



PMV

TECHNISCHE UNIVERSITÄT DARMSTADT

Progress in Paper Physics Seminar 2016

Conference Proceedings

ABB

Koehler PAPER GROUP

KRÜSS Advancing your Surface Science

MITSUBISHI PAPER MILLS LIMITED

VOITH





PMV

TECHNISCHE UNIVERSITÄT DARMSTADT

Progress in Paper Physics Seminar 2016

Conference Proceedings

ABB

Koehler PAPER GROUP

KRÜSS Advancing your Surface Science

MITSUBISHI PAPER MILLS LIMITED

VOITH

Scientific Committee

Program Secretary:

Heinz-Joachim Schaffrath	Technische Universität Darmstadt, Germany

Program Committee:

Warren Batchelor	Monash University, Australia
Wolfgang Bauer	Graz University of Technology, Austria
Jean-Francis Bloch	Grenoble Institute of Technology, France
Ulrich Hirn	Graz University of Technology, Austria
Thaddeus Maloney	Aalto University, Finland
Mark Martinez	University of British Columbia, Canada
Sören Östlund	Royal Institute of Technology, Sweden
Samuel Schabel	Technische Universität Darmstadt, Germany
Tetsu Uesaka	Mid Sweden University, Sweden

Schabel, Samuel; Schaffrath, Heinz-Joachim (eds.)
“Progress in Paper Physics Seminar 2016 Conference Proceedings”
Darmstadt, 2016

digital version:

URL: www.tuprints.ulb.tu-darmstadt.de/5636
URN: urb:nbn:de:tuda-tuprints-56362

print ISBN 978-3-00-054001-1

Cover photo:
Hochzeitsturm Mathildenhöhe (©Agentur für Mediendesign - Lichtenberg UG)

Presentations

Session I

”New Applications”

Conducting paper based photovoltaics

R. Schennach[1,2] and B. Friedel[1]

AUTHOR INFORMATION


R. Schennach

[1] Institute of Solid State Physics, Graz University of Technology, Austria

[2] CD-Laboratory for Fiber Swelling and Paper Performance

Email:
robert.schennach@tugraz.at

Functional organic photovoltaic devices on unmodified wood pulp fiber networks have been built. Long silver nanowires (AgNWs) have been adsorbed to their surface by help of naturally present hydroxyl groups by simple dip-coating, forming a well conductive and translucent fiber network. Low-density sheets of such treated cellulose fibers were characterized optically and electrically, showing hardly any absorption losses from silver content, but conductivities similar to ITO (Indium Tin Oxide), qualifying for a transparent electrode. The close contact of the AgNWs with the cellulose fiber minimizes the risk of short circuits when using this network as the anode of a thin film diode device. To proof this concept the AgNW-treated wood pulp fibers were coated with a mantle of hole-conductor PEDOT:PSS (Poly(3,4-ethylenedioxythiophene):poly(styrenesulfonate)) and a classic photo active layer of P3HT:PCBM (Poly(3-hexylthiophene):Phenyl-C61-butyric acid methyl ester) blend from solution, and finished with an evaporated metal cathode from only one side, to form a photovoltaic fiber network. The concept is shown in figure 1. The devices showed quite remarkable photoactivity, even without any optimization. Thereby nearly 0.1 % power conversion efficiency and up to 35 % fill factor were achieved under low-intensity white light illumination. Further it has been found that the scattering effect of the fiber sheets works as an advantage for the efficient capture of lowest intensity stray light. It has been shown that paper sheets despite their reputation of being too rough for diode substrates, can very well be used for photovoltaics if they are treated as a cellulose fiber network of quasi one-dimensional devices. A similar approach on viscose fibers will be presented too.

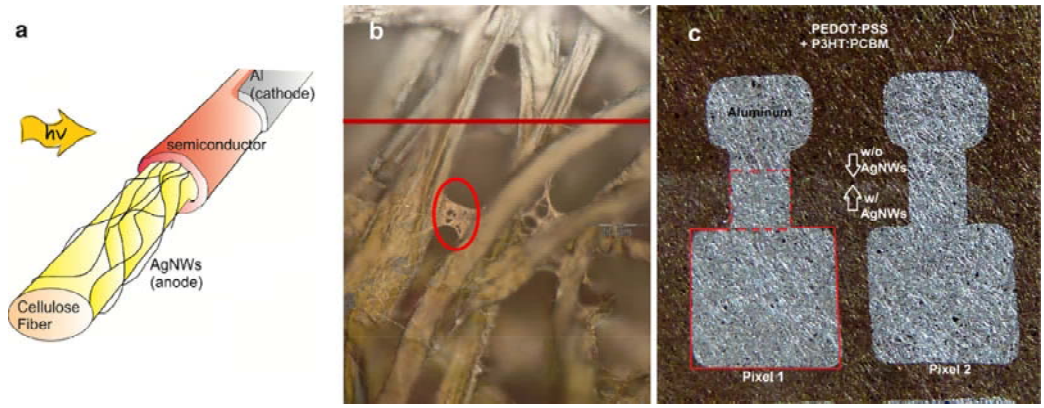

Figure 1: (a) The schematic architecture of a paper fiber photovoltaic device based on cellulose/AgNW anodes (illumination direction indicated) is depicted, (b) optical microscopy image of real individual photovoltaic fibers (the red line marks the border between fibers covered with AgNWs and P3HT:PCBM (below the red line) and fibers covered with AgNWs, P3HT:PCBM and then covered with the Aluminum counter electrode above the red line) and (c) photograph of a functional macroscopic device from the Aluminum side.

Enhancing the compression and shear properties of sandwich-honeycomb cores and foldcores using new paper-like materials

Alexander Bugiel[1], Falk Hähnel[1], Johann Strauss[2], Timo Kuntzsch[3]
[1] Institute of Aerospace Engineering, TU Dresden, Germany
[2] Papiertechnische Stiftung Munich, Germany
[3] Papiertechnische Stiftung Heidenau, Germany

Email: falk.haehnel@tu-dresden.de

High performance sandwich structures have a great significance in aerospace applications. Honeycomb cores are the most commonly used sandwich cores. Due to the closed cell structure of honeycombs, foldcores were developed to obtain a drainable sandwich structure. Both types of cores are usually made of aramid “paper” impregnated with phenolic resin. Because of this thin material and the relatively large unsupported areas, buckling of the cell walls is the typical failure mode under compressive and shear loads. In order to increase the load carrying capabilities of such cores, a new paper-like material is proposed in this paper. Therefore, materials with different fibre-network microstructures were created in order to investigate the influence of different pulp compositions on the bending stiffness. As a result, different kinds of three-layer materials have been developed. The face layers have a high stiffness due to the use of carbon and aramid fibres. In contrary, the middle layer is made of aramid fibres and lightweight particles. To determine and compare the mechanical parameters, standardized test methods have been used. Furthermore, compressive and shear test procedures for thin materials were improved. With these experimental determined parameters, numerical simulations have been performed to forecast the mechanical properties of the sandwich. The main outcome of the described analyses is the developed and experimentally investigated three-layer material. Experimental and numerical analyses show that the newly developed paper-like materials are capable of increasing the shear and compressive properties of honeycomb cores and foldcores significantly.

1. Introduction

The main failure mode of honeycomb cores and especially foldcores is a buckling of the cell wall material. Increasing the buckling resistance can

enhance the load carrying capability of such cores and sandwich structures. For honeycomb cores, the typical approach is to coat the aramid-paper with phenolic resin more than once. Thus, the cell wall thickness and the bending stiffness are increased [1]. Due to the high density of the phenolic resin, the strength to weight ratio cannot be increased significantly by this method. Another approach is to reduce the mean free path by using smaller cell sizes. Since more material is needed, the strength to weight ratio decreases [2]. In [3] Zakirov et al. describe a method to improve the bending stiffness of the cell wall materials of foldcores. This method includes grooving the material. Although the core compression strength could be improved, the strength to weight ratio seems to remain the same.

To the best of our knowledge, this paper presents a novel method to increase the strength to weight ratio of cores. New paper-like materials are developed that consist of three layers. This process is explained in section 2. To compare different materials, their mechanical parameters are determined. Thus, new and enhanced testing devices are suggested and applied to the materials in section 3. Furthermore, these mechanical parameters are needed for numerical simulations making it possible to forecast the behaviour of a whole sandwich core, which is explained in section 4. The simulations have been validated by compression tests on foldcores. Further numerical investigations showed a significant increase in the load bearing capabilities of cores made from the new materials.

2. Paper development

Main requirements to the development of adapted paper-like materials for core structures were non-combustibility and mechanical properties improving the buckling resistance of core structures. Step one was the production of material variations in the laboratory. A material screening was performed to test the suitability of a broad range of different potentially usable pulps for sheet forming, focusing on adequate strength, converting and impregnation properties besides general feasibility. As a result, paper materials modified with fibres that offer good sheet forming or formation and strength properties, for example aramid and carbon, were identified.

Sheet forming tests including the use of lightweight fillers were aimed at increasing the volume without weight gain. Filler-containing handsheets were successfully produced. The fillers make it possible to increase the specific volume of sheets, which does not necessarily lead to more bending stiffness.

The use of fillers reduces the static strength properties of non-impregnated sheets.

Using these findings, various test series were performed with promising pulp systems and fibre/filler systems to obtain multi-layer sheets in the laboratory. Aim of the tests was to increase the bending stiffness by combining stiff and high-strength face layers with a lightweight, voluminous middle layer to systematically create multi-layer paper structures. Three-layer paper materials with a grammage of around 150 g/m² (single layer grammage: 50 g/m²) could be successfully obtained in the laboratory. An improved weight-specific bending stiffness could be demonstrated for three-layer materials containing carbon fibres and impregnated with phenolic resin. An example of them is shown in the cross-sectional image in Figure 1.

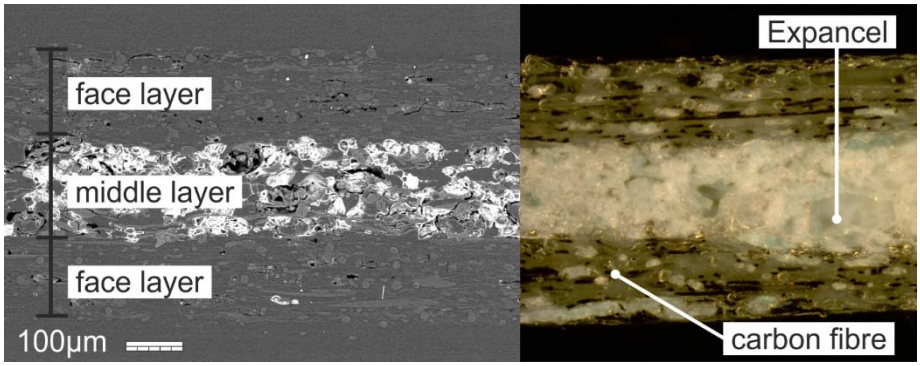

Figure 1: REM and light microscopic image of a developed paper

3. Paper testing

Parameters for stiffness and strength as well as plasticity were determined. Besides standardized test methods like the tensile test (DIN EN ISO 1924) and the bending test (DIN 53121), new methods for in-plane compressive, shear, and out-of-plane shear loads were needed. Therefore, a novel single-curved compression test has been developed, as can be seen in Figure 2 a) [4]. To determine the in-plane shear properties, the concept of a picture frame test device has been adapted for paper-like materials, see Figure 2 b) [5]. A modified Arcan fixture, which is based on the device suggested by Taher et al. [6], was used to determine the out-of-plane shear properties. The device can also be used to identify the mechanical behaviour under combined out-of-plane shear and tensile or compressive loads, see Figure 2 c).

Using these results, the different materials were compared to reduce the material diversity for further investigations. Furthermore, the experimental investigations have shown that three-layer materials seem to be most suitable for increasing the bending stiffness.

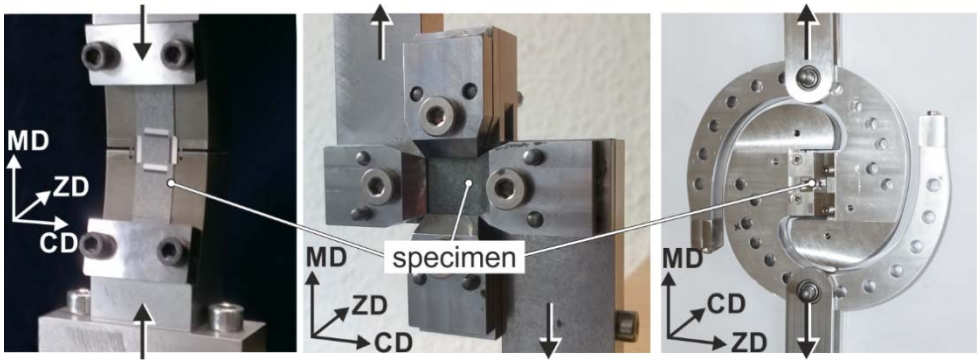

a) compression *b) in-plane shear* *c) combined out-of-plane*

Figure 2: Test devices for different load cases

4. Numerical investigations

In order to validate the numerical methods, foldcores made of common Nomex-paper impregnated with epoxy resin were tested and simulated. Experience has shown that standard constitutive laws are not suitable for this task. Hence, an adapted material law has been developed and implemented in an applicable finite element solver. Figure 3 a) shows a good agreement in terms of gradient and maximum force. Therefore, simulations are capable of predicting the mechanical behaviour of foldcores made of the developed materials. Only foldcores with the same geometry and grammage can be compared. Since the produced papers had grammage levels of approximately 350g/m² and Nomex is lighter, the thickness of the simulated material was adapted. The Nomex equivalent material has a thickness of 256µm and a grammage of 350g/m².

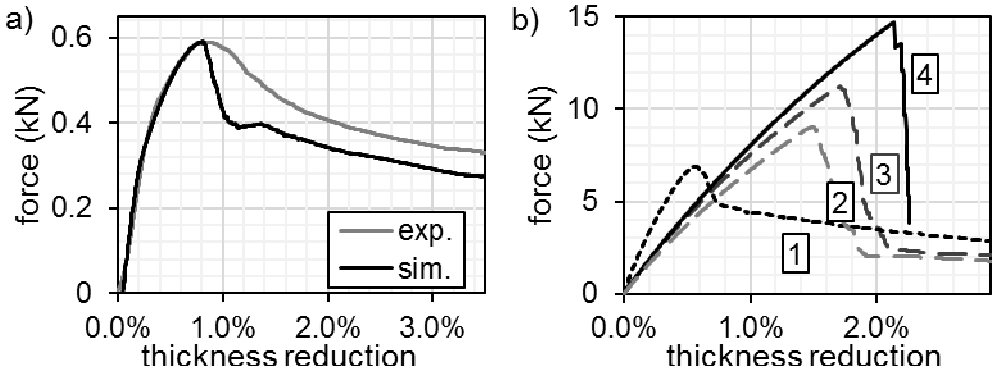

Figure 3: Results of the foldcore compression tests: a) comparison between experiments and simulation results; b) Simulation results of 350g/m² paper: 1 - Nomex equivalent paper, 2 – single-layer carbon paper (epoxy resin), 2 – three-layer carbon paper (epoxy resin), 4 – three-layer carbon paper (phenolic resin)

As can be seen in Figure 3 b), the Nomex equivalent (1) has the lowest compressive strength. In contrary, the three-layer carbon fibre material impregnated with phenolic resin (4) yields the highest strength. The same paper impregnated with epoxy resin (3) yields also good results. Graph (2) shows the behaviour of the same material without voluminous middle layer. The slightly lower compressive strength proves that the three-layer structure has a positive effect on the load bearing capability.

5. Conclusions

New paper-like materials have been developed. In order to compare their material and potential core properties, novel and enhanced testing devices as well as an enhanced constitutive law for numerical simulation have been suggested. Based on the experimentally determined mechanical parameters, it was possible to forecast the mechanical behavior of sandwich cores made of the new materials. By means of these methods, the best material was identified and optimized: a three-layer material. The face layers consist of carbon fibers and aramid fibrids, the middle layer is made of aramid fibers, fibrids and voluminous perlite. Further investigations are necessary to evaluate the benefits in structural components.

References

[1] F. Hähnel, Ein Beitrag zur Simulation des Versagens von Honigwaben aus Meta-Aramid-Papier in schlagbelasteten Sandwich-Strukturen, Dresden: Technische Universität Dresden, 2016.

[2] T. Bitzer, Honeycomb Technology, London: Chapman & Hall, 1997.

[3] I. Zakirov, A. Nikitin, K. Alekseev und C. Mudra, “Foldcore Structures: Performance, Technology and Production”, SAMPE EUROPE, International Conference, Paris, 2006.

[4] A. Bugiel, P. Reichenbach, F. Hähnel und K. Wolf, „Prüfvorrichtung für Druckfestigkeit dünnwandiger Materialien“. Patent DE 102015100467 A1 pend., 2016.

[5] F. Hähnel und K. Wolf, „Vorrichtung für die mechanische Werkstoffprüfung zur Bestimmung der Schubkennwerte von Werkstoffen“. Patent DE 102010006163 A1, 2011.

[6] S. Taher, O. Thomsen, J. Dulieu-Barton und S. Zhang, “Determination of mechanical properties of PVC foam using a modified Arcan fixture”, Composites: Part A, p. 1698–1708, 2012.

Potential of impulse drying technology for molded pulp products manufacture

DIDONE, MATTIA; TOSELLO, GUIDO; HOWARD, THOMAS J.

AUTHOR INFORMATION


M. Didone

Technical University of Denmark, Department of Mechanical Engineering, 2800 Kgs. Lyngby, Denmark

Email: matdid@mek.dtu.dk

ABSTRACT

The vision of the Green Fiber Bottle (GFB) project is to develop a paper bottle for beer, which will be both recyclable and biodegradable. The early prototypes of the bottle are very promising but there are huge technical and scientific challenges ahead to mature the production technology. The possibility of applying the concept of impulse drying during the drying stage is suggested. This would give benefits in terms of productivity and it would also reduce energy consumption.

With the aim of understanding and controlling the impulse drying phenomena, a simplified approach is proposed.

INTRODUCTION

The vision of the Green Fiber Bottle (GFB) project is to develop a paper bottle for beer, which will be both recyclable and biodegradable (Figure 1). The bottle is made out of paper pulp, which is a renewable resource. In order to enhance the green image of the product, the production technology has to offer the possibility of significant energy savings over the current approach, which is very heat and energy intensive.

Figure 1: The Green Fiber Bottle project main features and research partners

The manufacturing process involved in the production of the early prototypes of the GFB resembles the one used in the production of a thermoformed type of product. However, to enable the mass production of the product, technological improvements have to be introduced to meet the production throughput, product property and energy requirements.

Molded pulp products are made from cellulose fibers dispersed in water then formed, drained and dried. Like in the conventional papermaking process, the most energy intensive operation (also in terms of time) is drying.

It is in this process stage that an innovative way of drying the products based on the concept of impulse drying can be exploited.

The goal of this paper is to propose a simplified approach to understand and control the impulse drying effect, thus allowing its application in the manufacturing of molded pulp products.

In the next section, this paper provides an introduction of the main features of impulse drying. Section 0 discusses the applicability of this technology in the manufacturing of molded pulp products and a simplified approach to it is presented in Section 0.

It is the vision that the Green Fiber Bottle could be adopted for packaging drinks of various nature with the very ambitious goal “to bottle beer in a paper bottle”, which is highly relevant for the Danish industrial sector, and could have the potential of a global impact as well.

IMPULSE DRYING

Impulse drying is a process in which water is removed from a wet paper web by the combination of applied pressure and intense heat. It was introduced in the beginning of the 1980s by Wahren [1] and it attracted considerable interest from the paper industry as a means of reducing energy consumption in the drying process.

In this process, the wet web is exposed to pressures ranging from 10 to 80 bar and to hot surface temperatures typically between 100 – 350°C. The dwell or nip residence time is around 20 to 50 ms (hence the term “impulse”) and it

takes place in a so-called shoe-nip press, that replaces the conventional press nip [2].

Impulse drying is similar in nature to conventional wet-pressing operations but with the application of heat. The applied heat has two main roles: it reduces the viscous resistance of the water and it softens the structure of the paper pulp leaving it more compressible. It was also suggested that if the heat transfer rate is sufficiently high, a vapor phase can be generated on the wet paper side in contact with the high temperature medium [3]. This may assist in the dewatering process as the expanding steam can displace the bound water. This effect was recently studied and termed *flashing-assisted displacement dewatering* by Lucisano et al. [4].

Pilot scale experiments showed that some of the water present in the paper evaporates, and that some of it leaves the sheet in liquid form [5]. This means that less heat than what would be actually needed to evaporates all the water content has to be transferred resulting in a faster and a less energy consuming process [6].

Understanding the mechanism of steam forming and its motion through a fibrous and porous medium such as paper pulp is challenging. The phenomena was simplified and related to a class of heat transfer problems known as Stefan problems [7], but an exact interpretation, backed-up by experimental evidence, has not been obtained.

The introduction of the impulse drying technology in the paper industry has also been hampered by several operational problems. One such problem is delamination, which is defined as a sudden reduction of the strength in the thickness direction of the paper web. To prevent delamination, the fiber-to-fiber bonds must withstand the energy generated by the water, gases or steam moving in any direction during the impulse drying process [8]. A way to inhibit delamination consists of maintaining the pressure after opening the shoe-nip, allowing the paper to cool down gradually, avoiding an outburst of steam trapped inside. This results in a longer process time and increased investment in equipment. Re-wetting of the paper as it leaves the drying unit could also occur if the water is not effectively removed.

IMPULSE DRYING FOR MANUFACTURING THERMOFORMED MOLDED PULP PRODUCTS

In the production of the molded pulp products, the type of thermoforming is mainly characterized by the molding temperature, the pressure and the process time [9]. As explained in the previous paragraph, these are also the three main variables on which the impulse drying technology is based. These parameters must therefore be fine-tuned in order to achieve the benefits of the *flashing-assisted displacement dewatering effect*, which occur at a high and controlled temperature and pressure.

The operational problems that the impulse drying technology has encountered can be controlled and overcome. One such problem is the contact time between the impulse drying unit and the paper, required to control the energy transfer. In the manufacture of molded pulp products, molding and drying time

is not a major constraint, however, for mass produced goods like the Green Fiber Bottle time will be a factor to achieve the required throughput. To avoid delamination, the part can be kept inside the mold as long as the gases or steams trapped inside have been completely removed.

The technology can be applied in the production of any open geometry of molded pulp products. Extending this to the production of products with a three-dimensional closed geometry is still a work in progress.

Regarding the production of a bottle shaped molded pulp product, a patent has recently been filed by ecoXpac [10]. In its current state of development, the technology has proven to work for the production of prototypes but it does not exploit impulse drying that would give benefits in terms of energy saving as well as reduction in process time.

IMPULSE DRYING: HEAT CONDUCTION AND VAPOR-WATER DIFFUSION

With the aim of understanding and controlling the impulse drying phenomenon, a simplified approach is proposed. The idea is to describe the problem by looking at the thermodynamic state of the water content inside the paper.

The thermodynamic state of the system at a specific time is fully defined by knowing the values of the state variables, in this case, pressure and temperature. Some further assumptions have to be made regarding the thermodynamic equilibrium of the specific process stage considered.

The approach suggested refers to a conventional thermoforming process in which the pre-formed wet molded part is placed inside a mold. Assuming that temperature and pressure of the considered domain (i.e. the molded pulp part) can be controlled at each instant of time, two main process steps are identified:

1. Once the system is pressurized, the heat conducts from the heating element inside the wet paper part until a certain thickness of it reaches a definite temperature. At each instant of time, thermal and mechanical equilibrium is assumed.
2. Pressure is then released from one side of the system only and the water content in the top layers of the paper part flashes into vapor. The expanding steam diffuses through the paper thickness in the direction of the pressure gradient and it displaces the remaining liquid water. In this stage, a phase equilibrium is assumed, since only the diffusion of the vapor layer is taken into account.

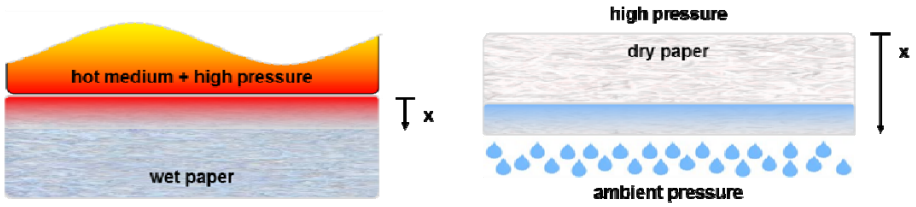

Figure 2: *Heat conduction stage (1); vapor-water diffusion stage through the paper thickness (2)*

The process can thus be summarized in a heat conduction stage followed by a vapor-water diffusion stage.

The duration of step one can be estimated by computing the heat transfer process along the thickness direction of the paper. The rate equation that appropriately quantifies the heat conduction is known as Fourier's law [11]. For the one-dimensional case the equation is as follow:

$$q_x'' = -k\frac{dT}{dx} \quad (1)$$

The heat flux q_x'' [W/m^2] is the heat transfer rate in the x-direction, in this case the thickness direction of the paper part, per unit of area perpendicular to the direction of transfer, and is proportional to the temperature gradient, dT/dx. The minus sign is a consequence of the fact that heat is transferred in the direction of decreasing temperature.

In the second step, the diffusive mechanism that can be considered is known as Stephan diffusion [12], which is also the dominating vapor transport mechanism in conventional paper drying. The driving force for Stephan diffusion is the gradient in the partial pressure of vapor:

$$\frac{\dot{m}_v}{A} = \varepsilon\,\Psi\frac{D_v}{R_v T}\frac{p_{tot}}{p_{tot}-p_v}\frac{dp_v}{dx} \quad (2)$$

Where:

ε void fraction of gas filled pores

Ψ labyrinth factor describing tortuosity of the flow path

D_v diffusivity of water vapor in air

R_v gas constant of water vapor (461,5 J/kg water/K)

p_v partial pressure of vapor

A major disadvantage of the Stefan theory is that the diffusion coefficients are not tabulated.

CONCLUSIONS

- Main features of the impulse drying phenomenon have been described, especially how the moving vapor layer can assist in the dewatering process by displacing the bound water.
- The applicability of the impulse technology during the drying phase of thermoformed products has been proposed. The packaging industry would benefit from such an improvement from a productivity point of view and it would also reduce energy consumption.
- A simplified explanation of the impulse drying effect has been proposed by considering two main process steps: heat conduction and vapor-water diffusion.

ACKNOWLEDGMENT

Support from Innovation Fund Denmark, funding a consortium between DTU Mechanical Engineering, EcoXpac and Carlsberg Group, is gratefully acknowledged. Particularly, the authors express their gratitude to Christian Carlsen and Kristian Søllner from EcoXpac for the invaluable discussions.

LITERATURE

[1] D. Wahren, “Impulse Drying,” in *The 47th Executives’ Conference*, 1983, pp. 54–60.

[2] P. Mendes, N. Belgacem, and J.-F. Bloch, “Impulse Drying Technology: the state of the art and the recent advances,” *ATIP*, vol. 58, no. 1, 2004.

[3] M. F. C. Lucisano, P. Mazzatorta, and D. M. Martinez, “On the mechanism of steam forming during impulse pressing of wet paper webs,” *Nord. Pulp Pap. Res. J.*, vol. 16, no. 4, pp. 355–361, 2001.

[4] M. F. C. Lucisano and A. R. Martin, “Visualization of liquid-vapor phase change phenomena in impulse technology,” *Tappi J.*, vol. 5, no. 6, pp. 15–21.

[5] J. C. Zavaglia and J. D. Lindsay, “Flash X-ray visualization of multiphase flow during impulse drying,” *Tappi J.*, pp. 79 – 85, 1989.

[6] H. Vomhoff and B. Norman, “Model experiments on wet pressing - The influence of felt surface structure,” *Nord. Pulp Pap. Res. J.*, vol. 12, no. 1, pp. 54–60, 1997.

[7] J. M. Hill, *One-dimensional Stefan problems: An introduction*. Longman Scientific & Technical, 1987.

[8] M. F. C. Lucisano and D. M. Martinez, “On the characterization of the delamination process during impulse pressing,” *Nord. Pulp Pap. Res. J.*, vol. 16, no. 4, 2001.

[9] S. T. Seana, B. Sanschagrina, B. V Koktab, and D. Maldasb, “Effects of

processing variables on the mechanical properties of compression molded polystyrene-wood fiber composites," *Die Angew. Makromol. Chemie*, vol. 184, no. 3128, pp. 157–166, 1991.

[10] K. Søllner, "A system and a method for producing a molded article, such as a bottle," WO2016/055073 A1, 2016.

[11] T. L. Bergman, A. S. Lavine, F. P. Incropera, and D. P. Dewitt, *Fundamentals of Heat and Mass Transfer*. 2011.

[12] M. Karlsson, *Papermaking Part 2, Drying*. TAPPI, 2000.

Improving the extensibility of thermoformable web structures with polymer dispersions

JARMO KOUKO[1], HARRI SETÄLÄ[2], JARMO ROPPONEN[2] AND ELIAS RETULAINEN[1]

AUTHOR INFORMATION

1: VTT Technical Research Centre of Finland Ltd, P.O. Box 1603, FI-40101 Jyvaskyla, Finland
2: VTT Technical Research Centre of Finland Ltd, P.O. Box 1000, FI-02044, VTT, Finland

Email:
jarmo.kouko@vtt.fi, harri.setala@vtt.fi
jarmo.ropponen@vtt.fi
elias.retulainen@vtt.fi

J. Kouko

SUMMARY

Paper-based packaging materials as renewable materials have growing market potential due to the sustainability potential of recycling. However, the development of new packaging concepts requires improvement in the mechanical properties of paper. Extensibility is one of those properties. Highly extensible papers have potential to replace plastics in several kinds of packaging.

The objective of this study was to produce a thermoformable network composed of cellulosic fibers and bio-based thermoplastic polymers with high formability. Bleached softwood kraft pulp was mechanically treated in two stages using high and low consistency refining sequentially. Chemical treatment using oxyalkylation method was applied to modify the fiber material, especially the fiber surface and its compatibility with polymer dispersions.

This study presents laboratory scale manufacturing methods for compositions that improved the extensibility of paper. The extensibility of the paper was measured with a novel experimental method that simulated the process conditions in thermoforming. The results showed that by choosing the pulp treatment method, the chemical composition and the thermoforming conditions, formability was improved. The results suggest that the formability of the paper is not a direct function of the extensibility of the applied polymer.

INTRODUCTION

Formability can be defined as the ability of a material to deform without breaking. However, formability is not a specific mechanical property, but can be regarded as a generic term for explaining how well paper deforms during a particular forming process [1]. In this study, formability was mainly estimated on the basis of a 2D experimental test method that simulated the process conditions in a fixed blank thermoforming process [2]. In the fixed blank process the formability is determined by the extensibility and tensile strength of paper [3].

Pulp fibers are the most important load-bearing component in paper. Kraft pulp fibers primarily consist of cellulose and hemicellulose. The chemical compositions of cellulose- and hemicellulose-polymers are well known, as are the general effects of refining on the fiber morphology and paper properties [4-5]. In this study, the influence of mechanical (two-stage refining) and chemical (oxyalkylation) treatments, on the formability of bleached kraft pulp, was investigated. The objective of the treatments was to modify the bonding ability of the fiber surface layer and change the fiber shape in such a way that the modifications are able to improve the elongation and bonding ability of the fiber network.

Elongation of some thermoplastic polymers such as Polyurethane (PU) (though it is not bio-based) can reach 450% and therefore it is reasonable to expect that the addition of such polymers to the fiber network will improve the formability of the paper [6]. Bio-based thermoplastic polymers are generally not hazardous to health and are also bio-degradable, which makes them suitable for use in food packages. Difficulties with polymer applications in wet-end additions are retention in the fiber network and adhesion to the fibers. On the other hand, in cases where the polymer is applied on a formed fiber network, difficulties arise in the impregnation of the polymer deep into the fiber network between the fibers. In this study several different thermoplastic polymers were applied onto, and into, the prepared undried fiber networks and then the influence of the application, on the formability of the paper was investigated.

Temperature is known to increase paper elongation and decrease tensile strength and tensile stiffness [7-10]. In this study, the influence of temperature on the formability of paper was investigated using a novel experimental method that simulated the process conditions in thermoforming.

EXPERIMENTAL

Bleached softwood kraft pulp (BSKP) from a Finnish mill was used as the raw material. The BSKP was mechanically treated in two sequential stages using high (HC) and low (LC) consistency refining. BSKP was chemically treated using oxyalkylation method (at low and high DS levels, 0.05 and 0.12, respectively) to modify the fiber material (see Table 1 for the pulps). This was done in order to modify fibers by introducing hydrophobic groups onto cellulose and improve their compatibility with polymer dispersions.

Table 1. The Studied Pulp Samples.

Pulp Abbreviation	Refining	Oxyalkylation Level
R	HC and LC sequentially	-
L	HC and LC sequentially	Low (DS_B 0.05)
H	HC and LC sequentially	High (DS_B 0.12)

Table 2. The Sprayed Thermoset Polymers.

Polymer Abbreviation	Polymer Name
WREF	Water (the reference)
PU-DL	Polyurethane (Impranil® DL 519)
PU-EPO	Polyurethane (Epotal® P 100)
PPC	Polypropylene carbonate (QPAC® 40)
PLA	PLA (LANDY PL-3000)
GL-PLA	Gelatin (2% of dry wt.) + PLA (18% of dry wt.)
PLA-CA	PLA + citric acid (4:1 mixture)
ST-AC	Starch acetate
NLAT	Nitrile latex (NYCHEM* 1561X604)
All polymer mixtures were sprayed with a 20% dry-weight of dry fiber amount, except gelatin was first sprayed with a 2% dry-weight and after that with a PLA 18% dry-weight of the dry fiber amount.	

The BSKP was made into 60 g/m^2 laboratory sheets. Table 2 presents the polymer dispersions (target 20% of dry-weight) that were sprayed onto the wet sheets. Vacuum was applied to the sheets to improve impregnation of the polymers. Unrestrained drying was utilized to allow the drying shrinkage that enabled the high extensibility of the structure.

The amount of the sprayed polymer was calculated using gravimetric measurement of the dry laboratory sheet. Target amount of the sprayed polymer was 20%. However, the deviation of the polymer amount compared to the target amount was systematical between pulps. The average amount of polymer in the R, L and H laboratory sheets was 17%, 27% and 19%, respectively.

2D formability strain was measured at several temperatures using the unique VTT tester [2]. The paper samples were set in the tester so that sprayed

surface was not in contact with the heated press. The paper samples were so thin that the there was only a minor temperature gradient through the paper thickness.

The tensile strength and the strain at break were determined with a Lloyd tensile tester, in accordance with ISO 5270:1998. Paper samples were conditioned and all testing of the samples took place in standard testing room conditions (temperature of 23 °C and 50% relative humidity).

RESULTS

Figure 1 shows that the low (L) oxyalkylation level yielded, on average, approximately 12% strain at break (in tensile test), which was the best average among the studied pulps (R, L, and H). The reference (R) and the high (H) oxyalkylation levels had an average strain at break approximately 9%. However, strain at break of the water reference (WREF) of the reference (R) pulp and low (L) level oxyalkylated pulp were similar and clearly higher compared to WREF of the high (H) level oxyalkylated pulp. This indicates that too heavy chemical treatment may not be beneficial for formability.

Strain at break of the water reference (WREF) of the reference (R) pulp was at the average level of the reference pulp group whereas strain at break of low (L) and high (H) oxyalkylation level pulps WREF was significantly lower compared to the average of the groups. That indicates that the chemical treatment improved the compatibility of the polymers to the fibers.

A simple linear regression analysis (the independent variables were the pulp type, polymer type and polymer amount) showed that the amount of polymer and polymer type in the paper samples probably had a significant influence on the tensile test results. This means that the systematically better strain at break of low (L) oxyalkylation has been partly caused by the higher polymer level in the sheets.

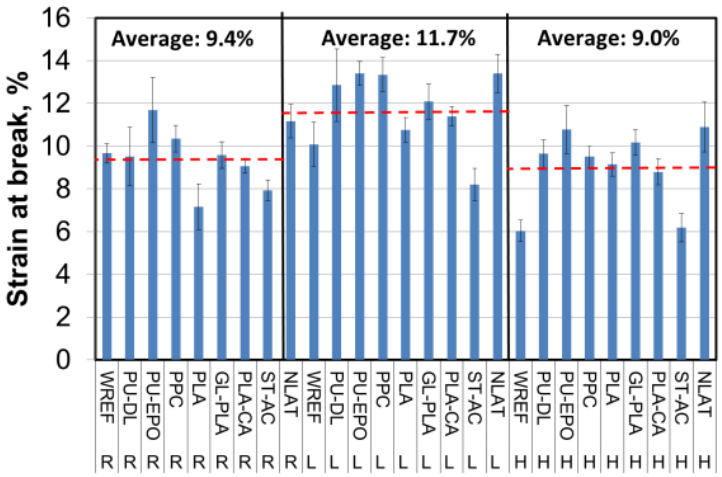

Figure 1. Strain at break of the paper samples.

The tension-strain curves, of the water reference (WREF) paper samples, are presented in Figure 2. The presented curves are repetitions that closely

represent the measured averages of the strain at break and tensile index. Figure 2 shows clearly that formability potential of the high (H) level oxyalkylated pulp was lower compared to the reference (R) pulp and low (L) level oxyalkylated pulp. For the formability potential of paper, the importance of the tensile index and especially the elastic modulus can be regarded as secondary, compared to strain at break.

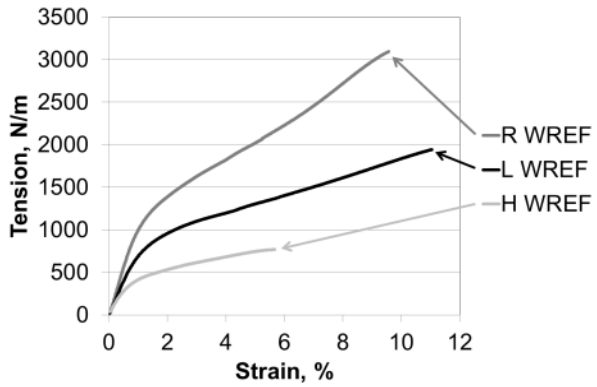

Figure 2. Tension-strain curves of the water reference (WREF) paper samples of the investigated pulps.

Figure 3 shows that the maximum formability strain was obtained at 60-90 °C temperature, whereas 120 °C clearly seemed to be above the optimal temperature in the most cases. Low (L) level of oxyalkylation had a clearly the highest formability strain compared to the other two pulps.

The 2D formability force could not be presented because of the limited space. However, the 2D formability force strongly decreased with temperature. This can be attributed to reduced hydrogen bonding. The maximum formability forces were measured at the lowest 23 °C temperature, while the 2D formability forces were 25-75% of the maximum value at 120 °C.

The most of the sprayed polymers improved the 2D formability strain of the low (L) level oxyalkylated paper samples, compared to the water reference (WREF). Both of the PU grades (PU-DL and PU-EP), polypropylenecarbonate (PPC), one PLA mixture (gelatin-PLA (GL-PLA)) and the nitrile latex (NLAT) improved the 2D formability strain. The strain at break of PU and PLA has been reported to be 450% and 7%, respectively. This indicates that the formability of the paper cannot be a direct function of the extensibility of the applied polymer. The tailor-made starch acetate (ST-AC) was the least promising of the studied polymers.

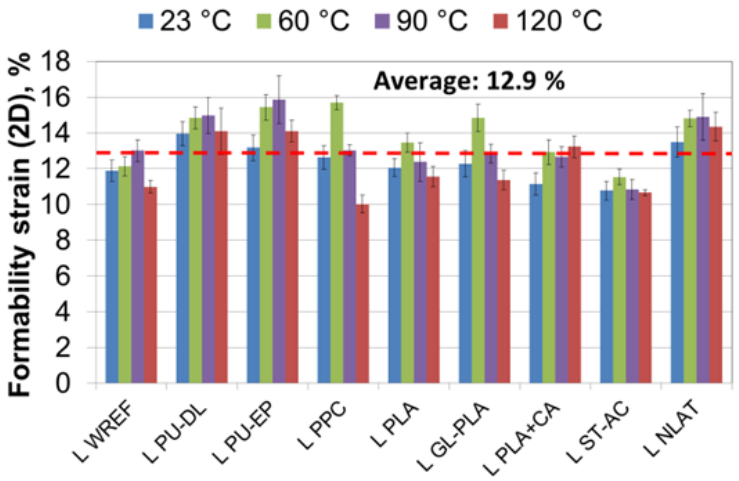

Figure 3. Formability strain of the paper samples with low (L) level oxyalkylation pulp. (Samples: Reference, two Polyurethane, Polypropylene carbonate, three PLAs, acetylated starch, and nitrile latex).

CONCLUSIONS

Low level oxyalkylation treatment of the bleached softwood kraft pulp is beneficial for the extensibility and thermoformability of a paper. Unrestrained drying significantly improves the extensibility and formability of paper and board. The optimal temperature for extensibility in thermoforming, in a fixed blank process, seems to be around 60-90 °C, for most of the investigated polymers and for the cellulose fibers. Increasing the thermoforming temperature deteriorates the strength of the paper. The formability of the paper is not a direct function of the extensibility of the applied polymer.

ACKNOWLEDGEMENT

This work was a part of the ACel program of the Finnish Bioeconomy Cluster CLIC Innovation. Funding by the Finnish Funding Agency for Technology and Innovation (TEKES) is gratefully acknowledged.

REFERENCES

[1] Vishtal, A. Formability of paper and its improvement. Doctoral thesis, 2015. VTT Science.
[2] Vishtal, A. and Retulainen, E. Improving the extensibility, wet web and dry strength of paper by addition of agar. *Nord. Pulp Paper Res. J.* 2014. Vol. 29, no. 3, pp. 434-443.
[3] Östlund, M., Borodulina, S., Östlund, S. Influence of paperboard structure and processing conditions on forming of complex paperboard structures. *Packaging Technology and Science* 2011. Vol. 24, no. 6, pp. 331-341.
[4] Alén, R. Structure and chemical composition of wood. In Stenius. P. (ed.) Forest Products Chemistry. Helsinki : Fapet Oy 2000. Section 1, pp. 11-57.
[5] Niskanen, K. Paper physics, 2000. Fapet Oy, Helsinki, Finland.
[6] Waterhouse, J. The deformation characteristics of polymer reinforced fiber networks. *Tappi* 1976. Vol. 59, no. 7, pp. 106-109.
[7] Salmén, L., Back, E.L. Moisture dependent thermal softening of paper evaluated by its elastic modulus. *Tappi* 1980. Vol. 63, no. 6, pp. 117-120.

[8] Salmén, L. Responses of paper properties to changes in moisture content and temperature. In Baker, C.F. (ed.) Products of Papermaking, 1993. Vol. 1, Pira International, Leatherhead, pp. 369-439.
[9] Back, E.L., Andersson, L.I. The effect of temperature on wet web strength properties. *Pan-Pacific pulp and paper technology* 1992. Vol. B, pp. 141-150.
[10] Kouko, J., Retulainen, E., Kekko, P. Straining and relaxation properties of wet paper during heating. *Mech. Time-Depend. Mater.* 2014. Vol. 18, no. 4, pp. 697-719.

Paper based all-cellulose composites - mechanical properties and anisotropy

Henri Kröling[1], Benoît Duchemin[2], Jan Dormanns[3], Mark P. Staiger[3], Samuel Schabel[1]

AUTHOR INFORMATION


H. Kröling

[1] Fachgebiet PMV – TU Darmstadt, Alexanderstraße 8, D-64283 Darmstadt
schabel@papier.tu-darmstadt.de
[2] LOMC, UMR 6294 CNRS-Université du Havre, Normandie Université, 53 rue Prony, 76058 Le Havre, France
[3] Department of Mechanical Engineering, University of Canterbury, Private Bag 4800, 8140 Christchurch, New Zealand

Email: kroeling@papier.tu-darmstadt.de

SUMMARY

In this work, the mechanical properties of paper-based all-cellulose composite (ACC) laminates were evaluated as a function of the fibre orientation of the precursor paper. Northern bleached softwood Kraft (NBSK) pulp was selected for this work as a cost effective precursor when compared with dissolving grade or cotton pulp. ACCs were fabricated by partially dissolving orientated NBSK paper using an ionic liquid and varying dissolution time. The resulting ACC laminates were tensile tested in both the machine and cross directions of the paper. The tensile properties of the ACCs in the machine direction achieved a tensile strength of 180 MPa and elastic modulus of 17 GPa, while that in the cross direction was 100 MPa and 8 GPa, respectively. The microstructure of the ACCs was evaluated *via* scanning electron microscopy and X-ray diffraction. The MD/CD ratio of the ACC was found to be close to that of the raw paper.

INTRODUCTION

A composite materials that consists predominantly of cellulose can be produced by partially dissolving cellulose fibres, followed by precipitation of the dissolved cellulose as a matrix that surrounds the remaining fibres [1]. All-cellulose composite are commonly prepared using ionic liquids or NaOH/urea

solutions as the cellulose solvents, contrasting with traditional processes for vulcanized fibres. ACCs have relatively high mechanical properties compared with other conventional bio-based composites (*e.g.* natural fibre-reinforced polypropylene) due to the strong fibre-matrix interface that forms in ACCs. Previous work has explored the use of filter paper or pulp sheets as a precursor for ACCs [2–5], with mechanical performance in the range of other ACCs. However, the cost of using filter paper and pulp sheet may be prohibitive in a commercial setting. In this work, 1-ethyl-3-methylimidazolium acetate (EMIMAc) was used to partially dissolve paper sheets based on a commercially available NBSK pulp as a more cost effective approach to paper-based ACCs. The paper was formed on a pilot paper machine at the Papiertechnische Stiftung PTS in Heidenau to investigate the effect of orientation on the mechanical performance of ACCs. A procedure was developed for fabricating the ACCs similar to that of Schuermann *et al.* [6].

RESULTS

The tensile strength of the ACCs was found to be significantly higher than that of the as-formed paper due to the formation of a matrix phase in the ACCs (Figure 3). The increase in strength is also partially due to densification of the material during processing into an ACC. The fibre orientation of the paper strongly influences the tensile properties of the as-formed paper and resulting ACCs (Figure 3). A cellulose film was also produced by fully dissolving the paper precursor.

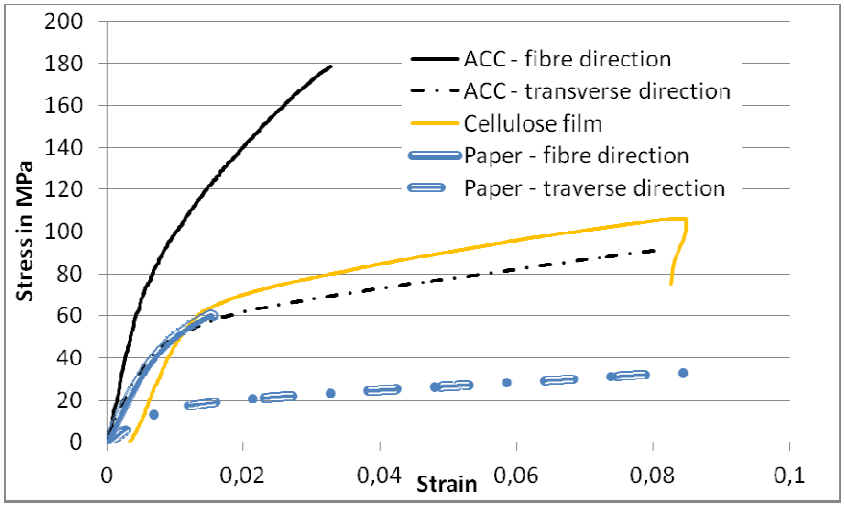

Figure 3: Tensile stress-strain behaviour of paper, ACCs and cellulose film

Following an initial increase in tensile properties, extending the dissolution time does not further enhance the tensile properties of ACCs (Figure 2). Changes in the crystal structure of the cellulose was determined from X-ray

diffraction (Figure 3). The diffractogram of the as-formed paper was typical of cellulose I. The diffractograms of the ACCs produced using varying dissolution times were similar, exhibiting mainly cellulose I. The crystallinity was calculated using the Segal's crystallinity index and two other methods (not shown), with all three methods confirming that all of the ACCs have similar crystallinity. A small minimum in crystallinity was observed at a dissolution time of 1 hour. The cellulose film consisted of amorphous cellulose and presumably cellulose II as expected.

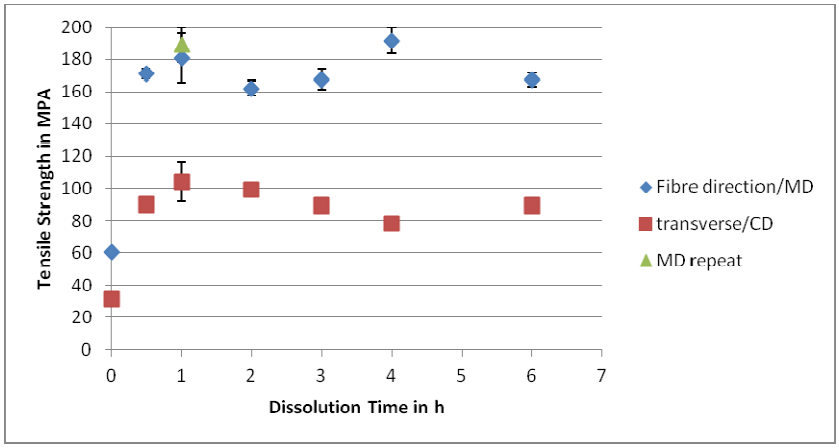

Figure 4: Development of the tensile strength over dissolution time

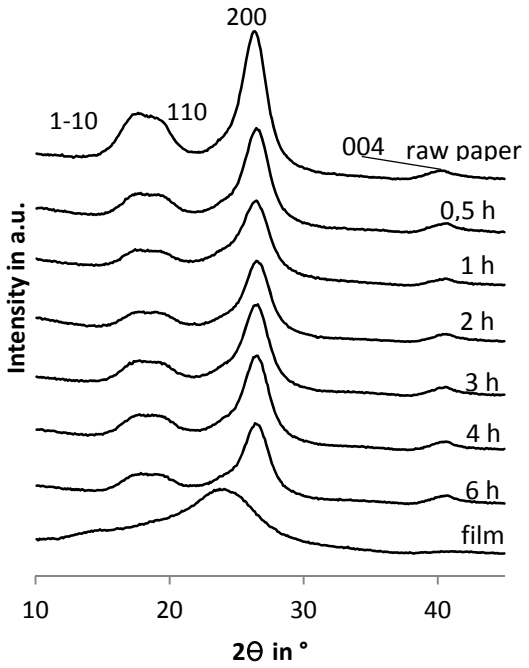

Figure 5: X-ray diffractograms as a function of the dissolution conditions.

CONCLUSIONS

ACCs with high tensile properties could be achieved by using a comparatively inexpensive NBSK pulp. The present work shows that the fibre orientation of the paper that originates from the paper making process strongly influences the mechanical anisotropy of ACCs. In the present case, the strength and stiffness were twice as high in the machine direction compared with the cross direction. The density-related strength of the ACCs is close to the specific fibre strength measured by the Zero Span Tensile. However, a clearer understanding of the effects of paper properties and dissolution on the micromechanical behaviour of paper-based ACCs is required. The anisotropy of the mechanical properties is also reflected in an orientation of the cellulose crystallites that is not diminishing with dissolution time. X-ray diffraction shows that the dissolution time does not strongly influence the phase transformation of cellulose I to cellulose II or amorphous cellulose that is presumed to be due to a low uptake of solvent due to a compact, dense paper structure. The presence of minimal solvent results in a low degree of cellulose dissolution of the paper fibres so that the final ACC structure is mainly retained as cellulose I. REFERENCES

[1] T. Huber, J. Müssig, O. Curnow, S. Pang, S. Bickerton, and M. P. Staiger, “A critical review of all-cellulose composites,” *Journal of Materials Science*, Jul. 2011.

[2] W. Gindl, T. Schöberl, and J. Keckes, “Structure and properties of a pulp fibre-reinforced composite with regenerated cellulose matrix,” *Applied Physics A*, vol. 83, no. 1, pp. 19–22, Jan. 2006.

[3] T. Nishino and N. Arimoto, “All-cellulose composite prepared by selective dissolving of fiber surface.,” *Biomacromolecules*, vol. 8, no. 9, pp. 2712–6, Sep. 2007.

[4] B. J. C. Duchemin, A. P. Mathew, and K. Oksman, “All-cellulose composites by partial dissolution in the ionic liquid 1-butyl-3-methylimidazolium chloride,” *Composites Part A: Applied Science and Manufacturing*, vol. 40, no. 12, pp. 2031–2037, Dec. 2009.

[5] B. J. C. Duchemin, D. Le Corre, N. Leray, A. Dufresne, and M. P. Staiger, “All-cellulose composites based on microfibrillated cellulose and filter paper via a NaOH-urea solvent system,” *Cellulose*, vol. 23, no. 1, pp. 593–609, Dec. 2016.

[6] J. Schuermann, T. Huber, and M. Staiger, “PREPREG STYLE FABRICATION OF ALL-CELLULOSE COMPOSITES,” in *19th International Conference on Composite Materials*, 2013, pp. 5626–5634.

DEVELOPMENT OF CELLULOSE NANOFIBRE QUALITY WITH MECHANICAL ENERGY: EFFECT OF STARTING CHEMICAL COMPOSITION

Praveena Raj[1], Alireza Mayahi[2], Thilina Gunawardhana[1], Swambabu Varanasi[1], Gil Garnier[1], Antonio Patti[3], Darren Martin[2], Warren Batchelor[1*]

[1]BioResource Processing Research Institute of Australia (BioPRIA), Department of Chemical Engineering, Monash University, Clayton 3800, VIC, Australia.

[2] The Australian Institute for Bioengineering and Nanotechnology (AIBN), The University of Queensland, St Lucia Qld 4072, Australia

[3] School of Chemistry, Monash University, Clayton 3800, VIC, Australia

[*]Corresponding author: warren.batchelor@monash.edu

Abstract

The gel point is the lowest solids content at which a fibre suspension forms a continuously connected network [1, 2] and is related to the fibre aspect ratio. We have previously shown that cellulose nanofibre aspect ratio is a critical fibre parameter controlling network formation in sheet forming and sheet mechanical properties [3-5] and that gel-point can be measured from data of final sediment height and initial solids concentration, for a range of dilute suspensions.

In this paper, we used gel point measurement to probe the development of nanofibre quality with increasing mechanical energy input for four different feedstocks: 1) Bleached Eucalypt Kraft Pulp (BEK), 2) commercial Microfibrillated Cellulose (MFC) with a very high crystalline cellulose composition, 3) de-lignified, bleached Spinifex pulp and 4) Softwood TMP pulp fines. By combining the data of the aspect ratio and average diameter, determined from SEM and TEM, we were able to compare the differences in feedstock processability.

The aspect ratio of all four feedstocks initially increased with increasing homogenisation energy, showing that the fibre delamination dominated over fibre shortening. The slope of the aspect ratio versus energy consumption showed the ease of processing of each sample.

The Spinifex fibres had the fastest rate of aspect ratio increase, followed by the BEK sample. The ease of processing of the spinifex fibres was due to the very high hemicellulose content, which facilitated separation of the fibrils. Both the commercial MFC and the TMP fines were difficult to process, but for different reasons. In the case of the commercial MFC, the strongly bonded crystalline cellulose structure was difficult to separate.

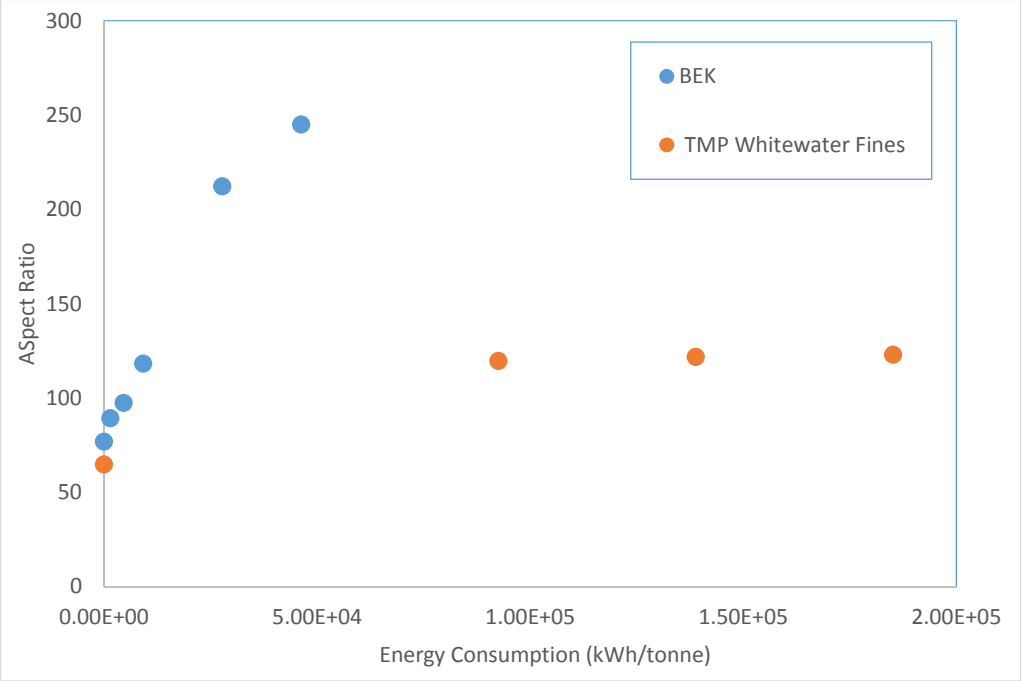

The data for the BEK and TMP fines is shown above. It can be seen that the BEK, with minimal lignin in the fibres, is far easier to process, with the aspect ratio continuing to increase with mechanical energy input from firstly a PFI mill and then a homogeniser. In contrast, the TMP fines are very slow to be further fibrillated, reflecting the high lignin content bonding the fibre structure, which has not been removed in the pulping process.

The use of the gel-point to measure aspect ratio is shown to be a promising approach to measuring nanofibre quality.

References

1. Celzard, A., V. Fierro, and R. Kerekes, *Flocculation of cellulose fibres:* new comparison of crowding factor with percolation and effective-medium theories. Cellulose, 2009. 16(6): p. 983-987.
2. Varanasi, S., R. He, and W.J. Batchelor, *Estimation of cellulose nanofibre aspect ratio from measurements of fibre suspension gel point.* Cellulose, 2013. **20**(4): p. 1885-1896.
3. Zhang, L., W. Batchelor, S. Varanasi, T. Tsuzuki, and X. Wang, *Effect of cellulose nanofiber dimensions on sheet forming through filtration.* Cellulose, 2012. **19**(2): p. 561-574.

4. Varanasi, S. and W.J. Batchelor, *Rapid preparation of cellulose nanofibre sheet.* Cellulose, 2013. **20**(1): p. 211-215.
5. Li, Q., P. Raj, F.A. Husain, S. Varanasi, T. Rainey, G. Garnier, and W. Batchelor, *Engineering cellulose nanofibre suspensions to control filtration resistance and sheet permeability.* Cellulose, 2016. **23**(1): p. 391-402.

Understanding and tailoring fluid flow in designed microfluidic papers

M. Biesalski

AUTHOR INFORMATION

M. Biesalski

Department of Chemistry,
Macromolecular Chemistry and Paper Chemistry
Technische Universität Darmstadt
64287 Darmstadt, Germany

Email:
biesalski@tu-darmstadt.de

The author didn‘t deliver an extended abstract. Instead he names the following papers covering the subject of his presentation:

1. Böhm, A.; Carstens, F.; Trieb, C.; Schabel, S.; Biesalski, M., Microfluidics and Nanofluidics 2014, 16 (5), 789-799.
   Engineering microfluidic papers: effect of fiber source and paper sheet properties on capillary-driven fluid flow.

2. Böhm, A.; Gattermayer, M.; Trieb, C.; Schabel, S.; Fiedler, D.; Miletzky, F.; Biesalski, M., Cellulose 2013, 20 (1), 467-483.
   Photo-attaching functional polymers to cellulose fibers for the design of chemically modified paper.

3. Jocher, M.; Gattermayer, M.; Kleebe, H.-J.; Kleemann, S.; Biesalski, M., Cellulose 2015, 22 (1), 581-591.
   Enhancing the wet strength of lignocellulosic fibrous networks using photo-crosslinkable polymers.

Modeling and characterisation of localized deformation of paperboard in the SCT and folding.

Eric Borgqvist[1,2], Mathias Wallin[2], Matti Ristinmaa[2] and Johan Tryding[1,2]

AUTHOR INFORMATION


E. Borgqvist

[1]Tetra Pak, Ruben Rausingsgata, 221 86, Lund, Sweden.
[2]Division of Solid Mechanics, Lund University, SE-221 00 Lund, Sweden.

Email:
eric.borgqvist@solid.lth.se

Summary

The localized deformation patterns developed during in-plane compression and folding of uncreased paperboard have been studied. The Short-span Compression Test (SCT) and folding have been studied using both experimental and numerical techniques. X-ray post-mortem images reveal that cellulose fibres have been reoriented along localized bands in both the compression and folding tests. A continuum model is utilized to predict the occurrence of the localized bands. It is shown that the in-plane strength in compression for paperboard can be correlated to the mechanical behaviour in folding. By tuning the in-plane yield parameters to the SCT response, it is shown that the global response during folding can be predicted. The simulations are able to predict the formation of wrinkles, and the deformation field is in agreement with the experimentally observed deformation pattern. The model predicts an unstable material response associated with localized deformation into bands in both the SCT and folding of paperboard.

Introduction

The paperboard occupies the largest volume of a paper-based package and becomes severely deformed during converting operations. To assess the quality of paperboard, simplified test methods that mimic the deformation modes present in converting and filling operations are typically performed. Two such test methods are the short-span compression test (SCT) and the

line folding operation. The results recorded in these tests can be correlated to the performance in the actual converting and filling processes. Even though these tests are designed to measure specific properties of the board, the deformation pattern of paperboard becomes complex. The SCT and folding have been investigated in this work using both numerical as well experimental techniques [1].

The 3-dimensional continuum material model established in [2] has been utilised to simulate the SCT as well as the uncreased folding of paperboard. The model takes into account the large degree of anisotropy in the continuum by utilising a set of director vectors representing the in-plane directions and a normal for the out-of-plane direction. Thermodynamic considerations at finite strains have been taken into account such that the dissipation inequality is fulfilled. The model has previously been shown to be able to predict the mechanical behaviour in creasing in [2] and [3].

Experimental setup

Schematics of the SCT and the line folding setups are shown in Fig.1a and Fig.1b, respectively.

a)

b)

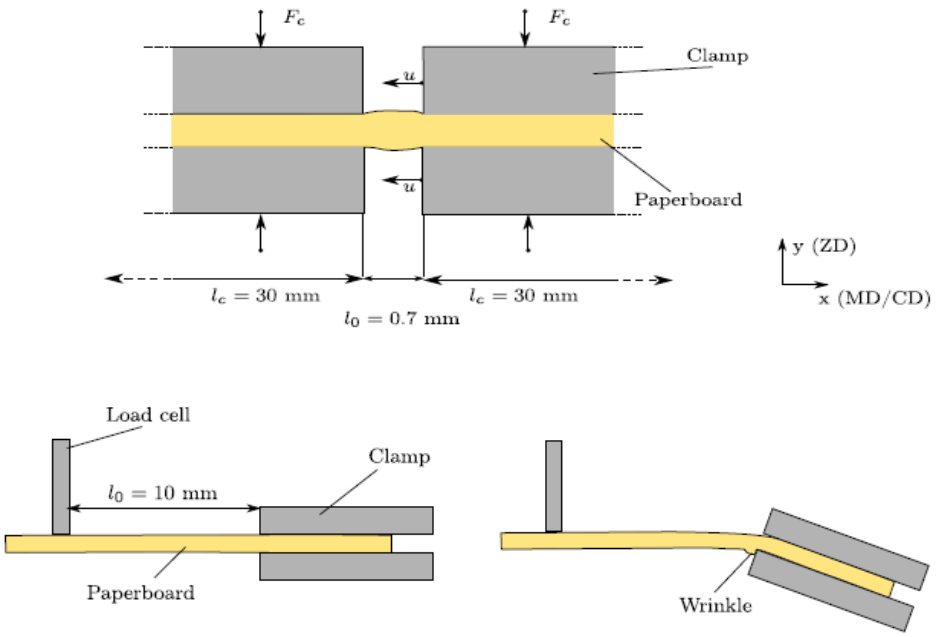

Figure 6: a) Schematic of the SCT-procedure. b) Schematic of the line folding.

In the SCT, the paperboard is initially clamped with a total pressure of ~5 MPa, where free span length $l_0 = 0.7$ mm is used, which separates the two

clamps. Boundary effects (from the clamp) influences the paperboard in the free span length due to the short length l_0 being used. In the folding operation, the paperboard is clamped on one end and there is a load cell acting as rigid support at a 10 mm distance from the clamps. During folding, one side of the paperboard will be under tension and the other side will experience compression. The failure stress of paperboard is lower in compression compared with tension and wrinkles are formed on the side which is under compression. The paperboard's strength in compression therefore has a significant effect on the folding behaviour of paperboard.

Post-mortem images of paperboard after the SCT and folding have been obtained using x-ray tomography. The processed images in Fig. 2a and Fig. 2b show typical local deformation patterns that are developed during the tests.

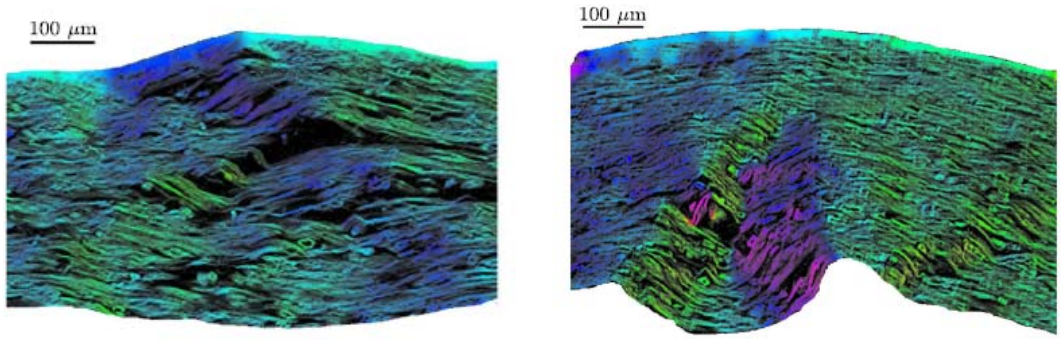

(a) *(b)*

Figure 2: Post-mortem images of *a) SCT b) Folding, obtained using x-ray tomography. The color coding in the images indicates the orientation of the fibers.*

As seen in Fig.2, the fibers become reoriented in localized bands both in the SCT and folding. From the folding test, it is seen that the fibers have been reoriented inside the wrinkle (on the side that is under compression), while the localization band is extended along the entire thickness in the SCT. The reorientation is approximately 25 degree in the SCT and approximately 45 degrees inside the wrinkle in the folding.

Numerical Results

In Fig.3, simulated deformation patterns of the SCT and the folding test are shown. As is seen in Fig.3, the model is able to predict the localized deformation patterns that occurs during these test, i.e. both the shear band in the SCT and the wrinkle formation in the folding operation can be predicted.

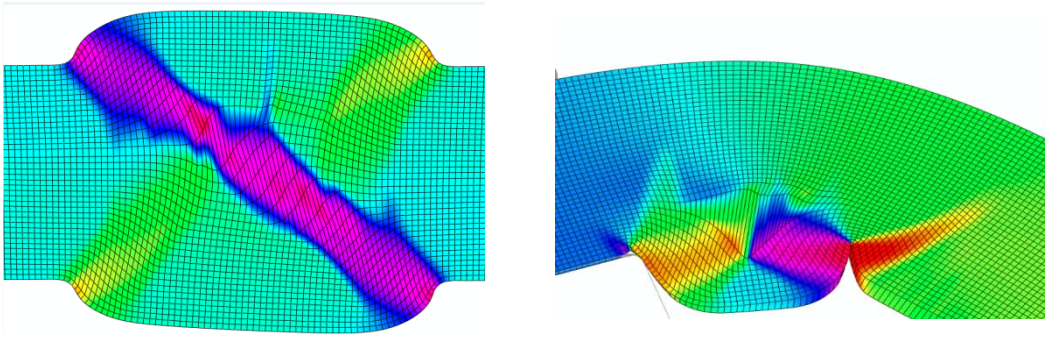

(a) (b)

*Figure 3: S*imulation images after *a) SCT- b) Folding- operation. The color coding in the images indicates the orientation of the fibers.*

The width of the localized bands are similar in the simulations as in the measurements, but the orientation angle is overestimated.

Specifically, the stress state present in the SCT prior to failure has been analysed and reveals that both in-plane compression and out-of-plane stresses are significant during the test. By tuning the model to fit the global force-displacement response from the SCT, it is further shown that the bending moment vs bending angle curve obtained from the folding can be predicted.

The shear bands observed for the paperboard material is common for other type of granular materials as well, when loaded in compression. This unstable material response is typically associated with a negative definite acoustic tensor and it has been shown in this work that the acoustic tensor becomes negative definite prior to failure in the SCT.

Conclusions

The mechanisms present in the SCT and folding have been analysed and it can be concluded that the SCT-value is correlated to the response in folding. The continuum model is able to predict similar deformation patterns that has been observed from x-ray post mortem images. Prior to failure in the SCT, significant in-plane compression as well as out-of-plane stresses occurs. The model is able to predict the unstable material response in the SCT and the formation of wrinkles in folding.

Literature

[1] E. Borgqvist, M. Wallin, M. Ristinmaa, J. Tryding and E. Tudisco. Localized Deformation in Compression and Folding of Paperboard. Packaging Technology and Science, Vol. 29, pages 397-414, 2016

[2] E. Borgqvist, M. Wallin, M. Ristinmaa and J. Tryding. An anisotropic in-plane and out-of-plane elasto-plastic continuum model for paperboard. Composite Structures, Vol. 126, pages 184-195, 2015.

[3] E. Borgqvist Continuum modeling of the mechanical response of paper-based materials, PhD-thesis, 2016

Session II

”Paper Mechanics”

Analysis of short-span uniaxial tests of paperboard samples

Johan Tryding* and Matti Ristinmaa

AUTHOR INFORMATION


J. Tryding

Division of Solid Mechanics, Lund University,
SE-221 00 Lund, Sweden
*e-mail: Johan.Tryding@solid.lth.se
web page: http://www.solid.lth.se

Summary

Analytical cohesive relations to describe experimentally measured stress-widening curves are often expressed in dimensionless quantities. These dimensionless quantities are obtained by use of the maximum strength and a length measure. The length measure used here is the ratio of the maximum strength to the maximum gradient of a stress-widening relation. An analytical cohesive relation, with maximum strength, length measure and a dimensionless material parameter, is suggested for paperboard. The cohesive relation is validated against experimental data; samples loaded in uniaxial tension and shear for in-plane and out-of-plane are used. A good fit is obtained for the proposed cohesive relation to the experimental data.

Introduction

Paperboards material properties are crucial for preventing defects, which can occur in converting and filling of packages. During folding out-of-plane delamination occurs in the filling machine and in-plane cracks may be initiated. To gain a better understanding of these processes an analysis of cohesive load-elongation measurements from short-span uniaxial tests have been performed, both in the in-plane and out-of-plane directions.

From short-span uniaxial tension tests, stable load-elongation relations have been measured up to complete failure separation. A cohesive stress-widening relation, σ_{max} vs. w, can be obtained from the stable post-peak part of the load-

elongation relation; using information of the elastic modulus for the specimen, cf. [1]. A normalization procedure for the stress-widening relation is presented in [1], which scale the experimental data, using the tensile strength, $\sigma_{\max}$, and the maximum slope of the stress-widening relation, $N_{\max}$. The stress σ is scaled as $y = \sigma/\sigma_{\max}$ and the widening w is scaled as, $x = w/w_N$, where $w_N = \sigma_{\max}/N_{\max}$. The length w_N, has been identified from a dimensionless analytical cohesive stress-widening relation derived from the Morse potential in [1].

Theory

As shown in [1], using the Morse potential for diatomic molecules, a cohesive stress-widening relation can be identified as,

(1) $$y = \operatorname{sech}^2\left(\frac{x}{x_c}\right) \text{ where } x_c = \frac{4}{3\sqrt{3}}.$$

Following the approach in [1], and utilizing a truncated Taylor series expansion of the natural logarithm of (1) around w = 0, the cohesive stress-widening relation is obtained as

(2) $$\ln(y) = -\left(\frac{x}{x_c}\right)^{1/c}.$$

In (2), $c = 1/2$ and higher order terms have been neglected. In [1] a rearrangement of (2) gave an exponential softening relation as $y = \exp\left(-(x/x_c)^{1/c}\right)$. It is noted that the same exponential softening relation has been proposed for concrete in [2], if x/x_c is replaced by Aw where A is a material parameter. Note also that A and c are independent material parameters. We will assume that $c > 0$ is an arbitrary dimensionless material parameter in the calculation that follows.

An additional softening relation from (2) can be obtained by making a truncated Taylor series expansion of the left hand side of (2) around y = 1 and neglecting higher order terms, i.e. $-\ln(y) = \ln(1/y) = (1/y - 1)$. Insertion into (2) gives after rearrangements the nonlinear cohesive relation

(3) $$y = \frac{1}{\left(\frac{x}{x_c}\right)^{\frac{1}{c}}+1}.$$

This format has been proposed for concrete in [3], if x/x_c is replaced by Aw. The slope is obtained by the derivative $-N(w) = d\sigma/dw = -\sigma_{\max}/w_N \cdot dy/dx = -N_{\max} \cdot dy/dx$, where we used the definition $w_N = \sigma_{\max}/N_{\max}$. Requiring that the second order derivative to be equal to zero, gives the maximum slope,

(4) $$-N_{\max} = \left.\frac{d\sigma}{dw}\right|_{\max} = -N_{\max} \cdot \frac{1}{x_c} \cdot \frac{c}{4}(c^{-1}+1)^{1+c}(c^{-1}-1)^{1-c}$$

Rearrangement gives

$$x_c(c) = \frac{c}{4}(c^{-1}+1)^{1+c}(c^{-1}-1)^{1-c}. \quad (5)$$

Material and methods

In [1], short-span in-plane tensile tests on six different paperboard materials (A-F) have been conducted. The paperboards have different structures, i.e. number of plies and fiber types. The entire paperboards and their individual plies were tested in a climate room at 23°C and 50% relative humidity (RH). The material parameters are tabulated in [1] and it is concluded that the investigated paperboards material data differ significantly between the paperboards and its plies.

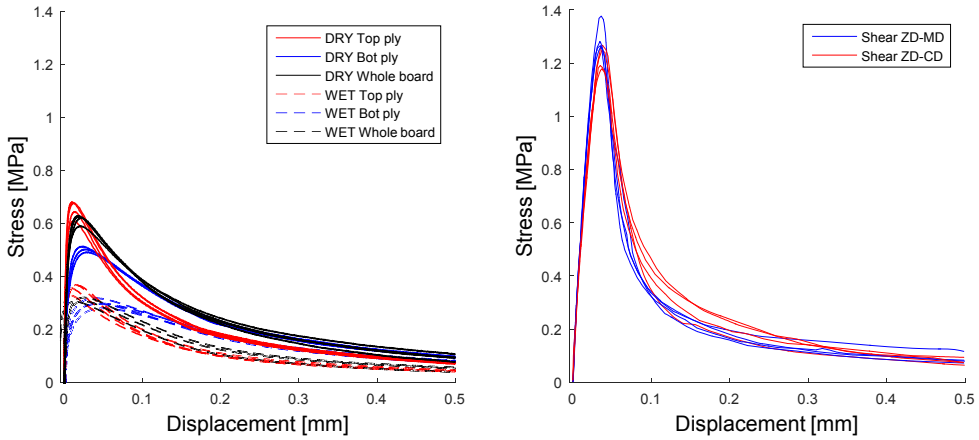

(a) (b)

Figure 7: Stress-displacement graphs. (a) Out-of-plane ZD tension loaded two-ply paperboard and its plies at two moisture content levels. (b) Out-of-plane ZD-MD and ZD-CD shear loaded triplex paperboard.

Additional experimental data are provided from uniaxial out-of-plane tension and shear tests. Figure 1 displays the stress versus displacement graphs of the two-ply paperboard and its plies together with a triplex paperboard. Figure 1(a) shows a two-ply paperboard and its plies in ZD tension loading and Fig. 1(b) shows a ZD-MD and ZD-CD shear loaded triplex paperboard. The two-ply paperboard is tested at two different moisture content levels. The DRY series refer to a moisture content level of 6.6%-8.1% and the WET series refer to a moisture content level of 15.1%-18.5%. The plies of the two-ply paperboard are denoted top ply and bottom ply. The two-ply paperboard were tested in a climate controlled laboratory at Innventia AB, [4], at 23°C and 50% RH for the DRY series and at 23°C and 90% RH for the WET series. The triplex

paperboard was tested in a climate controlled laboratory at Lund University, [5], at 23°C and 50% RH.

From the stress-displacement data in Fig. 1 the cohesive stress-widening parameters are obtained following the cohesive zone model by [6].

Results

In Fig. 2(a) the normalized stress versus normalized widening provided in [1] are plotted for both MD and CD. The tensile strength and the maximum slope for each individual curve was used, cf. [1]. The experimental relation shows that the normalization relations $y = \sigma/\sigma_{\max}$ and $x = w/w_N$ scales the experiments into a normalized cohesive relation approximately independent on the in-plane material properties, [1]. To calibrate (3) to the experimental data in Fig. 2(a), the dimensionless parameter *c* for each direction is obtained by a non-linear regression. A 3-parameters Weibull distribution gives an accurate fit to the distribution. The mode for *c* is in MD 0.4666 and in CD 0.4902. A mean value of the mode gives *c* = 0.4784. Figure 2(a) shows that the normalized cohesive relation with *c* = 0.4784, plotted as a dashed curve, and there is clear correlation between the analytical cohesive relation and the experimental data.

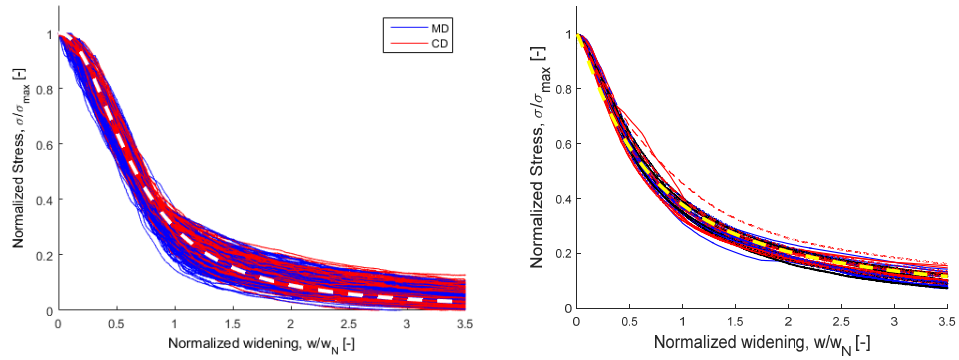

(a) (b)

Figure 8: Normalized stress vs. normalized widening curves. (a) Normalized in-plane data from [1]. (b) Normalized out-of-plane data corresponding to Fig. 1. In (a) and (b) Equation (3) are plotted with c = 0.4784 (dashed) and c = 0.8168 (dashed), respectively.

Data from the out-of-plane tension and shear loaded paperboards, using the same normalization as previously, are shown in Fig. 2(b). To calibrate (3) to the experimental data in Fig. 2(b) the dimensionless parameter *c* is obtained by a nonlinear regression for a combination of data series, giving *c* = 0.8168 ± 0.05632 for 31 samples, assuming a normal distribution. The analytical cohesive relation in (3), with *c* = 0.8168, is shown as a dashed curve in Fig.

2(b), and it is conducted that the normalized analytical cohesive relation fit well to the experimental data. Figure 2(b) reveals that the normalizations $y = \sigma/\sigma_{\max}$ and $x = w/w_N$, where $w_N = \sigma_{\max}/N_{\max}$ scales the experimental data into a relation that is independent of the moisture content levels and the out-of-plane material properties and loading condition.

Conclusions

Cohesive stress-widening relations are often expressed as dimensionless analytical cohesive relations, cf. e.g. [7], where the cohesive stress commonly is normalized using the maximum strength. The normalization of the widening is not as obvious as for the cohesive stress. Here, the length w_N is identified from a dimensionless analytical cohesive stress-widening relation derived from the Morse potential in [1]. An important observation was that by choosing the normalized widening w_N in the cohesive stress-widening relation given by (3) it was possible to show that the suggested material parameters were not independent. For the particular model only three material parameters, $\sigma_{\max}$, $N_{\max}$ and c are needed to fully characterize the cohesive relation.

The dimensionless cohesive relation was validated against experimentally obtained uniaxial tension data in the in-plane direction together with uniaxial tension and shear data in the out-of-plane direction. Samples with different sizes and paperboard properties were tested. The derived analytical cohesive relation was shown to fit all the investigated data. It was concluded that for the investigated paperboards the analytical cohesive relation and the experimental data suggests that the normalized cohesive data are collected into unique relations, one for the in-plane and one for the out-of-plane loading direction.

Literature

[4] J. Tryding, G. Marin, M. Nygårds, P. Mäkelä, G. Ferrari, International Journal of Damage Mechanics 1056789516630776, first published on March 11, 2016.
[5] V. Gopalaratnam, S. Shah, J. Am. Concr. Inst. 82 (1985) 310–323.
[6] A. Carpinteri, M. Corrado, M. Paggi, Strain 47 (4) (2011) 351–362.
[7] M. Nygårds, Innventia AB, Drottnings Kristinasväg 61B, SE-114 28 Stockholm, Contract work April 2014.
[8] K. Persson, Lund University, Contract work, June 2005.
[9] A. Hillerborg, M. Modeer, P. Petersson, Cement and Concrete Research 6 (1976) 773–782.
[10] S. Kumar, S. V. Barai, Concrete Fracture Models and Applications, Springer, 2011.

3D Structure & Strength Characterization of Northern Bleached Softwood Kraft Paper

Farzin Golkhosh[1], Majid Targhagh[1], Yash Sharma[2], Mark Martinez[3], Wendy Tsai[3,4], Loic Courtois[5], David Eastwood[5], Peter Lee[5], and André Phillion[6]

[1]School of Engineering, University of British Columbia, Kelowna, Canada
[2]Lehrstuhl für Biomedizinische Physik, Physik-Department and Institut für Medizintechnik, Technische Universität München
[3]Deptment of Chemical and Biological Engineering, The University of British Columbia, Canada
[4]Canfor Pulp Innovation, Canfor Pulp, Burnaby, Canada
[5]Manchester X-ray Imaging Facility, University of Manchester, Manchester, UK
[6]Dept. of Materials Science and Engineering, McMaster University, Canada

Email: philliab@mcmaster.ca

Summary

The strength of paper is linked to Low Consistency (LC) refining. While much is known about the changes in fibre morphology created from the beating effect, very little is known about how LC refining affects the microstructure of the sheet. Over the past 5 years, through collaborative research, innovative methods for characterizing the microstructure of paper products and the effect of LC refining have been developed using novel 3D X-ray tomographic imaging (μCT) and image-based modelling. In this talk, research from 3 studies will be presented:

(1) The development of a multi-step methodology for segmenting NBSK fibres in high-resolution μCT images that is able to isolate the individual fibres even with cracks and openings in their fibre walls. This method results in a robust 3D fibre segmentation that preserves the surface topology of the papermaking fibres, and enables quantification of fibre physical properties.
(2) The development of a finite element model to simulate the mechanical behaviour of a 3D network of NBSK paper based on “real” geometry from μCT images. By performing a series of simulations using different fibre morphologies and softwood / hardwood fractions, the effect of fibre geometry on tensile index has been quantified for low basis weight paper.
(3) The initial results from 4D imaging (3D images acquired over time while applying tensile load) of NBSK+ hardwood sheets.

Introduction

A key step in papermaking is the refining process, which modifies the fibre morphology. In LC refiners, papermaking fibres flow between rotor and stator discs in a slurry of 90% water and become “beaten” or “refined”, resulting in structure modification and strength enhancement. The action of refining

results in, amongst others, fibre fibrillation, shortening, and straightening, and the formation of fines [1]

While much is known about the changes in fibre morphology created from the beating effect, very little is known about how LC refining affects the microstructure of the sheet. X-ray tomographic microscopy (μCT) is a novel non-invasive visualization technique for acquiring high-resolution 3D images that can be used to characterize the internal structure of a wide variety of materials [2] including paper [3]. It is well known that X-ray tomographic microscopy can create beautiful images of paper products [4], but quantitative insight requires extensive development of bespoke numerical tools and experimental methods. This study reports the initial findings of three tools that can be used to gain insight into the relationships between paper architecture and tensile strength.

Applications of Quantitative μXCT to NBSK products

Fibre segmentation and 3D characterization of LC-refined fibre architecture [5]

The first and often most challenging task in the analysis of fibres is the isolation of each individual fibre in the 3D network, also known as fibre segmentation. Fibre segmentation gives access to the properties at the fibre level such as the length, cross-section area and orientation, as well as the properties at the network level including the coordination number of the fibre–fibre bonds. An automated algorithm to segment individual fibres from 3D μCT images has been developed using the lumen as base markers. The algorithm is able to segment uncollapsed fibres containing cracks and kinks, along with small regions where the fibres are locally collapsed. The three-step fibre segmentation algorithm segments the papermaking fibres by (i) tracking the lumen inside the fibres via a modified connected componenet methodology, (ii) extracting the fibre walls using a distance transform and (iii) labeling the fibres through collapsed sections by a final refinement step. Figure 1 shows a fully segmented dataset. This method is able to segment approximately 50% of fibres found in NBSK handsheets. The segmented dataset provides unique information about the architecture of refined papermaking fibres. Additional algorithms were also written to estimate the length, coarseness, shape factor, thickness, fibre wall thickness, and contact area. In one example handsheet section, size 1 mm^2, a coarseness of 0.16+/- 0.06 mg/m and a contact area of 68% /fibre was measured, with on average 9 contacts per fibre.

Mathematical Modelling of Tensile Strength in Low Density Paper [6]

NBSK is often mixed with hardwood furnished for strength enhancement. An approach has been developed to simulate the effects of basis weight, mixture fractions and fibre geometry on tensile strength. The simulation geometries were formed based on the true fibre geometries, extracted from the μCT images of paper handsheets. An example simulation geometry is shown in Figure 2(a). A series of simulations were then carried out to investigate the basis weight, and hardwood/ softwood fibre mixture ratios on the tensile index of the geometry. The results, given in Figure 2(b), showed that the simulation geometries with a higher basis weight and smaller elastic modulus at the fibre

scale lead to a lower tensile index. Further, it was shown that the increase in the softwood content of mixtures increased the bulk tensile index of paper. Finally, the results of the tensile strength simulations were compared to the results of experimental tensile strength tests [7]. The results of this research provide a new insight into the mechanical behaviour of paper and interaction of fibres under deformation of paper.

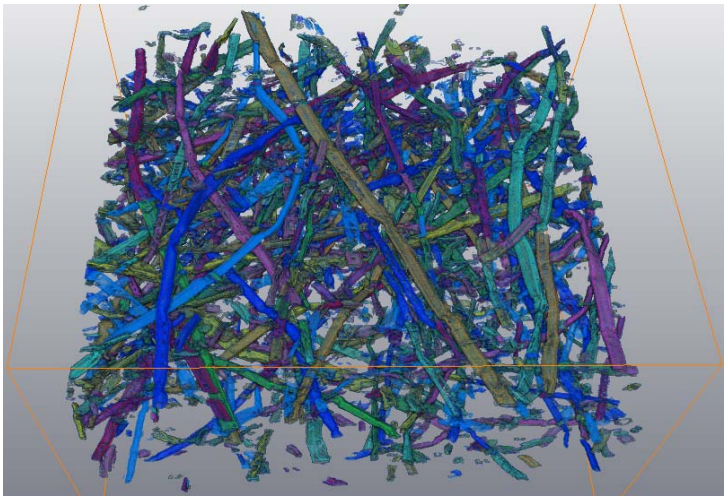

Figure 1: Segmented NBSK fibre dataset.

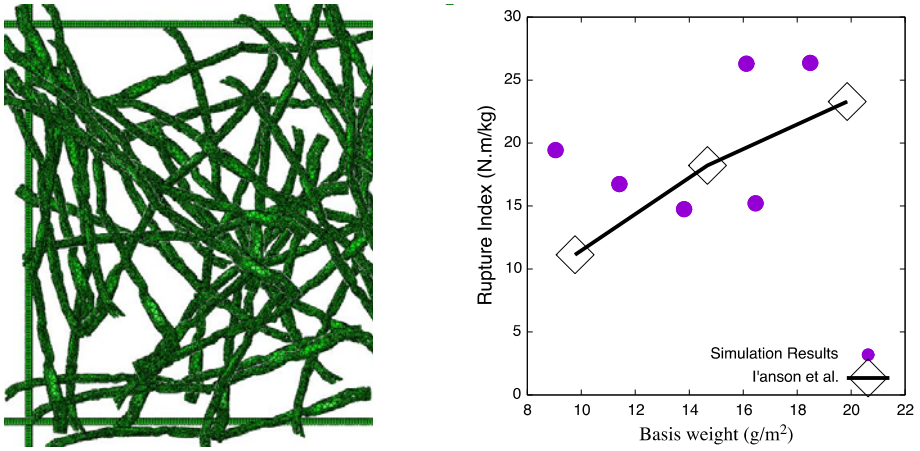

(a) (b)

Figure 2: (a) FE model of low-basis-weight paper showing structure of low basis weight paper; (b) Comparison between the fibre network simulations and experimental data by I'anson et al. [7]

4D tensile testing of NBSK and its mixtures

The preceding two studies focused on analysis of static µCT images and their use in order to model tensile strength. The high brilliance of synchrotron X-ray sources allows for 4D imaging, in which X-ray tomographic images are captured concurrently with physical specimen testing. Figure 3 shows the result of one such test, performed on a 100% NBSK specimen that was LC refined at 100 kW. Although only the initial and final fibre architectures are shown, the deformation sequence consisted of 10 µCT images. Our initial study of the 3D deformation indicates that at this refining intensity, many fibres break as a result of the tensile deformation instead of simply pulling apart,

indicating that the inter-fibre bonds are quite strong as compared to the intrinsic fibre strength. Further, the deformation localizes very quickly. The use of 3D μCT provides insight into deformation in the through-plane direction, and we are currently developing algorithms to determine the evolution of local fibre orientation and to calculate strain via Digital Volume Correlation [8].

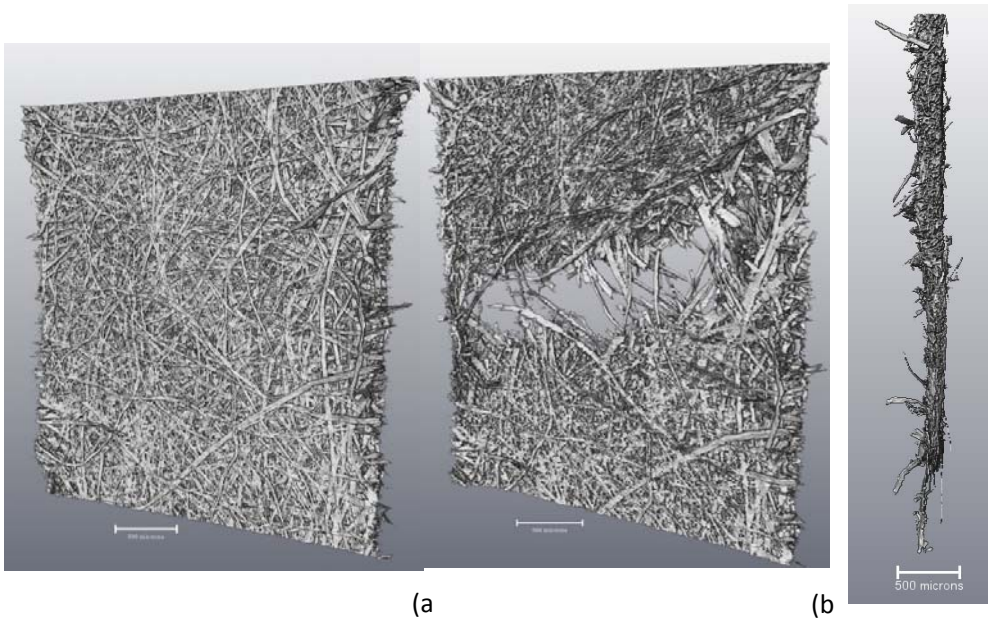

Figure 3: 3D synchrotron CT images showing the (a) initial and failed states, and (b) the cross-section view of the failed state of a 100% NBSK handsheet.

Conclusions

3D μCT is a powerful tool for exploring the microstructure of NBSK paper products. With appropriately-developed image analysis tools, the effects of refining parameters on fibre architecture can be quantified, and tensile strength can be simulated. Using 4D imaging at synchrotron X-ray sources, fibre deformation can be performed concurrently with the acquisition of 3D datasets, revealing new insight into the mechanisms of paper deformation.

Methods

The NBSK paper sample used for μXCT imaging was produced using a British handsheet maker at UBC's Pulp and Paper Centre. The papers were freeze-dried, after forming the sheet, to increase the percentage of fibres with un-collapsed lumens within the handsheet. The 3D dataset of the handsheets were then acquired using a Zeiss MicroXCT-400 X-ray tomographic microscope. For imaging purposes, the sheet was first cut to a size of 1.0 mm x 1.0 mm in cross-section and then firmly secured to a sample holder. The resulting 3D volume consisted of 2000 x 2000 x 300 voxels, each 0.58 μm in edge length. The automated fibre segmentation algorithm was written using the Matlab software, while the numerical simulations of tensile deformation were performed in the Abaqus finite element software. The 4D mechanical test was performed at the Diamond Light Source (Didcot, UK) on I13 using Lee's P2R tensile tester [2].

Acknowledgements

This work was made possible by financial support from the Natural Sciences and Engineering Research Council of Canada, Canfor Pulp, as well as the facilities and support provided by the Research Complex at Harwell, funded in part by the EPSRC (EP/I02249X/1 & EP/M009688/1). The authors also acknowledge the use of synchrotron beam-time at the Diamond Light Source, I13 through the Diamond/Manchester Collaboration (proposal MT13240).

References

1. D.H. Page, “The beating of chemical pulps- the action and effects,” in *9th Fundamental Research Symposium*, Cambridge, 1989, pp. 1-37.
2. C. Puncreobutr, P. Lee, R. Hamilton, A. Phillion, JOM, V64, pp: 89-95, 2012.
3. S.R. Roscoat, J-.F. Bloch, X. Thibau, “Synchrotron radiation micro-tomography applied to investigation of paper,” Journal of Physics D: Applied Physics, vol. 38, pp. A78-A84, 2005.
4. Y. Sharma, A.B. Phillion, D.M. Martinez, “Automated segmentation of wood fibres in microCT images of paper,” J. Microscopy, V260, pp: 400-410, 2015.
5. Y. Sharma, “Automated Fibre Segmentation in Micro CT Images of Paper,” UBC MASc thesis, 2014.
6. M. Targhagh, “Simulation of the mechanical behaviour of low density paper and an individual inter-fibre bond,” UBC MASc thesis, 2016.
7. S. I'Anson, W. Sampson, S. Savani, “Density dependent influence of grammage on tensile properties of handsheets,” J. Pulp Paper Science, V34, pp:182-189, 2008.
8. B.K. Bay, T.S. Smith, D.P. Fyhrie, M. Saad, Exp. Mech., V39, pp. 217-226, 1999.

Stress-strain behavior of paper affected by the actual contact area

Jian Chen, Edgar Dörsam, Dieter Spiehl, Arash Hakimi Tehrani and Jun Da

AUTHOR INFORMATION


J. Chen

Institute of Printing Science and Technology
Technische Universität Darmstadt
Magdalenenstr. 2, 64289, Darmstadt
GERMANY

Email:
chen@idd.tu-darmstadt.de

Keywords: actual contact area, actual stress-strain curve, actual modulus

SUMMARY

The surface topography of paper can range from very rough to extremely smooth, which has significant influences on mechanical properties of paper materials, especially the compressive behavior of paper in the out-of-plane direction. Normally, the stress-strain relations of most of the materials are calculated by using the nominal contact area, which is the whole area of the pressure head. The difference between actual and nominal contact area is ignored, but they are very different, and cannot be neglected in all situations. In this paper, a new experimental method for evaluating the relationship between the actual contact area and the normal load is proposed. A carbon paper is introduced in this method, and it is assumed that the measured contact areas between carbon paper and the actually tested paper are the same as the actual contact areas between the pressure head and the tested paper. Based on this assumption, the mechanical behavior of paper in the out-of-plane direction could be discussed by calculating the actual stress-strain relation and deducing the actual modulus. In addition, the force sensitivities of different carbon papers used for showing the actual contact areas were also compared. The calculation results show the crucial differences between the actual and nominal stress-stain behaviors.

INTRODUCTION

The relationship between the stress and strain that a particular material displays is known as that particular material's stress–strain curve. Generally, the stress-strain curve of the material is calculated based on the force-deformation curve. The force-deformation data obtained from tensile or compressive tests do not give a direct indication of the material behavior, because they depend on the specimen geometry.

For paper material, because of the existence of the surface roughness, the contact areas change continuously during the test. When the surface of the pressure head is very smooth, the actual contact area *A(z)* under force is usually smaller than the nominal contact area *A*.

The measurement and characterization of the actual contact area are very important not only for paper materials [1] but also for metal [2, 3] or other materials [4]. The researches about the actual contact area are very helpful to further investigate the surface roughness as well as the intrinsic characteristics of materials.

EXERIMENTAL SETUP

The laboratory of the Institute of Printing Science and Technology is equipped with the universal testing machine Zwick Z050, by which the deformation performance of specimen can be determined with high accuracy of the cross head speed (0.0005-2000 mm/min), position repetition accuracy (± 2 μm), drive system's travel resolution (27 nm) [5]. The travel sensor (Heidenhain-Metro MT 2581) is produced by the HEIDENHAIN firm, with the resolution of 50 nm and the repetition accuracy of 0.2 μm .

MATERIALS

The paper selected in this paper for doing the research is the normal copy paper (copy paper, DIN A4, 210×297 mm, 80 g/m^2), produced by the Steinbeis Paper GmbH. The average thickness is d = 84.7 μm.

For different carbon papers, the force sensitivities are very different. Seven different types of carbon papers (SH-1, SH-2, SH-3, DL-1, DL-2, DL-3, Geha-1) were tested. The effects of the ink on the copy paper are shown in Table 1.

Table 1. *Sensitivity tests of different carbon papers. SH carbon papers are produced by Shanghai Huideli Co., Ltd. DL carbon papers are produced by Deli Group Co., Ltd. Geha carbon papers are produced by Geha Werke Hannover.*

Carbon papers	100 N	20 N	10 N	2 N
SH-1	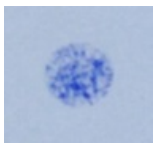			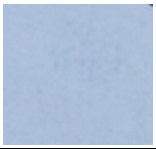
SH-2	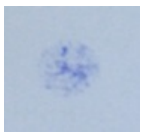			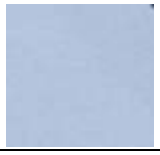
SH-3				
DL-1	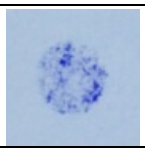			
DL-2				
DL-3	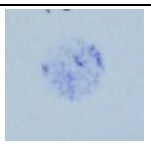			
Geha-1	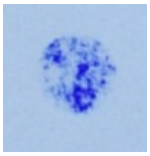			

It can be seen from Table 1 that the sensitivities of different carbon papers are quite different, only SH-1, Geha-1 can be used for measuring low pressure, especially, when the forces are smaller than 20 N. The SH-1 carbon paper was selected in the following parts to measure the contact areas under different forces.

METHOD

The method can be summarized as the following three steps [6]:

- Carrying out experiments: the forces are changed from 0 N to 100 N, with the length of the substep 2 N, which means 50 groups of experiments (2 N, 4 N, 6 N, 8 N,…, 96 N, 98 N, 100 N) are carried out. For each group, 20 tests are finished.

- Enlarging and transferring the pictures: the surface of the specimen is magnified 25 times under a binocular microscope and captured by a camera with pixels of 1200×1600. With the aid of MATLAB 8.1 [7], all pictures can be transferred into binary images.
- Calculating the contact areas: the image processing technique is used to separate the contact area from the background, then the contact areas can be calculated.

RESULTS

ACTUAL CONTACT AREA

Figure 1 shows the measured contact areas A_{mea}, the forces are changed from 0 N to 100 N with the substep of 2 N. The error bars represent the average (mean) values and the standard deviations of measured contact areas under different forces. The relationship between the measured contact area A_{mea} and force F can be drawn by the curve fitting method.

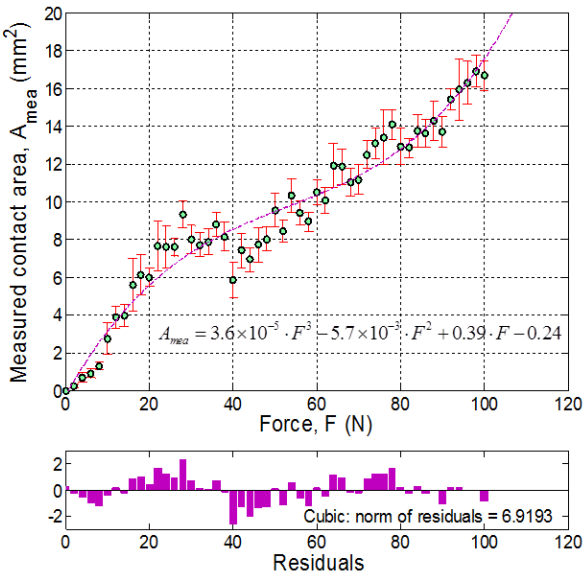

Figure 1. *Measured contact areas under different forces. The cubic curve fitting method (the coefficient of determination: R^2 = 0.953) is used in the above picture, the picture below shows the corresponding residuals.*

The cubic curve fitting method was used, the function is provided as follows:

$$A_{mea} = 3.6\times10^{-5}\cdot F^3 - 5.7\times10^{-3}\cdot F^2 + 0.39\cdot F - 0.24 \qquad (1)$$

It is assumed that the measured contact areas A_{mea} between carbon paper and copy paper are regarded as the actual contact areas $A(z)$ between the pressure head and copy paper. Based on this assumption, the mechanical

behavior of paper in the out-of-plane direction can be discussed by calculating the actual stress-strain relation and deducing the actual modulus.

ACTUAL STRESS-STRAIN CURVE

It can be seen from Figure 2 that by considering the surface roughness, the stress-strain curve of paper material is a typical elastic-plastic material, which is very similar to other engineering materials, such as steel.

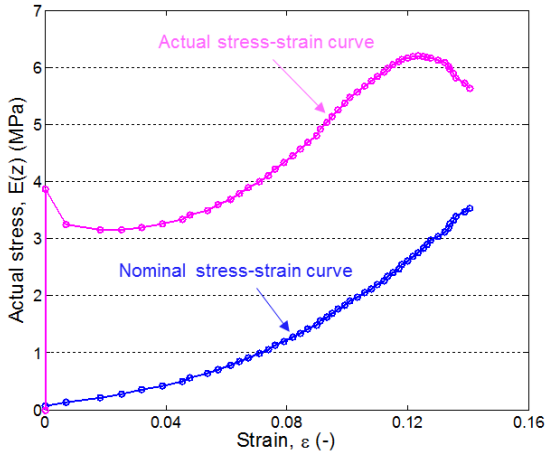

Figure 2. *Stress-strain curves of paper calculated by using the actual contact area and the nominal contact area. The actual contact areas under different forces are calculated by using Equation 1.*

Some typical characteristics used for determining the elastic-plastic material, for example, elastic part, plastic part, the yield stress, ultimate stress, etc., all of these behaviors can be found in the actual stress-strain curve.

For the nominal stress-strain curve, as we well know, the loading stage shows a typical J-shaped curve. Based on the results above, we can reasonably infer that the surface topography has a very big influence on the compressive behavior of paper materials.

ACTUAL MODULUS

When the changes of the forces are very small, it is reasonable to assume that the deformation behavior of the material under small forces accord with the theory of elasticity. Hooke's law is the law of elasticity under small deformation, which can be expressed in terms of stress (σ) and strain (ε) [8]:

$$\sigma = E \cdot \varepsilon \Leftrightarrow F = \frac{E \cdot A}{d} \cdot z \Rightarrow F(z) = \frac{E(z) \cdot A(z)}{d} \cdot z \qquad (2)$$

Where, *A* is the nominal contact area, *d* is the thickness of copy paper, *z* is the deformation under the force *F* (or *F(z)*). *E(z)* is the actual modulus, which is changing with the discrete force *F(z)*. *A(z)* is the actual contact area.

The actual modulus of paper can be expressed as the product of actual contact pressure, paper thickness and the inverse of the total deformation.

$$E(z)=\frac{F(z)}{A(z)}\cdot\frac{1}{z}\cdot d \tag{3}$$

Then, according to Equation 3, the actual modulus of paper can be calculated, the result is shown as the pink curve in Figure 3.

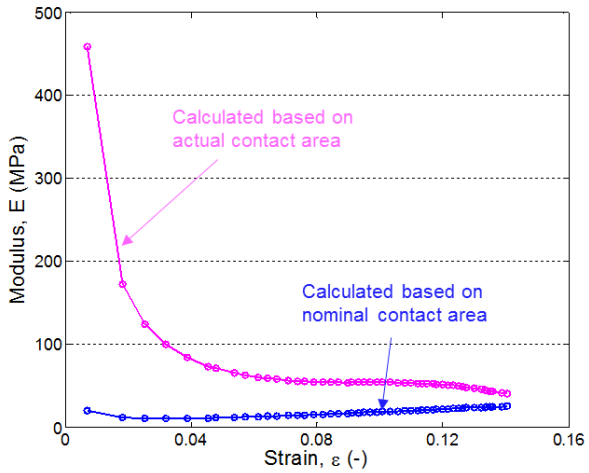

Figure 3. *Moduli of paper calculated by using different methods. The actual contact areas are calculated by using Equation 1.*

Figure 3 shows the moduli of paper calculated by using different methods. When the force is changing from 2 N (the pressure is about 0.07 MPa) to 100 N (the pressure is about 3.54 MPa), the actual modulus of paper is decreasing from 458 MPa to around 40 MPa. The modulus calculated based on the nominal contact area is changing from 20 MPa to about 25 MPa. With the contact area approaching to the nominal contact area *A*, the actual modulus decreases to a constant value (about 27 MPa), which is close to the result calculated based on the nominal contact area.

CONCLUSIONS

Three important concepts of paper materials were proposed in this paper: the actual contact area, the actual stress-strain curve and the actual modulus.

Firstly, the actual contact areas under different forces were calculated, it can be seen from the results that the actual contact area of paper is changing with the change of force, which is not a constant value as the nominal contact area.

Secondly, the concept of actual stress-strain curve was introduced to study the mechanical behavior of paper materials. The calculation results show the crucial differences between the actual and nominal stress-stain behaviors.

Thirdly, the concept of actual modulus was presented. The findings indicated that, with the contact area approaching to the maximum contact area, the actual modulus of paper is decreasing from about 458 MPa to about 40 MPa.

LITERATURE

[1] Endres, I., *Compression uniformity measurements on coated and uncoated paper surfaces*, in *Department of chemical engineering*. 2006, University of Karlstad: Karlstad, Sweden. p. 56.

[2] Buchner, B., M. Buchner, and B. Buchmayr, *Determination of the real contact area for numerical simulation.* Tribology International, 2009. 42(6): p. 897-901.

[3] Chen, L., et al., *Numerical and Experimental Study of the Roughness Effects on Mechanical Properties of AISI316L by Nanoindentation.* Modeling and Numerical Simulation of Material Science, 2014. 4(04): p. 153-162.

[4] Bachus, K.N., et al., *Measuring contact area, force, and pressure for bioengineering applications: using Fuji Film and TekScan systems.* Medical Engineering and Physics, 2006. 28(5): p. 483-488.

[5] Kaulitz, T. and E. Dörsam. *Highly accurate material characterization of paper for the simulation of printing process*. in *Proceeding of the 42nd International Research Conference of IARIGAI*. 2008. Valencia, Spain.

[6] Chen, J., J. Neumann, and E. Dörsam. *Investigation on deformation behavior of paper in Z-direction*. in *Proceeding of the Progress in Paper Physics Seminar*. 2014. Raleigh, North Carolina, USA

[7] MATLAB, *Documentation Center / image Processing Toolbox / Image Analysis / Region and Image Properties / Function*, in *MATLAB User's Help Manual*. 2013, MathWorks, Inc.

[8] Schaffrath, H. and L. Göttsching. *The Behavior of Paper under Compression in Z-direction*. in *Proceedings of the 1991 Tappi International Paper Physics Conference*. 1991. Hawaii, USA.

Prediction of box-failure by using paper data with enhanced McKee-formula

Heinz Joachim Schaffrath[1], Felix Reichenbach[1], Samuel Schabel[1]

AUTHOR INFORMATION


H.-J. Schaffrath

[1] Fachgebiet PMV – TU Darmstadt,
Alexanderstraße 8, D-64283 Darmstadt

Email:
schaffrath@papier.tu-darmstadt.de

SUMMARY

The well known McKee-formula was derived in 1963 for symmetric fluting constructions. This paper presents some investigations which show the influence of asymmetric properties, either geometric or concerning the elastic moduli. The theoretical considerations are verified by measuring paper parameters such as SCT, thickness and bending stiffness as well as ECT and bending stiffness of corrugated board and the BCT of the boxes.

INTRODUCTION

Since 1963, when McKee [1] published his formula to predict box-compression strength from edge-compression strength of corrugated board, the manufacturers of corrugated boxes have used this equation as a simple, practically usable and quite stable possibility to estimate the quality of their end product. The formula has been enhanced by Jonsen [2] in 1985 and Müller [3] in 2002 in order to be able to use paper data to predict box-quality. Both proposed the SCT-value to estimate the ECT-value, which can further be used to calculate the BCT-value.

However, the McKee-formula is submitted to some restrictions. Firstly, the connection of the flute to the liner is regarded to be ideal. Secondly, the ratio between box-perimeter and box-height must be higher than 7. Finally, the corrugated-board plate has to be assumed as symmetric in thickness. This last restriction needs to be eliminated as more and more boards with two different flutes are produced. Related to Germany, the amount of corrugated board with more than one flute increased from 26.0 % in 2000 to 32.7 % in 2015. In addition, the grammage of the papers used to produce corrugated boxes have decreased for a couple of years. The total mass of corrugated board declined from 531 g/m² in 2000 to 515 g/m² in 2015. [4] The single papers may only have 80 g/m² in todays manufacturing whilst a common grammage in 1963 was 120 g/m².

Therefore, it is necessary to evaluate whether the McKee formula can be used for low grammage corrugated papers too, and whether the formula can be enhanced to corrugated boards with two or three flutes.

Theory

McKee used the theory of buckling beams. The critical pressure P_{crit} causes buckling. The material can withstand the applied pressure until P_{max} is achieved. This leads to

$$\frac{P_{\max}}{P_{crit}} = c \cdot \left(\frac{P_{Mat}}{P_{crit}} \right)^{b} \qquad \text{respectively:} \qquad P_{\max} = c \cdot P_{Mat}^{b} \cdot P_{crit}^{1-b} \tag{1}$$

where P_{Mat} is a material property and will equal ECT in this case as well as P_{max} equals BCT. The perimeter of the box and the bending stiffness can be used to replace the critical load P_{crit} and leads to

$$BCT = 2{,}028 \cdot ECT^{0{,}746} \cdot \sqrt{S_{MD} \cdot S_{CD}}^{0{,}254} \cdot Z^{0{,}492} \tag{2}$$

which is known as the original McKee-formula. A second one uses ECT-values and thickness of the board instead of bending stiffness, which is less precise. The numbers of the parameters have been calculated by correlation with more than 100 boxes. [1] Although this formula is not as exact as a finite element analysis, it is often used in the industry because it is easy to handle and able to predict the BCT in a range of ± 10 %.

To enhance this formula to multilayer corrugated boards, a look back to the Euler-theory of buckling beams is necessary (figure 1). [5]

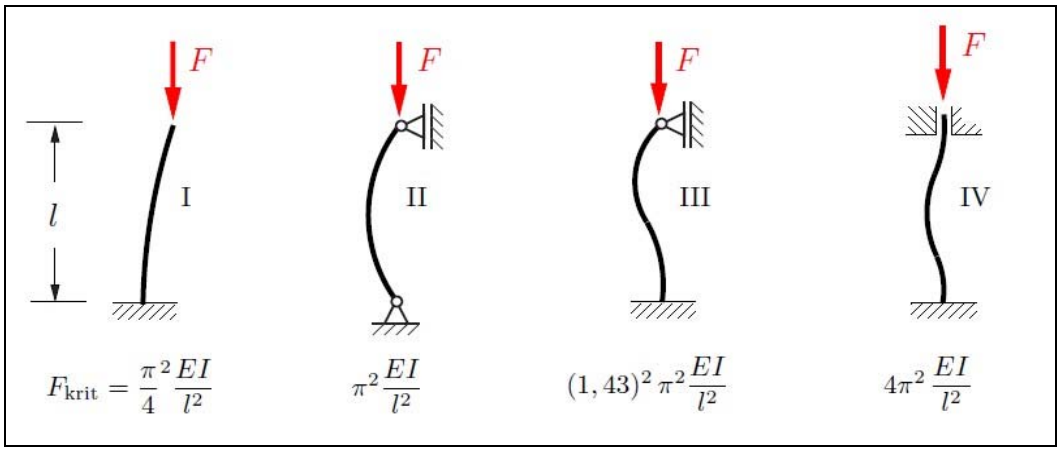

Figure 1: Four cases of buckling according to Euler [5].

In this paper, case II is assumed to be the one being closest to the situation of box failure. The geometrical moment of inertia is easy to calculate for symmetric structures. But e.g. a combination of B and C-flute or even B and E-flute will lead to a structure comparable to figure 2.

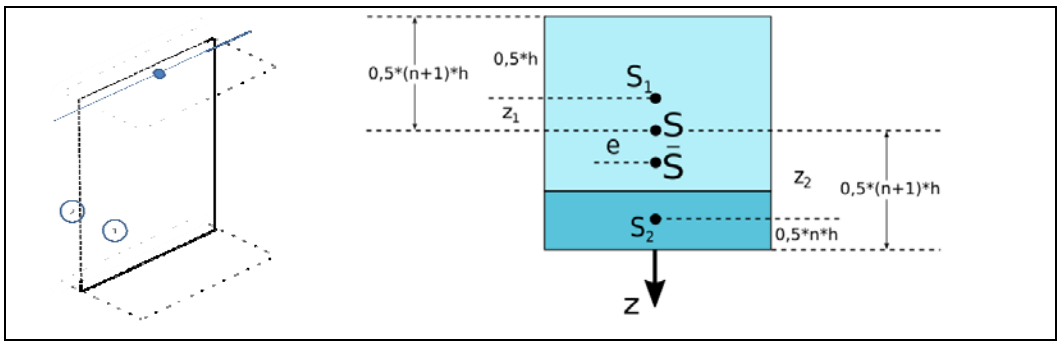

Figure 2: Unsymmetrical structures [6]

Layer 1 and layer 2 have different heights h_1 and h_2 as well as different E-moduli E_1 and E_2. The ratio of h_2 to h_1 is n. S_1 is the position of the neutral axis of layer 1, S_2 of layer 2, S the middle axis and $\bar{S}$ the neutral axis of the whole structure. With the parallel axis theorem the geometrical moment of inertia of the two layers can be calculated. Therefore, the distance between the neutral axis of each layer to the neutral axis of the whole structure has to be calculated with the help of z_1, z_2 and eccentricity e.

The values of z_1 and z_2 may be derived from geometrical conditions. The eccentricity is influenced by the elastic moduli E_1 and E_2 of the layers. Let m be the relation of E_2 to E_1, eccentricity e results to

$$e = \frac{n \cdot h_1 \cdot (m-1)}{2 \cdot (n \cdot m + 1)} \tag{3}$$

Using this together with the parallel axis theorem leads to

$$\overline{E \cdot I} = E_1 \cdot \left\{ \frac{b h_1^3}{12} + b h_1 \cdot \left[\frac{1}{2} n h_1 + e \right]^2 + m \cdot \left(\frac{b h_1^3}{12} n^3 + n b h_1 \cdot \left[\frac{1}{2} h_1 - e \right]^2 \right) \right\} \qquad (4)$$

as the bending stiffness of the whole structure. The width of the corrugated plate is b. These steps may be carried out for more than two layers as well and will lead to bigger formulas. With two different liners and one fluting medium, already three layers are given. [6]

The next step is to calculate a substitutional E-modulus for the flute. Sinus shapes cannot be analytically calculated; therefore the sinus is approximated by a triangular shape (figure 3):

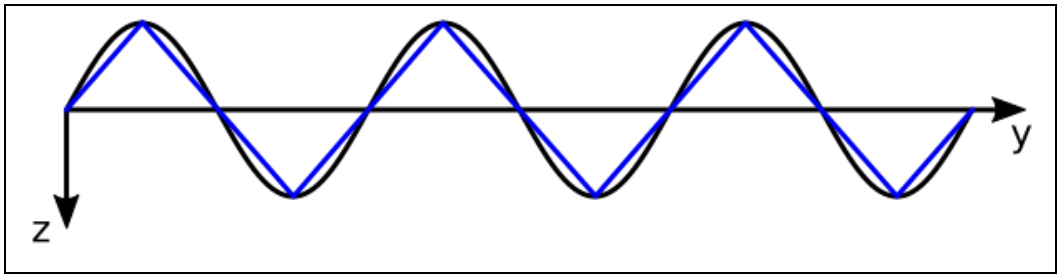

Figure 3: Approximation of a sinus-shape flute by triangles

Assuming that the width of a corrugated board is much larger than the pitch of the flute, the triangles may be displaced in a manner shown in figure 4. This will still lead to the same bending stiffness across the y-axis as the structure in figure 3:

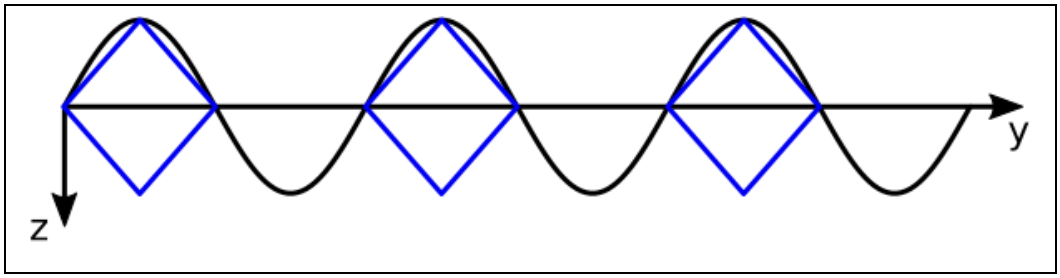

Figure 4: Displacing the triangles

Now the bending stiffness of the flute-layer is easy to calculate knowing the E-modulus of the fluting paper and the geometry. This bending stiffness can be used to calculate a substitutional E-modulus. Therefore, the flute-layer is theoretically substituted by a homogeneous layer with the thickness and the width of the flute-layer (which may be measured; the moment of inertia can then be calculated). As the theoretical homogeneous layer shall have the

same bending stiffness as the real layer, the substitutional E-modulus can now be calculated as well. [6]

With these instruments the stiffness of each liner/flute-construction, one flute as well as several flutes, with different paper properties (E-modulus, thickness) can be calculated.

EXPERIMENTS

Instead of the E-moduli the SCT-values of different papers were measured and used to calculate the ECT-value of the corresponding corrugated board. With the same SCT-values in MD and CD the bending stiffness of the papers were calculated and used to derive the bending stiffness of the board. From this board, boxes were manufactured and the BCT-value was measured and calculated according to the McKee-formula (2) and according to the theory demonstrated in the previous chapter (table 1). Surprisingly the 2-flute boards fit better than the 1-flute boards. The McKee-formula was least applicable to the C-flutes (box I: Z/h >7; box II: Z/h < 7). This may be regarded as an outlier as it is well known that the McKee-formula fits well to single layer, symmetric boards.

Table 1: Comparison of measured BCT to calculated BCT [6]

Board	BC-flute	EB-flute	C-flute I	C-flute II	B-flute
BCT measured	5.47 kN	2.69 kN	1.08 kN	1.85 kN	1.28 kN
BCT calc. ECT	5.22	2.49	1.44	1.44	1.14
BCT calc. paper	5.34	2.73	1.44	1.44	1.51

CONCLUSIONS

Both theory and the experiments lead to the result that unsymmetrical board structure, caused by the papers used or due to 2-flute structure, does not influence the mechanics as much that the McKee-formula becomes invalid. Prediction is still expected in the range of ± 10 %. However, much more data has to be generated to come to a final evaluation.

The thicknesses of the used papers and even more the thicknesses of the different flute-layers are the main influencing parameters of the total stiffness and the final box strength. Hence, the McKee-formula is robust enough to be

applied when using low-grammage papers as well as for multilayer board constructions.

REFERENCES

[1] McKee, R. C.; Gander, J. W.; Wachuta, J.: Compression strength formula for corrugated boxes. -
In: Paperboard Packaging. 38(1963)8. S. 149-159

[2] Jonson, G.; Ponton, S.: Utilizing liner/medium weight in corrugated board for best box performance. -
In: Boxboard Containers. 93(1985)11. S. 23-25

[3] Müller, G.: Die erweiterte McKee-Formel. -
In: Papier + Folien. 37(2002)5. S. 22-28

[4] N.N.: Zahlen und Fakten – Daten für die Wellpappenindustrie. Ausgabe 2016 – Verband der Wellpappen-Industrie e.V., Darmstadt

[5] Gross, D.; Hauger, W.; Schröder, J.; Wall, W.: Technische Mechanik 2. Heidelberg: Springer-Verlag, 2012. ISBN 978-3-642-19983-7

[6] Reichenbach, F.: Erweiterung der Formel nach McKee zur Vorhersage des Stapelstauchdrucks von Wellkisten aus Rohpapiereigenschaften und Überprüfung der theoretischen Ergebnisse an Wellpappen und Wellkisten. Darmstadt: Bachelor-Thesis, Technische Universität Darmstadt, 2016

Biaxial (In-Plane) Failure and Yield of Paperboard

Linvill, Eric[1] and Östlund, Sören[1]

AUTHOR INFORMATION


E. Linvill


S. Östlund

[1] KTH
Royal Institute of Technology,
Stockholm, Sweden

Email:
linvill@kth.se

Summary

Understanding the biaxial (in-plane) failure behavior of paperboard is crucial to understand the limits of 3-D forming of paper materials, because the biaxial strain failure limit determines the extent to which paperboard can be formed in different conditions.

A traditional cruciform biaxial specimen has been redesigned and modified with the help of laser engraving. By the use of laser engraving, 90 % of the effective thickness of the specimen in the center of the cruciform was removed, thus making the cruciform specimen more likely to fail in the center than at the edges. A variety of strain ratios were utilized to test the specimens with a biaxial testing machine, and the strain field was measured utilizing digital image correlation.

The results of the biaxial testing were analyzed in order to determine both the strain-based yield and failure surfaces. Additionally, the stresses in the center of the specimen were estimated based on the forces measured during the test. Based on these estimated stresses, stress-based yield and failure surfaces were also constructed. Furthermore, various models for the strain- and stress-based yield surfaces were applied to the data and compared.

Introduction

Paper and paperboard materials are oftentimes subjected to in-plane, biaxial loads. Examples of such instances include the loading and drying of the paper web in a paper machine, the stacking of paperboard boxes [1], and three-dimensional forming of paperboard (such as hydroforming [2] and deep-drawing [3]).

The traditional biaxial test (i.e. using a cruciform specimen) is inherently challenging, which is the reason why previous descriptions of stress-based [4-5] and strain-based [6] failure surfaces for paper materials have utilized either cylinders or bulge tests in combination with some traditional biaxial tests using cruciform specimens. Both the traditional bulge and biaxial tests are inherently difficult, because failure does not typically initiate in the desired, analyzed region (i.e. in the center of the specimen).

Experimental Method

Laser engraving has been utilized to reduce the effective thickness of the specimen by 90 %, which increases the probability that failure will occur in the center of the specimen. Similar methods (using milling techniques) have also been utilized for other materials, such as metals and polymers [7]. The specimen utilized in this study is shown in *Figure 1*.

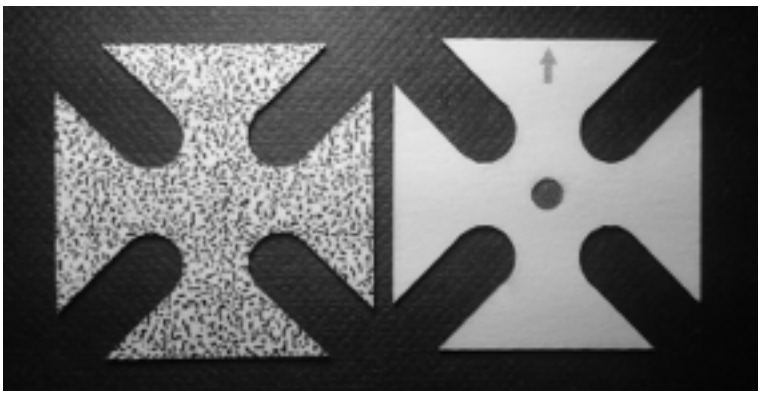

Figure 1: Speckle side (left) and engraved side (right) of the biaxial specimen.

The arrow in *Figure 1* was engraved into the specimen to keep track of the CD direction; this engraved arrow was under the clamps and therefore did not affect the results. The engraved circular region in *Figure 1* was where failure was meant to initiate. Out of the 214 tests conducted, 77 failed in that desired region. Only these 77 results were utilized in the following analysis.

In addition to capturing the stress- and strain-based failure surfaces, the stress- and strain-based yield surfaces were also obtained. The yield point

for paper materials can be difficult to define, so three separate definitions of the yield point were utilized: the 0.2 % method utilized often used for metals, the intersection of a bilinear fit, and the point with the minimum radius of curvature.

Results

The stress-based failure surface was found to be similar to the data previously published for paperboard [4] and envelope and sack paper [5], which provides further confidence in the results obtained with this method.

The definition of the yield point had little impact on the shape of the strain- and stress-based yield surfaces. Additionally, the strain- and stress-based yield surfaces had similar shapes to their corresponding failure surfaces. With the hypothesis that the deformation and failure mechanisms are related in paper materials, the similarity of the yield and failure surfaces seems to provide additional confidence in the results.

The overall shape of the obtained strain-based failure surface is shown in *Figure 2*, with certain points illustrating the areas of interest for various 3-D forming and tensile test operations:

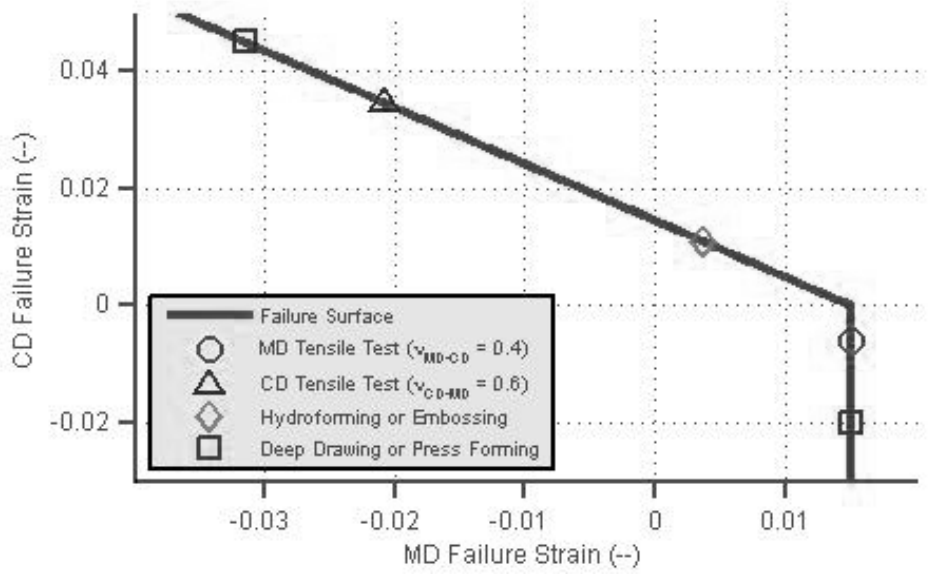

Figure 2: Strain-based failure surface with various points of interest.

In addition to the representation of the failure surface by the solid line in *Figure 2*, various points represent different strain ratios that may occur during various tests or 3-D forming operations. For example, the circle and triangle represent the failure strains for tensile tests in MD and CD, respectively. The diamond represents a strain combination that would be typical for hydroforming or

embossing: a biaxial tensile strain state. On the other hand, the two squares represent typical failure points for press forming of pre-creased specimens or deep drawing, during which large compressive strains in one of the in-plane material directions would cause wrinkling or compression of creases to occur. The greatest implication of the strain-based failure surface obtained in this study is the limited extent to which paper materials can be formed in biaxial tension; the strain-at-break in biaxial tension appears to be significantly less than that of the strain-at-break achieved through tensile tests.

The strain-based failure surface in *Figure 2* differs from the one obtained by Groche and Huttel [6], who utilized a different material at a high moisture content (15 %). The paperboard utilized in this study is significantly drier (around 6 % moisture content), so whether the difference in results is due to material, moisture, or method is difficult to determine.

Conclusion

The proposed method seemed to replicate previous results for stress-based failure surfaces, and the yield surfaces were found to have similar shape to the failure surfaces. Both of these points seem to provide additional confidence in the results.

The obtained strain-based failure surface was found to be different than the one previously published strain-based failure surface, although the previously published strain-based failure surface was obtained with different material, moisture, and methods. The obtained failure surface was found to show a limitation for the 3-D forming procedures with biaxial tensile strain, such as embossing and hydroforming.

Literature

[1] Johnson Jr. MW, Urbanik TJ (1987) *Buckling of Axially Loaded, Long Rectangular Paperboard Plates*, Wood and Fiber Science, 19(2): 135-146.

[2] Linvill E, Östlund S (2016) *Parametric Study of Hydroforming of Paper Materials Using the Explicit Finite Element Method with a Moisture-dependent and Temperature-dependent Constitutive Model*, Packaging Technology and Science, 29(3):145-160.

[3] Wallmeier M, Linvill E, Hauptmann M, Majschak JP, Östlund S (2015) *Explicit FEM Analysis of the Deep Drawing of Paperboard*, Mechanics of Materials, 89:202-215.

[4] Rowlands RE, Gunderson DE, Suhling JC, Johnson MW (1985) *Biaxial Strength of Paperboard Predicted by Hill-Type Theories*, Journal of Strain Analysis, 20(2):121-127.
[5] de Ruvo A, Carlsson L, Fellers C (1980) *The Biaxial Strength of Paper*, Tappi, 63(5):133-136.
[6] Groche P, Huttel D (2016) *Paperboard Forming – Specifics Compared to Sheet Metal Forming*, BioResources, 11(1): 1855-1867.
[7] Lamkanfi E, Paepegem WV, Degrieck J, Ramault C, Makris A, Hemelrijck CV (2010) *Strain Distribution in Cruciform Specimens Subjected to Biaxial Loading Conditions. Part 2: Influence of Geometrical Discontinuities*, Polymer Testing, 29(1):132-138.

Predicting the long-term mechanical behavior of corrugated cardboard packaging based on speed rate controlled short term tests

Hiller, Benjamin[1]; Köstner, Viktoria[2]; Dr.-Ing. Kuntzsch, Timo[1] and Prof. Dr.-Ing. Sadlowsky, Bernd[2]

AUTHOR INFORMATION

B. Hiller

[1] Papiertechnische Stiftung in Heidenau
[2] Institut für BFSV at Hamburg University of Applied Sciences

Email:
Benjamin.Hiller@ptspaper.de

Summary

The evaluation of long-term structural behavior of corrugated cardboard packaging is currently carried out on time and cost-intensive tests on the packaging. There are calculations that offer the possibility of a simple assessment of the structural behavior. These calculations are usually modeled on single material parameters and do not describe the complex behavior of the material sufficiently. The continuum mechanics offer the possibility to define the long-term structural behavior of corrugated cardboard by speed differentiated short-term tests. For this purpose a material model is developed which is defined by simple tests and can predict the behavior of the material. This task is performed by the frequency-dependent generalized Maxwell model with its idea of several parallel connected spring-damper-elements (Maxwell-elements). The frequency dependence can be converted on the time domain by use of the Prony analysis. This type of calculation is first compared with long-term studies on the material, to evaluate its accuracy. Furthermore, the influence of moisture is investigated and defined through specified studies in normal, humid and alternating climate. The developed method is incorporated into computerized simulations and offers the opportunity to describe the behavior of a corrugated cardboard shipping container by means

of simple and defined tests on material samples. So the interpretation of corrugated cardboard packaging is more specific to the material and there are ways generated to save material and to reduce the number of cases of failure in the delivery.

Introduction

During the last 10 years a constant development is recognized on the market for corrugated cardboard. The sales figures are on a high and mostly growing level and the number of employees is steadily increasing. This positive trend leads many companies to the idea that the production and trade of containerboard and corrugated cardboard is commercially more reasonable as for other types of paper. The first paper mills already established their production lines to containerboard. This development will probably continue in the next years. The increasing interest in packaging and other elements made of corrugated cardboard (e.g. purchase displays or decorations) goes hand in hand with the question of a precise interpretation of the material. The challenge for manufacturers and users of corrugated cardboard is particularly the structural behavior over a long period and under changing climatic conditions. Qualitative statements about the long-term structural behavior of corrugated containers are currently given only by time consuming and costly long-term studies. Due to these conditions, these tests are only used in rare cases. The design of the packaging is therefore usually based on simple calculations, such as the McKee-formula. These include only quasi-statically determined material parameters, general geometric relationships and are coupled with the assumption of many conditions (e.g. the ratio of height must agree to scope). In order to ensure a certain degree of security for the package, the results are subjected to general safety factors. Detailed considerations of climate- and long-term loads do not take place. Corrugated cardboard is a hygroscopic material and loses almost half of its strength with an increase in humidity from 50% to 90%. The following, inaccurate interpretation of corrugated packaging in the current sense will lead either to oversizing (waste material) or a failure (damage) by climatic or long time stress. An optimized use of the material does not take place in most corrugated containers. Investigations at BFSV Hamburg also revealed a limited correlation between research on materials and the packaging in short and long time stress. Packaging with similar BCT[1] values reveal significant

[1] box compression test

different behavior in long-term exposure [1]. Also, a direct link between long-term-ECT[2] and long-term-BCT has not yet been given [2]. The variety of issues associated with the long-term structural behavior of corrugated cardboard under climatic influences gave the idea for the IGF project 18876 BG "long-term structural behavior of packaging" in cooperation of Papiertechnische Stiftung in Heidenau with the Institut für BFSV at Hamburg University of Applied Sciences.

Objectives, definitions and measurements

The aim of the project is to develop a continuum mechanics justified method for calculating the climate-dependent creep behavior of corrugated containers by means of short-term tests, performed with different loading rates. The method sets the focus of research on the material-specific behavior of corrugated cardboard with respect to long-term and climate stress. Therefore it is possible to perform an application-oriented design of the packaging and dispense as far as possible on time and cost-intensive long-term tests on the packaging. In this way, a link between tests on the material and the behavior of the packaging is prepared.

For method development two-wave corrugated cardboards in wet strength and not wet strength design are used. The FEFCO 0201 is used as sample packaging with external dimensions of 1.200 x 800 mm, which corresponds to the basic dimensions of a euro pallet. Principal strains for a packaging made of corrugated cardboard in the long time shipping trade are the following forces:

- Pressure in the planes of the side walls caused by the stacking of the packaging during shipment and
- Bending perpendicular to the planes, caused by minimal deformations in the side walls.

The universal material testing, as the ECT (according to DIN EN ISO 3037:2013-12) or the measurement of the bending stiffness (according to DIN 53121:2014-8), are performed for these two major stresses. Some predetermined parameters of the standards need to be changed for the subsequent calculations, emphasizing especially the predetermined standard of loading rates. The experiments show for compression and bending the

[2] edge crush test

expected dependence of increase (E-modulus) and maximum value (strength) of the curves (Figure 1).

Figure 1: Speed rate dependent stress-strain-characteristics of corrugated cardboard from edge crush test measurements

Material model, calculations and comparison with long-term studies

The viscoelastic generalized Maxwell model is used as the material model for the development of this method. Without going into detail, the Maxwell model can describe the material behavior at different loading rates quite accurately. For this, the recorded speed dependent curves should be interpreted in the linear elastic regions only. By means of the evaluation it is possible to describe the required material-specific parameters (spring and damper constants) for the generalized Maxwell model. The relationship of stiffness and damping (referred as attenuation spectrum) also confirmed the assumption of an increasing stiffness (and strength) of the material at elevated loading rate (Figure 2).

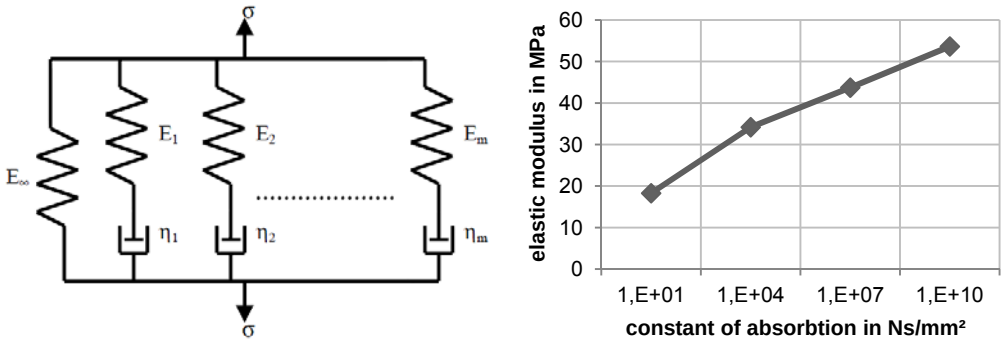

Figure 2: Scheme of a multiple Maxwell model to describe the viscoelastic material behaviour (left) [3] and a Spectrum of spring (E_i) and damper (η_i) constants for corrugated cardboard from the experiments (right)

At that point, the generalized Maxwell model gives only a frequency-dependent response to a defined loading rate. The analysis by Prony transfers this frequency-dependent behavior of the material samples in a time-dependent consideration of the modulus of elasticity (Formula 1, $\tau_i = \frac{\eta_i}{E_i}$, [3]).

$$E(t) = E_0 - \sum_{i=1}^{m} E_i \left(1 - e^{-\frac{t}{\tau_i}}\right) \qquad \textbf{(1)}$$

Using the resulting time-dependent modulus of elasticity, it is possible to predict the development of the creep behavior of a material sample by a correlation with a defined initial load. The results of the calculations are

compared with long-term studies on the material, to assess the effect of the previously non-considered viscoplastic behavior (example in Figure 3). In a first step 15, 25 and 33% of the measured maximum value for ECT and bending strength at standard atmosphere are used.

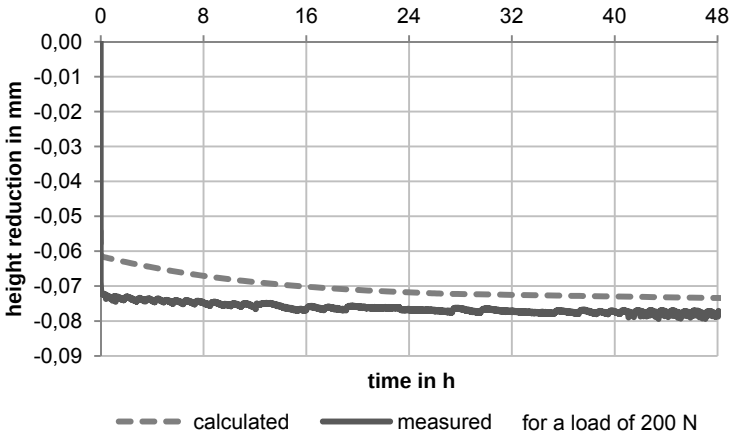

Figure 3: Calculated and measured height reduction of a corrugated cardboard sample during a long term edge crush test

Investigations under defined and varying climatic conditions determine the influence of humidity change. This influence is incorporated as a "moisture-Shift" in the calculation. The humid climate of the studies was determined with 23°C ambient temperature and 90% relative humidity. In this way, maximum equilibrium moisture is generated in the paper.

Outlook

Finally, the findings are transmitted to a computer-aided calculation model under the FEM[3]. The impact of packaging geometry should be detected and defined in its ratio by means of parameterized models. The results of the FEM calculations are verified afterwards by short- and long-term tests on the packaging itself.

The main task of the project is to develop the overall relationship between the results of the short-term studies on the material and the long-term studies on the packaging. For this purpose, an appropriate set of rules will be established, which allows providing the method towards a wider public, and so generating an improved interpretation of corrugated cardboard packaging.

[3] finite elements method

Literature

[1] Institut für BFSV an der HAW Hamburg, Wolfgang Reimers, 2009. *Entwicklung eines Qualitäts-Standards für Schwerwellpappe unter Berücksichtigung mechanisch/klimatischer Belastungen in internationalen Logistikketten* [AiF-Forschungsvorhaben Nr. 14836 N]. Hamburg

[2] Institut für BFSV an der HAW Hamburg, 2014. *Erarbeiten von Prüfnormen für das Kriechverhalten von Schwerwellpappe zur Ermittlung der Leistungsfähigkeit von darauf gefertigten Schachteln* [DLR-Forschungsvorhaben Nr. 01FS10018]. Hamburg

[3] KARA, Harun, 2005. *Untersuchung des viskoelastisch exzentrischen Knickens von Polymeren* [Dissertation]. München: Technische Universität

Linking paper structure to tensile deformation and fracture initiation

Jussi Lahti[1,2], Michael Dauer[1,2] and Ulrich Hirn[1,]

AUTHOR INFORMATION


J. Lahti


U. Hirn

[1]Institute of Paper, Pulp and Fiber Technology, Graz University of Technology, NAWI Graz, Inffeldgasse 23, 8010 Graz, Austria

[2]CD Laboratory for Fiber Swelling and Paper Performance, Graz University of Technology, Inffeldgasse 23, 8010 Graz, Austria

Email: jussi.lahti@tugraz.at

Summary

Meso-scale variations in structural properties largely define the tensile deformation distribution within paper. In order to study this relationship comprehensively, a procedure for correlating various structural properties, e.g. basis weight, fiber orientation and density, to tensile deformation (strain and damage) behavior in a meso-scale was implemented. The procedure was demonstrated by linking tensile deformation distribution, i.e. strain and temperature increase (damage) maps, to basis weight distribution. It was seen that the fracture initiated at the region with low basis weight surrounded by high basis weight regions in the stretching direction. However, the basis weight distribution only partly explains the distribution of deformation. Thus, other meso-scale structural properties will be also included to the procedure.

Introduction

In-plane tensile properties of paper are of utmost importance in various coating, converting, printing and packaging applications. These properties are by large extent defined by meso-scale structural non-uniformities. Meso-scale variations in structural properties, such as basis weight, fiber orientation and density, greatly influence on the tensile deformation distribution within paper, and thus determine the mechanical behavior of paper also on larger scales [1-7]. The aim of this study is to determine how the meso-scale variations in

different structural properties affect on the tensile deformation distribution within paper.

Experimental

The procedure for pursuing the aim of this study is described in Figure 1. Due to the fact that structural analysis includes also destructive methods, the procedure is started with deformation maps, i.e. strain and damage (temperature increase) maps. These maps are recorded simultaneously during tensile testing (Zwick/Roell Z010), as shown in Figure 2, which is stopped during/just prior to rupture. The damage map is measured with an infrared (IR) camera (Optris PI 450) by recording the increase in local temperature due to e.g. breaking of the interfiber bonds [7]. The strain map is in turn determined with a digital single-lens reflex (SLR) camera (Nikon D5100) combined with a macro lens (Nikon ED AF Micro Nikkor 200mm 1:4 D) and subsequent digital image correlation (DIC) analysis [8]. In order to increase the accuracy of the DIC analysis, the paper strip includes a laser printed random speckle pattern. Furthermore, the region of interest is identically marked on both sides of the paper strip with four dots (landmarks) before deformation measurements.

After the measurement of deformation maps, structure maps are determined. In this paper the focus is put on the basis weight map measured with a β-radiography (Formex Betaformation Box & Fujifilm BAS 1800-II scanner). The ROI marked with the silver dots is also visible in this map. Other structure maps which can be included to the procedure are e.g. thickness map measured with a twin laser profilometer [9], density map calculated with the aid of basis weight and thickness maps and layered fiber orientation map with a sheet splitting method [10].

The measurement of structure maps is followed by an alignment of the ROI's (see Figure 2) within the measured strips. This is performed through landmark based registration by utilizing the landmark dots [11]. The aligned maps can be then qualitatively as well as quantitatively correlated in the meso-scale. In this paper the focus is put on the qualitative analysis.

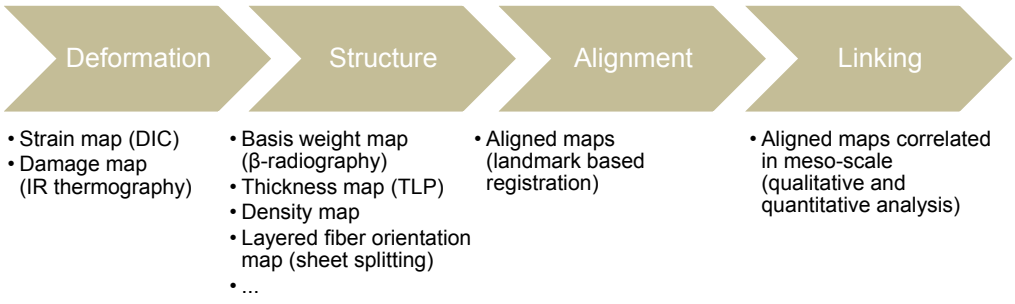

Figure 4. Procedure for linking paper structure to tensile deformation.

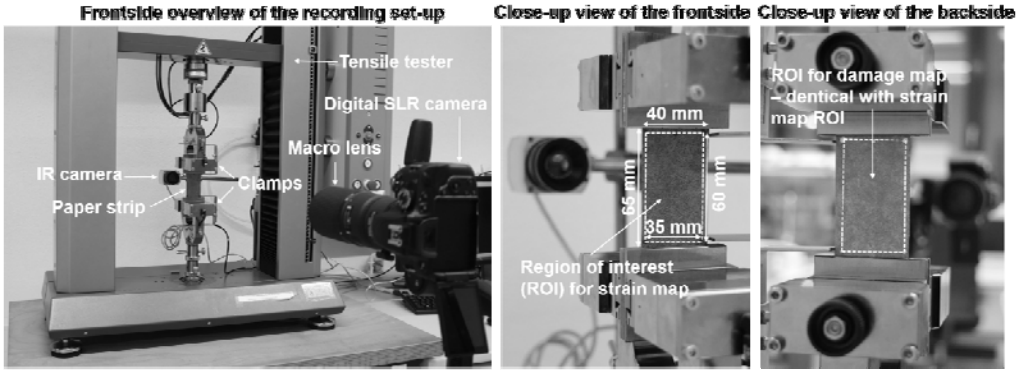

Figure 5. Set-up for recording both strain and damage (temperature increase) maps simultaneously during tensile testing.

Results and discussion

Figure 3 shows an example of the results gained with the above-described procedure. Here, a 70 g/m^2 packaging paper was analyzed. The deformation speed was 40 mm/min and the dimensions of the paper strip as shown in Figure 2. The tensile test was stopped in the middle of fracture propagation. The propagating approx. 5 mm long fracture line is marked with white circles to the deformation maps. It can be seen that the basis weight is low in this region of fracture initiation. On the other hand, the neighboring regions in the stretching direction (marked with white circles) deform insignificantly due to the high basis weights, i.e. these regions focus the deformation on the region with low basis weight.

Strain and temperature maps seem to represent the distribution of deformation similarly. The low basis weight regions seem to also correlate at some extent with the highly deformed regions. However, other meso-scale structural properties (see Figure 1) certainly influence the distribution of deformation as well, and thus will be included to the procedure.

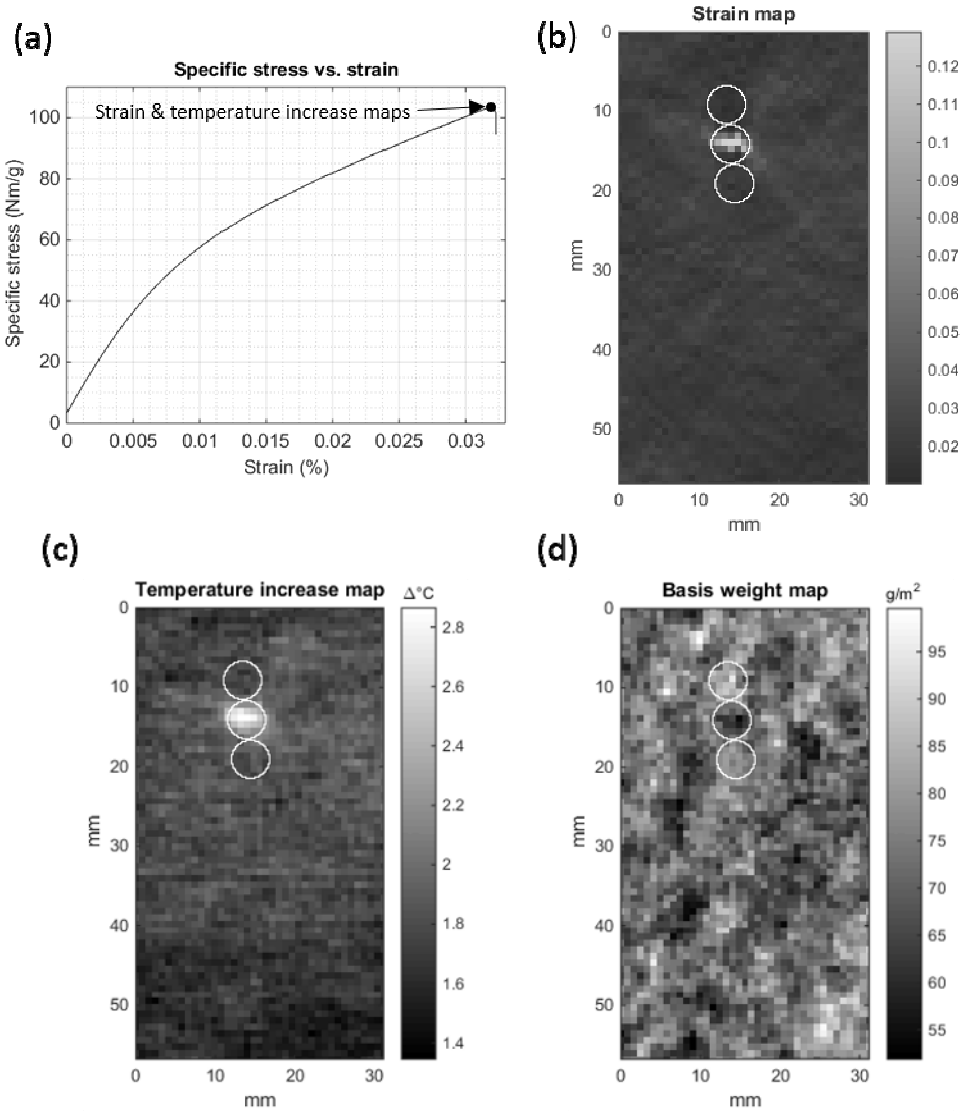

Figure 6. (a) Specific stress vs. Strain curve for a 70 g/m^2 packaging paper strip. The tensile test was stopped in the middle of the fracture propagation – fracture line length approx. 5 mm. (b & c) Strain and temperature increase (damage) maps at the moment of stoppage (maps slightly smaller than ROI in Figure 2). The Propagating fracture line and the surrounding considerably less deformed regions are marked with white circles. (d) Basis weight map measured after the deformation maps. Basis weights of the regions with large and small deformations are marked with white circles.

Conclusions

A procedure for correlating various structural properties to deformation behavior in a meso-scale was implemented. The procedure was demonstrated by linking tensile deformation distribution, i.e. strain and temperature increase (damage) maps, to basis weight distribution. It was seen that the fracture initiated at the region with low basis weight surrounded by high basis weight

regions in the stretching direction. However, the basis weight distribution only partly explains the distribution of deformation. Thus, other meso-scale structural properties will be also included to the procedure.

Literature

[1] B. Norman & D. Wahren. Mass distribution and sheet properties of paper. In Proceedings of 5th Fundamental Research Symposium (Editor F. Bolam). Technical Section of the British Paper and Board Industry Federation, London, UK. 269-298 (1966).

[2] D.P. Dumbleton, K.P. Kringstad & C. Soremark. Temperature profiles in paper during straining. Svensk Papperstidning. 76(14):521-528 (1973).

[3] M.J. Korteoja, A. Lukkarinen, K. Kaski, D.E. Gunderson, J.L. Dahlke & K.J. Niskanen. Local strain fields in paper. Tappi J. 79(4):217-224 (1996).

[4] M.J. Korteoja, K.J. Niskanen, M.T. Kortschot & K.K. Kaski. Progressive damage in paper. Paperi ja Puu. 80(5):364-372 (1998).

[5] M. Alava & K. Niskanen. In-plane tensile properties. Vol. 16 (2nd Edition) of Papermaking Science and Technology (Paperi ja Puu). Chapter 5, 181-228 (2008).

[6] C. Hyll, H. Vomhoff & M. Nygårds. Analysis of the plastic and elastic energy during the deformation and rupture of a paper sample using thermography. Nord. Pulp Paper Res. J. 27(2):329-334 (2012).

[7] T. Yamauchi. Application of IR thermography for studying deformation and fracture of paper. Infrared Thermography (InTech). Chapter 1, 3-26 (2012).

[8] C. Eberl, R. Thompson, D. Gianola, W. Sharpe Jr & K. Hemker. Digital image correlation and tracking. MatLabCentral, Mathworks file exchange server, FileID 12413 (2006).

[9] D.S. Keller, D.L. Branca & O. Kwon. Characterization of nonwoven structures by spatial partitioning of local thickness and mass density. J. Mater. Sci. 47(1):208-226 (2012).

[10] U. Hirn & W. Bauer. Evaluating an improved method to determine layered fiber orientation by sheet splitting. Proceedings of the 61st annual APPITA conference & 2007 paper physics conference. 71-80 (2007).

[11] U. Hirn, M. Lechthaler & W. Bauer. Registration and point wise correlation of local paper properties. Nord. Pulp Paper Res. J. 23(4):374-381 (2008).

Session III

“Pulp & Paper Processing”

Fines separation and thickening in the lab scale by means of screening and microbubble flotation

L.A. Jagiello[1,2], W.J. Fischer[1,2], R. Eckhart[1,2], W. Bauer[1,2]

[1]Institute of Paper, Pulp and Fiber Technology / Graz University of Technology, Inffeldgasse 23, 8010 Graz, Austria

[2]Flippr°- Future Lignin and Pulp Processing Research / Graz University of Technology, Inffeldgasse 23, 8010 Graz, Austria

Email: lukas.jagiello@tugraz.at

Introduction

Fractionation of pulp fibres is a common method used in the pulp and paper industry. This method often deals with the fine fibre fraction of chemical and mechanical pulps. In general, fines are defined as the fibre fraction which is able to pass through a screen having a hole diameter of 76 µm (200 mesh screen Bauer McNett fractionator) [1]. [2]. These particles are usually smaller than 100 µm.

Mechanical pulps contain 20 to 35 wt% of fines . These fines lead to a high opacity and reasonable strenght of the paper [3]. In 1953, Brecht et.al. [4] introduced the terms “Schleimstoff” and “Mehlstoff”. The first one refers to fibrillar material having a high bonding ability and the second one to chunky particles having a high lignin content and low bondability. Chemical pulps have less fines compared to mechanical pulps; the fines content ranges from a few percent to 10-12%, depending on the refining level [5]. Chemical pulp fines can also be divided into primary fines and secodary fines. Primary fines are already present after the cooking process, whereas secondary fines are generated during the refining process.

Conventional laboratory fractionation devices for fibre-fines fractionation are the Bauer Mc-Nett fractionator and the Britt Dynamic Drainage Jar (BDDJ) tester. The main drawback when using these devices is the small amount of pulp that can be treated in a single step (10 g BMcN, 5 g BDDJ) i.e. only small amounts of fines can be produced. In case of the Bauer Mc-Nett device, more than 240 l of water are needed for one separation run. Depending on the pulp type there are only few grams of fines diluted in huge amounts of water. To

allow further processing, thickening of such a highly diluted suspension is needed. Recently more and more research projects focus on areas of potential applications for fines. Therefore the need for new technologies for fines separation as well as fines thickening in a laboratory and industrial scale is of utmost importance in the current research field.

The present study should give insight in novel separation and fines thickening technologies. Here, two different process technologies have been applied to fulfil the technical and technological requirements. A pressure screen was implemented to separate the fines fraction from the fibre fraction. In order to thicken the obtained fines fraction, a dissolved air flotation (DAF) cell was designed at the Institute of Paper, Pulp and Fibre Technology at Graz University of Technology.

Materials and Methods

All tests were performed using unbleached mechanical pulp (spruce) as well as unbleached and bleached kraft pulp (mixture of spruce and pine) and the most important parameters influencing the separation and thickening process of fines were examined.The fibre and fines fractions obtained with the pressure screen and the flotation cell were analyzed with the L&W Fibre Tester Plus device.

Setup for separation of fines

Figure 1 shows the laboratory pressure screen which was implemented at the Institute of Paper, Pulp and Fibre Technology at Graz University of Technology in collaboration with the Institute of Paper Technology and Mechanical Process Engineering at the Technical University in Darmstadt.

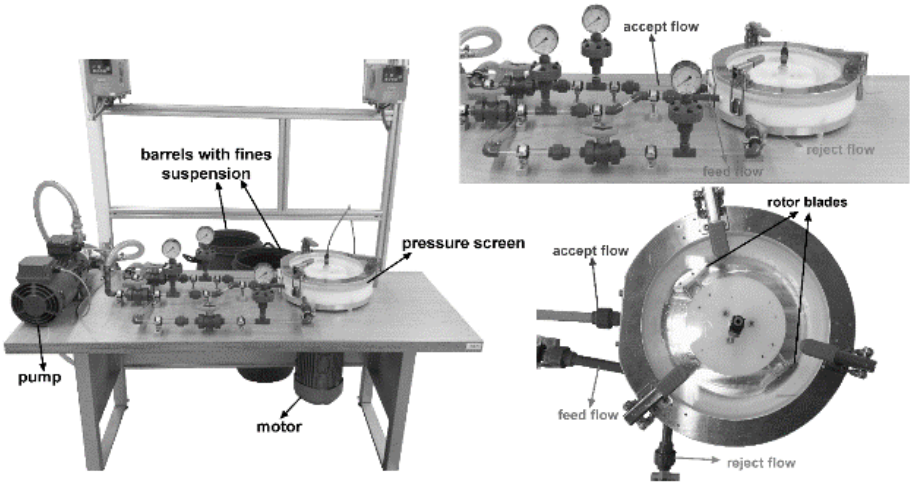

Figure 7. General view pressure screen

The pulp suspension is pumped from a feed tank to the pressure screen through the inlet. A rotor inside the chamber accelerates the pulp to a high tangential velocity. Furthermore, the rotor also introduces turbulence, which mixes the suspension and keeps the pulp fluidized. Positive pressure pulses are generated at the leading edge of the airfoil shaped rotor blades which push the fines through a perforated strainer (hole diameter 100 µm). Negative pressure pulses at the rear side of the foils remove fibres from the strainer to prevent plugging. The fines suspension (accept flow) is collected in a separate container and the remaining pulp is transferred back to the feed tank through the outlet port (reject flow). Several washing cycles are carried out in order to remove the fines from the pulp.

After separation the fines were analyzed and these measurements were compared with those of fines produced with the BDDJ ([2]). The L&W measurements showed that there is no difference between the fines produced with either the pressure screen or the Britt Jar Tester (BDDJ).

Depending on the type of pulp as well as on the feed consistency, the solid content of the fines suspensions produced with the pressure screen is below 0.1%. Due to the high water content further treatments such as chemical modification or forming of handsheets are more difficult to perform. To overcome this limitation, a method for thickening of fines suspensions is needed.

Thickening of the fines fraction

Figure 2 shows an image of the dissolved air flotation cell. The fines suspension is pumped from a feed tank to the flotation cell (1). A needle in the suction tube (2) of the jet pump injects a defined amount of air. High shear forces introduced by the impeller of the jet pump lead to collapse of the air bubbles and finally to dissolution. The amount of air can be adjusted by a control valve (3). Due to a pressure drop controlled by a pressure relief valve (4), the disolved air is released in the form of fine bubbles. The bubbles and the fines flow into the flotation tank. Different flow zones inside the flotation cell are needed for good separation efficiency. A stable froth layer is formed on the surface which contains the fines particles. This froth is removed by a hand-operated scraper.

Figure 8. Laboratory DAF cell.

One important aspect of this method is that it is operated without the use of any chemicals (e.g. flocculation agents, oils etc.) to avoid contamination of the material. Only water and small air bubbles are used for the thickening of fines.

Determination of the bubble size distribution

To learn more about the separation principle using disolved air flotation, the size distribution of the air bubbles was determined using a custom built measuring cell. A transparent box is connected with a jet pump and a pressure relief valve. The main liquid flow enters the measuring cell at the bottom and exists at the top. Again, air is injected into the jet pump with a needle and gets dissolved due to the overpressure of the pump. Small air bubbles are generated according to the principle disccused in the previous section. The bubbles are detected by a single reflex camera (Nikon D5100, Nikon AF micro nikkor 200mm 1:4 D). Trials at different pressure conditions (2.2 and 3.5 bar) were carried out to cover both the maximum and minimum pressure. Furthermore, comparative L&W measurements using polyamide particles were performed to verify the optical measuremnt procedure.

Results and Discussion

Pressure screening

In Figure 3, a comparison between an original unbleached kraft pulp sample and the corresponding fines fraction is shown. From this figure it is evident

that the laboratory pressure screen has a high separation efficency. The majority of the produced fines fraction (> 80%) consists of particles which are smaller than 100 μm.

Trials using different amounts of pulp showed that depending on the original fines content of a pulp (5 - 40% mass content [6]) quantities of several 100 g of fines (oven dry mass) can be produced within 1-2 hours on the laboratory pressure screen. The solid contents of the produced suspensions range from 0.01 to 0.1%. This indicates that for further processing such as chemcial modification an additional thickening step is needed.

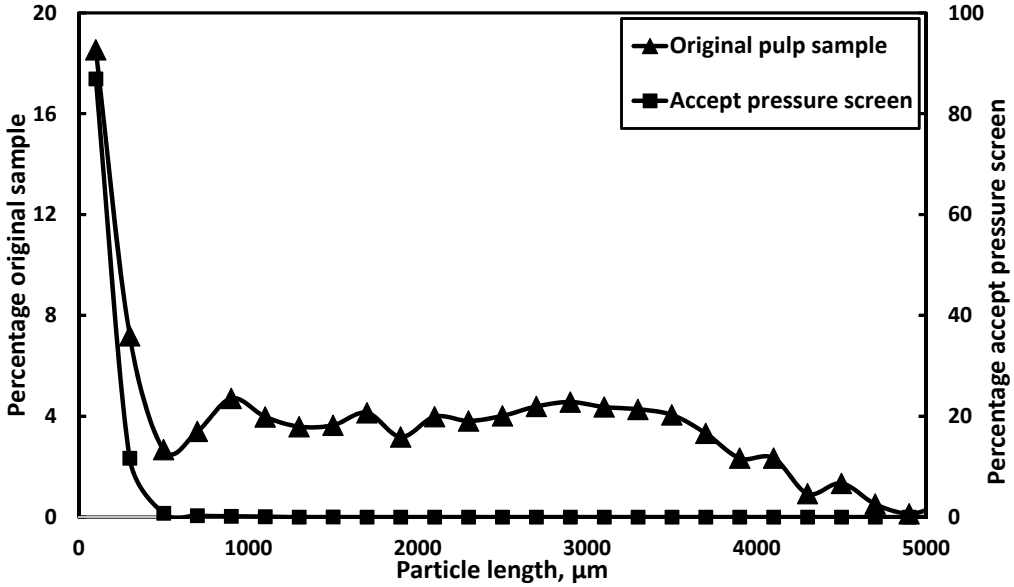

Figure 9. Original pulp sample and accept pressure screen fraction

Microbubble flotation

First results using the DAF device showed a high thickening efficiency. Fines fractions with a low fines concentration (0.01%) can be thickened up to 4% consistency by flotation.

Further experiments are in progress to determine the thickening and separation efficiency of the flotation cell.

Bubble size measurements

Table 1 shows first results of the bubble size measurements at different pressure levels and reference measurements using polyamide particles. It can be seen that there is no difference in mean bubble size between the two pressure levels. To verify the optical measurement method, L&W

measurements using the polyamide particles have been performed. From these results it is apparent that the two methods show comparable results.

Table 1. Results bubble size distribution measurements.

Sample ID	Mean diameter [µm]
Bubbles 3.5 bar	63.952 ± 2.288
Bubbles 2.2 bar	62.321 ± 0.795
Polyamide (optical method)	44.988 ± 2.267
Polyamide (L&W)	41.02 ± 10.81

Conclusions and Outlook

Results from pressure screening showed a high separation efficency, where the majority of the produced fines fraction (> 80%) consists of particles which are smaller than 100 µm. Trials using different amounts of pulp showed that depending on the original fines content of a pulp (5 - 40% mass content [6]) quantities of several 100 g of fines (oven dry mass) can be produced within 1-2 hours. Due to the low solids content further treatments such as chemical modification or formation of handsheets are more difficult to perform. To overcome this limitation, a dissolved air flotation cell for thickening of the fines suspensions was introduced allowing the thickening of fines fractions with a low consistency of 0.01% to a consistency of up to 4%. Evaluation of the bubble size in the dissolved air flotations cell showed no influence of the different pressure levels. The optical routine for bubble size determination was veryfied by comparative L&W measurements using polyamide particles.

Further investigations using the laboratory pressure screen in combination with the flotation technique will be carried out to reach an even higher separation efficiency and higher consistencies of the obtained fines fraction.

Literature

[1] O. Laintinen, L. Löytynoja and J. Niimiäki. Tube flow fractionator – A simple method for laboratory fractionation. Paperi ja Puu/Paper and Timber 88(6):351–355 (2006).

[2] SCAN-CM 66:05. Fines content. Scandinavian Pulp, Paper and Board Testing Committee, Stockholm, Sweden (2005).

[3] Retulainen, E., Moss, P., Nieminen, K. Effect of fines on the properties of fibre networks. InTrans. 10th Fund. Res. Symp., Oxford, Pira Int., Leatherhead, UK, 727-769 (Sept. 1993).

[4] Brecht, W., and Klemm, K. (1953). The mixture of structures in a mechanical pulp as a key to the knowledge of its technological properties Pulp and Paper-Canada 54(1), 72-80.

[5] Paavilainen, L. – The possibility of fractionating softwood sulfate pulp according to cell wall thickness, Appita 45 (5):319 (1992).

[6] Krogerus, B., Eriksson, L., Sundberg, A., Mosbye, J., Ahlroth, A., Östlund, I. and Sjöström, L (2002): Fines in closed circuits - final report, SCAN FORSK report 740

Determination of WRV from fiber and fine fractions and their impact on WRV in the pulp mixture

M. Mayr[1,2], R. Eckhart[1,2], W. Bauer[1,2]

AUTHOR INFORMATION

M. Mayr

[1]Institute of Paper, Pulp and Fiber Technology / Graz University of Technology
Inffeldgasse 23, 8010 Graz, Austria

[2]Flippr°- Future Lignin and Pulp Processing Research / Graz University of Technology
Inffeldgasse 23, 8010 Graz, Austria

Email:
melanie.mayr@tugraz.at

Summary:

WRV measurement is a standardized method for the measurement of the amount of water retained in a given pulp sample. For fine cellulosic materials the standardized procedure cannot be performed. Thus various modifications of the standard method were applied by different groups for the measurement of these materials. Due to these modifications the values obtained cannot be related to the standardized method. In this work a novel method was developed for the determination of the WRV of the fines fraction in a given pulp based on the normative procedure. WRV from fibers and the fines fraction were determined using this novel method. At a given fines content the WRV of the pulp was calculated and compared to the WRV measured with the standardized method for validation showing an excellent correlation with R^2 of 0.98. The WRV of fines fractions was found to be up to three times higher than the WRV of fibers. Considering the fines content present in refined chemical pulps, the contribution of fines to the WRV of a pulp can reach up to 30%.

Introduction:

The water retention value (WRV) is a measure for the ability of a cellulosic material to hold back or retain water. Thus it is a measure for fiber swelling. Swelling influences most of the process steps in pulp and paper

manufacturing. The water removal in the wet end, in wet pressing and in the drying section [1]. Swelling of fibers and fines (particles passing the 200 mesh) influences sheet consolidation and interfiber bonding. Swelling of pulp weather measured as WRV or FSP (fiber saturation point), correlates well with paper strength properties [2]–[4]. In this respect it is of interest to know not only the WRV of the pulp as a sum parameter, but also the WRV of the fiber and fines fraction to evaluate the separate effect of fibers and fines in terms of strength and other paper properties. Luukko has shown that the type of fines, specifically the fibrillar content of fines is responsible for the improvement of strength properties [5]. The swelling behavior of fines is highly related to the fibrillar content [6] and can therefore be applied as an indirect measure for it. Different raw materials and pulping processes deliver different WRV. And even within a given pulp source there is a difference between the fiber and the fine fraction, that cannot be determined or addressed based on the standard method. In this standardized procedure (ISO 23714) a fiber pad is formed by filtration of a suspension of cellulosic material over a buchner funnel. This fiber pad is then centrifuged under defined conditions. The parameters centrifugation time, centrifugation force, fiber pad dimension and fiber pad mass affect the final result [1], [7]. The method described above can be used for pulp suspensions. For fine cellulosic material like the fines fraction, it is hardly possible to form a pad within reasonable time following the normative. Several modifications were applied by other researchers for determination of WRV from fine cellulosic material:

- The mass of the sample was reduced in every modification.
- Centrifugation was replaced by other methods to remove excess water [7].
- Membranes were implemented to be able to hold back the fine material [8].
- Centrifugation time and force were varied [4].

Due to these modifications the values obtained for the fine fraction cannot be related to the standardized method. Thus the contribution of fibers and the corresponding fine fraction on the WRV of a given pulp sample cannot be determined. This work describes a novel method for the determination of the WRV of a fines fraction based on the normative procedure.

Materials and Methods:

Different pulps were separated into a fiber and a fine fraction based on a screening process. The determination of the fines content was done with the BDDJ (SCAN-CM 66:05). For WRV measurements fiber and fine fractions

were mixed to obtain proportions of 5, 10 and 15 % fines content for chemical pulps and 15 – 30 % for mechanical pulps. The WRV was determined according to the normative (ISO 23714). The fiber pad is to achieve a dry mass of the pad of 2.5 g. This fiber pad is then centrifuged (centrifugation time: 30 min, centrifugation force: 3000g). The pad was weighed after centrifugation (m_{wet}), dried and weighed again (m_{dry}). The WRV is determined according to eq. 1.

$$WRV\left[\frac{g}{g}\right] = \frac{m_{wet}}{m_{dry}} - 1 \qquad (1)$$

In Figure 1 the relationship between fines content and WRV is depicted. A linear increase of WRV with increased fines content is evident. The linear equation (eq. 2) obtained from this relation was solved according to the two boundary conditions w_{Fines} = 0 % and w_{Fines} = 100 % to determine the WRV of the single fractions (eq. 3, eq. 4). The WRV of a given pulp (WRV_{Pulp}) was then calculated based on the determined WRV of fines (WRV_{Fines}), fibers (WRV_{Fiber}) and the fines content (w_{Fines}) (eq. 5). The actual WRV of the pulp was also measured using the standard method (ISO 23714) in order to validate the calculation.

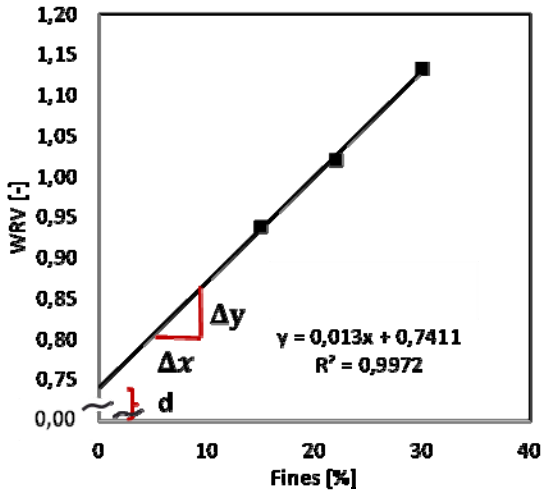

Figure 10: Linear relationship between fines content (x-Axis) and WRV (y - Axis)

$$WRV_{Pulp} = k * w_{Fines}[\%] + d \qquad (2)$$
$$x = 0 \rightarrow WRV_{Pulp} = d \triangleq WRV_{Fiber} \qquad (3)$$
$$x = 100 \rightarrow WRV_{Pulp} = k * 100 + d \triangleq WRV_{Fines} \quad (2) \qquad (4)$$
$$WRV_{Pulp} = WRV_{Faser} * \left(1 - w_{fines}\right) + \qquad WRV_{Fines} * w_{fines} \qquad (5)$$

Results:

For the validation of the novel method ten different mechanical and chemical pulps were measured. Using the given fines content of the original pulps the WRV_{Pulp} was then calculated based on the determined values for the separated fractions and compared to the WRV values measured with the standardized method (Figure 11).

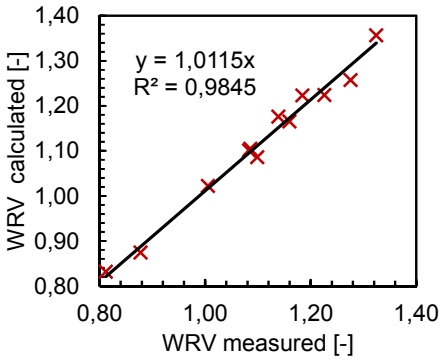

Figure 11: WRV of different pulps. Correlation between measured values (x – axis) and calculated values based on the novel method (y - axis)

As an exemplary application the swelling of fibers and fines can be determined together with the contribution of the single components in a pulp mixture. Figure 3 (left) shows the WRV of SW and HW bleached kraft pulps before and after refining. The black bars represent the WRV of the fiber fraction and the grey bars the WRV of the fines fraction. The WRV of the fines is up to three times higher compared to the WRV of fibers. SWBK fines show a higher WRV compared to HWBK fines, although the fibers give similar results for SWBK and HWBK. In Figure 3 (right) the contribution of fibers (black bar) and fines (grey bar) to the WRV of a pulp with defined fines content is displayed. The contribution of fines increases after refining for two reasons. The fines content is higher after refining and also the WRV of fines (Figure 3 left) is increased. In a chemical pulp refined under industrical conditions the contribution of fines to the WRV can reach up to 30 % based on these results although their mass proportion is only about 10 %.

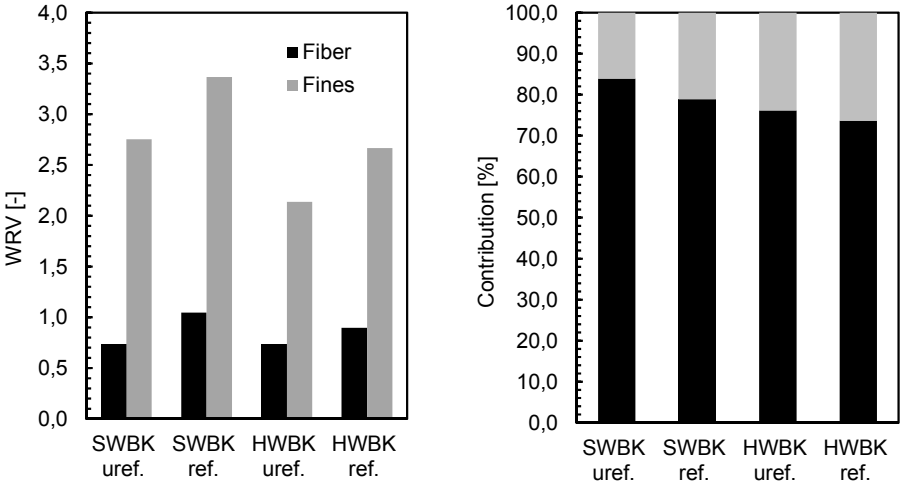

Figure 3: Exemplarily application of the novel method for SW and HW bleached kraft pulp before and after refining. left: WRV of 100% fiber (black bar) and 100% fines (grey bar); right: Contribution of fibers (black bar) and fines (grey bar) for the pulps with given fines content.

Conclusion:

In nearly every process area in paper manufacturing WRV is influenced, whether it is bleaching, refining or drying. Although only a low quantity of fines is present in a pulp mixture fines have a high impact on the WRV of the pulp as is shown in Figure 3. With the novel method the WRV of fibers and fines can be determined seperately. The contribution of the fibers and fines to the swelling of a pulp can then be calculated. The values obtained from this calculation are comparable to values obtained with the standardized procedure on the whole pulp sample and therefore show the validity of the method.

Literature:

[1] T. C. Maloney, J. E. Laine, and H. Paulapuro, “Comments on the measurement of cell wall water,” *Tappi*, vol. 82, no. 9, pp. 125–127, 1999.

[2] K. Koskenhely, H. Paulapuro, A. Ämmälä, and H. Jokinen, “Effect of refining intensity on pressure screen fractionated softwood kraft,” *Nord. Pulp Pap. Res. J.*, vol. 20, no. 2, pp. 169–175, 2005.

[3] Y. Chen, J. Wan, X. Dong, and Y. Ma, “Fiber properties of eucalyptus kraft pulp with different carboxyl group contents,” *Cellulose*, vol. 20, no. 6, pp. 2839–2846, 2013.

[4] Hii, “The effect of MFC on the pressability and paper properties of TMP

and GCC based sheets," *Nord. Pulp Pap. Res. J.*, vol. 27, no. 02, pp. 388–396, 2012.

[5] K. Luukko, "Fines Quantity and Quality in Controlling Pulp and Paper Quality," in *Tappi International mechanical pulping conference*, 1999, pp. 67 – 75.

[6] K. Luukko and T. Maloney, "Swelling of mechanical pulp fines," *Cellulose*, vol. 6. pp. 123–135, 1999.

[7] Q. Cheng, J. Wang, J. F. McNeel, and P. M. Jacobson, "Water retention value measurements of cellulosic materials using a centrifuge technique," *BioResources*, vol. 5, no. 3, pp. 1945–1954, 2010.

[8] M. Bäckström, M. C. Kolar, and M. Htun, "Characterisation of fines from unbleached kraft pulps and their impact on sheet properties," *Holzforschung*, vol. 62, pp. 546–552, 2008.

Wall investigations of pulp of paper flow in pipes-New model of behaviour or pulp of paper flow Paper

Salaheddine Skali Lami

AUTHOR INFORMATION

LEMTA - Lorraine University, 2 Avenue de la Forêt de Haye - 54518 Vandoeuvre-lès-Nancy cedex France

Email: salaheddine.skali-lami@univ-lorraine.fr

Summary

Start your paper with a 200 to 300 word summary

In papermaking the pulp and paper treatment processes needs the optimization of various unit operations which require a better knowledge of the pulp of paper behaviour. The Pulp of paper, which is a suspension of cellulose fibers in water, shows several regimes when flowing in pipes. These regimes are experimentally and qualitatively well described in the literature, they are related to the evolution of fibre flocculation characterizing different regimes (called: plug flow, mixed regime and turbulent flow). By against a quantitative descriptions of these regimes are limited and we don't find a model in the literature that describes entirety the behaviour of the pulp of paper flow from a plug flow (high shear friction at low velocities) to identical behaviour that of water at high velocities (turbulent Newtonian flow) going through drag reduction in intermediate velocities.

We propose an experimental analysis of the flow of pulp of paper for several concentrations of fibers in two diameters of pipes (evaluation of confinement effects). These results are compared to a model describing the behaviour of paper in any regimes. The proposed model is based on calculating an average shear stress which takes into account both the elastic moduli of the flocs and the network of fibres (floc agglomerates) and secondly the viscosity of the fluid (water) modified with dispersed fibres.

Introduction

The investigations of the pulp of paper flow in pipes have been the subject of numerous studies since the 50s (Masson [1], Takeuchi [2], Kerekes [3] Duffy [4]) to understand the various regimes of paper pulp including drag reduction regime resulting from interactions flocculation-turbulence. Other objectives are the description of the friction coefficients of the flow of the pulp of paper. Moller [5], on the basis of an elastic behaviour of the network of fibres and a Newtonian behaviour of the liquid film which surrounds, showed that the evolution of the wall shear stress changes with the bulk velocity to power1/3. Current investigations are moving towards determining the rheological characteristics of the pulp of paper as the apparent viscosity, the yield stress and the elastic moduli (see summary of different works B. Derakhshandeh [6]). Despite the difficulties of measurements (non-homogeneous suspensions, containment ...) the authors give orders of magnitudes of these properties and their evolution as a function of the concentration and nature of the fibres. In these rheological measurements, the constitutive law is given by the measuring device where the torque is linked the wall shear stress and the shear rate is linked the velocity and gap. This is valid for a homogeneous fluid but for pulp of paper we encounter many problems due to the heterogeneity of the suspension.

In the case of pipe flow the wall shear stress can be deducted from the pressure loss against the determination of the wall shear rate must use electrochemical techniques (Skali-Lami [7] and Ogawa [8]). The measurements obtained by these authors show that the behaviour of the paper pulp close to the wall is Newtonian whatever the flow rate and whatever the concentration. In fact the two variables vary non-linearly with the flow rate, but remain a constant ratio in average over time. This suggests that in the modelling approaches must, in a zone near the wall, consider the viscosity of water modified by dispersed fibres.

Experimental

Materials

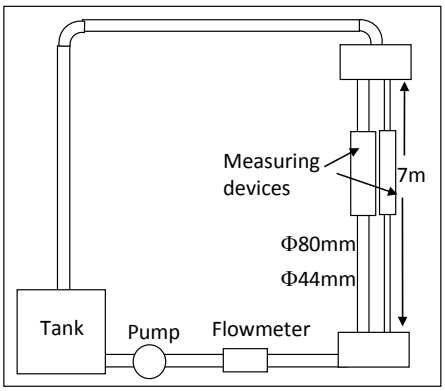

Fig.1 experimental setup

The experimental setup (fig.1) is composed of a tank, pump, flow meters, and two vertical pipes 7m in length and 80mm and 44mm diameters. Each of the pipes is equipped with an instrumented element by wall platinum electrochemical probes (ϕ 0.5mm).

Method:

The fibre suspension is realized in an electrochemical solution of water, potassium ferricyanide (Co = 210^{-3} M/l), potassium ferrocyanide (2 * Co) and potassium chloride 1/3 M/l.

Determining the wall shear rate is obtained from the mass transfer equation of a potassium ferricyanide on the parietal microelectrode:

$$\frac{\partial C}{\partial t} + \vec{U}.\vec{\nabla}\,C = D\,\Delta C$$

$$With \begin{cases} * \ C \ is \ the \ concentration \ of \ potassium \ ferricyande \\ * \ U \ volocity : Ux = \gamma\, y \ ; \ and \ Uy = -\dfrac{y^2}{2}\dfrac{\partial \gamma}{\partial x} \\ * \ \dfrac{\partial^2 C}{\partial x^2} \ll \dfrac{\partial^2 C}{\partial y^2} \\ * \ x \ is \ the flow \ direction \ and \ y \ is \ the \ normale \ to \ the \ wall \\ * \ \gamma \ is \ the \ local \ wall \ shear \ rate \end{cases}$$

This equation was solved by Hanratty [9] to determine the mass flux and therefore the electrical current collected at a microelectrode in the case of a high Schmidt number. $I \approx \gamma^{\frac{1}{3}}$

The measurement of current gives the instantaneous value of the local wall shear rate.

Theoretical analysis

We use theoretical approach to the calculation of the average stress resulting from that of a Newtonian fluid σ_{ij}^{w} in the liquid film of thickness δ and an elastic stress σ_{ij}^{f} in the radius of fibers of network (R-δ):

$$\sigma_{ij} = -\frac{\delta_{ij}}{V}\int_{V-\Sigma Vo} p\, dV + \sigma_{ij}^{f}\left(1-\frac{\delta}{R}\right)^2 + \sigma_{ij}^{w}\left(2-\frac{\delta}{R}\right)\frac{\delta}{R}$$

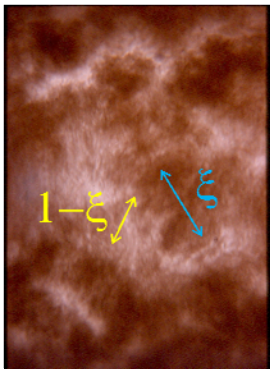

Fig. 2 Network

The elastic stress in the network can be described by a portion due to the splats and another portion surrounding floc because the elasticises are not the same: $\sigma_{ij}^{f} = \sigma_{ij}^{f1}(1-\xi) + \sigma_{ij}^{f2}\xi$

We can deduce from this equation the mean shear elasticity modulus: $G = G_{\infty} + (G_0 - G_{\infty})\xi$

This expression is similar to the Zener elasticity model, where ξ can be modelled by a kinetic 1 order according to the Reynolds number and a critical Reynolds number

Also at the interface of the network of fibres we can write the continuity of the tangential stresses where the network is assumed as a viscoelastic behaviour:

$\tau = \tau_0 + \mu(c)\frac{V}{\Delta} = \tau_0 + \mu(c)\frac{V}{R\frac{\Delta}{R}}$ and $\tau_0 = \tau\left(1 - \frac{\Delta}{R}\right)$ and $N = E\frac{\Delta}{R} = 2\left(\frac{\tau}{G}\right)^2$

Where τ_o : yield stress, N:normal stress E : elastic modulus ≈ G and Δ: mean thickness of liquid film (large deformation of the network $\frac{\Delta}{R} = \int_0^{\frac{\delta}{R}} \frac{d\left(\frac{\delta}{R}\right)}{\left(1-\frac{\delta}{R}\right)}$)

μ(c) is the shear viscosity in liquid film, we use theoretical approach given by Dinh&Amstrong [10]:

$\mu(c) = \mu_w\left(1 + \frac{4C\left(\frac{l}{d}\right)^2}{90\,Ln\sqrt{\frac{\pi}{C}}}\right)$ Where μ_w: viscosity of water l/d: aspect ratio of fibre (≈ 100) and C the concentration of fibres (0.3%≤C≤2%).

Solving all these equations allows establishing the evolution of wall shear stress as a function of the mean velocity for various concentrations of fibres and for the two pipe diameters. The comparison between experimental results and this model is given in Figure 3:

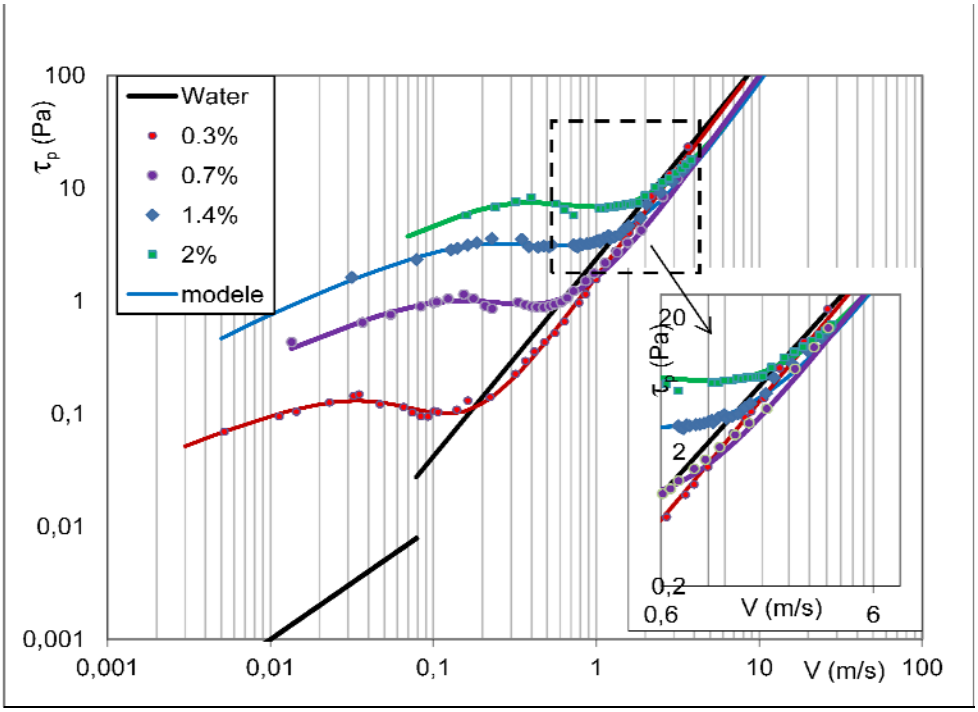

Fig.3 Wall shear stress vs mean velocity (pipe ϕ 80mm)

(■●▲experimental data – theoretical curves)

In Table 1, we postponed, versus the fibre concentration, the values of elasticities obtained by identification and those viscosities calculated by Dinh&Amstrong [10] equation. The critical Reynolds number is taken equal to 5000 and the values of G_∞ and G_o are obtained by identification to the experimental values. These elasticities values change with the concentration to the power 3.

C %	0,3	0,5	0,56	0,73	1,1	1,35	1,7	2
G_∞ (Pa)	1,39	2,20	6,09	13,36	15,84	44,88	82,47	177,85
G_o(Pa)	0,15	0,33	0,91	2,18	3,00	9,47	16,14	19,44
μ (C) *10^3 (Pa.s)	1,33	1,58	1,68	1,93	2,45	2,96	3,52	4,05

Tab. 1 Elasticities G_∞ and G_o and viscosities used

Conclusions

The proposed model is highly nonlinear but allows to describe all the behaviour of the flow of pulp with three adjustable parameters which are the thickness of the liquid film at rest, the elasticity of flocs and the elasticity in the inter-floc space. The viscosity in the liquid film is taken equal to that water modified by dispersed fibres.

Literature

[1] Mason S. G. (1948) “The flocculation of cellulose fiber suspensions” Pulp and Paper Mag. Can. 49 pp 99-104.

[2] Tkeuchi N., Senda S., Namba K. And Kuwabara G. (1983) “formation and destruction of fibre flocs in a flowing pulp suspension”APPITA,Vol 37, 223-230
[3] Kerekes R. (1983) “Pulp flocculation in decaying turbulence” A literature review T. Of pulp and paper Sci. 9 (3) TR 86.
[4] Duffy G. G. (2006) “Measurents, mechanisms, models : some important insights into the mechanisms of flow of fibre suspensions”. Annual Trans. of the Nordic Rheology Society 14 19-31.
[5] Moller, Duffy and Titechener (1971) “The laminar flow regime of paper pulp suspensions in pipe Svensk papperstiding Arg. 74, 828-834.
[6] Derakhshandeh B. Kerekes R.J., Hatzikiriakos S.G. and Bennington C.P.J. (2011) “rheology of pulp fibre suspensions:A critical review” Chem. Eng. Sci. 66 3460-3470.
[7] Skali-Lami S. (1991) “contribution à l’étude de l’écoulement de pâte à papier-Interaction flocculation-turbulence“ Thèse d’Etat INPL-Nancy
[8] Ogawa K., Yoshikawa S., Sugoro,A., Ikeda,J.Ogawa,H. (1990) “ Flow characteristics and circular pipe flow of pulp suspension“ J. Chem. Eng. Jpn. 23, 1-6.
[9] Hanratty, T.J. and Campelle, J.A. (1983) “Measurement of wall shear stress” Fluid mechanics measurements Ed. By Goldstein R.J. Hemisphere Publishing Corp. Ch. 11 p 559.
[10] Dinh, S.M. and Amstrong, R. G. (1984) “A rheological equation of semi-concentrated fiber suspension“J. Rheol. 28 (3) , 207-227.

The Volume under Load model for evaluating wet pressing performance

Patrick Leuk[1], Michael Dauer[1] and Ulrich Hirn[1]

AUTHOR INFORMATION

Ulrich Hirn[1]

[1]Institute of Paper, Pulp and Fiber Technology, Graz University of Technology, NAWI Graz, Inffeldgasse 23, 8010 Graz, Austria

Email:
ulrich.hirn@tugraz.at

Abstract

Press felts are optimized for their dewatering performance. Machine trials with new press felts are expensive and can easily lead to runnability problems. Therefore lab trials which can predict the dryness increase in a press nip are of great significance. At Graz University of Technology a method was developed to determine the area of contact under similar conditions to a press nip. This method is based on an imprint (4x4 cm²) of the felt under load which is afterwards digitized. A contact model is used to determine the contact regions between press felt and paper. The top figure shows the paper area in contact (colored) and not in contact with the press felt (white) according to the contact model.

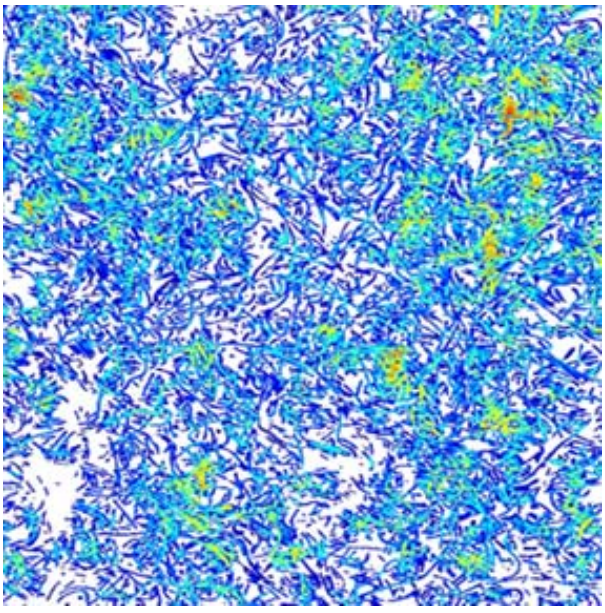

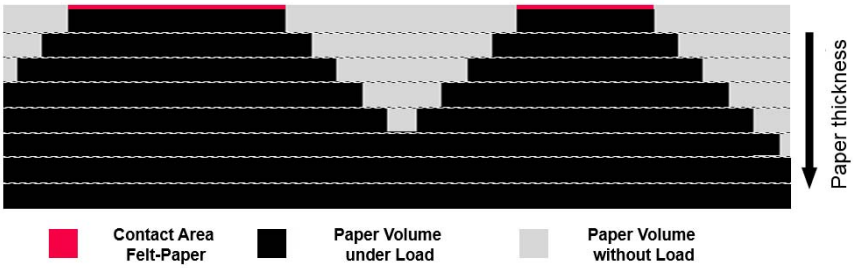

A load model is used to calculate the paper volume under load from the contact area between felt and paper (bottom figure). This model was validated in an extensive campaign of dewatering experiments using a press simulator. The volume under load model was found to correlate very well with the dryness increase during pressing (R^2>0.9).

It could be shown that not only the batt fiber diameter on the top layer of the felt influences the area of contact, but also other factors like the base wave construction.

Thickening and Dewatering of Cellulose Nanofibrils and Fines-Enriched Suspensions using Centrifugation

Maria Sedin, Eva Ålander, Elisabeth Björk, Hannes Vomhoff

AUTHOR INFORMATION

Innventia, Stockholm, Sweden

Email:
maria.sedin@innventia.com

Summary

In this study, thickening and dewatering studies were performed using an analytical centrifuge. During the centrifugation, the light transmittance of the samples was continuously measured as a function of time and height. The centrifugal force was varied up to 2320g. Different initial concentrations of the suspensions were investigated, which at the same initial volume of liquid varies the grammage of the sediment. Two fines-enriched pulps (FE) with different fibre length distributions were used to investigate the influence of fibre size. Two qualities of cellulose nanofibrils (CNF), based on enzymatic and carboxymethylation pre-treatment respectively were used to study the influence of total charge of the CNF.

Different thickening behaviour was observed for the FE-pulps; the coarser suspension could be dewatered faster and reach a higher concentration at equal compressive network pressure. Dependent on the initial concentration of the suspension and the grammage, the concentration of FE-pulp suspensions could be increased from about 10 up to 80 g/l.

The two CNF suspensions responded very differently to the centrifugal force. A final concentration exceeding 50 g/l of the lower charged CNF could be

achieved whereas the higher charged CNF was found to be much more difficult to thicken. Furthermore, the effect of the ionic strength on the thickening behaviour of CNF was investigated. A higher the ionic strength was found to beneficial for the thickening.

Introduction

Thickening and dewatering of suspensions comprising cellulose nanofibrils or a high fines content are challenging. Traditional filtration-based dewatering processes are very time-consuming, if at all possible. Once the solids of the suspension start forming a network, the permeability is very low due to small size-scale of the particles and the compressibility of the fibre network. In centrifugation the dewatering flow counteracts the compression of the network, thus maintaining a higher permeability during the thickening process. Thus, centrifugation may be a viable alternative separation method.

The thickening behaviour of four fibre suspensions was investigated in this study. Two FE-pulps were obtained by screening a highly beaten chemical Eucalypt pulp using two different screen baskets, 250 and 350 μm. Two qualities of CNF were produced by passing either enzymatic pre-treated or carboxymethylation pre-treated pulps [1, 2] through a homogeniser yielding CNFs with different size distributions and charge densities. Some properties of the fibre suspensions studied are given in *Tab. 1*.

Table 1. Some properties of the fibre suspensions studied. Fibre length distribution measured using Fiber Tester.

	Average fibre length, length weighted (mm)	Fibre fraction ≤0.2 mm
FE(250 μm)	0.278	51.2%
FE(350 μm)	0.377	35.7%
	Pre-treatment	Total charge (μeq./g)
CNF A	Enzymatic	approx. 60
CNF B	Carboxymethylation	approx. 600

Results and discussion

Using an analytical centrifuge (LUMiSizer [3]), the height of the supernatant was determined during centrifugation from *in-situ* light transmittance measurements (865 nm) at 25°C and the average sediment concentration and average compressive network pressure were calculated [4].

Both FE-pulps showed a very steep transmittance gradient at the supernatant-sediment interface but exhibited different thickening behaviour; the coarser suspension could be thickened faster and a obtained a higher final concentration at equal compressive network pressure, see *Fig. 1*.

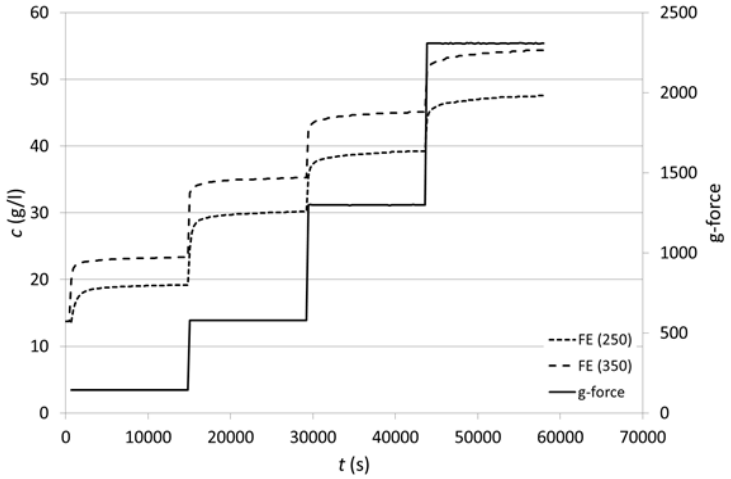

Figure 1. The response of the two FE-pulps' to stepwise increasing g-forces. Initial concentration of 11.5 and 10.7 g/l for FE (250 μm) and FE (350 μm), respectively.

Dependent on the initial concentration of the suspension and the grammage, the concentration of FE-pulp suspensions could be increased from about 10 up to 80 g/l. Interestingly, an expansion of the sediment was observed if the sediment was first formed at 2320g and then the g-forces were reduced. In *Tab. 2* the sediment expansion for FE-pulp (250 μm) is listed for two different initial concentrations and it can be seen that the sediment expansion is significant in both cases but is more pronounced for the lower initial concentration.

Table 2. Change in sediment concentration (g/l) for FE-pulp (250 μm) with decreasing g-forces.

Initial concentration	2320g	1310g	580g	9g
2.4	31.1	28.7	25.7	18.7
11.5	49.7	47.5	44.3	37.6

The two CNF suspensions responded very differently compared to the FE-pulps. Firstly, the CNF suspensions are stable below some g-force and secondly the top of the sediment exhibit a transmittance gradient. This is in contrast to the FE-pulps. This is illustrated in *Fig. 2* for CNF B at an initial

concentration of 3 g/l. From the figure it can be noted that the supernatant phase develops at about 4000 s/180g. At about 10000 s the relative highly concentrated sediment grows and after 10000 s the sediments is compressed.

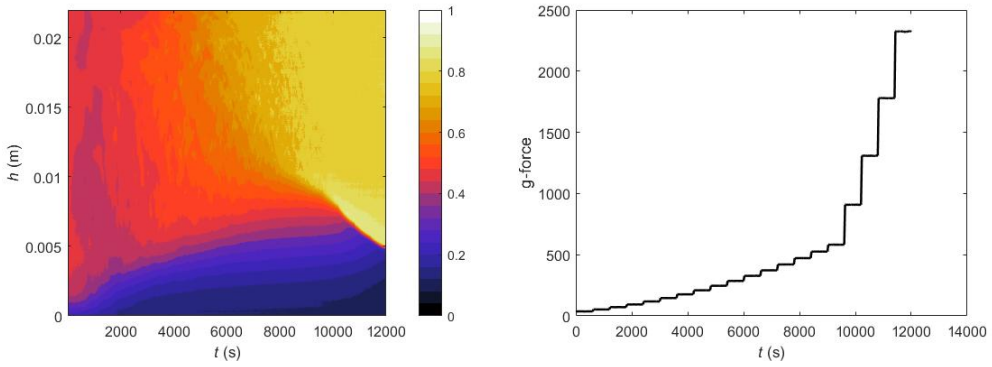

Figure 2. Transmittance measurement of CNF B with initial concentration of 3 g/l.

The two CNF suspensions responded very differently to the centrifugal force. A concentration of more than 50 and 12 g/l of the CNF A could be achieved from an initial concentration of 26 and 2 g/l, respectively, at 2320g.The higher charged CNF B was found to be much more difficult to thicken; at concentration greater than 3 g/l no phase separation occurred at 2320g. To improve the separation behaviour the ionic strength was increased up to 10 mM using with a phosphate solution. It was observed that increasing the ionic strength resulted in faster thickening and a much distinct supernatant-sediment interface, see *Fig. 3*.

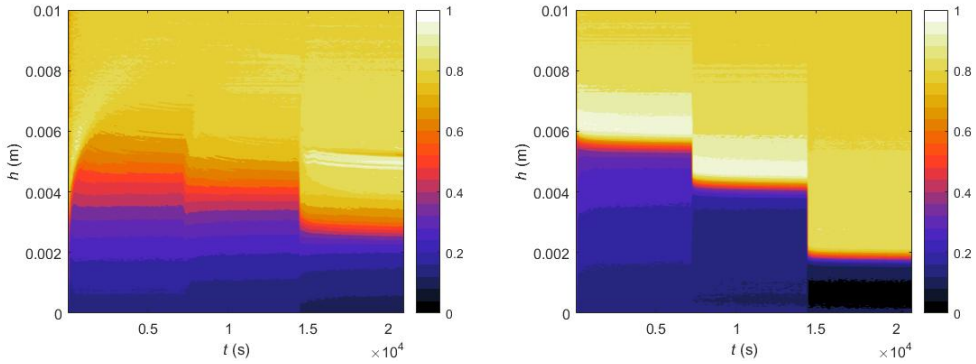

Figure 3. Transmittance measurements as a function of time and height illustrating the effect of ionic strength on CNF B with initial concentration of 1 g/l: ionic strength of 0.01 and 10 mM, respectively. g-forces corresponding to 36, 146 and 2320g. Transmittance equal to 1 and 0.85, respectively, corresponds to an empty cell and a water filled cell.

Conclusions

It was possible to increase the concentration of FE-pulp suspensions to more than 80 g/l at 2320g. Decreasing the average fibre length of the FE-pulp resulted in a more difficult thickening. The total charge of CNF has a great influence on the thickening behaviour. The concentration of CNF with the low total charge could be increased to 50 g/l. An increase in ionic strength of the CNF with the high total charge resulted in a faster phase separation. The analytical centrifuge has been shown to be an excellent tool for increased knowledge, up-scaling and process design on efficient thickening and dewatering of more challenging fibre suspensions.

Acknowledgement

RISE Research Institutes of Sweden is gratefully acknowledged for financial support.

Literature

[1] Pääkko, M., M. Ankerfors, H. Kosonen, A. Nykänen, et al. Enzymatic hydrolysis combined with mechanical shearing and high-pressure homogenization for nanoscale cellulose fibrils and strong gels. Biomacromolecules, 2007, 8(6), 1934-1941.

[2] Siró, I., D. Plackett, M. Hedenqvist, M. Ankerfors, et al. Highly transparent films from carboxymethylated microfibrillated cellulose: The effect of multiple homogenization steps on key properties. Journal of Applied Polymer Science, 2011, 119(5), 2652-2660.

[3] Sobisch, T. & D. Lerche Thickener performance traced by multisample analytical centrifugation. Colloids and Surfaces A: Physicochemical and Engineering Aspects, 2008, 331(1-2), 114-118.

[4] Loginov, M., M. Citeau, N. Lebovka & E. Vorobiev Evaluation of low-pressure compressibility and permeability of bentonite sediment from centrifugal consolidation data. Separation and Purification Technology, 2012, 92, 168-173.

Morphological and physical properties of pulps prepared from a dry defibration process

Schrinner, Thomas and Heinemann, Sabine

AUTHOR INFORMATION


T. Schrinner


S. Heinemann

Dresden University
of Technology

Email:
sabine.heinemann@tu-dresden.de
thomas.schrinner@tu-dresden.de

Summary

Contrary to wet disintegration, dry defibration enables the efficient reuse of difficult-to-recycle paper and board products such as release paper, liquid packaging, and other composite materials.

Numerous special paper grades contain high-valuable fibrous materials, but since they can only partly or not at all be treated in conventional recovery processes, those fibres are not available as raw material for new fibrous products. Lacking suitable other utilization processes, products from special papers become rather often waste products after only one utilization loop, requiring high disposal costs. Dry defibration is therefore a useful process to recover at least the fibrous part of those products incurring in considerable amounts, and a special dry defibration process for hardly-to-recover papers and boards was designed.

The mechanical principles occurring in dry defibration are impingement reactions with a solid surface, pressure-shear reactions in a refining gap, and reactions within a circulating turbulent flow, causing a fast separation of the special paper products into a fibrous material with properties different from those of conventionally wet disintegrated fibres.

With old newsprint and magazine as reference, a selection of special paper grades including wet-strength paper, release paper, and thermographic paper

was studied with respect of morphological and physical property developments depending on varied dry defibration process parameters.

Introduction and background

In order to sustainably reduce the specific energy consumption in papermaking the Professorship of Paper Technology at Dresden University of Technology has been working intensively on the development of new technologies for the preparation of different raw materials.

Background of this application-oriented focus was the fact that many state-of-the-art technologies employed today even in the most modern paper mills are the result of decades of experience and continuous evolution rather than innovation. It cannot be assumed that any further incremental development of these technologies bears the potential to meet the objectives defined in CEPI's roadmap 2050 in terms of CO_2-reduction and energy efficiency. On the other hand rather basic calculations have shown that the specific energy consumption of some of these state-of-the-art technologies – like de-inking or pulping – is way higher than the energy which should theoretically be sufficient to achieve the desired process objectives. Against this background the development of what is called breakthrough technologies is necessary and will become an indispensable prerequisite to run the production processes at much higher energy efficiencies and lower CO_2-emissions.

One of the main reasons for the inadequate energy efficiency of many stock preparation processes are low consistencies and the accompanying large amounts of water which have to be transported and thus render the processes uneconomical. This also applies to the defibration process at the beginning of any stock preparation line. Therefore, in a research project called "dry defibration" we examined, whether and how it is possible to comminute paper and board products either collected after having been used or as production residues from converting processes by completely dispensing with any addition of water in a purely mechanical way.

Dry defibration technology

The dry defibration technology is based on a mechanical airflow impact mill with a peripheral grinding track (Fig. 1). The paper product is comminuted due to high-impact collisions with the walls or special installations of the grinding chamber induced by a highly turbulent air flow as well as by the shear forces acting in the grinding gap.

Numerous dry defibration trials, however, showed that not only standard grades of recovered paper can be broken down into individual fibres, but – even more importantly – also difficult-to-recycle products such as board cores, release papers, composite materials such as beverage board or wet-strength filter papers containing high quality fibres. This would allow to turn hitherto entirely or at least partially unused raw materials into secondary sources for paper production. Especially against the background of increasing scarcity of and rising costs for fibre resources, this process might have the potential to become an attractive technology for the industry not only improving their economics but also increasing the security of raw materials supply.

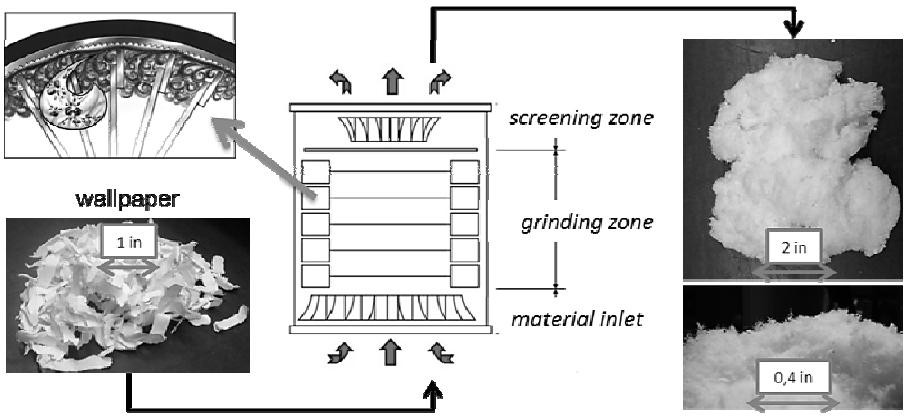

Fig. 1. Dry defibration principle [1]

Thus motivated, we have been searching for methods that would allow to make such material part of the paper cycle. However, a prerequisite for the use of such dry pulping technology is that the fibres obtained are qualitatively suitable for papermaking, for which reason in the following the properties of dry generated fibers will be considered more in detail.

Results

Comparison of dry defibration and conventional wet disintegration with a standard paper grade

A mixture of different paper and board grades, containing maximum 40% newspapers and magazines (Grade B12) was treated in the new dry disintegration technology, with varying rotor speed, initial moisture content, and dwell time (air flow). Additionally, a wet post-treatment was applied. For the reference, the same raw material was disintegrated in a conventional wet process.

The pulp character and deriving handsheet properties are determined by the fibre behaviour during the dry defibration treatments. Since the fibres in the dry state cannot slide apart gently, fibrils are not flexible and are pulled down from the fibre surface decreasing the external fibrillation. Concurrently, fibres are kinked and shortened, and both actions lead to an increased low-bonding fines content.

Generally, dry disintegration decreases the fibre-to-fibre bondability, concluded from higher bulk, strength drop, and accelerated pulp drainability. Schopper-Riegler values dropped down to approx. 30-40% of the reference, but could be lifted again to 83 % of the reference by controlling the initial moisture content, the dwell time and the post-treatment. In terms of strength, especially the wet post-treatment step re-activates both tensile index and tear index from a dropped value of around 50 % of the reference back to its original level near 100%. Fig. 2 gives an overview about obtainable pulp properties and the corresponding process design.

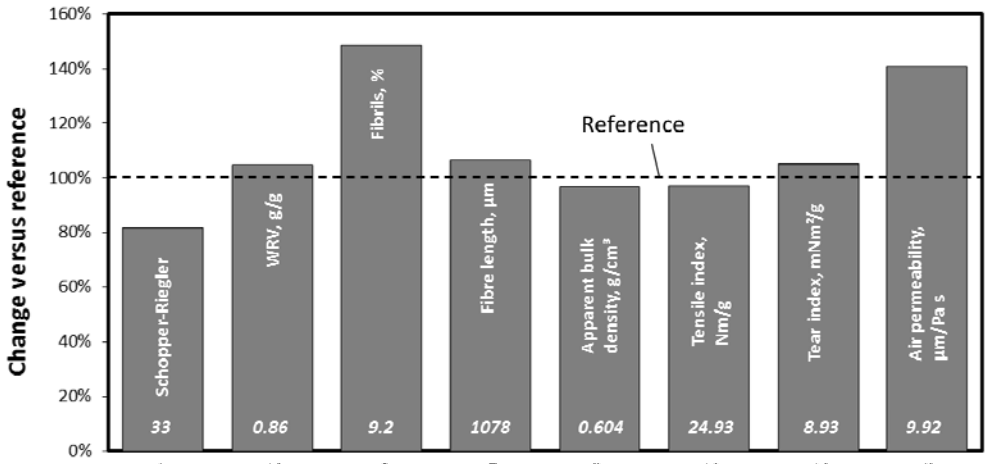

Fig. 2. Change of physical pulp properties of a dry disintegration process versus reference (wet disintegration, corresponding values are given). Conditions of the dry disintegration process: Rotor speed 55 Hz = 3,300 rpm, air flow 12 m/s, initial moisture content 41%, wet post-disintegration 10 min (50,000 rev).

Dry defibration for special paper grades

The dry disintegration process as described above was also applied to special hard-to-disintegrate materials such as wet-strength paper, silicon paper, and thermographic paper. As seen from Fig. 3, fibres of rather different character are produced – short and stiff fibres with some non-fibrous fines and small fibre bundles holding fibres in distance and preventing them from bonding

(wet-strength), slender and flexible fibres with some surface fibrillation (silicon), or short fibres with slight surface fibrillation for good bonding performance (thermo).

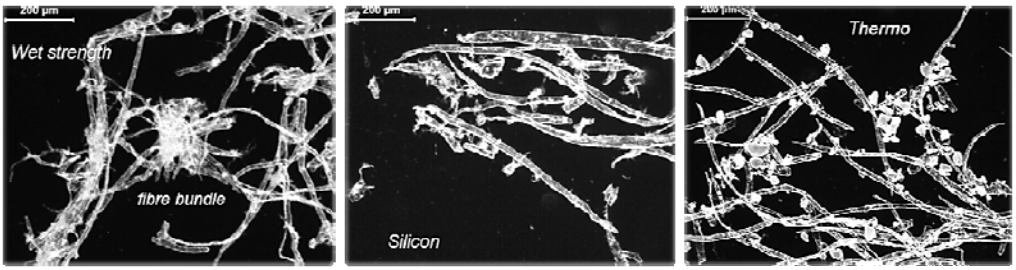

Fig. 3. Microscopic appearance of three hardly-to-disintegrate special papers using darkfield illumination – Wet-strength paper (left), silicon paper (centre), thermographic paper (right) [2].

In terms of physical handsheet performance, the non-fibrous constituents in these special papers affect strongly all structural properties from fibre-to-fibre bonding ability to z-dimensional formation, from sheet density to optical properties such as light-scattering.

Conclusions and outlook

In the novel dry defibration process, the material is comminuted; and short fibres and non-bonding fines are created, causing accelerated drainability and low strength properties. Pulp quality improvement is possible by special process design. Higher rotor speed decreases the number and size of fibre bundles and specks, higher initial moisture content supports the fibrillation effect, and a shorter dwell time improves all properties. Additionally, a special wet post-disintegration gives final quality improvement towards the reference pulp level.

Dry disintegration is working well for simple paper and board structures but becomes challenging for multi-component materials with higher proportions of non-fibrous components such as fillers, special coating or laminate layers, or special chemical additives. However, dry defibration has the capability to recycle difficult-to-recycle paper products at a higher energy-efficiency than standard wet processes.

Further investigations are aimed at optimizing the dry defibration technology by pre-treatments of the raw material to build a semi-dry defibration process improving fibre properties and reducing the energy demand. Such a process would be the prerequisite for one step further towards a dry or semi-dry paper

and cardboard production, already shown as essential for the development of new, e.g. hydrophobic or functional paper products thus providing the opportunity not only to save water and energy, but also to increase the added value – the two key objectives of the CEPI Roadmap 2050.

Literature

[1] Schrinner T. (2015) Dry defibration – A waterless preparation process for difficult-to-recycle paper and board products. International Austrian Paper Conference, 20-21 May.2015, Graz/A

[2] Schrinner T., Gailat T., Heinemann S., Lundberg M. (2015) Selected pulp properties after dry defibration of several paper products. PTS Pulp Symposium, 25-26 November 2015, Dresden/D

A First Principles Modelling Approach Probing the Chemical Suitability of Synthetic Strengtheners in Papermaking

Peter Deglmann[1], Anton Esser[2]

AUTHOR INFORMATION

[1] BASF-SE GME/MM
[2] BASF-SE , EVW/MI
Carl-Bosch-Str. 38
67056 Ludwigshafen, Germany

Email:
peter.deglmann@basf.com
anton.esser@basf.com

Abstract:

At a molecular level, wood pulps are fairly chaotic systems. Although approximate ratios of cellulose, hemicelluloses and lignin can be specified, little is known which parts of these bio-macromolecules are responsible for the main interactions with paper chemicals. Improvements of synthetic polymers for papermaking therefore had to rely so far mostly on trial and error. In our paper, calculations, are presented that were performed with the aim to develop a broader understanding of interaction strengths between synthetic polymers and cellulose as the only well-characterized pulp constituent. For our computational studies, we understood the question of mutual interactions as a docking problem between polymers (ligands) and representative molecular structures occurring at pulp surfaces (receptors). Typical docking strategies, however, require the existence of rather rigid and well defined receptors. This is impossible due to the huge diversity of receptors; additionally, also typical polymers exhibit numerous relevant conformational degrees of freedom. We therefore chose to study these interactions with the solvation model COSMO-RS, which allows for a calculation of interaction strengths between complex molecules from their electrostatic fingerprint. The results of our modelling approach will be discussed in the context of paper mechanical strength (initial wet web strength, wet strength, dry strength) provided by the treatment of wood fibers with synthetic polymers. In particular, we will discuss synthetic polymers like polyacrylamide, Polyvinylamine and Polyethyleneimine that, are commonly applied as strengthening aids in papermaking.

Wheat straw soda paper strengthened by nanofibrillated cellulose and Cationic Polyacrylamide (C-PAM)

Djafari Petroudy Seyed Rahman

AUTHOR INFORMATION

Seyed Rahman Djafari Petroudy, PhD
Assistant Professor at Cellulose Nanotechnology and Carbohydrate Chemistry Lab.
Department of Cellulose and Paper Technology Engineering,
Faculty of New Technologies and Energy Engineering,
Shahid Beheshti University (www.sbu.ac.ir)
TEHRAN, IRAN
P.O.Box: 47815-168
Email: sr_jafari@sbu.ac.ir

Introduction

There has been significant interest in Cellulose Nanofiber (NFC) for some time due to environmentally friendly, renewable, biocompatible and degradable, low cost in comparison with other synthetic nanomaterials as well as the wide range of potential areas of application. These include boosting paper properties (1, 2), as a barrier material in packaging, replacement for plastics and reinforcement of composite materials (3). Different technologies have been employed to produce NFC. The major mechanisms for NFC production are high mechanical shearing treatments via high pressure homogenizer, grinders and cryo-crushing. In addition, a lot of research works have been conducted on pretreatments such as enzymatic and TEMPO-mediated oxidation to facilitate the fibrillation and decrease energy demands during NFC production. It has been proposed that use of enzyme technology is preferred to chemical methods due to eco-friendly characteristics.

Now, thanks to energy-efficient preparation techniques the important barrier for the commercial utilization of NFC has been removed, but research work is still needed to obtain an optimal and stable production process. Wood has been the most used source for production of NFC fibers. However, fibers from annual crops such as flax, hemp, kenaf, sisal in addition to agricultural residues like sugar cane bagasse, wheat and rice straw has attracted interest

due to their wide abundance, low-cost, availability and renewability (1). Presently, conversion of such agricultural waste into value-added materials is thus of high industrial interest.

Many researchers have shown that NFC has great potential in papermaking applications; as strength enhanser, to enhance barrier properties in food packaging, to improved paper gloss, to reduce paper basis weight and to enable smart packaging (3). Addition of NFC to paper yields significant increment in the corresponding tensile index, however the sheet drainage is impaired.

Cationic polymers have been used as a fixative for retention of NFC as well as for better suspension drainability. Recently, we have shown that MFC produced from sugarcane bagasse can be applied as strength enhanser in soda bagasse paper (1). Here, this paper is intending to show the interaction between NFC, fibers and Cationic Polymer (C-PAM) from a structurally point of view and the objective of the current research work is to assess the effects of WS NFC on relevant properties of paper produced from soda wheat straw pulp. Bleached soda wheat straw pulp was used as raw materials for the production of NFC. The pulp was firstly highly refined (30000 revolutions) then enzymatically treated (Endoglucanase, 0.17 µL mono-component endoglucanase (Novozyme 476, 5 ECU/_L) per gram fiber 50°C, 2 hours). Different NFC enzymatic pretreatment and without pretreatrment grades were produced by homogenization using an ATS AH Pilot High Pressure Homogenizer (HPH) operated at 1500 bar pressure. The pulp consistencies during homogenization were 1%. The CNF samples were collected after 5 passes and will be referred to as “UWS NFC” and “EWS NFC” for the mechanical and enzymatic produced NFC, respectively. Bleached soda wheat straw pulp was produced in laboratory. This pulp was used for the hand-sheet production. The initial freeness of the pulp was 650 mL, CSF (Canadian Standard Freeness). The soda wheat straw pulp was swollen, disintegrated and refined in a PFI mill according to the ISO 5264-2 standard and stored at approximately 10% (w/w). Impurities, such as remaining metal ions, were removed by hydrochloric acid treatment. Cationic Polyacrylamide (C-PAM) was kindly supplied by BASF SE in Germany. C-PAM was diluted to a solution concentration of 0.05% 12 h before application. The PAM applied in this study was Percol®540) and had low charge density and high molecular weight properties. The NFC suspension (1% or 5% MFC) was added to the fiber suspensions. The resulting fiber/NFC suspensions were mixed for 20 min at 500 rpm before C-PAM (0.1 or 0.3%) was added. After 20 min of additional

mixing at 500 rpm, hand-sheets were formed in a laboratory sheet former. Different series of hand-sheets produced with varying amounts of NFC and C-PAM. The target grammage including MFC was 60 g/m2. The hand-sheets were produced according to ISO 52697/1-1979(E) and further air dried in a climate room. The standards used for conditioning and physical, mechanical and optical paper properties. The results have shown that enzymatic pretreatment has facilitated the fibrillation of the fibers. The sample EWS NFC has a minor fraction of poorly fibrillated fibers, compared to the UWS NFC sample. Also, it seems that enzymatic pretreatment can reduce the energy consumption of fiber during homogenization. As expected, addition of UWS NFC in different amounts increased the drainage time of the suspensions considerably (Fig. 1) compared to the wheat straw pulp (starting pulp). However, application of C-PAM decreased the retention time of the suspensions which contained NFC.

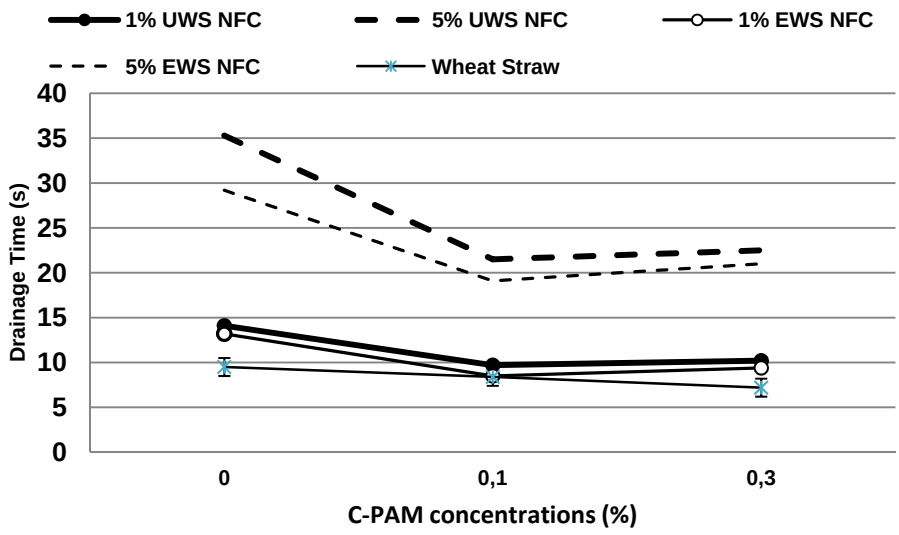

Fig. 1. The effect of different contents of NFC and varying percentage of C-PAM on the drainage time of hand-sheets produced from soda wheat straw pulp.

The drainage time can be related to the dewatering efficiency of the pulp in a paper making process, which in turn affects the energy required to press and dry a given furnish. Therefore, High level addition of NFC will be challenging in an industrial situation due to the high level of energy that would be necessary to dewater and dry the paper. The thickness of hand-sheets decreased with addition of NFC, compared to the thickness of the starting sheet. With addition of C-PAM, the negative fines and fibrils are partly neutralized, the double-layer

forces are reduced and the fines start to flocculate. As a result, the amount of bonds between fibers and fibrils outreaches (Fig.2). The sample containing 5% EWS NFC and 0.3% C-PAM was the thinnest and having compacted structure, indicating that this paper had a more packed structure in comparison to the other hand-sheets.

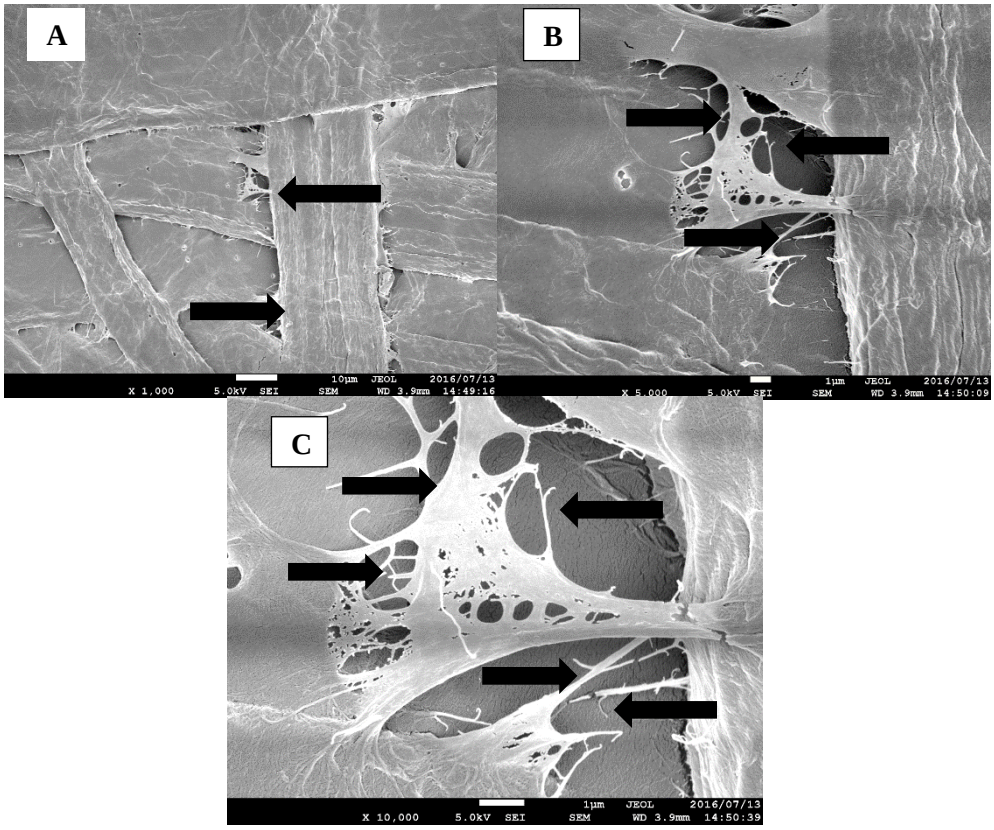

Fig. 2. FE-SEM analysis of sheet structures composed of soda wheat straw pulp, NFC and C-PAM. Soda wheat straw paper with 5% UWS NFC, 0.3% C-PAM and 95% wheat straw pulp. The corresponding images acquired at 1000× (A), 5000 x (B) and 10000 x (C) magnifications. The black arrows indicate the additional bonding between fibers and fibril structures.

Addition of NFC remarkably developed the tensile strength of the hand-sheets (Fig. 3), which was promoted by the creation of bonding between fibrils and fibers (Fig. 2). The strength of the furnish network may have been enhanced by the increased mechanical and chemical entanglement of the fibrils. The results also show that both WS NFCs had a positive effect on the tensile strength (18-38 % improvement). Addition of CPAM fraction increases the tensile index of all samples even samples have no NFC. In this regard, Samples containing 5% EWS NFC yielded higher tensile index compared to

all other samples. Addition of 0.3% C-PAM improved the tensile index with about 22% and 40% for the sheets containing 5% UWS NFC and 5% UWS NFC, respectively. However, it is also worth to emphasize that addition of only 1% MFC increased the tensile index significantly.

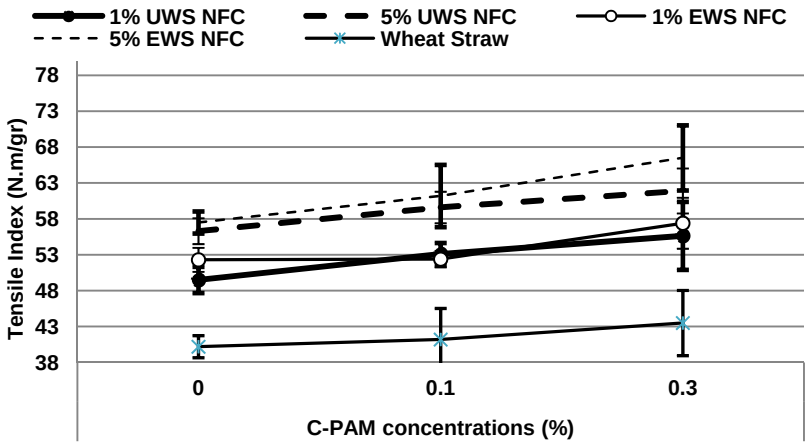

Fig. 3. The effect of different contents of NFC and varying percentage of C-PAM on the tensile index of hand-sheets produced from soda wheat straw pulp.

Conclusion

The current study has illustrated that Nanofibrillated cellulose (NFC) has excellent capability for using as a strength-enhanser additive in paper and paperboard applications. Two different types of NFC (with and without enzymatic pretreatment) were produced from soda wheat straw pulp. The enzymatic pretreatment of fibers facilitated the fiber fibrillation. Both WS NFCs had a positive effect on the tensile strength (18-38 % improvement) and considerably decreased the thickness of the papers with 3-5 wt% dosages. Although this study ascertains the strength-enhancing effect of NFCs but small fractions of NFC in combination with C-PAM can be recommended for writing and printing papers, without major affecting the pulp drainage and paper opacity, which is most interesting from paper machine runnability and paper printability point of views.

Literature

[1] Djafari Petroudy, S.R, Syverud, K., Chinga-Carrasco, G., Ghasemian, A., Resalati, H. (2014). Effects of bagasse microfibrillated cellulose and cationic polyacrylamide on key properties of bagasse paper. Carbohydr Polym, 99:311–318.

[2] Mörseburg, K., Chinga-Carrasco, G., (2009). Assessing the combined benefits of clay and nanofibrillated cellulose in layered TMP-based sheets. Cellulose, 16(5), 795-806.
[3] Osong, H. S, Norgren, S., Engstrand, P. (2016). Processing of wood-based microfibrillated cellulose and nanofibrillated cellulose, and applications relating to papermaking: a review. Cellulose, 23 (1), 93-123.
[4] Zimmermann, T., Bordeanu, N., & Strub, E. (2010). Properties of nanofibrillated cellulose from different raw materials and its reinforcement potential. Carbohydrate
Polymers, 79(4), 1086–1093.

Session IV
„Characterisation of Pulp & Paper“

Improvement of ultraviolet-visible diffuse reflectance spectroscopy for chromophores research

M. Missori(1), A. Mosca Conte(2), L. Teodonio(3), O. Pulci(4), J. Lojewska(5)

AUTHOR INFORMATION


M. Missori

(1) Institute for Complex Systems, CNR, Piazzale Aldo Moro 5, Rome, Italy

(2) ISMN, CNR, Via Salaria Km 29.300, Monterotondo Stazione (Rome), Italy

(3) ICRCPAL, MIBACT, via Milano 76, Rome, Italy

(4) ETSF, MIFP, Dept.of Physics, University of Rome Tor Vergata, Via della Ricerca Scientica 1, Rome, Italy

(5) Faculty of Chemistry, Jagiellonian University,Ingardena 3, Kraków, Poland

Email: mauro.missori@isc.cnr.it

Summary

Paper represents a striking example of optically inhomogeneous material characterized by the presence of light scattering which affects both absorption and reflectance measurements. In the visible (Vis) and ultraviolet (UV) spectral regions scattered light usually exceeds absorbed light so largely that it is no longer possible to obtain a useful absorption spectrum of paper without taking account of scattering even for thinned samples.

On the other hand absorption spectra measured over the UV-Vis region give direct information on the nature and chemistry of the chromophores that regulate the optical quality of paper. Kubelka-Munk (K-M) theory, recently extended by Yang and Miklavcic, allows an estimation of paper absorption spectra from measurements of diffuse reflectance spectra. This is true for low-basis weight sheets, i.e. optically thin samples. For optically thick sheets, singularities in the K-M equation for the scattering coefficient (S) prevents for the recovering of the optical absorption.

In this presentation a new approach to estimate S and, consequently, the optical absorption from reflectance measurements of highly absorbing paper sheets will be shown. This approach is based on the estimation of S in the wavelength region where samples are optically thick, obtained by using the measured diffuse reflectance spectra. This allows the optical properties to be

recovered up to the UV region where paper sheets can show strong chromophores' absorption.

Results have been compared to theoretical ab-initio quantum-mechanical computational simulations carried out within time-dependent density functional theory. In this way quantitative chemical information on the chromophores causing paper yellowing can be obtained in non-destructive way. Applications to modern paper samples aged in different environmental conditions and highly absorbing in the ultraviolet region, as well as ancient paper used by Leonardo da Vinci for its drawings, will be shown.

Introduction

A medium is optically inhomogeneous when it is characterized by variations of the dielectric function ε over distances comparable to those of the wavelength of light impinging on it (1). In general, irregularities in the propagation medium, presence of particles, or roughness in the interface between two media are cause of optical inhomogeneity. This induces the scattering of light, namely the deflection of photons from a straight path. The complicated inner structure of paper, composed of fibres, pores and particulate, is responsible for light scattering (2)

Scattering makes transmission measurements of paper sheets more difficult than diffuse reflectance (3). Therefore obtaining the absorption spectrum from the measured diffuse reflectance of a sheet is of great practical importance for the study, in detail, of the chemistry of chromophores which contribute to the yellow colour of paper. The Kubelka-Munk theory (3), widely used in paper optics, has been recently extended by Yang and Miklavcic (Y-M) to describe a wider range of optical absorption by taking into account the effect of photon scattering on path length of propagating light (4). However, even with these advances, for optically thick sheets singularities in the K-M equation for the scattering coefficient (S) prevents for the recovering of the optical absorption.

In this work an approach for recovering scattering and absorption coefficients from non-destructive reflectance measurements of paper sheets is presented. In this way, the optical properties can be obtained up to the ultraviolet (UV) region where chromophores' absorption peaks are localized. This knowledge combined with calculations of chromophores' theoretical spectra allows chemical information at the molecular level to be extracted.

Methods

In the K-M theory the change in light transmittance due to scattering and absorption are characterized by the phenomenological scattering coefficient S. and K, respectively. K is related to the concentration chromophore responsible for paper yellowing. K-M theory provides expressions connecting diffuse reflectance measurements to S and K. The most famous result of K-M theory is $A_{KM} = \frac{K}{S} = \frac{(1-R_\infty)^2}{2R_\infty}$, where A_{KM} is the so-called K-M pseudo-absorption or remission function and R_∞ is the reflectance of a sample with infinite thickness. Details of K-M calculations and their application to paper optics can be found in several textbooks (1) (2).

In order to recover K it is necessary to calculate S from reflectance measurements. A suitable method is to measure the diffuse reflectance of a paper sample over two different backgrounds, for instance on a poor-reflecting (black), R_b, and a good-reflecting (white), R_w. (reflectance of black and white backgrounds are R_{bb} and R_{wb} respectively). Therefore (1):

$$S = \frac{1}{t\left(\frac{1}{R_\infty} - R_\infty\right)} \ln \frac{\left(1 - R_b R_\infty\right)\left(R_\infty - R_{bb}\right)}{\left(1 - R_{bb} R_\infty\right)\left(R_\infty - R_b\right)} \quad (1)$$

The reflectance R_∞ that would have an infinite layer of the same sample can be also recovered from R_b, R_w, R_{bb} and R_{wb}. However, if samples are optically thick, R_b and R_w assume the same value, and singularities in eq. (1) appear. In addition, experiments demonstrated an inherent nonlinear relationship between K and S and the physical intrinsic optical properties of the materials, represented by the absorption and scattering probabilities, α and s, respectively. The K-M model was then extended by Yang and Miklavcic (Y-M) in order to face these problems (4). This leaded to new analytical relationships between the K-M phenomenological scattering S and absorption K coefficients and the intrinsic scattering s and absorption α coefficients of a material. Following these advances an approach to estimate s in the wavelength region where samples are optically thick and eq. (1) diverges was recently obtained (5). It is based on the consideration that the portion of radiation scattered throughout the solid angle by a layer of an inhomogeneous medium, in a given time interval, can be expressed as:

$$s_\infty \propto tT(\lambda)\sigma(\lambda)$$

where t is the layer thickness, $T(\lambda)$ is the layer transmission coefficient and $\sigma(\lambda)$ is the total scattering cross-section per unit volume. t depends on the

penetration depth of photons for the incident radiation and can be calculated by the Y-M approach (4). The sample transmission coefficient $T(\lambda)$ can be obtained according to the results of the K-M theory (1). For materials like paper, which are made of a collection of not uniformly-sized rough-surfaced fibres, the total scattering cross-section $\sigma(\lambda)$ per unit volume varies smoothly with the wavelength and can be considered constant (4). Thus, it is possible to demonstrate that:

$$s_\infty(\lambda) \propto \sqrt{\frac{e^{-\frac{1}{\sqrt{1+\frac{2}{A_{KM}}}}}}{\left[4\left({A_{KM}}^2+2A_{KM}\right)\right]^{\frac{1}{4}}}} \quad (2)$$

Eq. (2) (valid for $K > S$ equivalent to $\alpha > s/2$) can be easily calculated from the measured reflectance spectra even in case of optically thick samples and allows experimental measurements of the optical properties of paper to the UV region. In Fig. 1, α, s and s_∞ are shown as a function of λ for a low grammage paper sample where it was possible to recover s from eq. (1) in all measured spectral range: it is possible to verify the goodness of the estimation of s by s_∞.

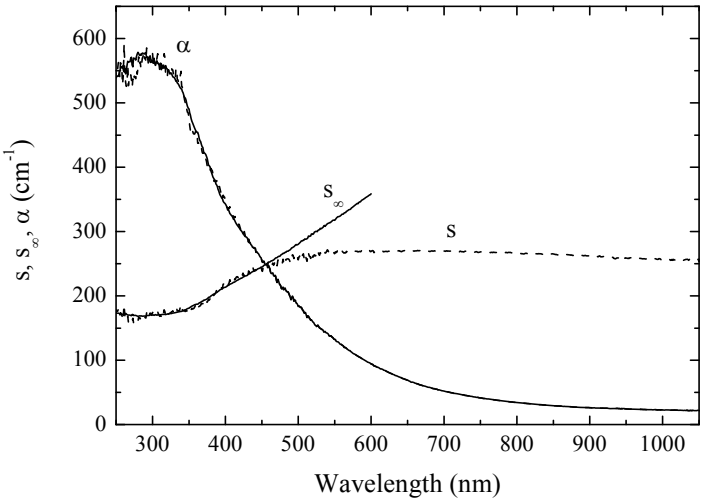

Fig.1 The behavior of α, s and s_∞ as a function of wavelength for a low grammage paper sample. α is show as obtained from s (dashed line) and from s_∞ (continuous line).

Results

Since our method is based on non-destructive reflectance measurements it is particularly suited for diagnostic studies of precious samples, i.e. ancient documents. The 16th-century Leonardo da Vinci's self-portrait presents in rather poor condition due to intense widespread and localized yellowing of the

paper it was made on. It consists of a drawing in red chalk executed on a sheet of handmade paper measuring approximately 33.3 cm x 21.3 cm, with a thickness t of about 220 μm and a grammage of about 124 g/m^2. Absolute diffuse reflectance spectra in the UV-Vis and near infrared regions were measured in different spots by using a portable non-invasive set-up supplied by Avantes BV (The Netherlands) (6). Due to the grammage and heavy absorption at about 450 nm R_b become indistinguishable from R_w within the measurement error and eq. (1) diverged. By applying the approach described before it was possible to extract the intrinsic absorption coefficient $\alpha(\lambda)$ at any λ for comparison with theoretical calculations of chromophores spectra. It should be pointed out that the complexity of the local chemical environment in cellulose precludes the possibility of identifying individual chromophores in the optical spectrum by drawing analogies with reference compounds. For this reason, in order to interpret the results, oxidized cellulose was modelled using different configurations of ketone, diketone, and aldehyde groups within the β-D-glucopyranose units. For each structure, the optical spectra were calculated according to time-dependent density functional theory. It was found that the total concentration of chromophores span from 3 to 6 mmol/100 g of cellulose, depending on the measured spot. Diketone was found to be directly correlated to visual degradation due to the appearance of their absorption peaks in the visible spectral range. Their concentration was found to be about 1 mmol/100 g of cellulose. Most interestingly the relative concentrations of chromophores are very similar to those measured in modern and ancient samples aged in humid environments. This finding tallies with accounts regarding the deterioration which has occurred during its documented history, its misguided conservation behind glass in a closed frame, in particular.

This analysis quantifies the present level of optical degradation of the Leonardo da Vinci's self-portrait which, compared with future measurements, will assess its degradation rate.

Literature

(1) Kortum, G. *Reflectance Spectroscopy (Principles, Methods, Applications)*. Berlin-Heidelberg-New York: Springer-Verlag, 1969.

(2) Pauler, N. *Paper Optics.* Kista, Sweden: AB Lorentzen & Wettre, 2002.

(3) Borch, J. Optical and appearance properties. J. Borch, et al., *Handbook of Physical Testing of Paper*. New York: Marcel Dekker, 2002.

(4) Yang, L. and Miklavcic, S. J., J. Opt. Soc. Am. A, Vol. 22, pp. 1866-1873, 2005.

(5) Missori, M., Pulci, O., Teodonio L., Violante, C., Kupchak, I., Bagniuk, J., Łojewska, J. and Mosca Conte, A., Phys. Rev. B, Vol. 89, p. 054201, 2014.

(6). Mosca Conte, A., Pulci, O., Misiti, M. C., Lojewska, J., Teodonio, L., Violante, C. and Missori, M., Appl. Phys. Lett., Vol. 104, p. 224101, 2014.

Improving the understanding of paper formability by applying new methods of material mechanics characterization

Timo Kuntzsch, Martin Zahel

AUTHOR INFORMATION

Papiertechnische Stiftung Heidenau

Email:
timo.kuntzsch@ptspaper.de

Abstract

The special advantages of natural fibre based network structures as resource-efficient and recyclable multilayer materials make them attractive for a broad range of different fields outside conventional paper usage where they might substitute established materials based on crude oil or other fossils. This enables new applications for cellulosic paper materials, for example in customized three-dimensional packaging solutions and in construction or lightweight applications. An essential prerequisite for utilizing this potential is, however, that usual processing e.g. state-of-the-art plastics technology can be applied to the new paper based materials. Particularly with regard to forming or moulding processes conventional paper or board grades are in general unsuited without further developments of furnish composition, stock preparation or network forming. As a consequence of this unsatisfying situation a number of research activities is ongoing that deals with single fibre modification, control of fibre bond and network characteristics as well as the buildup of special multilayer structures. All these efforts aim at the enhancement of board formability as much as possible to achieve a lower risk level of breaking, unwanted wrinkling and improved processing properties. Unfortunately up to now favourable material and process conditions can only be determined by trial and error using extensive forming trials. In addition it is

very difficult to identify characteristic material parameters that are related to the paper forming ability due to the unavailability of suited characterization methods.

To overcome this unfavourable situation a number of efforts have been taken at PTS during the last years to make available improved characterization and evaluation methods to support material development and simulation activities by providing continuum mechanical parameters and corresponding constitutive laws. Basic mechanical tests are of special interest to determine material parameters directly e.g. by performing in-plane or out-of-plane tension, compression and shear tests, as well as optical deformation analyses with regard to local mechanical stresses and cross direction strain. Moreover, existing laboratory standard measuring procedures, which in some cases operate with rather complex mechanical stress states, have been identified as a suitable complement to basic experiments in answering questions of workability with the help of reconstruction methods using mechanical modelling in reverse engineering. In order to provide a compact but adequate basis for numerical simulations, relevant parameters in adapted simplified constitutive laws for paper in a methodical material modelling framework were identified as well.

The objective of the contribution is to discuss the results of recent experimental investigations on how to control fibre and network structure characteristics to improve the formability of the resulting papers. The forming behaviour was tested for a variety of paper samples using an experimental hydroforming setup (ongoing joined research project with PMV at Technical University of Darmstadt). The findings indicated a very differing forming behaviour of the samples. The undeformed materials were also tested by a setup of conventional and newly developed paper testing methods to identify parameters that might be crucial for the observed behaviour. Fig.1 shows exemplarily the “good” or “bad” forming behaviour during the tests due to a differing multilayer structure for the very samples. For the investigated samples also the strain field in tension direction during a conventional tensile test was observed. Fig. 2 highlights that a strongly non-uniform strain field also showing an initiating localisation occurs much earlier (at lower strain levels) for the “bad” sample than for the “good” one.

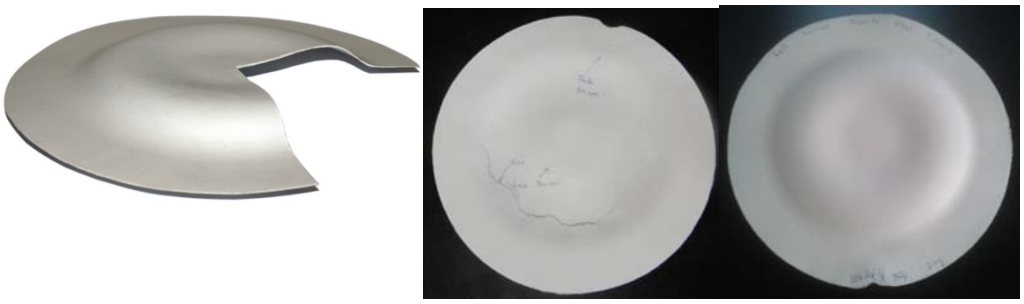

Fig.1: Moulded parts after hydroforming: schematic (left, source: PMV, TU Darmstadt), "bad" forming behaviour (middle), good forming behaviour (right)

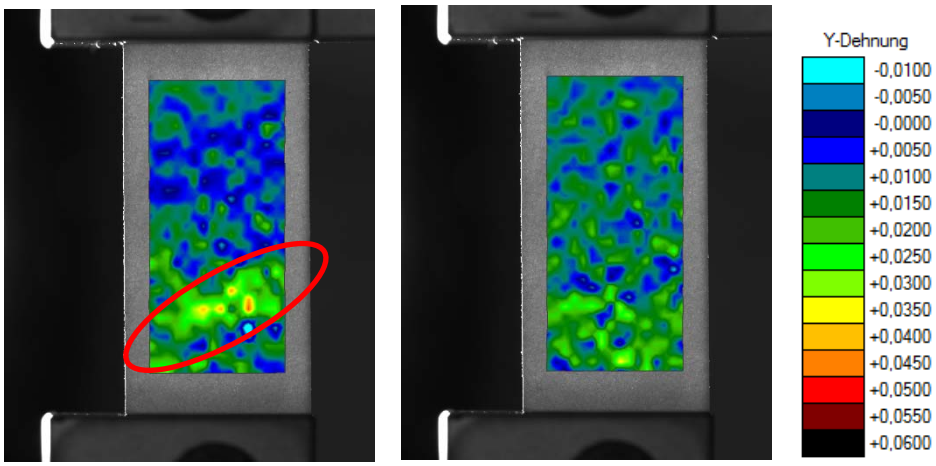

Fig.2: Result of an optical strain field analysis showing a beginning localisation for the "bad" sample (left) whereas the "good" sample (right) behaves more homogeneously, both images for ca. 2% strain level in tensile direction (strain at break ca. 4%)

Soft Radiography for the Structural Characterization of Paperboards

Keller, D. Steven and Hossein, Abedsoltan

AUTHOR INFORMATION

Miami University
650 E. High St.
45056 Oxford, United States

Email:
kellerds@miamioh.edu

Summary

The in-plane distribution of mass, or paper formation, of paperboard products is a critical property that influences strength properties, cockle and curl, as well as the surface uniformity and print quality. In seeking a precise imaging method to study paperboards with grammage values, $w > 130$ g·m^{-2}, and with sufficient spatial dynamic range for statistical significance, we studied the use of 6 keV soft X-radiography, with both film/scanner and storage phosphor screens (SPS), to obtain grammage maps for 70 mm square regions with element size of <10 μm. Beam artifacts were addressed by using image processing.

This presentation describes the investigation of the use of both X-ray film/scanner and storage phosphor plates to acquire grammage maps that have a dynamic range spanning four orders of magnitude from fiber dimensions, ~10 μm, through large scale flocked structures approaching 100 mm. The method that enables the acquisition of images suitable for advanced statistical and spectral formation analysis. The objective of this investigation was to determine if this approach is viable for accurately characterizing the formation of containerboard and high grammage kraft papers. The ash present in samples caused an over estimation of the grammage, and was addressed using an empirical correction based on measured ash content. The results suggest that X-radiography is viable for imaging paperboard formation. It may

also be used to examine the size and distribution of internally contained mineral matter.

Introduction

For most paper and paperboard grades, the distribution of fibrous mass within the structure has a significant influence on the perceived quality and end use performance of the final product. This has motivated the study of paper formation and how unit processes can be modified to control its uniformity.

While optical methods remain the principal method for characterizing formation of papers throughout the industry, such methods are unsuitable for paperboards greater than 130 $g \cdot m^{-2}$ due to the opacity of these products. A successful emissive source must penetrate the web structure and provide sufficient contrast of the material distributed along the transmission path. To minimize effects of beam scattering and to enable the measurement of higher grammage materials, higher energetic sources such as β-ray, soft X-ray and electron beam have been used for both research and industrial application. The Beer-Lambert law provides a valid representation of mass for a given sample zone, i.e. grammage, w, ($g \cdot m^{-2}$), through the relationship:

$$I = I_0 e^{-\kappa' w} \tag{1}$$

where the transmitted radiation intensity, I, is a function of the incident radiation, I_0 and the mass attenuation coefficient, κ', ($m^2 g^{-1}$) of the material.

The use of soft X-ray for imaging the formation of paper was first reported by Lambot [1] in 1947, and later by Pelgroms [2]. Soft X-ray refers to relatively low energetic emission, 1 keV to 10 keV, within the X-ray spectrum. Soft X-rays are readily attenuated by the papermaking fibers and yield a reasonable contrast for images captured by either X-ray film or storage phosphor screens [3]. Farrington [4] and Yuhara et al. [5, 6] used soft X-radiography to study mean fiber orientation in printing papers. More recently, Feng et al. [7] applied the method to tissue and towel papers where the point source illumination resulted in high depth of field projections of the fibrous mass.

Experimental

The 21 samples tested in this study were production retain samples ranging from 26 lb to 56 lb, supplied by the manufacturers. TAPPI standard methods were used to condition,and then measure gravimetric grammage, thickness and ash content (525°C).

Soft X-radiography was conducted using a Minishot X-Ray cabinet (AXR, Corp.). Grammage was internally calibrated using a Mylar internal standard. Exposures were 30 min at 6 kV / 4.5 mA. Films were developed and then scanned using an Epson V700 optical scanner at a 5.3 µm pixel size. Storage phosphor plates were processed using a Storm 860 (Molecular Dynamics/GE Healthcare Life sciences and had a 50 µm pixel size.

Results: Radiography

Figure 1 shows a typical radiographic image acquired by film/scanner. Shown at the left is a contrast enhanced image of the 63.75 mm square region used for analysis. Note the spatial sensitivity to features within the structure, e.g. flocs and fiber shives and dirt particles. Figure 1 right shows a 5 mm subregion, magnified to illustrate the limits on spatial resolution. The digital resolution of the film/scanner is 5.37 µm. Lighter regions indicate low grammage and black regions are fully opaque to X-ray transmission. Fiber fragments and shives can be identified. Inorganic dirt particles are the dark spots with low aspect ratios. The ash content confounds the direct calculation of grammage using the Mylar standard and eq 1, since ash has a higher absorption coefficient resulting in erroneously high values.

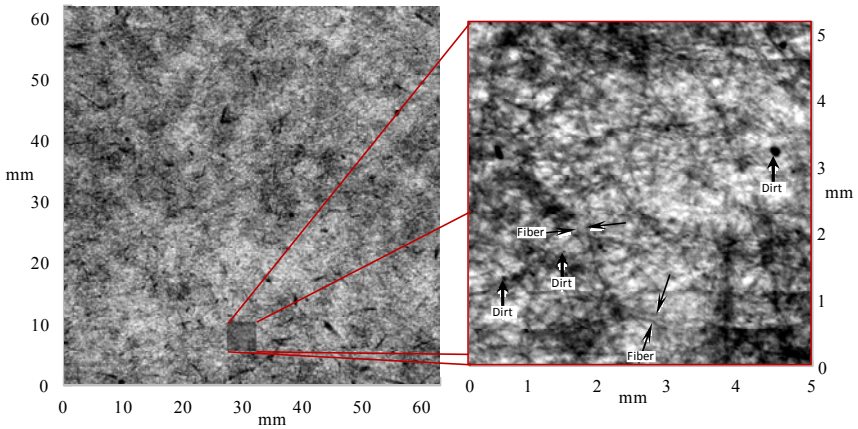

Figure 1. *X-radiograph of a 26 lb. Linerboard. Grammage increases from light to dark. The region of interest (left) and the subregion (right) shown dynamic range of flocs, fiber segments, shives and dirt particles.*

Results: Correction for Inorganic (Ash) Content

In Fig 2., the grammage estimated from X-radiographic images is plotted as a function of the grammage determined gravimetrically using the TAPPI standard for 21 different containerboard samples. The raw radiometric grammage, shown as the symbol (**X**), clearly overestimates the actual

grammage by more than 20 g·m^{-2} for all samples. The concentration and size distribution of the mineral matter in the sample affects the mean grammage and its local distribution. Furthermore, X-radiography alone provides insufficient information to resolve the superimposed spatial distributions of fibrous and inorganic matter.

The first step to address this simply involved the measurement of the ash content in each sample. Ash content measured by firing at 525°C to preserve the carbonate content that is likely present in recycled pulp. It is assumed that the particle size distribution of inorganic matter is not the same in each sample and that the ash is distributed within the sample at concentrations that correlate well with the local fiber grammage. Since the ash contents are under 5 wt.%

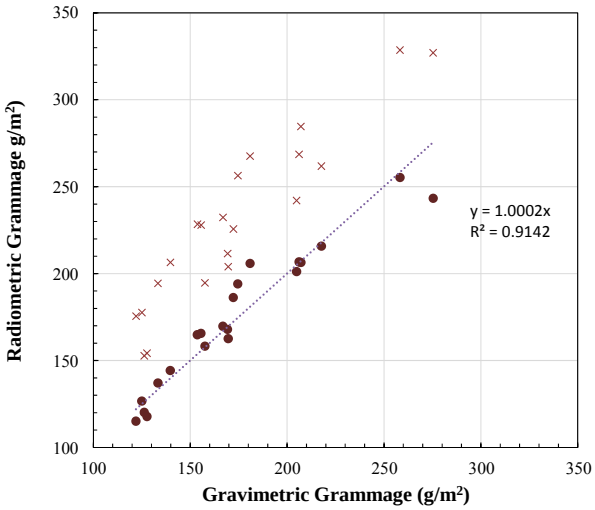

Figure 2. *X-radiometric vs. gravimetric grammage for containerboard samples. The mean radiometric grammage was calculated from a 63.75 mm square region of the film exposure.The uncorrected values (×) and values corrected for ash content (•) are shown The trend line for the corrected values is illustrated as a dotted line.*

except for two samples, the effect of the ash distribution on the overall distribution of mass will be minimal. However, significance will increase as the analyzed zone size decreases.

An empirical analysis of the relationship between X-ray attenuation and ash content was determined. The grammage correction, w_{corr}, was determined from the difference between the radiometric and gravimetric grammage values, and the low temperature ash content, A_{525}, of the samples was fitted to the equation:

$$w_{correction} = 32\sqrt{Ash_{525}} \quad (2)$$

Applying eq (2) to the measured radiometric grammage gives the empirically corrected values shown in Fig. 2. The trend line indicates the equivalence between the radiometric and gravimetric grammages with R^2 = 0.9142. For this sample set, ash content and sample grammage are independent. Therefore, the scatter about the line of equivalence may be due to the nature of the distribution of the ash, or another factor that has yet to be identified. From this relationship, cf. Fig. 2., radiographic images can be corrected to accurately calculate the local in-plane distribution of grammage to some minimum zone size at which the particle size and spatial distribution of the inorganic matter interferes with the determination.

Results and Discussion: Grammage Maps

Figure 3. shows an example of the radiographic image and the corresponding grammage map. The contrast of radiograph was arbitrarily optimized to enhance the structural features for viewing clarity. Grammage maps were determined for each of the linerboard samples from the radiographs at each 5.37 μm square pixel based on the internal calibration. Grammages that are at, or exceed the maximum value for the color range are assigned black. In most

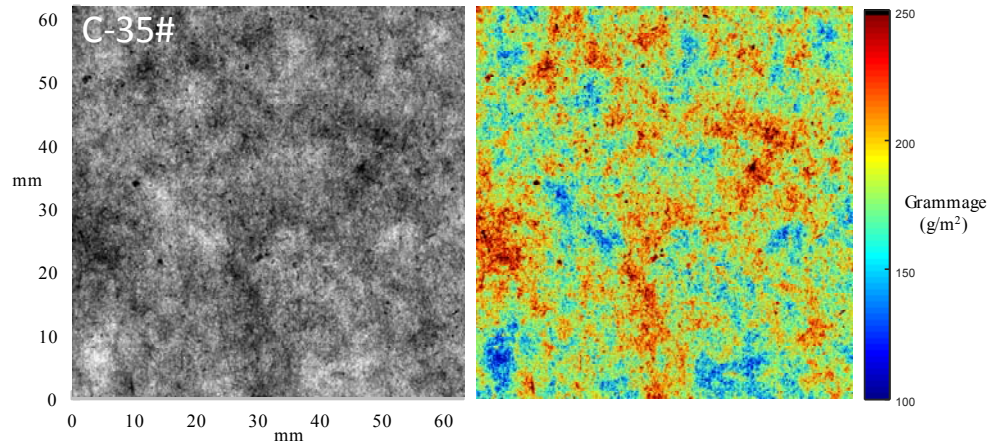

Figure 3. *X-radiographic (film) image of 35 lb. linerboard sample with poor formation by the manufacturer. The contrast adjusted image of the sampled region, shown at the left.The calculated grammage map is shown at the right.*

cases this identifies dirt or fiber shives as suggested by the size and shape of the black regions. In this example, a 35 lb. sample with $w \approx 170$ g·m^{-2} is shown. The formation of this sample is considered poor due to the high variability and large flocs. There appear to be few shives, although large dirt particles are evident. The ash content is 1.11 wt%. The mineral size

distributions of the different samples appear to vary significantly. For basis weights greater than 26 lb., it is more difficult to detect individual fibers. This is expected since the small grammage differences within, and at the edges of individual fibers that are used to detect position of fibers, either visually or analytically, is lost as the number of fibers along the path length increases.

Results and Discussion: Characterization of Inorganic Matter (Dirt)

Although the inorganic dirt contained in the containerboard samples typically constitutes < 5% of the mass and of grammage, with a much higher value of κ', their X-radiation absorption is much greater than papermaking fibers. Also, the particle size distribution may extend to sizes that are within the spatial measurement range or finer, e.g. <5 μm, which will cause an increased background absorption, causing grammage to appear greater than it actually is.

Based on the empirical relationship between grammage correction and ash content, it is possible to estimate the ash content based on the mean radiographic grammage. As expected, good correlation exists between the estimated and actual ash content for several samples tested in this study. A deeper examination of this relationship, as a function of zone size and considering the measured ash particle size distribution could provide important insight into the influence that dirt properties have on end use performance. While there is a lower limit to the particle size that may be detected, the method may find use for estimating the particle size distribution at larger sizes, e.g. >25 μm. It may also be useful for predicting the ash content of a paperboard using the differences between the mean radiometric and gravimetric grammage.

Literature

[1] H. Lambot. Sur La Microradiographie Des Papiers. *Industrie Chimique Belge* (5) 1947.
[2] J.D. Pelgroms. *Paper Trade Journal* (1):25-32, 1952.
[3] D.S. Keller and J.J. Pawlak. *Journal of Pulp and Paper Science* 27(4):117-123, 2001.
[4] T.E. Farrington. *Tappi Journal* 71(5):140-144, 1988.
[5] T. Yuhara, M. Hasuike and K. Murakami. *Japan Tappi* 41(6):523-529, 1987.
[6] T. Yuhara, M. Hasuike and K. Murakami.. *Journal of Pulp and Paper Science* 17(4):J110-J114, 1991.
[7] D.S. Keller, C. Feng, J.F. Bloch and S. Rolland Du Roscoat. Local S. In *15th Fundamental Reseasrch Symposium*, (ed. S. I'anson), p. 3, Cambridge, UK. The Pulp and Paper Fundamental Research Society, UK, **A**, 2013.

An Operating Window for Acceptable Creasing of Paperboard

Coffin, Douglas W.[1] and Panek, Joel C. [2]

AUTHOR INFORMATION


D.W. Coffin

1 Miami University, Oxford OH USA
2 WestRock, Richmond, VA USA

Email:
coffindw@muohio.edu

Summary

Creasing and folding are essential converting operations in the production of folding cartons. The ability to produce a high–quality crease is essential to the success of the subsequent folding to produce corners that are well formed, free of cracks, and allow for proper interaction of the sides of the carton. The rich history of literature on creasing and folding was reviewed and several key-components were identified as being important to creasing. A kinematic model was developed to characterize a generic creasing operation. The results of this model combined with limits of creasing gleaned from the literature were utilized to develop a window of allowable process parameters leading to acceptable creasing. Laboratory results were obtained to verify that this approach is reasonable. The result is an engineering approach that board producers and converters can use to obtain acceptable creasing in paperboard.

Introduction

The desire to place a well-defined fold into paper is likely as old a paper itself. Whether the application is for secrecy (an envelope), convenience (a book over a scroll), utility (a carton), or even art (origami), the ability of the paper to be creased and/or folded while maintaining appearance and functionality is critical. Consider the folding carton that has been a mainstay for packaged

goods since the early 1900's. De F. Shelton [1] outlined good and bad creasing in his 1876 patent and identified (1) reducing tension on the outer face to minimize cracking, and that by (2) bending against the creased ridge to form an inner bead would yield improved corners. In 1912, Bird [2] showed that delamination of the sheet into multiple layers was essential to produce a good fold from a creased paper.

The earliest scientific study of creasing located by the authors, was that of Halladay and Ulm [3] from 1932. They made observations of the deformation during creasing and folding and developed two terms which they termed the angle of break (γ) and the Half-draw (d):

$$\gamma = \tan^{-1}\left(\frac{4z/c}{1-4(z/c)^2}\right), \text{ and } d = \frac{c}{2}\left[\left(\frac{c}{4z}+\frac{z}{c}\right)\gamma - 1\right] \quad (1)$$

Where z is the crease draw or total travel depth of the male rule and c is the channel width. They suggested that the minimum crease spacing is $L_{min}=\varepsilon_f/d$, where ε_f is the tensile strain at failure. Halliday and Ulm [3] advocated that these equations be used to determine reasonable creasing set-up parameters.

In 1959 and the 1960's, Hine [4-6] presented results of creasing studies including the introduction of equipment to evaluate creasing. He suggested that there was an operating window of creasing parameters that will yield an adequate crease. Emslie and Brenneman [8] re-developed much of the previous work from Halladay and Ulm [3] obtaining the same equations (1) in slightly different form. In addition, they described the geometry of a 180-degree fold and related it to the crease geometry.

A review of these early studies of creasing leads to the following conclusions:

1) During creasing the paper experiences a combination of in-plane tensile strains, bending strains, ZD-compression, and transverse shear resulting in large plastic deformation. The transverse shear strain developed during creasing appears to be important and is related to the geometry of the tooling, the thickness of the paperboard, and the crease draw.

2) If either the ratio of crease depth to board caliper or if the crease width is too small, the board does not form an adequate bead. This could result in excessive stretch of the top liner and possible fracture during bending, but more likely just a fold that is not uniform.

3) If the crease depth is too deep, the damage in the sheet is excessive and board failure may result.

4) The bending moment required to fold a crease can be used to determine the performance of a board to creasing. The maximum moment decreases with crease depth and the measure of Relative Crease Strength, *RCS* (ratio of creased to un-creased maximum bending moment).

For an overview of recent research on creasing, the reader is referred to [9, 10], but for the present work the concept of an operating window for creasing operations alluded to in the early literature [1-8] is investigated.

Development of Creasing Operating Window.

Figure 1 provides a simplified depiction of the creasing geometry and tooling, with parameters identified. From the geometry shown in Figure 1, we developed new relationships for the angle of the crease, θ, and a dimensionless crease draw, χ, as:

$$\tan(\theta) = \frac{\sqrt{(1-\kappa)^2+\lambda(2+\lambda)}-(1-\kappa)(1+\lambda)}{\lambda(2+\lambda)} \ , \ = \frac{\kappa(2-\kappa)}{2(1-\kappa)} \text{ for } \lambda = 0 \qquad (2)$$

$$\chi = \frac{\theta+\sqrt{(1+\lambda-\sin(\theta))^2+((\kappa-1+\cos(\theta))^2}}{1+\lambda} \text{-1} \ , \qquad (3)$$

where $\kappa = z/(r_c + r_a + t)$ and $\lambda = \frac{(c-a-2t)}{2(r_c+r_a+t)}$ are the dimensionless crease displacement and crease clearance respectively.

Equations (2) and (3) illustrate that the severity of a creasing operation can be described with two dimensionless parameters. Our initial studies show that the RCS strength correlated very well with the crease angle and can serve as a lower limit to the minimum extent of creasing required as defined by an angle of break for the paper. For severe creasing we found that the dimensionless draw correlated well with the percentage of cracked crease and can be used as an upper limit defined by a maximum crease draw.

One can form a range of creases that yield a fold that does not induce damage, but that could lead to other issues. Thus, we place an upper limit on creasing geometry that would lead to loose corners and a lower limit that would likely lead to inadequate bead formation. These limits do not just depend on the dimensionless parameters but the specific scale of the crease.

The result of all these considerations is a creasing operating window as shown in Figure 2. The shaded region represents the set of crease-tool parameters that one could expect to obtain adequate 180-degree folds.

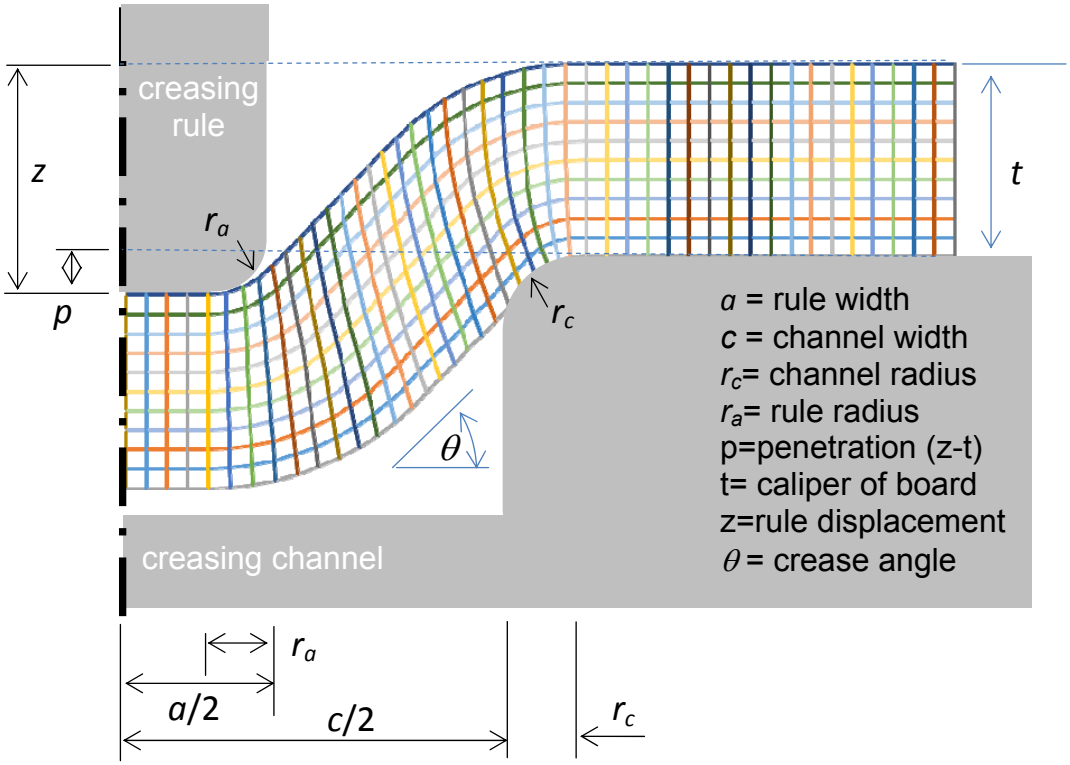

Figure 1. Idealized creasing geometry

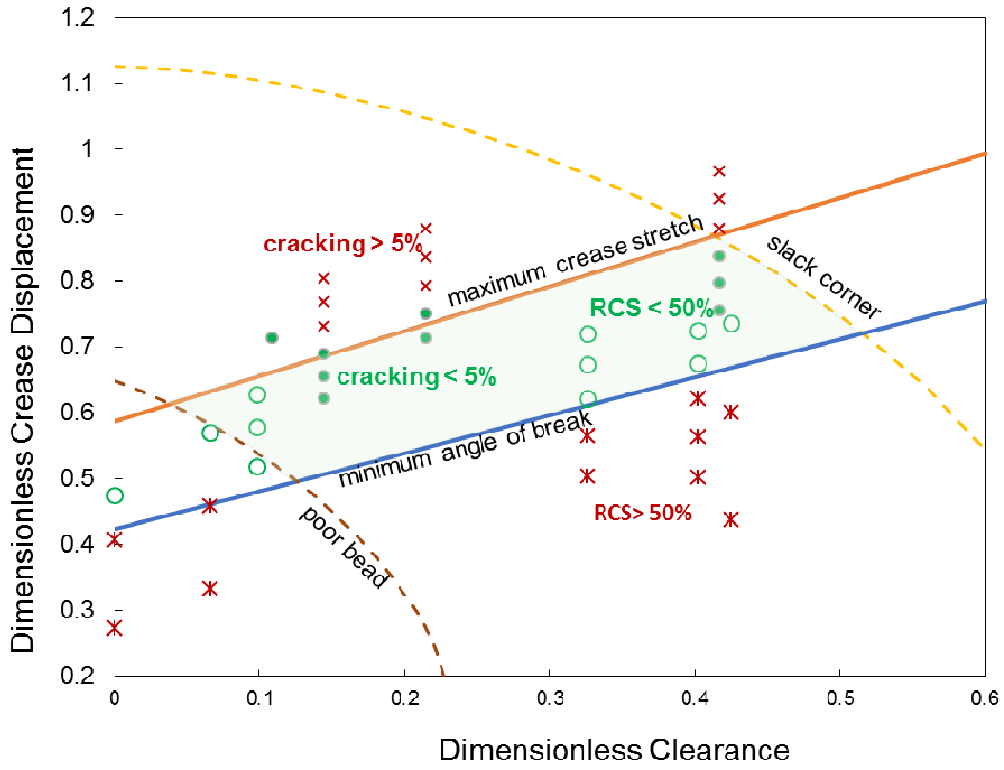

Figure 2. Example of Adequate Creasing Operating Window (shaded region). Markers represent a composite of data. The dashed line limits are for a specific rule radius.

The data contained in Figure 2 was taken from a composite set of laboratory creasing experiments and used to show good creasing (circles) and poor creasing (x's) based on cracking for the upper limit and RCS strength for the lower limit to illustrate the concept of the operating window. The sloped lines are from Equations (2-3) for constant draw and angle of break. The dashed curves represent the self-imposed limits of a loose tight corner for a specific rule width.

Conclusions

The kinematic description of an ideal crease that includes corner radii appears to adequately capture the severity of creasing operations and allows for the development of an operating window of creasing tooling for a given paper. The preliminary experimental results suggest a minimum crease angle (angle of break) is required to get a crease that will easily delaminate and form a bead upon folding. Furthermore, a critical draw ratio limits the extent of creasing that will not lead to folds that crack.

Literature

1. Shelton De F. E, Improvement *in Paper Boxes*, US Patent 183423, Oct. 17, 1876.
2. Bird C. S. *Method of Reinforcing Paper Boxes*, US Patent 1,022,923, April 9, 1912.
3. Halladay J. F. and Ulm R. W. K. "Creasing and Bending of Folding Boxboard," *Paper Trade Journal*, TAPPI Section, **108**(5): 36:40 (Feb. 2 1939)
4. Hine, D. J. "Testing boxboard creasing," *Modern Packaging* **32**(8):122-128 (1959).
5. Hine D. J. "Creasing for Appearance, Research and the Carton Maker Part 1. (1964) (Possibly published in "The Converter" December 1964.)
6. Hine D. J. "Creasing for Performance, Research and the Carton Maker Part 2. (1965)
7. Hine D. J. "Creasing for Consistency, Research and the Carton Maker Part 3. (1965)
8. Emslie A. G. and Brenneman R. S. "A Theoretical and Experimental Study of the Scoring and Bending of Boxboard," *Tappi Journal* **50**(6):289-297 (June 1967)
9. Nygårds M. "Behavior of corners in carton board boxes." *Mechanics of Paper Products ed.* K. Niskanen, de Gruyter, (2012)

Huang H., Hagman A., and Nygårds M. "Quasi static analysis of creasing and folding for three paperboards." *Mechanics of Materials* **69**(1): 11-34 (2014)

Characterizing hydraulic properties of paper coatings using FIB-SEM tomography and 3D pore-scale modeling

H. Aslannejad[a], S.M. Hassanizadeh[a], A. Raoof[a], S.A.M de Winter[a] , N. Tomozeiu[b]

AUTHOR INFORMATION

[a] Department of Earth Sciences, Utrecht University, Utrecht, The Netherlands
[b] R&D Department, Océ Technologies B.V., P.O. Box 101, 5900 MA Venlo, The Netherlands

Email:
H.Aslannejad@uu.nl

Abstract

Paper used in printing industry generally contains a thin porous coating layer covering a relatively thick fibrous base layer. The three-dimensional pore structure of coatings can have a major effect on fluid flow patterns inside the paper medium. As such, understanding and quantifying the flow properties of thin coating layers is crucial. Pore spaces within the coating are relatively small with an average size of about 180 nm. We have used focused ion beam- scanning electron microscopy (FIB-SEM) to visualize nano-scale pore structures and image post-processing resulted in the reconstruction of the entire pore space of the coating in three dimensions. The 3D pore space was analyzed in detail for the porosity, pore size distribution, and the permeability of the coating. Porosity values were obtained directly from the 3D FIB-SEM images and the permeability was estimated by solving the Stokes equation. Determining the pore size distribution and the permeability for different domain sizes resulted in a representative elementary volume (REV). The REV was found to be 60 μm^3 which is well within the volume analyzed by the FIB-SEM. The porosity and the permeability of the REV were 0.34 and 0.09 mDarcy respectively. Subsequently, the capillary pressure-saturation (P_c-S) and relative permeability curves were determined for the REV, using the pore morphology method. From the P_c-S curves it was found that the coating has a high air entry suction, which is very favorable for printing purposes (as the ink or droplet) will invade the coating nearly immediately (as soon as the droplet touches the surface of the coating layer). The results are essential for improved understanding of the coating layer in the inkjet industry to optimize the penetration depth and spreading of ink on and within paper substrate.

1. Introduction

During inkjet printing, once an ink droplet reaches the paper surface, spreading and evaporation processes determine overall ink penetration. The dynamics of these processes affect the final print quality. In order to optimize

ink penetration during inkjet printing, paper is often coated with a layer of ultra-fine mineral particles, usually composed of kaolin or calcium carbonate and bound together with an adhesive. Surface-modified calcium carbonate and clays, colloidal-precipitated calcium carbonate, alumina silicate and zeolite are considered to be among the most promising pigments [1] and [2]. The extent of ink penetration depends on the structure of this coating as well as on the characteristics of the employed ink [3].

The porosity and pore size distribution of a coating determines the extend, speed and final distribution of the injected ink. Fig. 1. shows an overview of the processes that occur during inkjet printing [4]. The specified times in Fig. 1 indicate the approximate moment at which various phenomena are expected to start. The forces that cause lateral spreading of a droplet on the paper surface competes with the capillary suction of liquid into the paper [5]. Capillarity is the dominant force drawing ink into the pore structure. Micro capillary penetration starts typically within 0.1 ms after the droplet arrives [6] and [7].

Several studies have been conducted to explore the performance of ink in different papers. Dalton et al. [8] used secondary ion mass spectrometry and X-ray photoelectron spectroscopy (XPS) to determine the final distribution of ink components in a single cross section of paper samples.

Alam et al. [9] used computational fluid dynamics simulations in order to calculate permeability for three packing structures which represented the coating layer of paper. The calculated permeability values were within one order of magnitude of experimental equivalents. Matilainen et al. [10] studied the spreading and penetration of bio-based ink, containing laccase enzyme and its substrate ABTS, on three different coated printing substrates. Optical and confocal microscopy techniques were used, together with a tape laminating method [10]. The pore size distribution of the printing substrate was explored using Mercury Porosimetry. Pore sizes were found to be 1–5 μm for base layer, 0.05–0.5 μm for coating pores. Air permeability was also measured (6 ml/min).

Lamminmäki et al. [11] studied the coupled effect of pore structure and swelling of the binder of coating layer on ink imbibition (penetration and spreading). The coating structure was studied with respect to its absorption behavior for polar and non-polar liquids. The measurements were performed on compressed tablets containing polyvinyl alcohol (PVOH) or styrene acrylic latex (SA) as the binder. Results indicated that small pores play a dominant role in the ink imbibition process during the first two seconds Simultaneously, water diffusion into the hydrophilic PVOH binder caused its swelling. The swelling reduced the diameters of the remaining pores, thus slowing capillary flow. In contrast, the SA latex binder did not absorb water. The dominant process hence was found to be capillary absorption.

Short time-processes during the early stages of ink penetration cannot be described using equilibrium flow simulation methods. The liquid advance in a porous structure is usually simulated using some approximate method that is consistent with experimental data [11]. A well-known method is based on using Lucas–Washburn equation, which assumes that the coating consists of a collection of vertically placed capillary tubes. The method was improved later by Schoelkopf et al. [12] and Ridgway and Gane [13], who employed the Bosanquet equation [14] to show the role of pore sizes and viscous drag [13].

The spreading and penetration of ink is generally very much affected by bulk properties such as porosity, permeability, thickness, paper moisture content, temperature and layer structure. Gane et al. [15] showed that standard ground

calcium carbonate coatings, because of their relatively broad particle size distributions and low permeability, produce slower initial rates of adsorption of ink than more specialized ones having narrower pore size distributions and higher permeability. They found that coatings with higher specific surface areas and permeability have a faster initial moisture uptake rate.

The aim of this work is to obtain a detailed pore structure of coating layer with a very high resolution. We first introduce a visualization method of extracting the 3D structure of the layer by using FIB-SEM imaging technique; The resolution can be up to 3 nano meter. It consists of many cycles of removing a very thin cross sectional layer by ion beam, and imaging by electron microscopy. Image analysis was used to obtain pore morphological information about the coating layer. Finally, using the pore morphology method, pore-scale simulation was used to calculate effective hydraulic parameters of the coating, which are required for continuum scale-models of ink movement in the coating layer.

4. Conclusion

FIB-SEM is an effective and powerful technique for visualizing the three-dimensional morphology of coating layer of paper. In combination with image analysis methods, it was used to extract 3D pore network of the layer. By analyzing segmented images, pore size distribution and porosity of the layer were determined. The minimum domain size for obtaining stationary meaningful volume for porosity and permeability (REV) was found to be 60 μm^3. P_c- S curves of the layer were obtained using Geo-dict software, based on pore morphology method. By fitting van Genuchten equation to Pc- S curves data, required parameters for calculation of permeability and conductivity were determined. Also, the relative permeability was determined. Hydraulic parameters can be used for characterization of the layer. Also this work makes a contribution to the 3D reconstruction of the coating layer which will be used in continuum models in order to study ink penetration and spreading inside coating layer of paper.

References:

[1] P.B. MALLA, S. DEVISETTI, Pap. Technol. 46 (2005) 17–27.
[2] K. Vikman, T. Vuorinen, 48 (2004) 138–147.
[3] P.J. Heard, J.S. Preston, D.J. Parsons, J. Cox, G.C. Allen, Colloids Surfaces A Physicochem. Eng. Asp. 244 (2004) 67–71.
[4] J. Kettle, T. Lamminmäki, P. Gane, Surf. Coatings Technol. 204 (2010) 2103–2109.
[5] F. Girard, P. Attané, V. Morin, Tappi J. 5 (2006) 24–32.
[6] C.J. Ridgway, P.A.C. Gane, Nord. Pulp Pap. Res. J. 17 (2002) 119–129.
[7] G. Desie, G. Deroover, F. De Voeght, A. Soucemarianadin, J. Imaging Sci. Technol. 48 (2004) 389–397.
[8] J.. Dalton, J.. Preston, P.. Heard, G.. Allen, N.. Elton, J.. Husband, Colloids Surfaces A Physicochem. Eng. Asp. 205 (2002) 199–213.
[9] P. Alam, T. Byholm, J. Kniivilä, L. Sinervo, M. Toivakka, Calculating the Permeability of Model Paper Coating Structures Comprising Incongruent Particle Shapes and Sizes, 2009.
[10] K. Matilainen, T. Hämäläinen, A. Savolainen, T. Sipiläinen-Malm, J. Peltonen, T. Erho, M. Smolander, Colloids Surfaces B Biointerfaces 90 (2012) 119–128.
[11] T.T. Lamminmäki, J.P. Kettle, P.J.T. Puukko, C.J. Ridgway, P.A.C. Gane, J. Colloid Interface Sci. 365 (2012) 222–235.
[12] J. Schoelkopf, P.A.. Gane, C.J. Ridgway, G.P. Matthews, Colloids Surfaces A Physicochem. Eng. Asp. 206 (2002) 445–454.

[13] C.J. Ridgway, P.A.C. Gane, J. Schoelkopf, J. Colloid Interface Sci. 252 (2002) 373–382.
[14] C.H. Bosanquet, Philos. Mag. Ser. 6 45 (1923) 525–531.
[15] P.A.C. Gane, M. Salo, J.P. Kettle, C.J. Ridgway, J. Mater. Sci. 44 (2008) 422–432.
[16] Y. Song, C.A. Davy, P. Bertier, D. Troadec, Microporous Mesoporous Mater. 228 (2016) 64–85.
[17] V.P. Schulz, E.A. Wargo, E.C. Kumbur, Transp. Porous Media 107 (2014) 13–25.
[18] M. Hilpert, C.T. Miller, Adv. Water Resour. 24 (2001) 243–255.
[19] L. Cheng, R. Kirsch, A. Wiegmann, P. Gervais, N. Bardin-monnier, D. Thomas, M. Gmbh, T. Str, Proc. FILTECH Conf. Filtech Exhib. Ger. Meerbusch (2013).
[20] J. Järnström, M. Väisänen, R. Lehto, A. Jäsberg, J. Timonen, J. Peltonen, Colloids Surfaces A Physicochem. Eng. Asp. 353 (2010) 104–116.
[21] M. Van Genuchten, Soil Sci. Soc. Am. J. 44.5 (1980) 892–898.
[22] L. Luckner, M.T. Van Genuchten, D.R. Nielsen, Water Resour. Res. 25 (1989) 2187–2193.
[23] M. Oostrom, J.H. Dane, R.J. Lenhard, Fluid Contents, J.H. Dane and G.C. Topp; Soil Science Society of America , Madison, WI, United States(US)., 2002.

ACA Ash Content Analyzer: Optimizing the filler content in paper and board

Grüner, Giselher

AUTHOR INFORMATION


G. Grüner

emtec Electronic GmbH, Leipzig, Germany

Email:
g.gruener@emtec-papertest.de

Summary

Fillers play an increasingly important role in the paper production, which is also due to the enlarged usage of waste paper.
The waste paper leads to an automatic but unknown supply of minerals in the production process.
With the combustion method, which is traditionally applied in the paper industry, the total content and few selected individual fillers can only be determined through an extremely time- and energy-consuming and in routine operation relatively inaccurate combustion of the samples at different temperatures (± 5% rel., operator dependent!). The combustion method is also disadvantageous due to its destructive measuring procedure.

By the use of the newly developed ACA Ash Content Analyzer with its really new and innovative measuring procedure, the total filler content but also the percentage content of the individual typical fillers in the paper industry can be determined within seconds without combustion of the samples, i.e. nondestructive.

The quick measuring procedure leads to an instant availability of measuring results and therefore allows for an indeed immediate reaction to changes in the process.

Introduction

The content of mineral fillers in paper and board is an important quality and production parameter. Fillers can be dosed or are automatically added with recycling paper. One target of the application of fillers is that it can help to save costs, because the price for fillers is lower than for fibers, but fillers also play a role as functional components to guarantee specific quality parameters.

The use of waste paper leads to an automatic supply of minerals in the production process. This represents a problem, because the single components of minerals and their amounts are unknown. The type of contained minerals strongly affects the characteristics of the finished paper.

Typical fillers in the paper industry are: Clay, Calcium carbonate ($CaCO_3$), Titanium dioxide (TiO_2), Talcum. Minerals can have a positive influence on the degree of whiteness, opacity and on the flatness/printability of paper. Furthermore, their use can enable to reduce the costs of the raw material.

The wanted and unwanted addition of mineral fillers into the paper leads to the need for: permanent and accurate monitoring and control, determination of the total content as well as the single components and their percentage distribution, quick supply of this data, and measurement at different points of the production chain.

Combustion method: Previous method for the measurement of filler content

Traditionally in the paper industry, the ash content or the combustion residue is determined by the combustion method according to ISO 1762 and 2144, DIN 54370, TAPPI T 413 or 211. First, the ash content is determined by combustion at 525°C ± 25°C. Second, the combustion residue is determined at 900°C ± 25°C. The amount of calcium carbonate is determined by the difference between the combustion residue and the ash. With the practically often-used fast combustion at 900°C, which leads to a lower accuracy, the calcium carbonate is not determinable.

Disadvantages of the traditional combustion method

The traditional combustion method has various shortcomings, as it is a time-consuming, user-dependent and a destructive measuring method, which offers only the determination of the content of few selected fillers.

Besides the total content, only calcium carbonate and the combination of titanium dioxide with clay can be measured. The measurement takes approx. 3 – 7 hours in total when requiring high accuracy in accordance with the standards. The delayed availability of measuring results leads to a non-optimal process control as well as overdosage. The measured ash content of one and the same sample varies from company to company, depending on the used standards and combustion temperatures. Although under optimal conditions, it is assumed that the accuracy of the combustion method is ± 2 % (rel.), a relatively inaccurate combustion (± 5 % rel.) of the samples arises in routine operation. Often the quick combustion is used, which takes place 10 – 20 minutes at 900°C (depending on the type of paper), whereby calcium carbonate cannot be determined. The heating of the oven is skipped partly.

These disadvantages led to the need to develop a new measuring instrument to overcome the shortcomings of this method.

ACA Ash Content Analyzer: New method for the measurement of filler content

Emtec's ACA Ash Content Analyzer and its new and innovative measuring principle without combustion of the paper samples, meaning without destruction, enable to determine both within seconds: the total filler content as well as the percentage content of typical fillers in the paper industry. This means that the respective percentage content of calcium carbonate, kaolin, talcum, and titanium dioxide as well as further used mineral fillers in the paper industry can be detected. The results are shown after about 20 seconds. The accuracy of measurement is approx. ≤ ± 0.1 – 0.3 % (abs.) for grade-specific calibration and approx. ≤ ± 1 - 3 % (abs.) for global calibration.

Measuring principle of the ACA

The measuring method of the ACA is based on the combination of X-ray fluorescence analysis and the X-ray transmission. The initial radiation will be generated by a Fe 55 X-ray source. Using complex mathematical functions from the captured X-ray fluorescence spectra together with the measured X-

ray transmission, the concentration of the detected filler components will be calculated. Figure 1 illustrates the measuring principle.

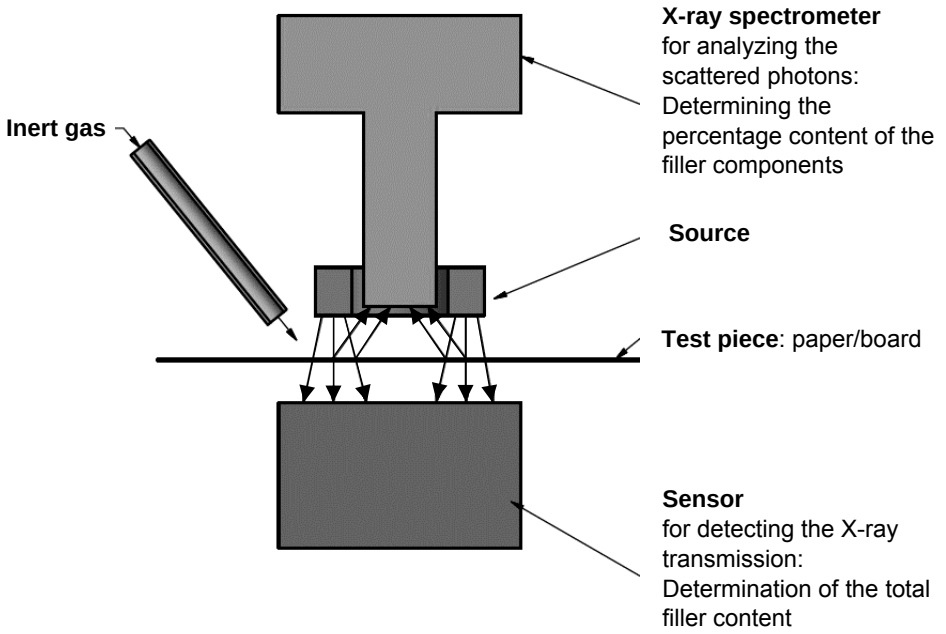

Figure 1: Measuring principle of the ACA

Advantages of the ACA Ash Content Analyzer

The ACA has diverse benefits over the traditional combustion method, as it uses a quick, user-independent and nondestructive measuring method, offering the determination of the content of various selected fillers separately and quantitatively. The results have only low dependency on the moisture of the sample. The device can be applied for efficient process optimization and monitoring, control and R&D. For example, the benefits are:

- Efficient process optimization: Improve of **filler retention**. The different types of fillers have a different retention, which results in unknown content of the individual filler types. With the ACA, the end product can be improved as the dosage of different retention agents can be optimized by a fast, easy and accurate measurement, also lowering the costs.
- Significant savings of working time by rapid determination of the cross profile of the filler distribution
- Optimal process control through prompt measurement results, mainly in case of short cycles of grade changes

- Monitoring the filler development along the entire production process, from raw material input to the finished product. Samples for measurement can e.g. be taken at the dump chest, at the input and output of flotation, bleaching tower, headbox and paper from PM.

  [Suspensions can be examined as follows: Creation of sheets on filter paper using the so-called “Büchner funnel” or a sheet former (also on filter paper), drying, and measurement with ACA.]

- Fast and targeted influence on the filler content respectively **de facto instant response to changes in the process**
- Reduction of process fluctuations
- Targeted control of the filler composition and content along the entire production chain (filler content in waste paper, before / after flotation)
- Faster attainment of the target values of the individual filler components during grade changes
- Targeted, effective product and quality development

Compared to the combustion, immense savings can be achieved such as savings in time, personnel and energy. The consumption of pigments can be reduced, as the accuracy of the ACA and the rapid availability of results allow for a narrowing down of the specifications for the filler content in the finished product (for process optimization).

Conclusions

The ACA replaces the time-consuming traditional combustion methods. Furthermore, it offers significant advantages and delivers information, which is not possible to achieve by combustion. The application of the new measuring instrument guarantees a quick Return on Investment by means of significant savings, while increasing the measuring accuracy over traditional methods.

Fully automatic time dependent contact angle mapping on paper sheets facilitated by the novel liquid needle based dosing technique

Martin Kirchner*, Daniel Frese, Thomas Willers

AUTHOR INFORMATION

M. Kirchner

KRÜSS GmbH, Borsteler Chaussee 85,
22453 Hamburg, Germany
*M.Kirchner@kruss.de

Wettability is an important parameter characterizing paper and pulp [1]. Sorption of water characterizes the quality of paper with respect to its application; tissue paper is expected to be highly adsorbing, packaging paper has to be water repellent. Spreading and the adhesion of inks, glues or hotmelts is a pivotal question for the handling of paper. Wettability is characterized using contact angle measurements. The method has been considered that important that it has been standardized within paper industry [2, 3]. These standards have been established in times when contact angle was a rather subjective technique. Today, high speed camera, digital image processing and automated sample positioning are available. With respect to drop deposition, so far two different ways of applying the droplet onto the surface are most frequently used in paper research and industry: A droplet hanging on a solid needle is carefully brought into contact with the paper and thereby transferred onto the surface. Alternatively, a rocking motion causes detachment of a droplet hanging on a needle which then falls onto the paper surface. Both techniques have their particular disadvantages of a partially not very reproducible way of drop deposition resulting in enlarged standard deviations and reduced repeatability of the measured contact angles. In addition the time “zero”, when the liquid touches the surface is not well-defined which can be disadvantageous for papers that absorb the liquid within a rather short amount of time. Here, we present a new way of applying droplets onto paper surfaces using a liquid jet acting just like a *liquid needle*. This method facilitates drop deposition within less than 0.1 seconds with a well-defined time “zero” and intrinsically eliminates experimental errors caused by the two other drop deposition techniques [4]. From the chemical point of view, paper exhibits a rather heterogeneous surface. Consequently a single droplet will not characterize the complete sample. The more heterogeneous the sample the more droplets should be placed also to identify undesired spots of

heterogeneity. We will use the liquid-needle dosing to do a fully automatic mapping of wettability on different types of paper in A4 sheet size; i.e. the time dependent water contact angle of a minimum array of 20 x 20 drops on the sheet is measured automatically. From those data we would like to deduce a mean value for the wettability of the different papers and, more importantly, precise information about the spatial homogeneity of the papers' surface and / or wettability properties.

[1] Arne Krolle, Thesis, *Benetzbarkeit der Papieroberfläche,* Dr. Hut, 2014
[2] TAPPI T 458
[3] TAPPI 558
[4] M. Jin, R. Sanedrin, D. Frese, C. Scheithauer and T. Willers, "Replacing the solid needle by a liquid one when measuring static and advancing contact angles", Colloid Polym. Sci., Volume 294, Issue 4, pp 657-665; DOI 10.1007/s00396-015-3823-1 (2016).

Highly dispersible synthetic fibers for paper manufacturing

Joel J. Pawlak[1], Ph.D., Hasan Sadeghifar[1], Ph.; John Allen[2] and Steve Perri[2]

AUTHOR INFORMATION

J. Pawlak

[1] Department of Forest Biomaterials,
North Carolina State University,
Raleigh, North Carolina

[2] Eastman Chemical Company, Kingsport,
Tennessee, USA

Email:
jjpawlak@ncsu.edu

Abstract

The use of synthetic fibers in the papermaking process has a number of difficulties associated with it. One of the most significant problems is related to the ability of the fiber to become well dispersed in the papermaking furnish. Without proper dispersion, the formation of the paper sheet suffers greatly resulting in a sheet that has flocs of synthetic fibers. In this work, we use a novel easily dispersible polyethylene terephthalate micro-fiber for the formation of paper sheets with various concentration of the micro-fiber. The associate physical properties are evaluated as well as the recyclability. Results indicate that the fibers are highly recyclable, but exhibit some reduction in bonding characteristics upon recycling. This is believed to be associated with the removal of surface active agents from the synthetic fibers resulting in reduced bond strength between cellulose fibers and the synthetic fibers as well as between the synthetic fibers themselves. These fibers impart unique physical characteristics to the paper sheet in terms of appearance and hand feel that may be desirable for some papermakers. This is one of the first commercially available synthetic micro-fiber that can be seamlessly integrated in the paper making operation without concerns for the process-ability of the fiber.

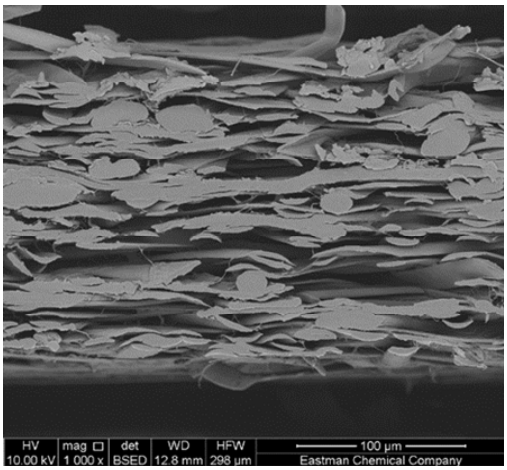

Figure 1: SEM image of 36 % softwood and 64 % microfiber blend shows seamless integration of microfiber into laboratory handsheet.

Thermal fiber orientation tensors – a novel approach for characterizing the local fiber orientation in paper and paperboard

Matti Schneider*, Matthias Kabel* and Heiko Andrä*

AUTHOR INFORMATION


M. Schneider

*Fraunhofer Institute for Industrial Mathematics ITWM, Kaiserslautern

Email:
matti.schneider@itwm.fraunhofer.de

SUMMARY

We estimate the orientation of wood fibers in porous networks like paper, paperboard or fiberboard by computing digital thermal conductivity experiments on micro-computed tomography (µCT) images with artificial isotropic thermal conductivity parameters.

The accuracy of mechanical and thermal constitutive models for porous wood fiber based materials crucially depends on knowing the local wood fiber orientation. Unfortunately, due to the high porosity, the micro-heterogeneity of wood fibers, the high carbon content of organic materials and the unknown additives present in industrial paper µCT-scans often exhibit low contrast and strong artifacts. Conventional image processing approaches encounter difficulties, as they rely upon convex fiber cross sections.

We propose a solution by circumventing the segmentation of single wood fibers in µCT images, by performing thermal conductivity simulations on binary wood fiber structures, where an artificial isotropic thermal conductivity is associated to the fibers and the pore space is considered as isolating. The

local and global temperature fluxes are assembled into a fiber orientation tensor. This method overcomes the limitations of the mentioned local image processing approaches, as individual fibers need not be resolved.

We use our novel method to analyze large three-dimensional µCT -scans and a synchrotron scan of a deep-drawn paperboard sample, serving as the starting point of an accurate micromechanical modelling of the effective anisotropic mechanical behavior of paper and paperboard in the deep-drawing process.

This is joint work with the Chair of Processing Machines and Processing Technology (TU Dresden), the Institute for Machine Tools and Control Engineering (TU Dresden) and Math2Market GmbH.

Introduction

Multiscale models of paper and paperboard offer a deeper understanding of the mechanisms governing their elastic and inelastic behavior. Imaging techniques like micro-computed tomography enable snapshots of the complex three-dimensional fiber networks underlying paper and paperboard. Unfortunately, the obtained data comes in the form of a density value for each voxel (= volume pixel), leading to a severe limitations for mechanical computations on such CT data. For a resolution of the order of 1 µm individual fibers can be segmented, but the mechanical properties of the wood fibers are not isotropic. Rather, they exhibit orthotropic behavior based on their fine-scale structure which remains hidden for such a resolution.

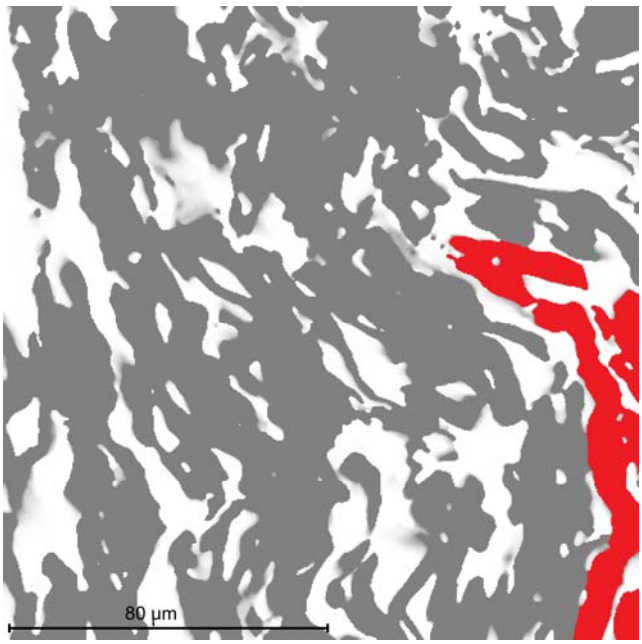

Fig. 1: Synchrotron scan of deformed paperboard with a single highlighted fiber (red)

To enable mechanical simulations it is necessary to furnish the binary three-dimensional images with reconstructed orientation data. Determining the fiber orientation from CT images constitutes a classical task for fiber reinforced polymers, and a variety of image processing solutions are available, e.g. [1]. Unfortunately, these tools are of limited use in the

context of wood fibers, as they rely upon a model fiber, preferably with convex cross section. The reinforcing particles in fiber reinforced plastics are man made and have the shape of bent cylinders. In contrast, the wood fibers in paper and paperboard show a broader variety of shapes. Their cross-sections have (approximately) the shape of thickened ellipses – but their major axes may vary over the length of the fiber, corresponding to a partial flattening of the fiber. The situation becomes even more difficult when the fibers are malformed during the production process, like the deep-drawing of paperboard, considered for instance in Hauptmann et al. [2]. The situation is illustrated in Fig. 1.

In this work we circumvent the identification of single fibers by relying upon digital thermal conductivity simulations on binary volume images. The intuitive idea is the following. Suppose you have a heat conduction wire placed in an insulating medium. If you apply a thermal gradient onto the ends of the wire, the heat is transported along the wire from the end with the higher temperature to the end with the lower temperature. As the surrounding medium is insulating, the temperature gradient is tangent to the wire. In particular, the tangent of the wire can be determined from this heat conduction experiment. The latter observation generalizes to more sophisticated structures consisting, for instance, of pipes with a non-circular cross section. The heat flow is always tangent to the structure and points in the principal direction of a fiber, for instance. Furthermore, the direction of heat flow is independent of the (isotropic) heat conductivity which was associated to the solid.

In the subsequent paragraphs, we will formalize the preceding discussion, exhibit their mathematical properties and apply these so-called thermal orientation tensors to examine the change of paperboard fiber orientation during the deep-drawing process of Hauptmann et al. [2].

Thermal fiber orientation tensor – definition and basic properties

Consider a rectangular box Y occupied by a solid, partially filled with a solid structure S and a porous part Y\S. Fix a scalar thermal conductivity k and solve, for the three cases i=1,2,3 the thermal conductivity equation according to Fourier's law

$\operatorname{div} q_i = 0$ with $q_i = -k\left(e_i + \nabla T_i\right)$,

where e_i is the unit vector in the i-th direction and the temperatures T_i obey periodic boundary conditions. The effective thermal conductivity tensor L is assembled as

(*) $$L = -\sum \sum_{i=1}^{3} \langle q_i \rangle_Y \otimes e_i \ ,$$

where $\langle \ \rangle_Y$ denotes taking the mean value over the cell Y. The effective thermal conductivity tensor L depends on the thermal conductivity k in a linear fashion. Thus, the quantity L/k is independent of k and captures morphological information of the distribution of the solid S within the cell Y. The thermal orientation tensor A^{ThOr} is obtained from L/k by rescaling its trace to one. A^{ThOr} has the following properties:

1. A^{ThOr} is a symmetric and positive definite 3x3-Tensor with trace 1, and has thus similar characteristics as the Advani-Tucker fiber orientation tensor (of second order) [3]. In particular, by an eigenvalue decomposition the principal axes of the specimen and the relative distribution of the fiber orientations in these directions can be determined.
2. A^{ThOr} is defined through the solution of a partial differential equation, which can be solved by a variety of different methods, like finite difference or finite element methods, see [4]. Apart from the discretization error A^{ThOr} is independent of the solution method used. In particular, and in contrast to most image processing methods, the definition (*) of A^{ThOr} does not depend on a variety of finely tuned parameters like the filter width etc.
3. Omitting the mean value brackets in (*) leads to a local thermal conductivity tensor which recovers the macroscopic thermal conductivity L upon averaging. With this local thermal conductivity tensor, a local thermal orientation tensor can be computed accounting for the principal directions of the wood fibers in a paperboard sample.

An example for the computed local orientation tensors can be found in Fig. 2. For the computation of the thermal conductivity fields we use the Fraunhofer ITWM software FeelMath [5].

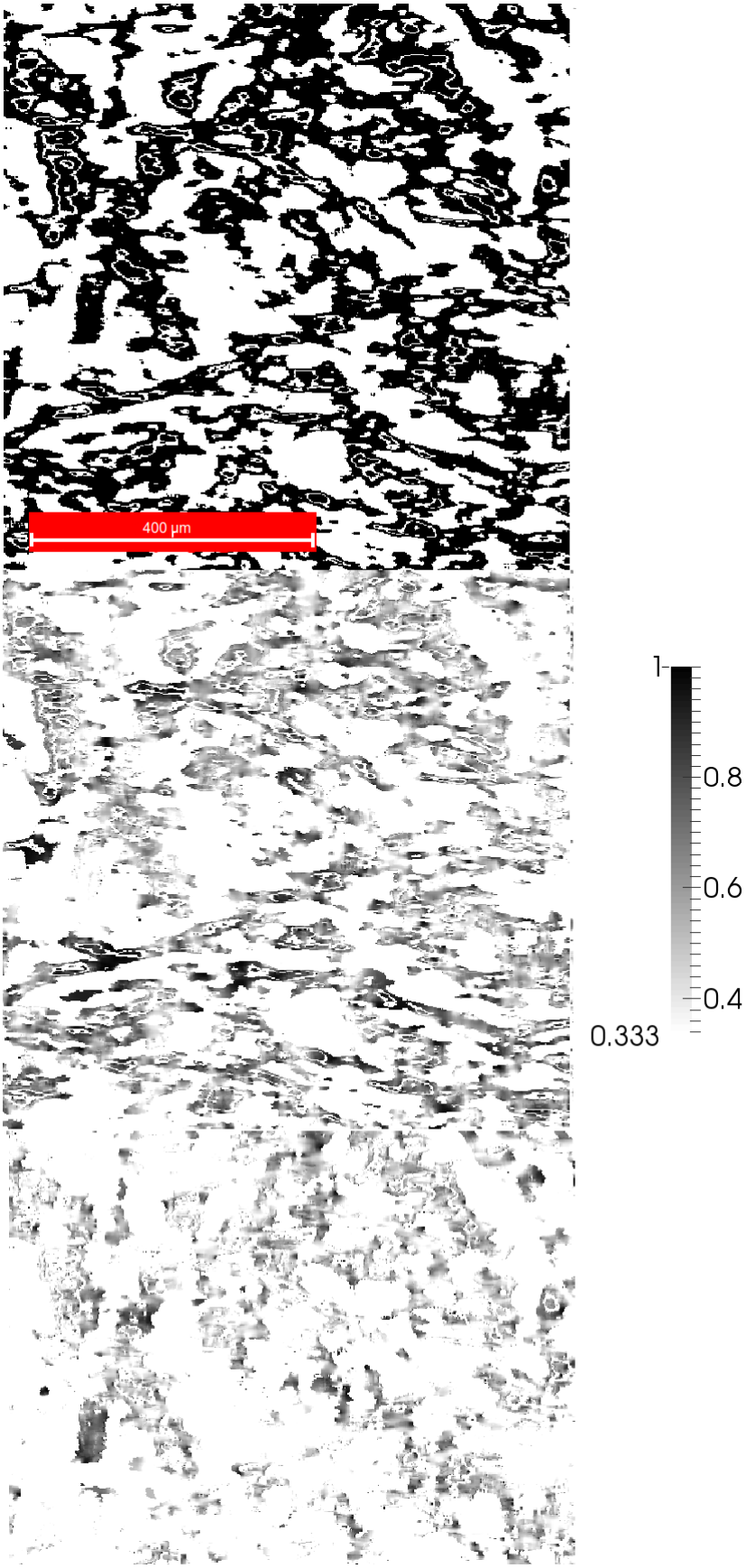

Fig. 2: 500x500 Pixel slice of a µCT-scan of a paperboard sample – geometry (top), Axx (middle) and Ayy (bottom)

Conclusions

We have presented a novel fast and robust method to furnish microCT images of porous paper(board) microstructures with local orientations based upon digital thermal conductivity simulations on regular voxel grids.

Acknowledgements

The IGF-research project 18047BR was supported by the German Federal Ministry for Economic Affairs and Energy through the German Federation of Industrial Research Associations AiF. The authors would like to that all funding organizations. This work was co-financed by the European Regional Development Fund (ERDF). We thank Alexander Rack (X-ray Imaging Group – ID19, European Synchrotron Radiation Facility ESRF Grenoble) and Michael Godehardt (Department of image processing, Fraunhofer ITWM Kaiserslautern) for the µCT-scans.

Literature

[1] H. Altendorf, D. Jeulin, 3D directional Mathematical Morphology for Analysis of Fiber Orientations, Image Analysis and Stereology 28 (3) (2011) 143-153.

[2] M. Hauptmann, J.-P. Majschak, New Quality Level of Packaging Components from Paperboard through Technology Improvement in 3D Forming, Packaging Technology and Science 24 (7) (2011) 419-432.

[3] S. G. Advani, C. L. Tucker, The Use of Tensors to Describe and Predict Fiber Orientation in Short Fiber Composites, Journal of Rheology 31 (8) (1987), 751-784.

[4] F. Willot, B. Abdallah, Y.-P- Pellegrini, Fourier-based schemes with modified Green operator for computing the electrical response of heterogeneous media with accurate local fields, International Journal for Numerical Methods in Engineering 98 (7) (2014) 518-533.

[5] FeelMath – Finite Elements for elastic Materials and Homogenization, Fraunhofer ITWM.

Continuum Modeling of Wrinkles and Explicit FEM Modeling of Paperboard Deep-Drawing

Östlund, Sören[1] and Linvill, Eric[1] and Wallmeier, Malte[2]

AUTHOR INFORMATION

S. Östlund

E. Linvill

M. Wallmeier

[1] KTH Royal Institute of Technology, Stockholm, Sweden

[2] TU Dresden, Dresden, Germany

Email: soren@kth.se

Summary

Deep drawing of paperboard requires the creation of wrinkles for successful forming of a paperboard cup. A phenomenological model for the mechanical response of wrinkles is proposed and based on the assumption that the wrinkles have a mechanical response equivalent to that of a plastic hinge (i.e. the internal moment in the hinge is held constant during deformation). This 1-D model has been verified with two experiments.

Furthermore, this phenomenological model has been expanded into a 3-D continuum constitutive model, which considers the initiation and propagation of wrinkles, large deformations due to wrinkle formation and wrinkle compression, and permanent deformations. This 3-D continuum model

has been compared to and verified against experimental deep-drawing results. Experiments and simulations have been compared in terms of springback, wrinkle propagation, and punch force. Additionally, the model provided insight into the deep-drawing process by establishing better understanding of the initiation of wrinkling.

Introduction

Deep drawing of paperboard has been studied extensively in recent years, including the development of quality analysis techniques [1], the increased understanding of deformation mechanisms [2], and the study of more complex deep-drawn products [3]. With precise control of manufacturing conditions, one can control the extent of wrinkling and produce a high-quality paperboard cup. These paperboard cups could potentially replace some packaging that is traditionally made out of plastic, such as yoghurt cups.

Recent progress regarding the explicit finite element simulation of the deep-drawing of paperboard materials has been limited up to the onset of wrinkling [4]. With current technology and paperboard properties, wrinkling must occur for successful creation of a deep-drawn paperboard cup. In order to capture the entire process in a finite element framework, the model must account for the development and loading of wrinkles in the paperboard.

Constitutive Model

The development, propagation, and mechanical response of wrinkles were included by the assumption that the wrinkles have a mechanical response equivalent to that of a plastic hinge. This assumption was tested utilizing two uniaxial methods: a compression test of an unwrinkled specimen, and a tensile test of a previously wrinkled specimen. In both cases, the plastic hinge approximation was found to match the experimental data well.

The plastic hinge approximation was incorporated into the continuum, elastic-plastic constitutive model previously developed by Wallmeier et. al. [4]. The initiation of wrinkling was determined by the elastic strain energy balance within each element (i.e. whether the more favorable state is the wrinkled state or the unwrinkled state). Once each element wrinkled, the mechanical response of that element was determined by three new material directions: the wrinkle direction, the in-plane direction perpendicular to the wrinkles, and the through-thickness direction. Each direction was coupled to the straining of the wrinkles in the element, due to the geometric, large deformation effect that the wrinkles have on the element. Otherwise, these three new material directions were assumed to be independent from each other.

Explicit Finite Element Model

The same explicit finite element model that was utilized by Wallmeier et. al. [4] has also been utilized with this new constitutive model. Utilizing the explicit finite element method (FEM) allows for combined mechanical and thermal finite element solution with thermo-mechanical contact. The contact friction was modelled as temperature dependent. This model only had one element through the thickness direction in order to accurately capture the physics of wrinkling (i.e. once a wrinkle is formed in an element, it must affect the entire thickness), and elements with only one integration point through the thickness of the element were utilized. Having only one element with one integration point through the thickness causes hourglass stiffening of the bending response. Therefore, the thickness of the element was reduced in the simulation to better capture the bending stiffness of the paperboard.

Results

The results of the simulation were compared to experimental deep-drawing results in three separate ways: the springback of the final cup, the progression and development of wrinkles, and the force of the punch during deep drawing.

The simulated cup after springback is shown *Figure 1*, and the springback was measured and compared to the experimental springback. The average experimental springback was 7.0 mm while the simulated springback was 8.6 mm, which shows fairly good agreement between the experiments and simulations.

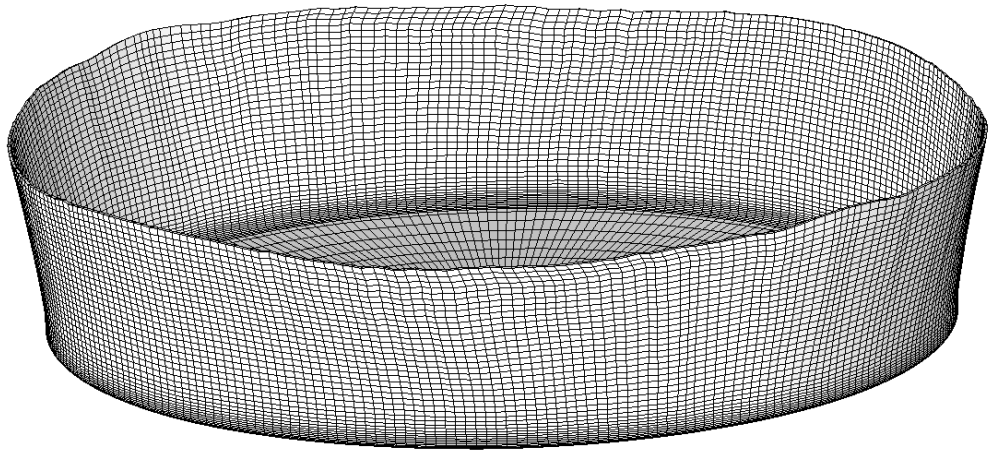

Figure 1: Simulated cup after springback.

Figure 2 shows the progression of wrinkles along the height of the cup, where the number of wrinkles increases with cup height. The cup height is measured

from the base of the cup. For a highly stochastic process, *Figure 2* illustrates that the model is capable of capturing a significant amount of the process with fairly good accuracy.

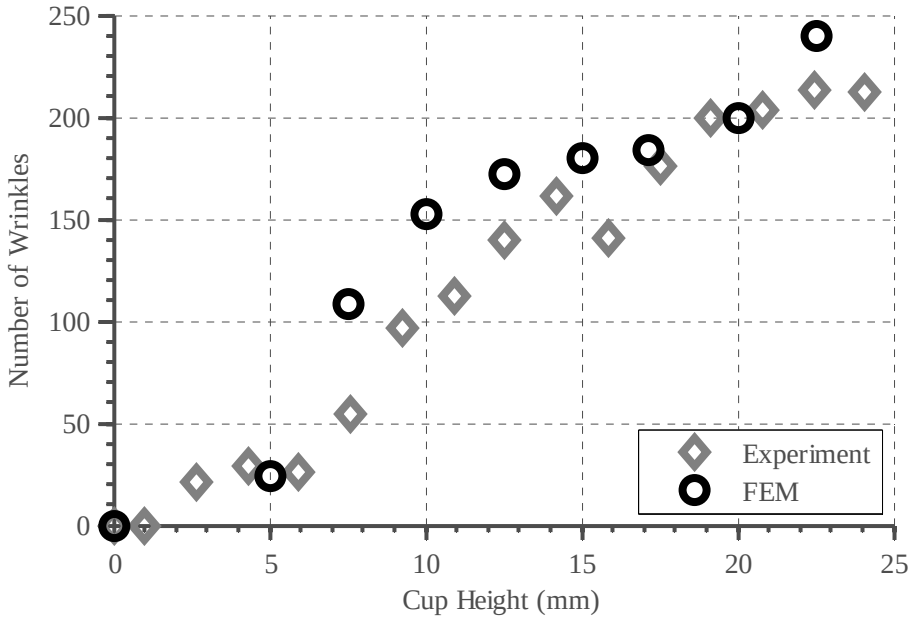

Figure 2: Development of Wrinkles.

The punch force is illustrated in *Figure 3* for both the simulation and experiment. Although the curves do not match exactly, a similar trend is observed in experiment and simulation. The overestimation of the maximum punch force peak in *Figure 3* is likely due to the fact that only one element is utilized through the thickness, so the bending response is not accurately captured even with the reduction in thickness.

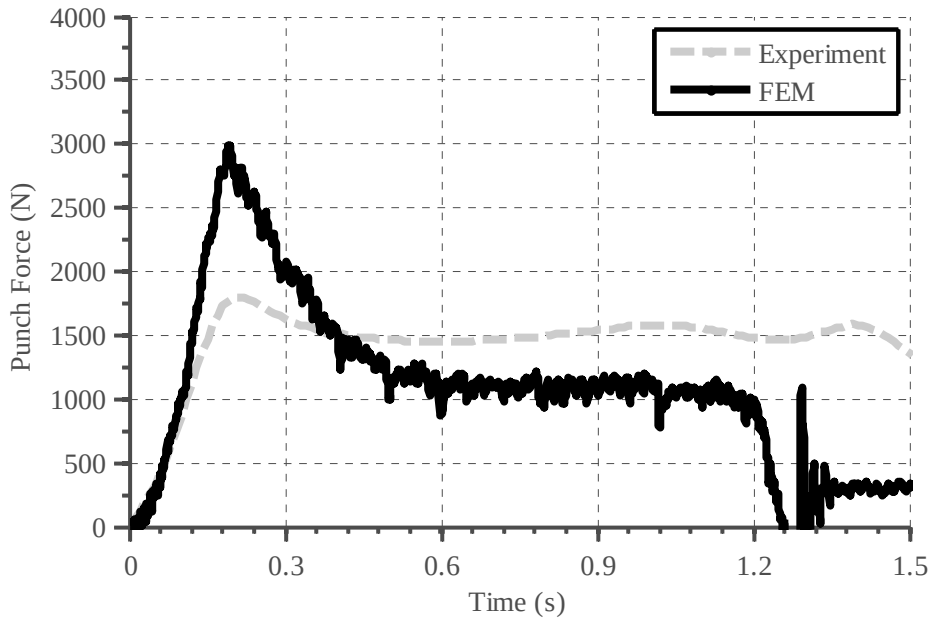

Figure 3: Punch Force.

The above results seem to indicate that the material model qualitatively captures the mechanisms of the paperboard deep-drawing process. In addition to capturing the mechanical response of the deep-drawing process, the model also confirms the suspicion that the first peak in the punch force curve is the same point at which wrinkling begins to occur in the paperboard.

Conclusions

A constitutive model for the wrinkling and permanent deformation of paperboard has been developed, implemented, and validated against simple experiments as well as experimental deep-drawing experiments. The model seems to capture the basic mechanisms in the deep-drawing process, and the model can be utilized to better understand deep drawing of paperboard materials.

Literature

[1] Wallmeier M, Hauptmann M, Majschak JP (2015) *New Methods for Quality Analysis of Deep-Drawn Packaging Components from Paperboard*, Packaging Technology and Science, 28(2):91-100.

[2] Hauptmann M, Wallmeier M, Erhard K, Zelm R, Majschak JP (2015) *The Role of Material Composition, Fiber Properties and Deformation Mechanisms in the Deep Drawing of Paperboard*, Cellulose, 22(5):3377-3395.

[3] Hauptmann M, Ehlert S, Majschak JP (2014) *The Effect of Concave Base Shape Elements on the Three Dimensional Forming Process of Advanced Paperboard Structures*, Packaging Technology and Science, 27(12):975-986.

[4] Wallmeier M, Linvill E, Hauptmann M, Majschak JP, Östlund S (2015) *Explicit FEM Analysis of the Deep Drawing of Paperboard*, Mechanics of Materials, 89: 202-215.

X-ray nanotomography of fibre bonds

Elias Retulainen[1], Joni Parkkonen[2] and Arttu Miettinen[2]

AUTHOR INFORMATION


E. Retulainen

[1:] VTT Technical Research Centre of Finland Ltd, P.O. Box 1603, FI-40101 Jyväskylä, Finland

[2]: Jyväskylä University, Jyväskylä, Finland

Email:
elias.retulainen@vtt.fi

SUMMARY

X-ray nanotomography has successfully been applied for studying individual fibre bonds. X-ray nanotomography is a powerful tool for observing the three-dimensional structure of the fibre crossings with a resolution better than is possible with optical methods. Typical challenges encountered were the demanding sample preparation process, and movement of the sample during the scanning. A long scanning time was needed (60 h), which apparently also degraded the cellulose molecules in the fibre wall. In spite of several problems, a small number of fibre bonds between springwood fibres (unrefined and refined, bleached softwood kraft) were successfully imaged. The results showed that only a fraction (i.e. 15-88%) of the crossing areas were in contact.

INTRODUCTION

The importance of interfibre bonds for strength and optical properties has been recognised for decades. Page et al. [1–3] in the 1960s significantly increased the understanding on fibre bonds. By using light microscopy with polarized vertical illumination, they showed that the overlapping area of two fibres is often only partially bonded. They also assumed that the areas of optical contact are the actual areas of adhesion. Using light microscope in the diffraction interference contrast mode and a special kind of negative staining, it has also been shown [4] that in the contact zone of rayon fibres the “optical contact” is only partial, but it increases with increasing surface charge.

The resolution of optical measurements is, however, limited by the wavelength of light. Scanning and transmission electron microscopy (SEM and TEM) has given valuable information on the cross sectional areas of paper and fibre bonds [5–7] and the three- dimensional structure of them. The bonded fibres have, for example, been claimed to form a saddle structure due to the laterally larger shrinkage tendency of fibres. In an extensive TEM study by Nanko and Ohsawa [7] it was shown that the bond areas of unrefined fibres can contain unbonded areas.

Recently, also fluorescence microscopy and fluorescence resonance energy transfer (FRET) have been applied in order to examine the interphase of two fibres [8]. These methods give information of distances from 1 to 10 nm, which is relevant for molecular level interactions. The information obtained suggested that molecular level interactions take place only in a few areas at the interphase. With the introduction of tomographical imaging techniques using light (confocal laser scanning microscopy) [9] or X-rays (X-ray tomography), new information is available and it is possible to get a better 3D image of paper structure [10,11] and even single fibre bonds.

X-ray nanotomography

X-ray tomography is a non-destructive imaging technique where the three-dimensional structure of a sample is computationally reconstructed from two-dimensional X-ray projection images [12]. Cellulosic materials have been studied at the bulk and fibre network levels, including paper and board [10,11], pigment coatings [13], films [14] and composites [15]. In the context of organic fibrous materials, X-ray microtomography with imaging resolution near 1 μm has routinely been applied to e.g. composite materials and paper. Recent advances in X-ray optics have enabled resolutions even better than 100 nm even in laboratory-scale devices [16, 17].

The objective of this study was to examine the suitability of X-ray nanotomography for fibre bond research and examine how well the fibres are in contact and how the contact areas are located within the crossing areas.

EXPERIMENTAL

The bonds studied were fabricated by placing a highly diluted suspension of fibres between two PTFE plates and keeping them under 50 kPa pressure for 5 minutes, after which the plates were dried in an oven at 80°C for 90 minutes. X-ray tomographic imaging was performed using an Xradia NanoXCT-100 device (at 8 keV). The samples were scanned at 25°C and 30 % relative

humidity for 60 h, during which time 1,081 shadowgraphs were taken over 180 degrees at 65 nm pixel size, 150 nm spatial resolution and 65 µm field of view. The 3D model of the sample was then reconstructed with a voxel size of 65 nm.

To facilitate segmentation of the non-bonded part of the intersection, the image was denoised with Gaussian blur (σ=2) and binarized using the Otsu method [18]. The remaining imaging noise and artefacts caused by the gold particles used as a marker were suppressed by removing all small regions from the image, taking care that regions contributing to the contact area were retained.

The approximate direction of the normal of the intersection area was determined, and a projection of the binary image in the direction of the normal was calculated. The region where the two fibres intersect was determined visually from the projection image. Non-bonded parts in the intersection region were extracted from the three-dimensional image. Their thickness in the direction of the normal was determined, to provide a function $A(d)$ that gives the area of the intersection, where the distance between the two fibres is d.

Based on $A(d)$ and the total area of the intersection region A_0, the relative contact area r as a function of maximum separation of the two fibres, δ, was calculated as

$$r(\delta) = \frac{A(d<\delta)}{A_0}, \quad (1)$$

where $A(d < \delta)$ gives the area of the intersection region where the fibres are closer to each other than δ. The uncertainty of r was estimated based on uncertainties in A_0 and A, the former mainly being caused by the visual estimation of the intersection area and the latter by areas occluded by the gold particles.

RESULTS

Obtaining acceptable images from the samples proved to be more complex than had been assumed. Due to the low contrast typical of biological materials, a long (60 h) imaging was needed. Often some movement in the sample took place during the scanning time, ruining the result. Therefore, only a limited number of fibre bonds (6 bonds) could be examined successfully. An example of the results can be seen in Figs 1–2. Although the fibre bonds inspected were made from springwood fibres that are typically flattened to

ribbon-like structures, the bonding at the overlapping areas was far from perfect. The contact area between the fibres in Fig. 1 was only 16% of the overlapping area. The contact areas in this case seem to be located in the corner areas.

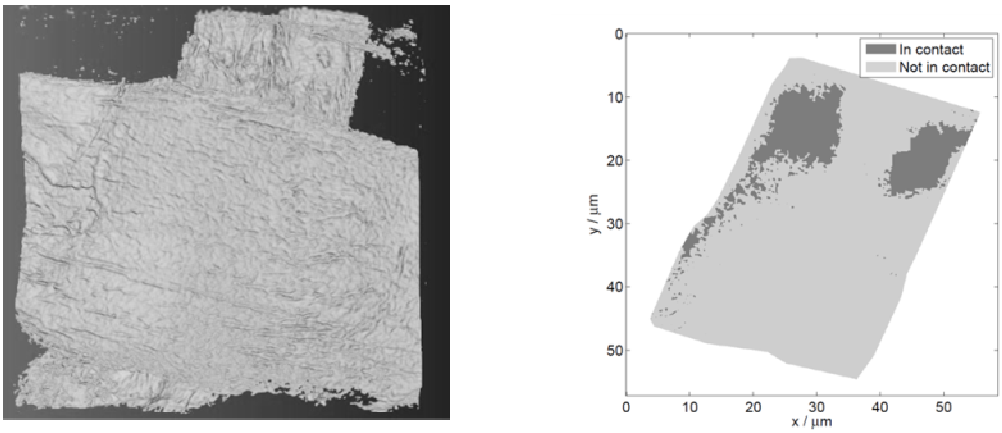

Figure 1. Left: The crossing area of two unrefined springwood fibres. Right: The overlapping area (grey) of the same crossing and the contact area (dark) determined from the x-ray tomography data.

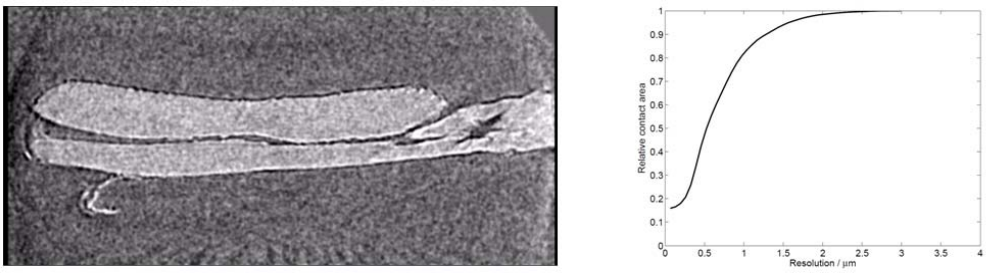

Figure 2. A cross-section of the overlapping area of the same fibres as in Fig. 1. In this cross-section the fibres are not bonded. Right graph shows the relative contact area r(δ) in the whole bond as a function of resolution.

A summary of the properties of the studied fibre bonds can be found in Table 1. There seems to be a large variation between the bonds studied, and the relative contact areas measured are small, as low as 15–16%. The refined fibres seem to have slightly higher relative contact areas, although, due to the small number of samples, the difference is not statistically significant.

Table 1 Properties of the analysed fibre crossings

Sample	Contact area [µm²]	Overlapping area [µm²]	Relative contact area [%]
Unrefined fibres, sample 1	154	1045	15 ± 2
Unrefined fibres, sample 2	1202	4792	67 ± 5
Unrefined fibres, sample 3	246	1548	16 ± 6
Average	**534**	**1462**	**33**
Refined fibres, sample 1	302	1550	20 ± 2
Refined fibres, sample 2	620	926	67 ± 13
Refined fibres, sample 3	1337	1519	88 ± 6
Average	**753**	**1332**	**58**

The determined relative contact areas as a function of separation r(δ) (like in Fig. 2) suggested that the measured contact areas are to a great extent dependent on the resolution.

After the X-ray imaging, some of the fibres measured were inspected in a light microscope, and one bond sample was taken for nanorobotic testing. However, in both cases the fibres were found to be very fragile, and often the fibre broke at the edge of the bond. This is probably due to the fact that X-rays have cut cellulose molecules, reducing the degree of polymerisation below a critical level. Cutting of cellulose molecules and subsequent release of drying stresses may also be one reason for the movements of most samples during scanning.

CONCLUSIONS

A method to examine single fibre bonds using X-ray nanotomography has been developed. X-ray nanotomography is a promising tool for observing the three-dimensional structure of the fibre bonds with a resolution better than is possible with optical methods. The fibre bonds were imaged using a 65 µm field of view and a spatial resolution of 150 nm. Digital image analysis was used to determine the apparent contact area between the two fibres as a function of imaging resolution. A total of six successful samples were analysed, showing a large variation in the structure of the bonds. In spite of several challenges, the methods seem to provide a suitable tool for analysing the 3D structure of fibres and inter-fibre contacts at the crossing area.

Typical challenges encountered were the movement of the sample during scanning and the demanding sample preparation process. The long scanning time (60 h) was also a problem, but that could be improved by utilising staining with heavy metal compounds or applying lower X-ray energy, yielding a better contrast.

Some general conclusion regarding the fibre bonds studied can be made:

- A large part of the overlapping area of two fibres, even in the case of collapsed springwood fibres, can be unbonded.
- The bonded area measured is to a great extent dependent on the resolution.
- Fibre structure affects the location of the bonded area at the crossing area. Bonds are not just crossings of two homogeneous ribbons.
- No saddle type of structures were observed
- There seems to be a great potential to improve the contact area with methods such as fines, polymers, surface treatment, refining etc.

ACKNOWLEDGEMENT

This work has been supported by the PowerBonds project belonging to the EU WoodWisdom-Net program and ExtBioNet project supported by the Academy of Finland.

REFERENCES

1. Page, D. H., Tydeman, P. A. and Hunt, M., A study of fibre-to-fibre bonding by direct observation, in The formation and structure of paper, Bolam, F., Ed. Tech. Sect. British Paper Board Makers' Assoc.: Oxford, 171–193, 1962.
2. Page, D. H., Tydeman, P. A. and Hunt, M., The behavior of fibre-to-fibre bonds in sheets under dynamic conditions. The formation and structure of paper, Bolam, F., Ed. Tech. Sect. British Paper Board Makers' Assoc.: Oxford, 249–263, 1962.
3. Page, D.H. and Tydeman, P.A., Physical processes occurring during the drying phase. In Consolidation of the Paper Web, Trans. IIIrd Fund. Res. Symp. Cambridge, 1965, (F. Bolam, ed.), 371–392, FRC, Manchester, 2003.
4. Torgnysdotter, A., Kuachenko, A., Gradin P. and Lars Wågberg, L., The Link Between the Fiber Contact Zone and the Physical Properties of Paper: A Way to Control Paper Properties. Journal of Composite Materials July 2007 vol. 41 no. 13 1619–1633.
5. Jayme, G. and Hunger, G., Electron microscope 2- and 3-dimensional classification of fibre bonding. In Formation and Structure of Paper,Trans. IInd Fund. Res. Symp. Oxford, 1961, (F. Bolam, ed.), pp. 135–170.
6. Page, D.H. and Sargent, J.W., The fine structure of fibre bonding. In Formation and Structure of Paper, Trans. IInd Fund. Res. Symp. Oxford, 1961, (F. Bolam, ed.), pp 195–200, FRC, Manchester, 2003.
7. Nanko H , Ohsawa J., Mechanism of fibre bond formation. Paper presented at 9th Fundamental Research Symposium 'Fundamentals of Papermaking' held 17-22 Sept. 1989 at Cambridge, UK, pp 783–830.
8. Thomson C., Lowe R., Page D.H., Ragauskas A., Exploring fibre-fibre interfaces via FRET and fluorescence microscopy. J. Pulp Pap. Sci. vol. 34, no. 2, Apr.-May-June 2008, pp 113–120,

9. Moss, P., Retulainen, E., Effect of fines on fibre bonding: Cross sectional dimensions of TMP fibres at potential bonding sites. Journal of Pulp and Paper Science 23(1997)8, J382–J388.
10. Koivu, V., Seppänen, R., Turpeinen, T., Mattila, K., Hyväluoma, J., Kataja, M., Combining X-ray micro-tomography and image analysis to study imbibition and void space in liquid packaging board, Journal of Pulp and Paper Science, 36(3–4), 2010, 1–8.
11. Marulier, C., Dumont, P.J.J, Orgéas, L., Caillerie, D., Rolland du Roscoat, S., Towards 3D analysis of pulp fibre networks at the fibre and bond levels, Nordic Pulp and Paper Research Journal, 2012 vol 27, no 2, 245-255.
12. Kak, A. C. and Slaney, M., Principles of Computerized Tomographic Imaging, IEEE Press, 1988.
13. Järnström, J., Väisänen, M., Lehto, R., Jäsberg, A., Timonen, J., Peltonen, J., Effect of latex on surface structure and wetting of pigment coatings, Colloids and Surfaces A, 363(2–3), 2010, 104–116.
14. Miettinen, A., Chinga-Carrasco, G., Kataja, M., Three-Dimensional Microstructural Properties of Nanofibrillated Cellulose Films, International Journal of Molecular Sciences, 2014, 15(4), 6423-6440.
15. Joffre, T., Miettinen, A., Berthold, F., Gamstedt, E.K., X-ray micro-computed tomography investigation of fibre length degradation during the processing steps of short-fibre composites, Composites Science and Technology, 2014, 105, 127–133.
16. Yun, W., Wang, Y., United States Patent No. US7119953 B2, 2006.
17. Holzner, C., Feser, M., Vogt, S., Hornberger, B., Baines, S.B., Jacobsen, C., Zernike phase contrast in scanning microscopy with X-rays, Nature Physics Letters, 6, 2010, 883–887.
18. Otsu, N., A threshold selection method from gray level histograms. IEEE Transactions on System, Man and Cybernetics, 1979, 9, 62–66.

Modeling multi-phase transport and swelling of paperboard using hybrid mixture theory

M. Alexandersson[1], P. Mäkelä[2], H. Tufvesson[2] and M. Ristinmaa[1]

AUTHOR INFORMATION

M. Alexandersson

[1] Division of Solid Mechanics, Lund University, PO Box 118, SE - 221 00 Lund, Sweden
web page: http://www.solid.lth.se

[2] Billerud Korsnäs AB, Kontorsvägen 1, SE-801 81 Gävle, Sweden

Email:
Marcus.Alexandersson@solid.lth.se

Summary

A thermodynamically consistent model aiming towards application on paperboard based package materials is developed within the framework of hybrid mixture theory. Transport of pore water, water vapor, and fiber-wall water are included as well as mass exchange between the different states of water. Modes of transport considered in the model includes, capillary transport, in-fiber diffusion, vapor diffusion and gas convection. The swelling and its effect on the transport properties is also accounted for. The derived model is used to simulate deformation and edge wicking of hydrophobic and hydrophilic boards.

Introduction

To be able to adapt and develop new competitive paperboard packages it is necessary to understand processes inside the material and how they are coupled. In this work paperboard is viewed as a porous material with fibers and voids. Here the fibers consists of dry material and fiber wall water and the inter-fiber space are filled with pore water and humid air. The fibers have a high affinity towards water, thus water vapor is readily adsorbed from the environment. Similarly pore water is absorbed by the fibers as well as evaporated, the separation of paperboard into phases and constituents is illustrated in figure 1. The presence of water in the fibers strongly

influence the mechanical properties of the board and it is therefore important in many paperboard applications. Swelling of the material due to interaction with water changes the transport properties which consequently alters the material response. In this work a hybrid mixture theory approach is adopted and mixture theory balance laws for mass, linear momentum and energy are established for each constituent [1]. The dissipation inequality is derived in the same fashion as in the work by Bennethum and Cushman [2], Alexandersson *et al*. [3] and is used to derive the macro-scale constitutive relations in a consistent fashion.

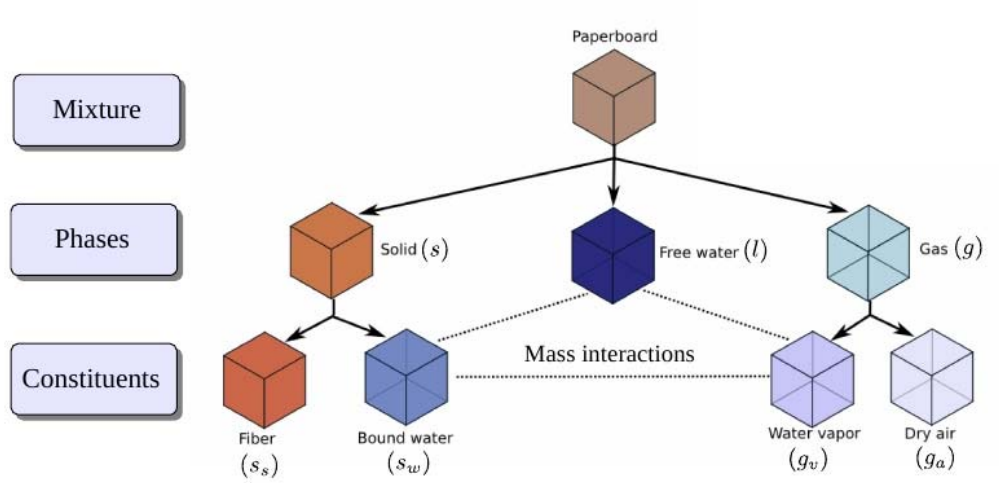

Figure 1: Separation of paperboard into immiscible phases and miscible constituents.

Theory

As a consequence of the up-scaling of the governing equations from micro-scale, information is lost about the micro-scale configuration. On macro-scale the up-scaling results in volume fractions which are not naturally associated with any balance equation, hence additional closure assumptions are required. In this work it is assumed that the free liquid in the pore space is incompressible and that the fiber density evolution as a function of moisture can be given explicitly.

The Helmholtz free energy of the phases are postulated to have the following dependencies: $A_l = A_l(S)$, $A_g = A_g(\rho_{g_v}, \rho_{g_a})$, $A_s = A_s(W_b, \mathbf{F}^{\mathbf{e}}_{\mathbf{s_s}})$, where the subscript (l), (g) and (s) denote free liquid phase, gas phase and fiber phase, respectively. Moreover S is the liquid saturation, ρ_{g_v} the vapor density, ρ_{g_a} the dry air density, W_b moisture ratio of bound water and $\mathbf{F}^{\mathbf{e}}_{\mathbf{s_s}}$ deformation gradient of the solid component. The interface energies are considered to be lumped into the liquid free energy hence the distinction between hydrophilic and hydrophobic material is given by the sign of the derivative and as a

consequence $\frac{\partial A_l}{\partial S} < 0$ defines a hydrophilic material.

Through careful treatment of the dissipation inequality using Liu's Lagrange multiplier method a set of constitutive relations are derived, including generalizations of Fick's law for species diffusion, Darcy's law for seepage flow as well as mass transfer relations. In table 1 some of the constitutive relations are given.

Quantity	Relation
Vapor diffusive flux ($\boldsymbol{J}_{g_v}$)	$\boldsymbol{J}_{g_v} = -\boldsymbol{D}^{\varphi}_{eff} \cdot \nabla(\varphi)$
Gas flux ($\boldsymbol{J}_g$)	$\boldsymbol{J}_g = -(\phi(1-S))^2 \rho_g \frac{\boldsymbol{K}^0 \kappa_g}{\bar{\mu}_g} \cdot \nabla(p_g)$
Pore water flux ($\boldsymbol{J}_l$)	$\boldsymbol{J}_l = -\phi^2 S \rho_l \frac{\boldsymbol{K}^0 \kappa_l}{\bar{\mu}_l} \cdot [S\nabla(p_g) - p_l^s \nabla(S)]$
Fiber-wall water flux ($\boldsymbol{J}_{s_w}$)	$\boldsymbol{J}_{s_w} = -\boldsymbol{D}^{s_w}_{eff} \cdot \nabla(W_b)$
Mass transfer $s_w - g_v$ ($\hat{m}_{s\to g}$)	$\hat{m}_{s\to g} = \zeta_{sg} \frac{R\theta}{M_{g_v}} \ln(\frac{a_w}{\varphi})$
Mass transfer $l - s_w$ ($\hat{m}_{l\to s}$)	$\hat{m}_{l\to s} = \zeta_{ls} \frac{R\theta}{M_{g_v}} \ln(\frac{a_l}{a_w})$
Mass transfer $l - g_v$ ($\hat{m}_{l\to g}$)	$\hat{m}_{l\to g} = \zeta_{lg} \frac{R\theta}{M_{g_v}} \ln(\frac{a_l}{\varphi})$
Dry solid stress ($\boldsymbol{S}^{eff}_{s_s}$)	$\boldsymbol{S}^{eff}_{s_s} = \boldsymbol{D}^H \boldsymbol{E}^e_{s_s}$
Moisture swelling ($J^{\omega}_{s_s}$)	$J^{\omega}_{s_s} = \exp(\mathrm{tr}(\boldsymbol{S}) W_b)$
Fiber density (ρ_{s_s})	$\rho_{s_s} = \rho^0_{s_s}(1 + \frac{\rho^0_{s_s}}{\rho_l}\gamma W_b)^{-1}$
Porosity (ϕ)	$\phi = 1 - (1-\phi^0)\exp(-\mathrm{tr}(\boldsymbol{S}) W_b)(1 + \frac{\rho^0_{s_s}}{\rho_l}\gamma W_b)\frac{1}{J^e_{s_s}}$

Table 1: Constitutive relations, where $\mathbf{D}^{\varphi}_{\mathbf{eff}}$, $\mathbf{K^0}$, κ_α, $\mathbf{D}^{\mathbf{s_w}}_{\mathbf{eff}}$, $\zeta_{\alpha\beta}$, $\mathbf{S}, \mathbf{D^H}$, $\gamma, \tilde{\mu}_\alpha$ *are material parameters.* a_w *is the water activity of bound water and is given by the sorption isotherm whilst* a_l *is the water activity of free water related to the solid-liquid interaction pressure via the relation,* $\frac{\partial \ln(a_l)}{\partial S} = -\frac{M_{g_v}}{\rho_l R\theta}(\frac{p_l^s}{S} + \frac{\partial p_l^s}{\partial S})$.

Numerical example

The saturation, moisture ratio, relative humidity, gas pressure and displacements are used as primary variables. The governing equations being the mass balances for free water, bound water, water vapor, gas as well as the linear momentum of the whole mixture. To compare the different response of a hydrophilic and a hydrophobic material to edge penetration, a simulation is set up representing a laminated rectangular sheet submerged in a water bath. In the simulation it is assumed that no pore gas leaves the sheet and the surrounding pressure of the water is kept at 1 atm. The simulated water uptake of for a hydrophilic and a hydrophobic material is shown in figure 2.

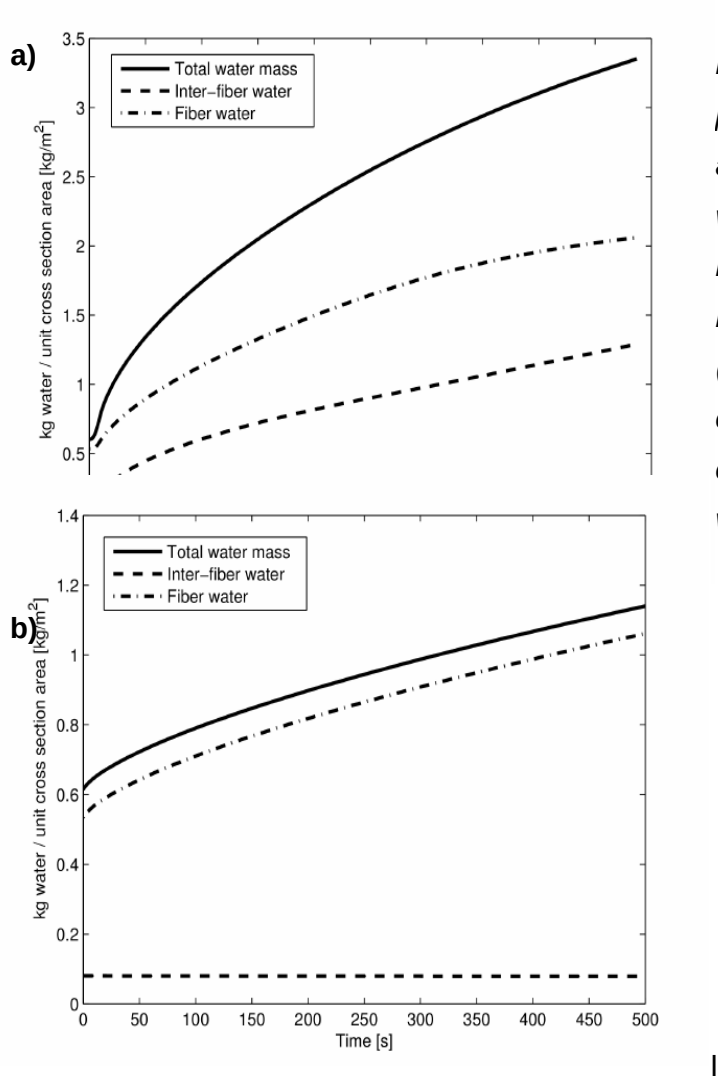

Figure 2: Water uptake per unit cross section area in contact with water time. ***a)*** *Hydrophilic material* ***b)*** *Hydrophobic material. (solid line – total water, dashed – fiber water, dot-dashed – inter-fiber water).*

It is seen that the amount of water is higher in the untreated (hydrophilic material) as expected, in this case several mechanisms drive water into the board and most notably the free water transport in the pore space by capillary actions. However also fiber diffusion at high moisture and vapor transport provide pathways. For the hydrophobic material the external pressure of water is not sufficient to overcome the hydrophobic forces, instead the contact with water provide a source for vapor and water-fiber sorption and in-fiber diffusion and vapor diffusion will act as pathways of water transport.

References

[1] L.S Bennethum and J. Cushman. Multiscale, hybrid mixture theory for swelling system I: Balance laws, *International Journal of Engineering Science*, 34, 125-145 (1996).

[2] L.S Bennethum and J. Cushman. Multicomponent, multiphase thermodynamics of swelling porous media with electroquasistatics: II.

Constitutive theory. *Transport in Porous Media,* 47, 309-336 (2002).

[3] M. Alexandersson, H. Askfelt and M. Ristinmaa. *Triphasic Model of Heat and Moisture Transport with Internal Mass Exchange in Paperboard. Transport in Porous Media*, 112, 381-408 (2016).

Influence of different relative humidity on the strength of individual hardwood and softwood fibres and joints

Marina Jajcinovic[1,2], Wolfgang Johann Fischer[1,2,3], Ulrich Hirn[1,3], Wolfgang Bauer[1,2,3]

AUTHOR INFORMATION

M. Jajcinovic

[1] Institute of Paper, Pulp and Fibre Technology, Graz University of Technology, NAWI Graz, Inffeldgasse 23, A-8010 Graz

[2] Dok'In'Holz, Graz University of Technology Inffeldgasse 23, A-8010 Graz

[3] CD Laboratory for Fiber Swelling and Paper Performance, Graz University of Technology Inffeldgasse 23, A-8010 Graz

Email:
marina.Jajcinovic@tugraz.at

Abstract

Natural materials i.e. cellulose fibres are susceptible to fluctuation in temperature and especially relative humidity. Besides morphological changes such as swelling and shrinking, the mechanical properties of individual pulp fibres and fibre-to-fibre joints are also influenced by the aforementioned. The present study compares the forces needed to break individual hardwood as well as softwood fibres and fibre to fibre joints at different relative humidity (30%, 50%, 80% RH). A decreasing trend in breaking force of fibres and joints is noticeable but no statistically significant difference was obtained in neither of the cases.

Introduction

It is well known that wetting or drying of pulp leads to changes of morphological properties of fibres i.e. shrinking or swelling. However, not only morphological fibre properties are influenced by the presence of water, dry or humid air. The mechanical properties of individual pulp fibres [1, 2, 3, 4] and fibre-to-fibre joints [5, 6] in the wet state differ from those in the dry state.

Several studies have shown that the fibre strength reduces upon exposure to humid air [1, 4], whereas others have shown the opposite, i.e. increase in breaking load [2, 3]. According to previous research, the absorbed water either helps distribute load more evenly across the fibre surface [2, 3], or leads to breaking between cellulose structural units [4], thus lowering the fibre strength. When it comes to the influence of different relative humidity on the force needed to separate two bonded fibres, the literature data is scarce. To the author's knowledge, there have been only two studies dealing with wet and dry strength of fibre to fibre joints, where the strength of joints decreases upon contact with water [5, 6]. If the above mentioned premise of increased spacing between cellulose structural units is accepted, it is presumable that the same increase in spacing will happen between two constituent bonded fibres. However, the influence of reduced or elevated humidity has never been investigated directly.

Materials and methods

All investigations have been performed using softwood and hardwood pulp. Softwood pulp was a once dried, unbeaten, unbleached kraft pulp (mixture of spruce and pine). Hardwood pulp was a once dried, unbeaten, bleached kraft pulp (mixture of Eucalyptus nitens and Eucalyptus globulus). Individual fibres and fibre to fibre joints were prepared according to Kappel et al. 2009 [7]. After the preparation, the samples were conditioned at 50% RH and 23°C.

Testing setup

Fibre and joint testing has been performed using a micro bond tester developed at Graz University of Technology [8]. As an additional part, a conditioning chamber was developed. By means of a humidity generator, the different relative humidity can be adjusted and maintained between 25 to 95% RH. The conditioning and testing setup is shown in Figure 1.

Figure 1. Conditioning and testing setup
1 – conditioning chamber, 2 – microscope camera, 3 – humidity generator, 4 – RH and temp. recording

Sample fixation and testing procedure

Individual fibres and joints were glued onto specially designed sample holders described in detail Fischer et al. 2012 [8] and Jajcinovic et al. 2016 [9]. After mounting of the sample holder carrying the fibres and joints on the micro bond tester, the chamber was closed. Subsequently, dry or humid air was blown in through a plastic tube connected to the humidity generator. During conditioning, it was observed that upon drying the fibres exhibited load increase due to shrinking. To avoid such drying stresses, similar to restrained drying, individual fibres were unloaded during conditioning according to the tension signal of the load cell. After reaching the defined RH (30% and 80%), the humidity was kept constant for 120 min. Subsequently, fibres and joints were loaded until failure and the entire testing procedure was recorded.

Results

Joint testing

Table 1 shows a comparison between forces needed to break individual softwood joints at different relative humidity (30%, 50% and 80% RH).

Table 1. Breaking load of fibre-fibre joints tested at different RH

	Breaking load at different RH [mN]		
	30%	50%	80%
Softwood	4.27 ± 2.67	6.58 ± 4.45	3.11 ± 1.31

As to be expected, joints tested at 30 and 80% RH show lower values when compared to 50% RH values. Those tested at 30% RH show a 35% reduction in breaking load whereas joints tested at 80% show a 52% reduction when compared to 50% RH. According to a t-test, no statistically significant difference between joints tested at 30 and 50% RH could be obtained. However, there is a significant difference in case of joints tested at 80% RH ($\alpha = 0.05$, p-value = 0.023). If it is assumed that the moisture absorption is great enough to swell the fibres, it is plausible that the distance between two adjacent fibres increases as well. This in turn would decrease the size of the bonded area, thus lowering the strength of interfibre interactions. Even though the water absorption is not enough to break the joint prior to loading, its absorption seems to induce some changes in the bonded area lowering the

breaking load. The reduction in case of joints tested at 30% RH could be attributed to the stresses in the bonded region caused by differences in transversal shrinking potential and restraint of shrinkage in the joint [6]. None the less, it appears that the loss of moisture affects the joint to a lesser extent than the moisture regain. However, it should be noted that the joints were conditioned in partially restrained state. It is possible that some changes in the joints have already taken place due to restrain during conditioning and further tests without restraining should be carried out.

To ensure that the exposure time of 120 min was enough for the joint to reach an equilibrium, tests with 8 h exposure time have also been performed. No significant difference was found between the breaking load values after 2 and 8 hours of conditioning.

Single fibre testing

Table 2 shows a comparison of the breaking load of individual softwood and hardwood fibres tested at different RH (30, 50 and 80%).

Table 2. Breaking load of individual fibres tested at different RH

	Breaking load [mN]		
	30% RH	50% RH	80% RH
Softwood	186.72 ± 97.72 143.38 ± 46.78*	235.97 ± 56.62	193.97 ± 82.72
Hardwood	24.05 ± 11.81	38.81 ± 16.31	27.39 ± 14.85

*conditioned under restraint

As can be seen from the table 2, individual fibres tested at 30 and 80 % RH of both softwood and hardwood show slightly lower values when compared to fibres tested at 50% RH. In case of softwoods, the breaking load is around 20% smaller when the fibres were tested either in elevated or decreased humidity. No statistically significant difference was obtained in neither of the cases. The only significant difference was obtained between fibres conditioned under restraint at 30% RH ($\alpha = 0.01$, p-value = 0.0047). The reduction of nearly 40% could be attributed to possible development of strength reducing flaws during drying [4]. Higher occurrence of such weak spots, in combination with tension forces during conditioning, could result in a fibre that is already damaged prior to testing, thus having lower breaking load. The same could be applied when comparing the values of fibres tested at 30% RH (restrained and unrestrained) where a reduction of 23% in breaking load is visible. In case of hardwood fibres, the same behaviour as in case of softwoods was observed.

For fibres tested at 30 and 80% RH a reduction of 29 and 38% can be seen, respectively. No statistically significant difference was obtained in neither of the cases. Figure 2 shows a comparison and distribution of values of softwood and hardwood fibres.

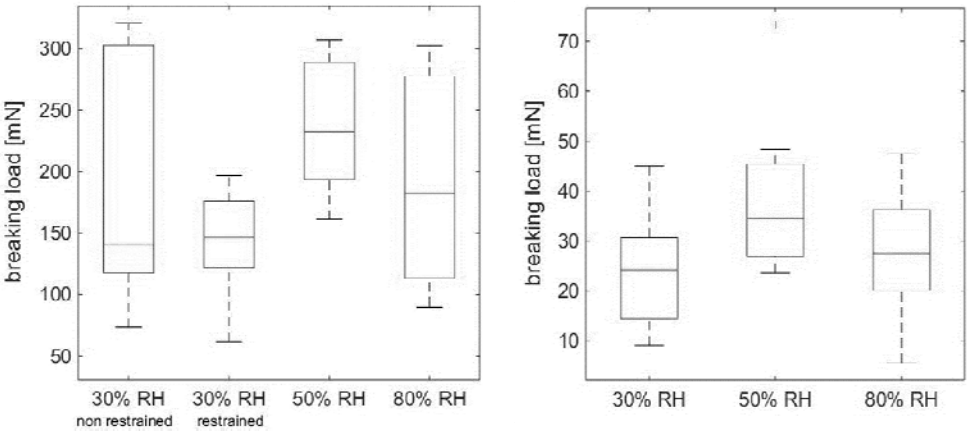

Softwood Hardwood

Figure 2. Breaking load of individual softwood and hardwood fibres

One should note that even though the fibres were conditioned in a "non-restrained state", they were still fixed at both ends. The large standard deviations in breaking loads could be attributed to the fibre morphology. If the real influence of RH on fibre properties is to be determined, the type of fibre (earlywood/latewood) should be known and the fibres should be conditioned in a fully unrestrained state.

Conclusion

The breaking load of individual fibre to fibre joints reduces when exposed to high or low relative humidity. The reduction shown in these preliminary results suggests that fibre joints are more sensitive to elevated than decreased humidity. When it comes to individual fibre breaking loads, a decreasing trend is visible and additional tests in completely unrestrained state will be performed. Furthermore, investigations of the influence of humidity of hardwood joints are in progress.

References

[1]Klauditz, W., Marschall, A. and Ginzel, W. (1947) Zur Technologie verholzter pflanzlicher Zellwände. Ermittlung der Zugfestigkeit von Zellstofffasern aus Pinus merkusii-Holz. Holzforschung, Heft 4, 98-103

[2] Wardrop, A.B. (1951) Cell wall organization and the properties of the xylem. I. Cell wall organization and the variation of breaking load in tension of the xylem in conifer stems. Aust. J. Sci. Res., B, Vol. 4, No. 4, 391-414
[3] Leopold, B. and Thorpe, J.L. (1968) Effect of pulping on strength properties of dry and wet pulp fibres from Norway spruce. Tappi, Vol. 51, No. 7, 304-308
[4] Kersavage, P.C. (1973). Moisture content on tensile properties of individual douglas-fir latewood tracheids. Wood and Fiber 5(2): 105-117
[5] Russell, J., Kallmes, O.J. and Mayhood, C.H. (1964) The Influence of Two Wet-Strength Resins on Fibers and Fiber-Fiber contacts. Tappi, Vol. 47, No. 1, 22-25
[6] Schniewind, A.P., Nemeth, L.J. and Brink, D.L. (1965) Fiber and Pulp Properties. I. Shear Strength of Single-Fiber Crossings. Tappi, Vol. 47, No. 4, 244-248
[7] Kappel, L.; Hirn, U.; Bauer, W. & Schennach, R. A novel method for the determination of jointed area of individual fibre-fibre joints Nordic Pulp and Paper Research Journal, 2009, 24, 199-205
[8] Fischer, W. J.; Hirn, U.; Bauer, W. & Schennach, R. Testing of individual fiber-fiber joints under biaxial load and simulataneous analysis of deformation Nordic Pulp and Paper Research Journal, 2012, 27, 237-244
[9] Jajcinovic, M., Fischer, W.J., Hirn, U. and Bauer, W. (2016) Strength of individual hardwood fibres and fibre to fibre joints. Cellulose, 23(3), 2049-2060

The effect of geometry on the mechanical properties of the fiber bonds

Brandberg, August

AUTHOR INFORMATION

KTH Royal Institute of Technology

Email:
augustbr@kth.se

A. Brandberg

Summary

In this work, we investigate the mechanical properties of fiber bonds as a function of their geometrical configuration and loading conditions, particularly how the stiffness of the bonded, collapsed and semi-collapsed fibers varies. The study is performed using a detailed finite element model of a fiber-fiber bond which comprises the essential characteristics of the fiber such as layered structure, chemical composition, fiber cross section geometry, boundary layer between the fibers.

1 Introduction

Optimizing the properties of paper products is an important task to reduce waste and increase efficiency in the paper and packaging industry. The mechanical properties of a sheet of paper stem from the strength of individual fibers as well as the strength of bonds between fibers in the fiber network. The fiber bond properties are sometimes the limiting factor in enhancing product strength. Gathering information about the properties of individual bonds experimentally is difficult, as it requires performing tedious and precise manipulations on the bond length scale.

A finite element model is constructed to study the behavior of fibers as they come into contact. The cellulose and non-cellulose content is resolved as

independent materials in the model to permit unambiguous interpretation of the results of non-linear deformation. Lignin and hemi-cellulose is represented as a single material whose properties are determined using the rule of mixtures which is assumed to have a yield limit after which it follows an ideal plasticity law. The material parameters are given in Table 1.

The model is depicted in Figure 1 where cellulose content indicated in lighter, lignin/hemi-cellulose mix in darker material. The cellulose is distributed using the Fisher-Yates shuffling algorithm [1].

Table 1: Implemented material parameters in the model.

	Matrix	**Fibril**	**Unit**
E_L	6.5[2],[3]	134[4]	GPa
E_T	2.5[2],[3]	27.2[5]	GPa
G	1.3[2],[3]	4.4[5]	GPa
ν	0.25	0.1	-
Volume fraction	0.58[6]	0.42[6]	-
σ_y	30[7]		MPa
H	0[7]		MPa

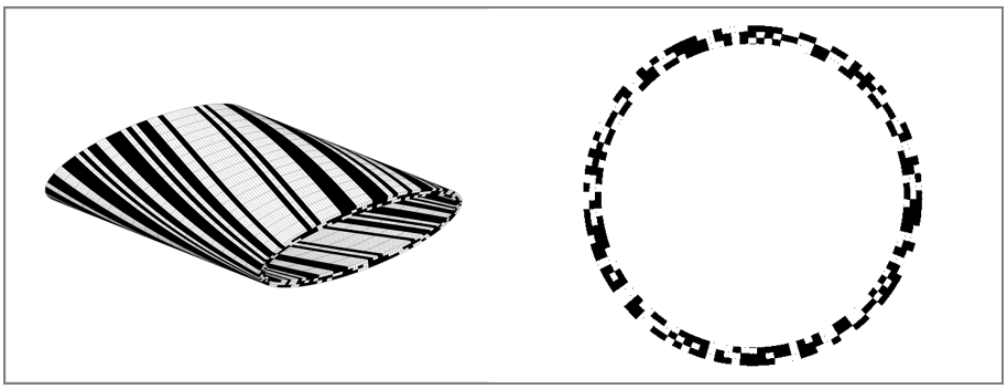

Figure 1: The fiber model. Cellulose content indicated in lighter, lignin/hemi-cellulose mix in darker material.

The loading is performed in several steps, starting with compression to simulate the processing of the fiber during drying. To study the properties of the bond, a model with two fibers is created. In the initial configuration, the fibers are positioned on top of each other. The loading is applied along two rigid plates on the top and bottom of the two fibers as enforced displacement.

This load case is comparatively hard to perform in physical experiments due to the difficulty of applying a distributed shearing or normal load onto the fiber without resorting to additives that risk altering the mechanical properties of the fibers or the bonds.

The effect of changing the numerical formulation of the model with a particular focus on the contact surfaces is studied. In particular, the effect of using a fully bonded contact once contact is achieved is compared with bonding the contact only in the normal direction, and for the inner lumen of the fiber the effect of allowing the lumen to reopen after compression is compared with a strictly enforced bond.

Conclusions

The results show that the response of the bond is a strong function of pressing conditions and is drastically affected by the closed lumen (inner surface of the fiber) as shown in Figure 2. The difference between using the two contact formulations is small, indicating that introducing finite friction in the contact interface does not yield interesting results.

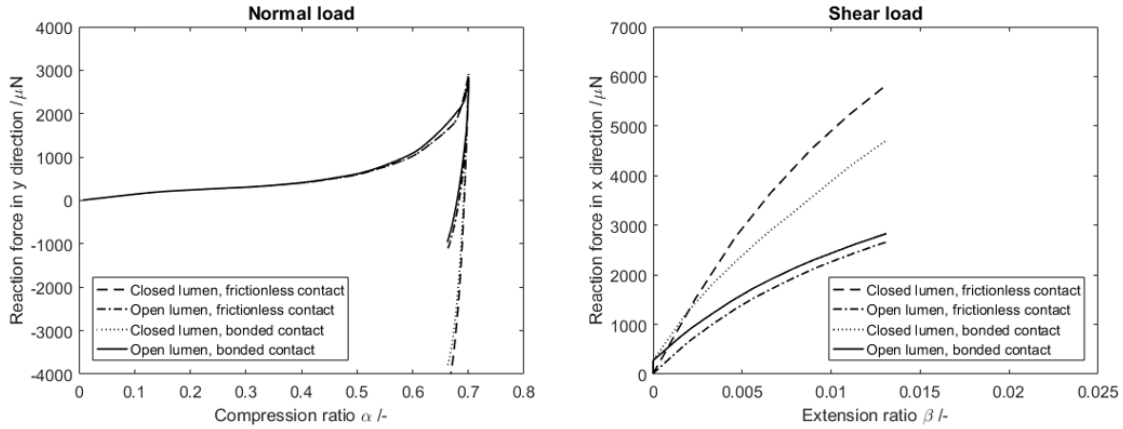

Figure 2: Response as a function of lumen and contact condition for load in the normal and tangential direction. The compression and extension ratio is the ratio between enforced displacement and the original size in the y-direction, e.g. 0 % compression ratio is undeformed and 100 % compression is completely flattened.

A comparison between the area that would appear bonded to an external observer and the area that is reported as in contact shows that the two differ by a factor of about 2 in the conducted simulations.

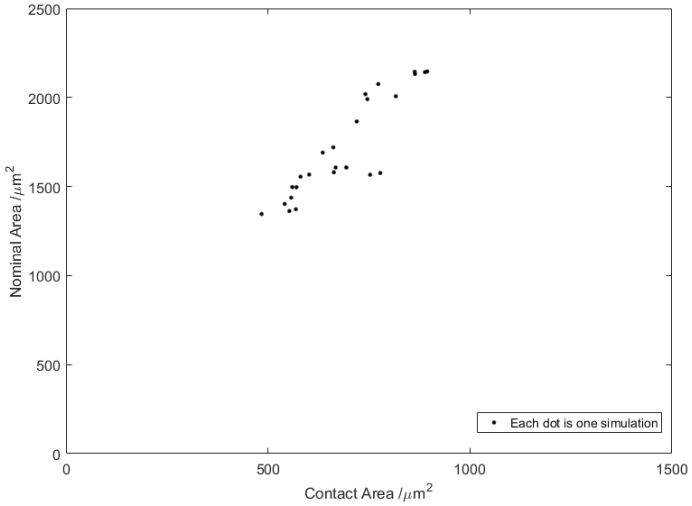

Figure 3: Nominal area defined as the area appearing bonded to an outside observer compared to the area reported to be in contact in the FEM simulation. Each dot represents one unique combination of the parameters wall-thickness, fiber radius, micro fibril angle and drying pressure.

Among the geometrical properties the fiber wall thickness shows the greatest impact on fiber elasticity while the diameter has a limited effect. The effect of the micro fibril angle after compression is also shown to be secondary.

Going forward, the study will refine the formulation of the contact interface using a discrete boundary layer made up of fines and starch additives as well as explore the possibility of using a cohesive zone to capture the stiffness during the delamination of fibers. Furthermore, hygrodynamics and shrinkage will be introduced to capture the contribution of these physical phenomena to the overall fiber bond strength.

Literature

1. Knuth, D.E., *The art of computer programming / Vol. 2, Seminumerical algorithms*. 1969, Reading, Mass.: Reading, Mass. : Addison-Wesley.

2. Cousins, W.J., *Elastic modulus of lignin as related to moisture content.* Wood Science and Technology, 1976. **10**(1): p. 9-17.

3. Cousins, W.J., *Young's modulus of hemicellulose as related to moisture content.* Wood Science and Technology, 1978. **12**(3): p. 161-167.

4. Kroon-Batenburg, L., J. Kroon, and M. Northolt, *Chain modulus and intramolecular hydrogen bonding in native and regenerated cellulose fibers.* Polymer Communications, 1986. **27**(10): p. 290-292.

5. Mark, R.E., *Cell wall mechanics of tracheids*. 1967: JSTOR.

6. Norman, B., *Pappersteknik*, ed. J.A. Bristow and p. Tekniska högskolan i Stockholm. Institutionen för. 1991, Stockholm: Stockholm : Institutionen för pappersteknik, Tekniska högsk.

7. Rozite, L., et al., *Nonlinear behavior of PLA and lignin-based flax composites subjected to tensile loading.* Journal of Thermoplastic Composite Materials, 2013. **26**(4): p. 476-496.

Simulation of an idealized sealing of two sheets of paperboard

H. Askfelt*, M. Alexandersson†, and M. Ristinmaa†

AUTHOR INFORMATION


H. Askfelt

† * Division of Solid Mechanics, Faculty of Engineering, Lund University, PO Box 118, SE - 221 00 Lund, Sweden
* e-mail: Henrik.Askfelt@solid.lth.se
web page: http://www.solid.lth.se

Summary

The response of moist paperboard exposed to extensive compression and heating in a short period of time is investigated. The transient transports of mass, momentum and energy, as well as specific interaction terms are considered for orthotropic paperboard. The elasto-plastic response is taken into account in a large strain setting. The dynamic mass exchange between the water bound to the fibers and the water vapor is also considered. Simulations of an idealized sealing of two sheets of paperboard are performed and the predicted distributions of moisture, temperature, vapor pressure, and out-of-plane stresses are studied.

Introduction

Paperboard is a base material in many package solutions. The process of producing a sealed package involves several steps where paperboard is exposed to severe load situations. In order to be able to guarantee the integrity of a package containing food, it is important to understand how paperboard will react to different load situations such as significant changes in moisture and temperature as well as significant deformations.

A continuum model able to predict the elasto-plastic deformation of paperboard in a large strain setting has been developed in [1]. The transient transport of heat and moisture in paperboard has been treated in [2]. This work combines these two models in a hybrid mixture theory framework such that a the coupled transport of moisture, temperature and momentum is

derived in a thermodynamically consistent manner.

Modelling approach

A hybrid mixture theory framework [3] is adopted and paperboard is considered to be a continuum where each point in the body is viewed as a superposition of the components of the board. Moisture ratios below the hygroscopic moisture content are considered and the board is assumed to be composed of three phases, namely, a solid phase defined by the dry fiber network, a liquid phase defined by the liquid water bound to the fibers, and a gas phase defined by the moist air. Furthermore the gas phase is considered as a mixture of the two miscible constituents, dry air and water vapor, cf. Figure (1).

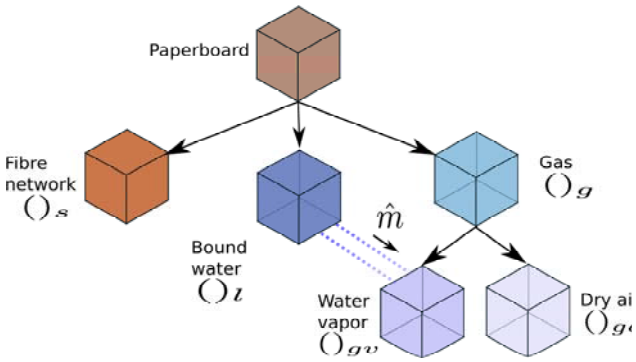

Figure 1 : Illustration of the decomposition of paperboard into phases and constituents. The dynamic mass exchange between the bound water and the water vapor is illustrated with .

Each component of the board is viewed as a continuum governed by its own balance laws and allowed to have its own motion, [4]. For the assumed composition the general format may be reduced to the following set of equations governing the response of moist paperboard in conditions similar to those of a sealing process of a food package [5].

Balance of mass of the bound water, the dry air and the water vapor :

$$\rho_l \frac{D_s(n_l)}{Dt} + \bar{\rho}_l \nabla \cdot (\mathbf{v}_s) + \hat{m} = 0$$

$$\rho_{g_d} \frac{D_s(n_g)}{Dt} + \frac{\bar{\rho}_{g_d}}{p_{g_d}} \frac{D_s(p_{g_d})}{Dt} - \frac{\bar{\rho}_{g_d}}{\theta} \frac{D_s(\theta)}{Dt} + \nabla \cdot (\mathbf{J}_{g_d}) + \bar{\rho}_{g_d} \nabla \cdot (\mathbf{v}_s) = 0$$

$$\rho_{g_v} \frac{D_s(n_g)}{Dt} + \frac{\bar{\rho}_{g_v}}{p_{g_v}} \frac{D_s(p_{g_v})}{Dt} - \frac{\bar{\rho}_{g_v}}{\theta} \frac{D_s(\theta)}{Dt} + \nabla \cdot (\mathbf{J}_{g_v}) + \bar{\rho}_{g_v} \nabla \cdot (\mathbf{v}_s) - \hat{m} = 0$$

Balance of linear momentum of the fiber network :

$$\nabla \cdot (\boldsymbol{\sigma}) + \rho \mathbf{b} - \hat{m}(\mathbf{v}_{g,s} + \mathbf{w}_{g_v}) = \mathbf{0}$$

Balance of energy of the mixture :

$$c^p \frac{D_s(\theta)}{Dt} + \rho \mathbf{b} \cdot \mathbf{w}_s + \nabla \cdot (\mathbf{q}) - \sum_{j=d,v} h_{g_j} \nabla \cdot (\mathbf{J}_{g_j}) + \hat{m} \Delta H_{ads} = 0$$

where ρ_α denote the densities, n_α the volume fractions, p_α the pressures, θ the absolute temperature, $\hat{m}$ the rate of evaporation, $\boldsymbol{\sigma}$ the total Cauchy stress tensor, h_α the enthalpies, ΔH_{ads} the enthalpy of adsorption, **b** the body force tensor, **q** the total heat flux.

Furthermore, $\mathbf{J} = n_g \rho_{g_j} (\mathbf{v}_{g,s} + \mathbf{w}_{g_j})$ denotes the combined mass flux, $\mathbf{v}_{g,s}$ the inter-fiber gas-solid seepage, and $\mathbf{w}_{g_j}$ the inter-fiber diffusion. Explicit formats of all constitutive relations, appearing in the balance laws, are derived in [6].

Numerical example

Simulations are carried out in order to investigate the response of paperboard in conditions similar to those present during a local sealing of two sheets of paperboard. During the sealing process, two sheets of paperboard are pressed together locally and a polymer is melted between them. The sheets are wide in CD and the idealized sealing is viewed as a 2D problem where plane strain is assumed to prevail. The initial state of the board is determined such that it is in equilibrium with an ambient climate defined by the relative humidity of 50%, the gas pressure of 1 atm, and the temperature of 298.15 K. The external loads, applied on the paperboard, during the sealing process are simulated by a local compression of 40% of the board thickness as well as a local heating of 250 K in 0.1 s. The predicted distribution of the absolute temperature is shown in Figure (2a). It is seen that due to the rapid nature of the sealing process, the temperature distribution is far from an equilibrium state. Due to the very local form of the temperature increase the elevated vapor pressure also appears very local. In Figure (2b) it is seen that the increase in vapor pressure is in the magnitude of 1000 % locally. This increase is partly due to the explicit temperature dependence in the ideal gas law but also due to the evaporation of the water bound to the fibers. This evaporation is illustrated in Figure (2c) where the element wise volume specific change in liquid mass, $(\Delta m_l)_e / v_e^0$, is shown. The initial volume of element *e* is denoted, v_e^0, and the change in liquid mass in element *e*, is denoted $(\Delta m_l)_e$ and calculated by

$$(\Delta m_l)_e = (m_l)_e - (m_l^0)_e = -\int_0^t \left[\int_{\Omega_e^d} \hat{m} dv \right] dt$$

A consequence of the increased pressure inside the board is that the board will experience out-of-plane tension stresses, cf. Figure (2d). The failure stress

in out-of-plane tension is approximately 0.36 MPa [7] and it is seen that the increased inter-fiber pore pressure will, for the current simulation, not cause

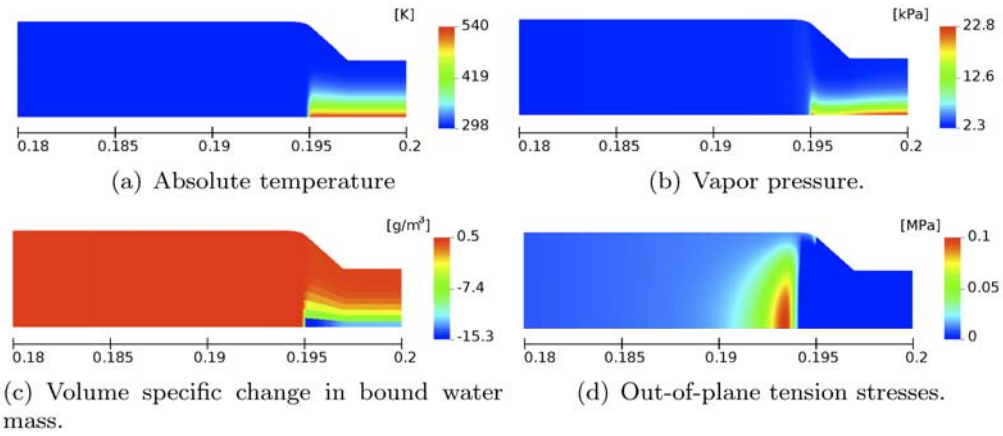

Figure 2 : Distributions after a local heating of 250 K and compression of 40% in 0.1 s a) absolute temperature, b) vapor pressure, c) volume specific change in bound water mass, and d) out-of-plane tension stresses.

failure in out-of-plane tension.

REFERENCES

[1] Borgqvist, E., Wallin, M., Ristinmaa M. and Tryding J. : An anisotropic in-plane and out-of-plane elasto-plastic continuum model for paperboard. Composite Structures **126** (2015) 184-195.

[2] Alexandersson M., Askfelt H. and Ristinmaa M. : Triphasic Model of Heat and Moisture Transport with Internal Mass Exchange in Paperboard. Transport in Porous Media (2016) 1-28.

[3] Hassanizadeh M., & Gray W. G. : General conservation equations for multi-phase systems: 1. Averaging procedure. *Advances in Water Resources*, **2,** (1979), 131–144.

[4] Bennethum L. S. : Multiscale, hybrid mixture theory for swelling systems with interfaces. Ph.D. thesis Prudue University (1994).

[5] Askfelt H., Alexandersson M. and Ristinmaa M. : Transient transport of heat, mass, and momentum in paperboard including dynamic phase change of water. Submitted for publication

[6] Askfelt H. and Ristinmaa M. : Response of moist paperboard during rapid compression and heating. Submitted for publication

[7] Stenberg, N. : A model for the through-thickness elastic-plastic behaviour of paper. International Journal of Solids and Structures **40** (2003) 7483-7498.

3D-modelling of cellulose fibers

Kazakov Yakov, Lebedev Ivan, Guriev Timur

AUTHOR INFORMATION

Y. Kasakov

Northern (Arctic) Federal University
named after M.V.Lomonosov,
Arkhangelsk, Russian Federation

Email:
j.kazakov@narfu.ru

Summary

The application of computer models of pulp fibers for visual analysis and prediction of the properties of the obtained pulp-and-paper product receives widespread in recent years. This paper presents a method of obtaining 3D model of the cellulose fibers. Getting the model done according to the algorithm includes three main stages: calculation of a fibers trajectory using Béziers curves; design of the fiber cross section; the performance of the resulting 3d model on the screen. The Béziers curves based on the obtained original data: fiber length, *l*, mm; form factor *f* (curvature); angle to define the direction □; the coordinates (x_c,y_c) of the fiber center. The structure of the cross section of the fiber is carried out by use of information about fiber width *b*, mm, the wall thickness of fiber □, μm and the degree of oblateness *t*, %, and set the number of edges *n*. To obtain the computer model affine coordinate transformations, and algorithms for removing hidden lines and change the illumination fiber are used.

Introduction

Well-known that paper consists of fibers, which are heterogeneous and stochastic stacked in a unified structure. This structure has a significant influence on the physical properties of paper. For example, the paper strength depends on the fibers strength, the points number of fiber contacts and fibre-fibre bonding forces between them.

Computer simulation is a promising and popular method of cognition. This offers great opportunities to find ways to produce pulp and paper materials with predetermined properties. The three dimensional structure of most the paper fibers is distributed in a plane of the sheet. To quantify the structural anisotropy of the paper the characteristics of individual fibers: length *l*, the angle of the fiber orientation in a machine direction □, the degree of curved – shape factor *f* are used. Stochastic properties of the structures are also used: distribution of fiber length and distribution of fiber width, distribution of the angle of the fiber orientation, distribution of fiber shape factor. In this case, the

key role belongs to the characteristics of the individual fibers forming the stochastic structure [1].

In the simulation of three-dimensional paper structure, the first and necessary step is the simulation of the individual fibers. The model requires more detailed information not only about the total and average degree of fibers curvature, but also on the location of the fibers and the trajectory of the bend in the plane of the sheet structure. Three-dimensional model is constructed on the basis of information about: 1) the trajectory of the fibers described curved line; 2) information about the cross section of the fiber having the shape of an ellipse with different values of oblateness.

Materials and methods

For simulating, the program for the PC was developed. A three-dimensional model of the fiber on basis of the trajectory construction and the cross section of the fiber is generated. Algorithm includes 3 stages: 1) Calculation of the in-plane fiber path; 2) The calculation of the fiber cross section;3) Three-dimensional representation of the fiber image.

It was found that the trajectory of the fibers described by third order Bezier curves, which are based on the 4-point. The initial data for modeling the trajectory of the location of the fibers in the plane of the sheet are: fiber length, *l*, mm; form factor *f* (curvature); angle to define direction □; the coordinates (x_c,y_c) of the fiber center. The coordinates of the base points of the Bézier curve (x_i,y_i, where i = 0..3) are selected according to the developed algorithm to the length and curvature of the curve corresponded to the task. By varying the number of units in the polyline, part of a Bezier curve, it is possible to achieve a given smooth of the curve.

The initial data for modeling of the cross section (profile) of the fiber are: fiber width *b*, mm, the wall thickness of fiber □, μm and the degree of oblateness *t*, %. As the geometric framework adopted by the polygon in the shape of an ellipse with number of fins *n* from 4 to 36.

When building a three-dimensional fiber image in the form of a polyhedron, calculates the coordinates of its vertices in three-dimensional space. The number of faces depends on the adopted number of links in the fiber path and the number of edges of the ellipse cross-section. The ends of the fibers are simulated by reducing the cross-section dimensions of the fiber. When you receive a flat three-dimensional image of the body uses affine coordinate transformations and a projection of the selected type – oblique, isometric, dimetric. Also in this program implements the algorithms for removing hidden lines and change the illumination fiber depending on whether it is in screen space.

Results

Examples trajectory modeling softwood pulp fibers in the plane of the sheet are shown in Figure 1. The fiber length *l* is assumed constant - 3 mm; form factor *f* and the orientation angle □ varies in limits experimentally determined. Shape of the models corresponds fiber images obtained by the visual analysis of the form of colored fibers in the sheet. This confirms the correctness of the approach using Bezier curves.

Fig.2 shows the results of simulation fiber profile with different parameters. The form of models correspond to images obtained by the cross-sectional SEM-images of paper.

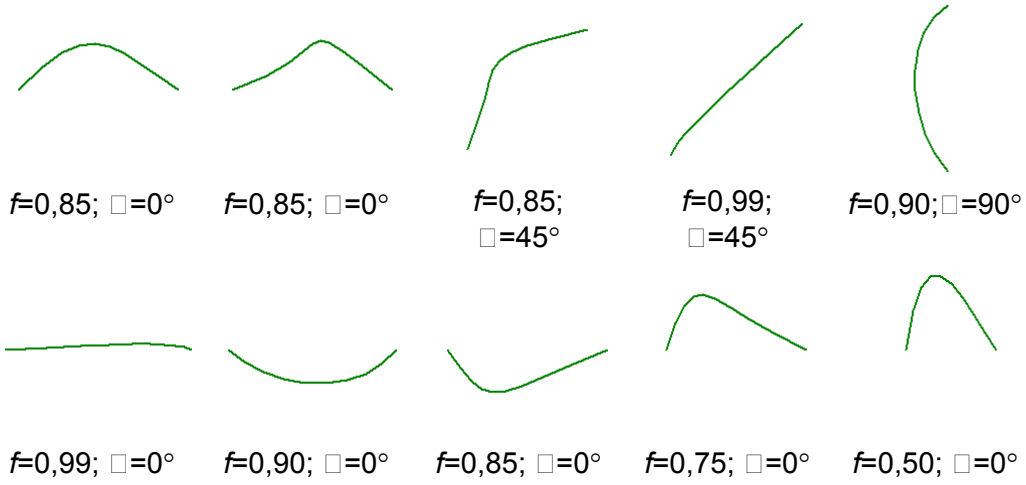

Figure 1. Results for simulation the fiber in-plane trajectory with different parameters

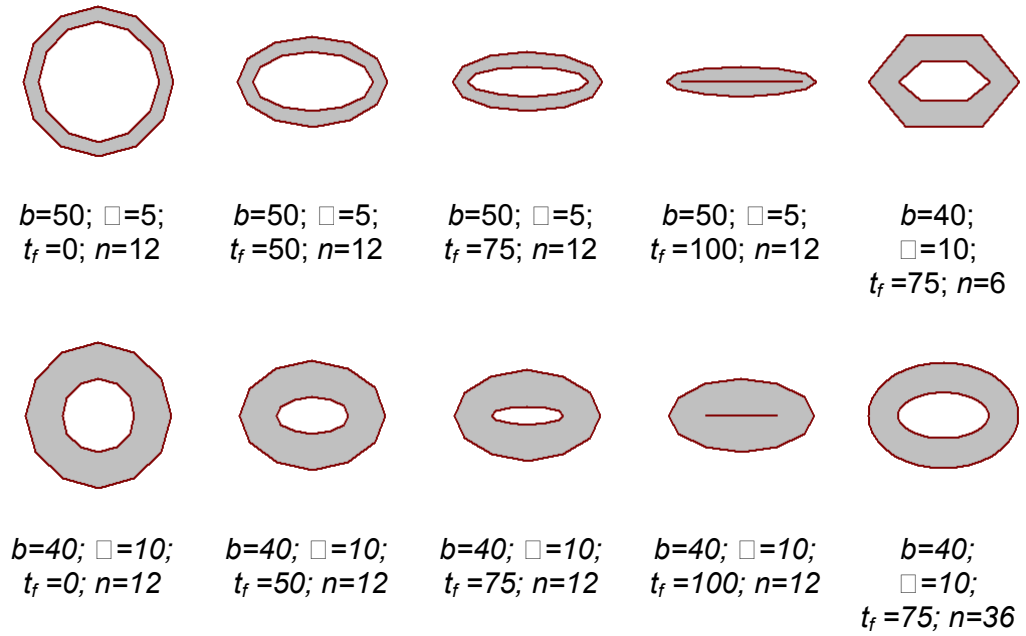

Figure 2. Results of simulation fiber profile with different parameters

Simulation results softwood fibers with length l = 2,9 mm, width b = 50 mm with a different form factor f and the orientation angle to the X axis □ are presented on Figure 3.

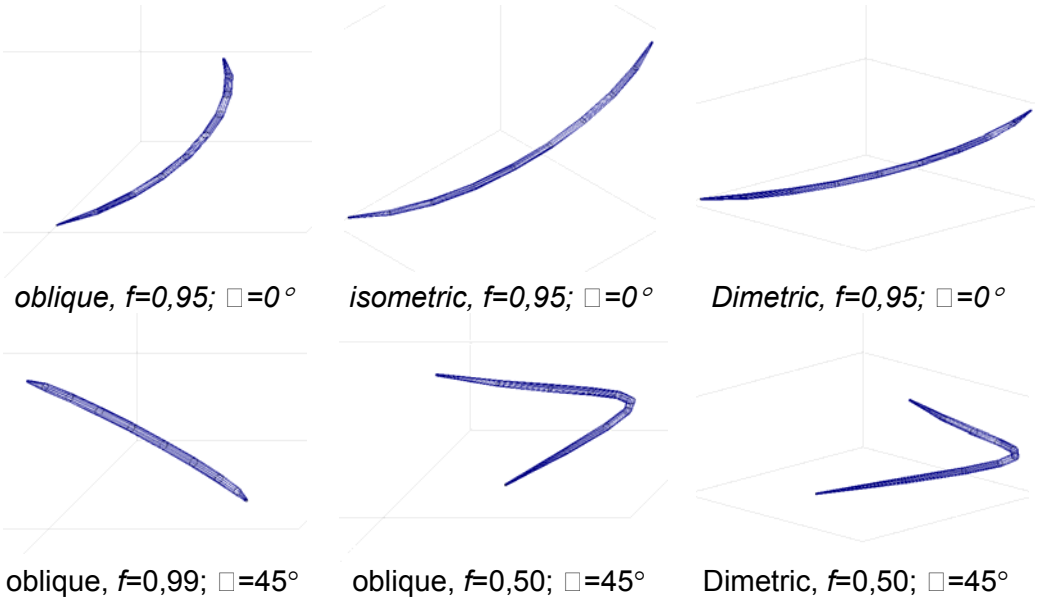

Figure 3. Results of 3D modelling of fibers used different projections

Conclusions

The used approach allows you to obtain 3D models of individual fibers with specified geometric parameters. Subsequently in these models it is possible to impart strength properties and to use them to build 3D model structure of a paper sheet. Using the parameters distribution laws of length, width and shape factor open the way to the modeling of three-dimensional structure of the paper with adequate probabilistic characteristic of fiber geometry.

Literature

1. Lebedev I., Kazakov Ya. A mathematical model of the paper sheet structure //"The Issues in mechanics of pulp and paper materials": Proceedings of 3rd International Conf. (Arkhangelsk, September 9-11, 2015) // North. (Arctic.) Federal Univ. Arkhangelsk: NArFU, 2015. P.288–293.

2. Kazakov Ya. Three-dimensional modeling of cellulose fibers // New advances in chemistry and chemical technology of plant raw materials: Proceedings of IV All-Russia. Conf. Barnaul: Publishing House of Altay University Press, 2009. Book I. pp 57-59.

3. Stefan B. Lindstrem Modelling and simulation of paper structure development. Thesis for the degree of Doctor of Technology, Sundsvall, Sweden. 2008. 64 p.

4. Marketing Authorisation. Number 2012612983. Russian Federation. Certificate of state registration of computer software. The program for three-dimensional modeling of the cellulose fibers (3D Fiber). / Y.V. Kazakov; The applicant and the holder NARFU (RU). N 2012610543; appl. 30.01.2012; publ. 26.03.2012. The registry of the computer programs. 1 p.

The effect of inhomogeneous material properties in explicit dynamic simulation of paperboard forming

Wallmeier, Malte[1] and Linvill, Eric[2] and Hauptmann, Marek[1]

AUTHOR INFORMATION

M. Wallmeier

E. Linvill

[1] TU Dresden, Dresden, Germany

[2] KTH Royal Institute of Technology, Stockholm, Sweden

E-mail:
malte.wallmeier@tu-dresden.de

Summary

Paper and Paperboard are heterogeneous materials whose mechanical and thermal properties are strongly influenced by the properties of the fibers and the network structure. The heterogeneity of the structure affects forming processes on the macroscopic scale, for example the occurrence of rupture in deep drawing of paperboard. Other forming processes, like creasing and folding, involve local deformations that are influenced by the network structure. Micromechanical models can be used to capture stochastically differing material properties of paperboard in simulations, but they are currently not used to simulate complex processes.

An approach for the implementation of stochastically varying material properties in material models based on continuum mechanics is evaluated in this paper. The stochastic variation of material prioperties has a smoothening effect on the stress-strain curve in the simulation of a uniaxial tensile test. Variations of the yield stress are found to have a high impact on the local variations of the strain in the simulations. Measurement methods to determine the stochastic variation of local material properties are needed. Strain field measurements are found to lead to different variations and strain values depending on the homogenization and the scale of measurement.

Introduction

Paper and paperboard are highly heterogeneous materials even though considerable efforts have been made to reduce the randomness of their mechanical and optical properties. Although the heterogeneity of paperboard is predominant on the microscopic scale, large scale forming processes - like press-forming, creasing and deep-drawing - are affected by the local differences in mechanical properties, as well. A recent investigation of the

occurrence of ruptures in deep-drawing of paperboard showed the influence of heterogeneity by finding smooth conversions between areas of low and high probability of rupture (1). Ruptures occur randomly when parameter combinations are chosen that induce stresses close to the breaking strength of the material. In simulations of processes that are strongly affected by local differences in material properties, methods for measurement and determination of input parameters are needed.

Different methods have been used to obtain information about local strains in paper, like holography (2), laser spectrometry (3), photo spectrometry (4) and digital image correlation (DIC) (5). The DIC-method is widely accepted and commonly used, even for micro- and nanoscale deformation measurements (6). Applying the DIC-method to paper, Considine (5) found that the local variation of strain in uniaxial tensile tests is much larger than previously reported in other publications, reaching up to 400%. It is also found that the strain variation can be fitted with a 3-parameter-Weibull distribution and that the measured strain variations depend on the resolution of the measurement. The highest resolution was 0.6 mm x 0.6 mm. Ostoja-Starzewski and coworkers (7) studied the effects of local variations of the basis-weight on the mechanical behavior of paper and paperboard under biaxial loading, finding that the stiffness-coefficients on the length-scale of 1 mm are linearly proportional to the basis-weight. Furthermore, homogeneity can only be assumed for scales 10 times larger than the floc size.

Insights in correlations between scale effects and local properties are an important step to the implementations of locally varying mechanical properties in simulation with continuum models. This publication aims to investigate the effects of the implementation of stochastic variations of mechanical properties in a continuum model. Furthermore, the scale effects in strain field measurements using digital image correlation of tensile tests are examined to conduct first steps concerning the transfer into simulations of tensile tests.

Methods

Simulations were executed with a user defined material model presented in (8) with LS-Dyna. The model was supplemented with the possibility to add stochastic variations to all mechanical properties by the equation:

$$P_V = P * (1 + r * SF).$$

P_V is the value assigned to an element, P is the mean value of the parameter, r is a random number following a standard normal distribution and SF is a scaling factor. SF (e.g. 5% variation of the nominal value) can be set to all MD, CD, ZD or shear parameters and switched on or off for each individual parameter.

A uniDAC® fast system by Chemnitzer Werkstoffmechanik GmbH with a Guppy Pro F-201B telecentric lens was used to record the images for the strain field measurement. The resolution of this system was 0.0395 mm/pixel. Strain fields were measured using a strong light source located on the backside of the sample and digital image correlation to identify and follow the microstructure of the paperboard. The reference field was 20 x 20 pixel on a grid with distances between the central pixel of 5, 6, 8, 10, 20, 50 and 100 pixel to alternate the resolution of the strain field measurement. The

trajectories for the local material distortion were calculated using the VEDDAC 6.2 software by Chemnitzer Werkstoffmechanik GmbH.

Results

Simulation

16 simple simulations of stress strain tests in CD were performed using the identical material properties listed in (8). Additionally, variations were included following the design of experiment in Table 2, where 1 indicates that the variation was switched in, and 0 represents variation switched off. The amount of variation is defined as percentage of the mean value. The amount of variation was arbitrarily chosen to investigate the effects and may not represent a realistic magnitude.

Table 2: DoE for the investigation of influence of variation of mechanical properties.

Number	E-modulus	Yield strength	Tangent modulus	Variation
1	0	0	0	5%
2	0	1	0	5%
3	1	1	0	5%
4	1	0	1	5%
5	0	1	1	5%
6	1	0	0	13%
7	0	0	1	17.5%
8	1	1	1	17.5%
9	0	1	0	20.125%
10	0	0	0	30%
11	1	0	0	30%
12	1	1	0	30%
13	0	0	1	30%
14	1	0	1	30%
15	0	1	1	30%
16	1	1	1	30%

The results of the simulations are presented in *Fig. 1*. The response for the t-ratios in *Fig. 1 left* is the standard deviation of strains of all elements at 5% strain of the sample. The variation parameter has the most dominant effect on the variation of strain in the proposed model.. Among the material properties, variations of the yield strength have the strongest effect on the variation of the strain. The interaction coefficient of variation and yield strength, and variation and tangent modulus indicate that the respective effect increases with the variation.

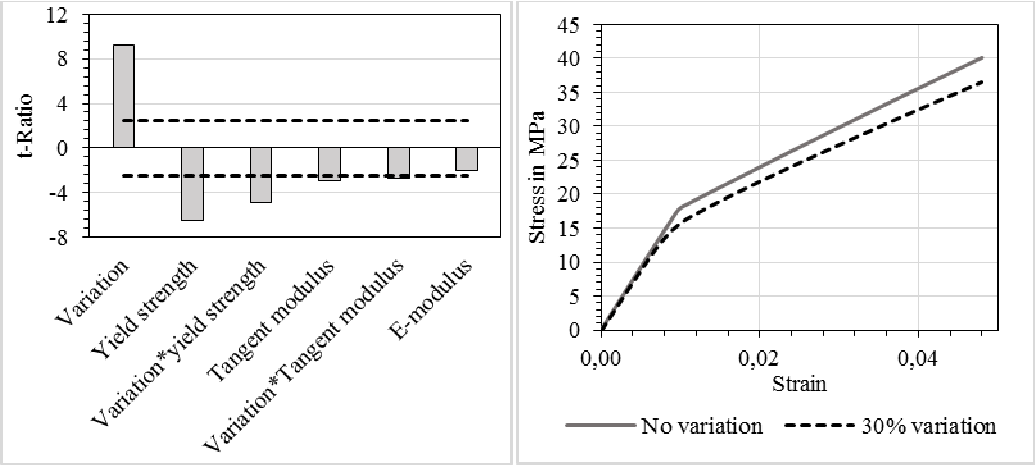

Fig. 1: left: t-Ratios for the DoE, right: stress-strain curves for simulations with and without stochastic variation of parameters.

The diagram in *Fig. 1* on the right side shows the influence of the variation on the resulting stress-strain curve of the tensile test. The material model uses a bilinear elastic-plastic model with a yield point. Including 30% random variation of E-modulus, tangent-modulus and yield strength results in the dashed line in *Fig. 1*. Especially remarkable is the smooth transition between elastic and plastic behavior which accounts for a much better resemblance of the stress-strain curve to a measured stress-strain curve of paperboard.

The results show the possibilities that arise when variations are included in a continuum model, but measurement methods are needed to determine input parameters for the variation of the different mechanical properties. In the following section, scale effects of strain field measurements will be discussed.

Strain field measurement

The first step of strain field analysis is the calculation of strains out of the trajectories. Several methods exist for this purpose. The easiest and most obvious one is subtraction of the trajectories of adjacent points of measurement and division by the original distance. The abbreviation SD is used to appoint this procedure in *Fig. 2*.

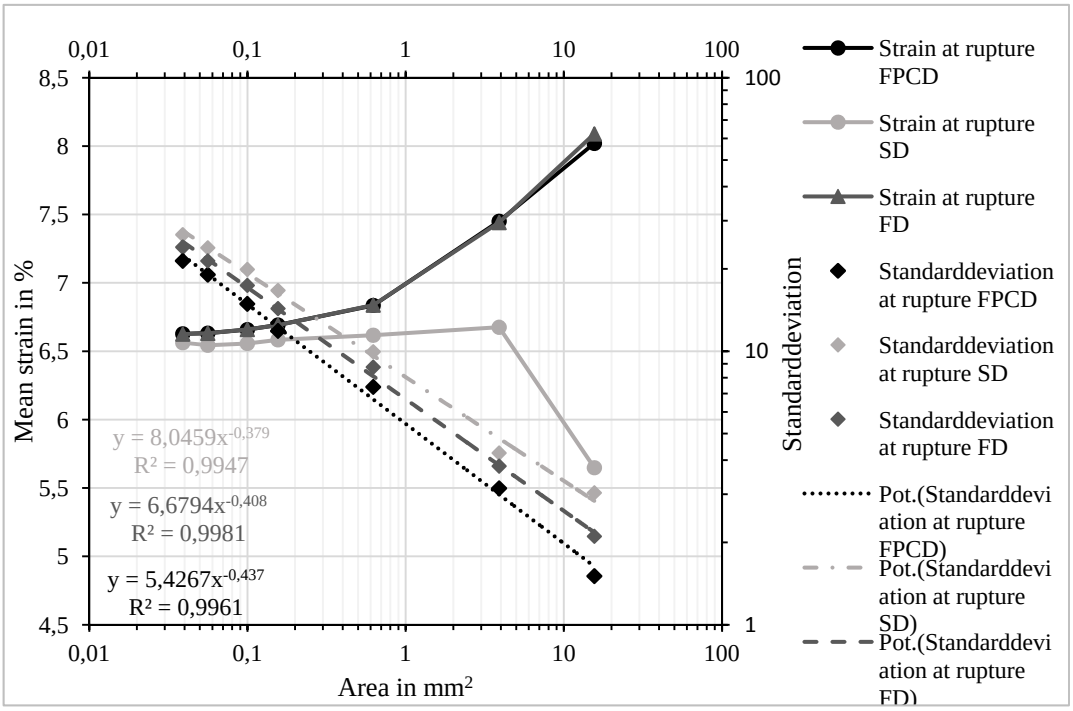

Fig. 2: Influence of homogenization and resolution on global strain and standard deviation in strain field measurement.

This method has the disadvantage that small errors in one trajectory lead to errors in two strain values, producing a noisy outcome of the measurement. Therefore, methods for the homogenization are often used, like the four-point central differences method (FPCD) (5), or the forward differences (FD) or pointwise least squares (9). *Fig. 2* shows that these methods can – and as expected – do result in different standard deviations. FPCD results in the lowest standard deviations, followed by FD and SD. However, the method of homogenization also influences the measured mean strain. It is noticeable that FPCD and FD lead to constantly increasing mean strains at rupture for increasing measuring area while the mean strains calculated with SD remain almost constant up to 3.9 mm of measurement area.

In contrast to (5), the Weibull-distribution provided a rather poor fit of the local strains; instead, the normal distribution and the Beta distribution provided better fits. Standard variation and mean strain both increase linearly in strain field measurements. Normalizing the standard deviation with the mean strain and the size of the measurement field leads to a linear relationship of the normalized standard variation and the measured area on a log-log scale (*Fig. 3*).

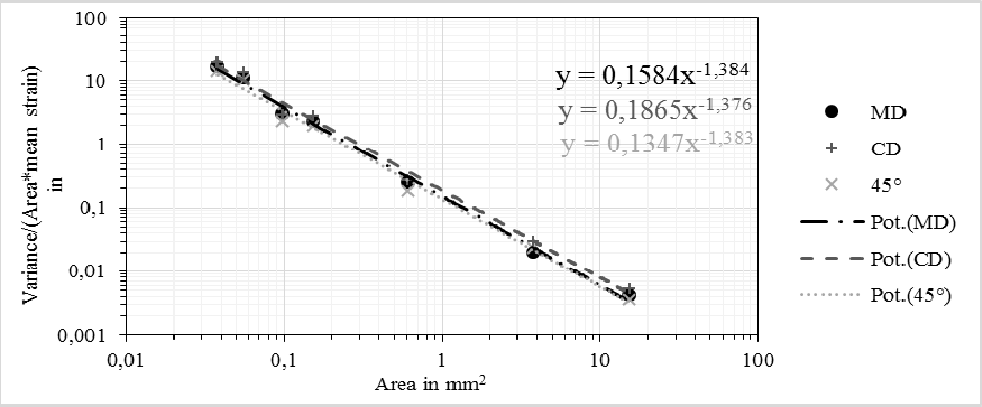

Fig. 3: Normalized standard deviation of local strains over measurement area for samples strained in MD, CD and 45°-direction.

Slightly higher normalized standard deviations were measured for CD than for MD and 45°-direction. The power function provides a good fit for all measurements; consequently, a universal behavior can be assumed.

Conclusions

Different methods for homogenization of strain field measurements result in drastically different standard deviations and different global strain values when a low resolution is used. A universal scaling law for the relationship between standard deviation and measurement resolution may exist in strain field measurement. Including variations in simulations of tensile tests smoothens a bi-linear elastic-plastic stress-strain relationship and results in better fitting stress-strain curves.

Acknowledgements

Measurement strain fields were performed by Dr.-Ing. Timo Kuntzsch at PTS (Papiertechnische Stiftung e.V.).

Literature

1. **Wallmeier, M., Hauptmann, M. and Majschak, J.-P.** The occurence of rupture in deep-drawing of paperboard. *BioResources.* 2016, Vol. 11, 2, pp. 4688-4704.

2. **Lyne, M. B. and Hazell, R.** Formation testing as a means of monitoring strength uniformity. *The Fundamental Properties of Paper and its Uses, Transactions of the 5th Fundamental Research Symposium.* 1973.

3. **Lyne, M. B. and Bjelkhagen, H.** The application of speckle interferometry to the analysis of elongation in paper and polymer sheets. *Pulp Paper Can.* 1981, Vol. 82, 6, pp. TR29-TR35.

4. **Choi, D., Thorpe, L. J. and Hanna, R.B.** Image analysis to measure strain in wood and paper. *Wood Science and Technology.* 1991, Vol. 25, pp. 251-262.

5. **Considine, J. M., et al.** Use of digital image correlation to study the local deformation field of paper and paperboard. *13th Fund. Res. Symp. Cambridge.* 2005.

6. **Pan, B., et al.** Two-dimensional digital image correlation for in-plane displacements and strain measurement: a review. *Measurement Science and Technology.* 2009, Vol. 20, pp. 1-17.

7. **Ostoja-Starzewski, M. and Castro, J.** Random formatio, inelastic response and scale effects in paper. *Philosophical Transactions of the Royal Society.* 2003, Vol. 361, pp. 965-985.

8. **Wallmeier, M., et al.** Explicit FEM analysis of the deep drawing of paperboard. *Mech. Mater.* 2015b, Vol. 89, pp. 202-215.

9. **Pan, B., Asundi, A., Xie, H. and Gao, J.** Digital image correlation using iterative least squares and pointwise least squares for displacement field and strain field measurements. *Optics and Lasers in Engineering.* 2009, Vol. 47, 7-8, pp. 865-874.

Multi-scale Modeling of Paper

Li, Yujun[1,*]; Stapleton, Scott[2]; Reese, Stefanie[1] ; Simon, Jaan-Willem[1]

AUTHOR INFORMATION

Y. Li

[1]Institute of Applied Mechanics,
RWTH Aachen University, Germany

[2]Department of Mechanical Engineering,
University of Massachusetts Lowell, USA

**E-mail address*:
yujun.li@rwth-aachen.de

Summary

Laminated paperboard is widely used in packaging products. It is generally composed of several pulp fiber layers bonded to each other by starch or adhesive material, leading to macro anisotropic elastic-plastic behavior. The aim of this study is to predict the mechanical properties of a paper layer by using a three-scale approach consisting of the fiber wall scale, the fiber network scale, and the layer scale. The homogenization was first performed on the fiber wall scale, where the fibrils were considered at some orientation embedded in a polymeric matrix. The obtained homogenized response was then input to the single fibers in the network model, which was the second scale considered. At this level, the virtual microstructure was generated first by creating the individual fibers in different layers, and then by simulations of artificial compression to obtain the practical fiber volume fraction. Thereafter, the interaction between fibers was described by an interface-based cohesive zone model introduced in all fiber-fiber contact areas. Finally, the macroscopic mechanical properties were obtained by applying periodic boundary conditions, and subsequent numerical homogenization was performed on the generated fiber network.

1. Introduction

Laminated paperboard is widely used in packaging products. Depending on the specific requirement, it can be easily designed as a single layer paper or multi-layer sandwich structure. Paper is generally composed of several pulp fiber layers bonded to each other by starch or adhesive material. Its mechanical properties are strongly controlled by single fiber properties and inter-fiber bonds. In addition, the stochastic nature of the drainage process leads to a planar network structure with more fibers along the machine direction (MD).

Paper typically has three scales of importance: the fiber scale, the network scale, and the paper layer scale. Due to the importance of paper products in packaging and printing industry, there are lots of studies on the paper layer or laminated paperboard, see e.g. Nygårds et al. [1] and Li et al. [2]. At the fiber

level, the single fibers are actually composite materials themselves, since the cell wall of pulp fibers consists of a layered structure of cellulose micro-fibrils embedded in a lignin and hemicellulose matrix. The micro-fibrils are around the axis of the fiber and form a helical assembly in the bundles. The fibril orientation angle governs the mechanical properties of the fiber, as shown in [3]. Recently, a 3D finite element model that accounts for the presence of micro-fibrils has been developed to study the fiber cyclic loading behavior [4]. Similar models have been used in other studies focusing on either the elastic properties of the fiber or the bond properties [5].

In order to predict the macro mechanical properties of paper, a three-scale approach was adopted, with focus on the two lower scales in this work. The following section of this study outlines the general model framework, along with the implementation of a homogenization and modeling strategy at different scales. This model provides the framework for determining the effect of microstructural parameters such as fiber orientation, fiber length, and inter-fiber bond on the network behavior.

2. Modeling framework

Regarding the aforementioned microstructures of the paper layer, the lower scale architecture has much lower length scales than the upper scale characteristic structure. Therefore, a three-scale algorithm was used to evaluate the effect of the micro architecture on the macro material behavior in this study. Figure 1 shows the paper morphology at different scales and the corresponding representative volume element (RVE). The homogenization was performed first on the fiber wall scale, where the fibrils were considered at some orientation embedded in a polymeric matrix. The homogenized response was used to characterize single fibers in the network model, which was the second scale considered. At this level, the analysis was conducted on the generated virtual network. The homogenized stress-strain curves could then be used in macroscale modeling.

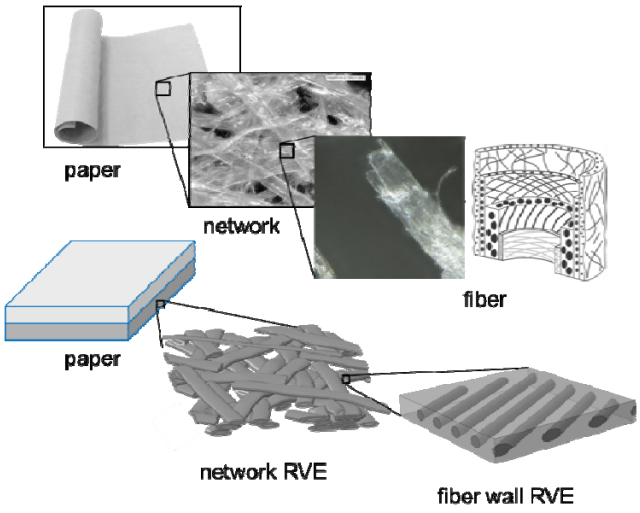

Figure 1. *Comparison of the multi-scale nature of paper and the multi-scale framework for simulation.*

2.1 Single fiber scale

The original wood fiber typically consists of four major layers: the primary wall and three secondary layers S_1, S_2, and S_3. The secondary layers are

composed of cellulosic micro-fibrils and a relatively compliant polymeric substance, comprising of hemicellulose and lignin, which is often treated as a matrix. Since the pulping process removes some contents of the surface layers, the thickest S_2 layer is assumed to dominate the mechanical behavior the fiber. Thereby, the fiber's structural stiffness can mainly be characterized by the properties and the amount of cellulose micro-fibrils embedded in a polymeric matrix of the S_2 layer, as well as their orientation along the fiber. In this study, the fiber was assumed to be purely elastic, because the measured force to break the inter-fiber bond was much smaller than the force for the fiber to achieve nonlinear deformation. In addition, several studies have found the dependence of MFA change on the fiber axial strain, and this will result in a stiffening effect in the case of fiber tension. However, the degree of stiffening is significantly small for high initial MFA, and the measured elastic modulus is not sensitive to the MFA change in experiments. Hence, the MFA was assumed to be constant in the current study.

Since the fiber wall was a composite reinforced with transversely isotropic micro-fibrils, the analytical micromechanical model developed by Chamis [6] was adopted to achieve the homogenized stiffness with sufficient accuracy.

2.2 Network scale

In order to perform analysis at the network level, the first step is to generate a network RVE large enough to represent the actual behavior of the microstructure. Using the experimentally obtained fiber length, diameter, and orientation distribution, the periodic RVE was constructed with a drop-down procedure. During this process, the fibers were deposited one by one on a flat surface. The orientation of these fibers was selected to follow the input statistical distribution. Then, the fibers were brought into contact and deformed by an artificial compression in order to obtain realistic values for the fiber volume fraction. The compressed geometry is shown in Fig. 2(a). It should be noted that the periodic geometry was maintained by applying appropriate boundary conditions. Finally, the interaction between fibers was described by interface-based cohesive zone elements introduced at all fiber-fiber contact areas.

To achieve the macro mechanical properties, six simulations, corresponding to uniaxial loading and pure shear loading states, were performed using periodic boundary conditions. The stress-strain curves could be obtained to compare with experimental results. Figure 2(b) shows the schematic diagram of a stress-strain curve obtained from the uniaxial tension on RVE.

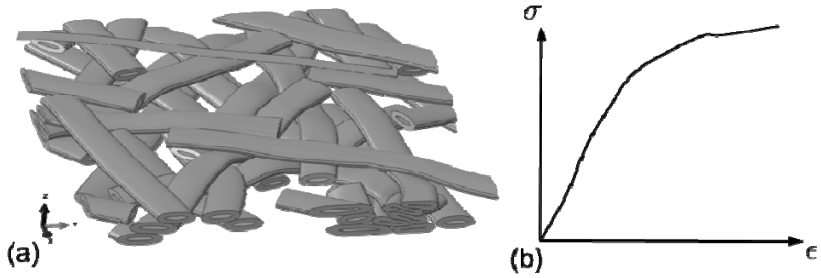

Figure 2. *(a) Compressed 20 fibers network, and (b) schematic diagram of stress-strain curve.*

The network scale analysis allowed simulating the RVE with various fiber structure and orientation. Therefore, it was possible to evaluate the influence of fiber length, diameter and distribution on the macro mechanical properties of paper.

3 Conclusions

This study presented a three-scale approach to predict the mechanical properties of paper. Using this approach, the effect of MFA on fiber properties at the single fiber scale and the effect of the statistical fiber distribution on paper macro properties at the network scale can be evaluated. Furthermore, it is also possible to study the role of inter-fiber bonds in the network deformation. Consequently, the current study established a framework to study the fiber property and pass the information to the upper scale for fiber network analysis.

Acknowledgments

The first author gratefully acknowledges the financial support of the China Scholarship Council (CSC). The last author is grateful for financial support of the Ministry of Innovation, Science and Research of the State of North Rhine-Westphalia.

References

[1] Nygårds M, Just M, Tryding J. Experimental and numerical studies of creasing of paperboard. International Journal of Solids and Structures. 2009;46(11-12):2493-2505.

[2] Li Y, Stapleton SE, Simon J-W, Reese S. Experimental and Numerical Study of Paperboard Interface Properties. Experimental Mechanics. 2016;1-12.

[3] Burgert I, Fratzl P. Plants control the properties and actuation of their organs through the orientation of cellulose fibrils in their cell walls. Integrative and comparative biology. 2009;49(1):69-79.

[4] Borodulina S, Kulachenko A, Tjahjanto DD. Constitutive modeling of a paper fiber in cyclic loading applications. Comp Mater Sci. 2015;110:227-240.

[5] Magnusson MS, Östlund S. Numerical evaluation of interfibre joint strength measurements in terms of three-dimensional resultant forces and moments. Cellulose. 2013;20(4):1691-1710.

[6] Chamis CC. Mechanics of composite materials: past, present, and future. Journal of Composites, Technology and Research. 1989;11(1):3-14.

Posters

Temperature rise at an imbibition front

H. Aslannejad[a], Alexandros Terzis[b], S. M. Hassanizadeh[a]

AUTHOR INFORMATION

[a] Department of Earth Sciences, Utrecht University, Utrecht, The Netherlands Austria
[b] Institute of Aerospace Thermodynamics, University of Stuttgart

Email:
H.Aslannejad@uu.nl

Summary

Spontaneous imbibition of a wetting phase into a porous medium is believed to be driven by energetic forces. The nonwetting phase-solid interface is known to have a higher interfacial energy than the wetting phase-solid interface. Thus, the imbibition process is expected to lead to the release of energy and thus a rise of temperature at the water front. In order to investigate the occurrence of this effect, experiments were performed involving the penetration of water into three different paper types (Plain, glossy and plastic based). A CCD and an infrared (IR) camera were used for the quantitative visualization of the imbibition process. First water and paper were brought to the room temperature. Then, water was injected to one end of a strip of paper. The temperature was found to rise gradually as the water front approached. The temperature rise was 0.6, 0.5 and 0.2 ºC for plain, glossy and plastic based papers.

Introduction

Spontaneous imbibition of water is an important process in many natural and industrial porous media. Water rushes into a relatively dry hydrophilic porous solid despite resistance from viscous drag and even against gravity. Only if the resident phase (e.g. air in the case of unsaturated soil) is put under high pressure, the wetting of the porous medium can be halted. One may pose the questions why spontaneous imbibition occurs and/or which driving force is it that can overcome gravitational and viscous forces. The usual answer is: capillary forces, induced by interfacial tension. In two-phase flow in porous media, there exist indeed three interfaces: two fluid-solid interfaces and one

fluid-fluid interfaces, each with their own interfacial tension. A given solid has (a larger) affinity for one of the fluids, called the wetting phase. The other fluid is called the non-wetting phase. The interfacial tension of the non-wetting fluid-solid interface is always larger than that of the wetting fluid-solid interface. But, we can still pose the question what physical explanation there is for the difference in magnitude of interfacial tension.

Given the fact that the interfacial tension is directly related to the interfacial energy per unit area, a porous solid filled by the non-wetting phase has a higher energy than when it is filled with the wetting phase, under isothermal conditions. That is why the solid phase would spontaneously imbibe the wetting fluid; the solid-fluid system goes to a lower energy state. The spontaneous imbibition would be stronger the larger the affinity of the solid phase for a given fluid is. This is clearly reflected in the definition of capillary pressure on both microscale and macroscale. For a capillary tube, the capillary pressure p^c is given by Young-Laplace equation as:

$$p^c = \frac{2}{r}\gamma^{wn}cos\theta$$

where r is the tube radius, θ is the contact angle, and γ^{wn} is the interfacial tension between the two fluid phases. This equation can be combined with Young's equation (equilibrium balance of forces for a contact line) to obtain:

$$p^c = \frac{2}{r}(\gamma^{ns} - \gamma^{ws})$$

where γ^{ns} and γ^{ws} are the solid-nonwetting phase and solid-wetting phase interfacial tensions, respectively. Clearly, the larger the difference between these two interfacial tensions (i.e., the larger the affinity of the solid for the wetting phase), the larger the capillary pressure. A similar link can be established between macroscale capillary pressure and interfacial surface energies. According to Hassanizadeh and Gray (1993), the macroscale capillary pressure, P^c, can be defined as:

$$P^c = \frac{1}{\varepsilon}(-\frac{\partial F^{wn}}{\partial S^w} + \frac{\partial F^{ns}}{\partial S^n} - \frac{\partial F^{ws}}{\partial S^w})$$

where $F^{\alpha\beta}$ is the total free energy of all $\alpha\beta$-inerfaces within an averaging volume per unit volume, ε is porosity, and S^w and S^n are the saturations of wetting and nonwetting phases, respectively. Here, the changes of free energies of bulk phases are neglected. Obviously, for P^c to be positive, there

must be a net decrease of the energy of all interfaces when the saturation of the wetting phase increases. This is the basis of spontaneous imbibition.

This reasoning suggests that during spontaneous imbibition, energy should be released. Such a release of energy should result in a (temporary) rise of temperature. This was shown to be the case as early as 1960 (Anderson and Linville [3]). A temperature spike was observed at a front when a nonwetting phase was displaced by a wetting phase. The rise ws of limited duration as the amount of released energy is limited and the fluid arriving behind the front dissipates the generated heat. Early explanation of the observed temperature spike was based on the heat of condensation of vapor on soil grains (Anderson and Linville (1960) [3]). It was only later that it was shown that the energy needed for the observed temperature rise is much more than the heat of vapor condensation.

In this research, we have revisited the question of occurrence of temperature spikes during spontaneous infiltration. We have used infrared imaging in order to monitor temperature changes in time and space continuously and simultaneous optical imaging to monitor the water movement in the porous medium. As porous medium, we have used six various paper types with different thicknesses. First, we provide a detailed review of the literature on the occurrence of a temperature spike at a front where a wetting phase displaces a nonwetting phase. Next, various paper types used in our studies and the experimental setup are described. Results are presented and their significance and how they correspond to the results by other authors are discussed.

References

[1] G. Claxton, Detector for liquid-solid chromatography, J. Chromatogr. A. 2 (1959) 136–139. doi:10.1016/S0021-9673(01)86273-7.

[2] M. Blumer, Thermometric Monitor for Chromatographic Streams, (1960).

[3] D.M. Anderson, A. Linville, Temperature Fluctuations at a Wetting Front: I. Characteristic Temperature-Time Curves, Soil Sci. Soc. Am. J. 26 (1962) 14. doi:10.2136/sssaj1962.03615995002600010005x.

Modeling of the fluid flow in tailor-made paper substrates

Franz Carstens

AUTHOR INFORMATION


F. Carstens

Fachgebiet PMV – TU Darmstadt,
Alexanderstraße 8, D-64283 Darmstadt

Email:
carstens@papier.tu-darmstadt.de

Summary

In the present work, the flow of deionised water in tailor-made paper substrates was studied. Therefore, handsheets of different fibre sources, cotton linters, eucalyptus sulphate and a mixture of pine and spruce sulphate, were formed at the same freeness and grammage. Firstly, the thickness and the porosity of the paper substrates in dry state as well as in wet state were respectively determined. Some differences between the three fibre types were revealed. In addition, the capillary rise of the lab-engineered paper substrates was determined according to the Klemm method. Moreover, a mathematical model that matches the mentioned method and describes the fluid flow was introduced. Afterwards, the experimental and the theoretical results were compared.. Furthermore, the model was also compared to the Lucas-Washburn equation in order to show the differences between them.

The findings suggest a considerable improvement in the description of the fluid flow in tailor-made paper substrates. By changing the fibre types and some paper values, it was possible to reduce or raise the capillary rise, which eventually allows us to modulate and control fluid flow in a more accurate and desirable way. Finally, the introduced mathematical model allows describing the fluid flow more accurately than the Lucas-Washburn equation.

Introduction

Paper-based microfluidic devices have successfully proven to be a novel system for fluid handling and fluid analysis for a variety of applications; such as environmental monitoring, disease diagnostics and even food quality testing. Over 1000 articles in the field of microfluidic paper-based analytical devices (μPADs) have been published [1]. In order to optimized the μPADs, it is essential to understand the fluid flow. The first researchers who studied the dynamics of capillary flow were Poiseuille [2], Lucas [3], and Washburn [4]. The latest is well known for its capability to describe the capillary rise. However, it does not properly work with paper substrates since it assumes parallel, cylindrical capillaries with homogeneous radii or evaporation of the fluid during the capillary rise. Several research groups have since presented modified equations to improve the predictive accuracy of fluid flow. Szekely et al. took for instance inertial and gravitational forces into account [5]. Cai et al. extended Washburn's equation to characterize the water absorption [6]. Other groups have developed a non-uniform capillary model, considering pore size distribution instead of a mean pore value [7, 8]. Liu et al. proposed another model under consideration of water evaporation [9].

However, these models either consider the evaporation of water, or the swelling of the fibres, or some physical properties of fibres and papers; but not altogether. Therefore, this work introduces a model, which describes the fluid flow in tailor-made paper substrates by considering the influence of mentioned properties.

Materials and methods

For this work three different bleached fibre sources were used: cotton linters (CL), eucalyptus sulphate (ES), and a long fibre sulphate mixture (LFS, 50 % pine sulphate, 50 % spruce sulphate). In addition, deionised water was used for the Klemm method.

For the preparation of the lab-engineered paper substrates, the fibre types were first refined in a Voith LR 40 laboratory refiner with different effective specific energies, in order to obtain a freeness value of 21±1 SR, which was determined according to ISO 5267. Afterwards, the lab-engineered paper sheets were fabricated on a conventional Rapid-Koethen handsheet mould (ISO 5269/2) with a grammage of 80 ± 1 g/m^2 (ISO 536:2012).

The capillary rise of the lab-engineered paper substrate samples was determined according to the Klemm method (ISO 8787). During the tests, the samples were also weighed with a digital lab-balance and recorded with a

video camera, in order to determine the water's mass and height, respectively.

The proposed model is a numerical method based on the mass balance of the paper substrate sample, which is expressed as

$$m_0 = m_r + m_{ev} \quad (1)$$

where m_0 is the mass entering the sample, m_r the remaining water mass in the sample and m_{ev} the evaporating water mass (see *Figure 1*).

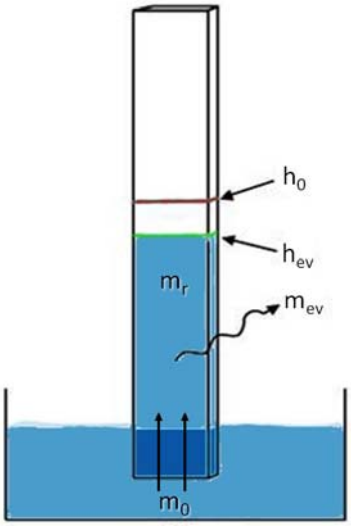

Figure 1: Mass balance of paper substrate sample

After several assumptions, substitutions and differential calculation, one can solve the equation (1) to

$$h_{ev} = 2 \cdot N \cdot e^{-M \cdot t} \cdot \int_0^{\sqrt{t}} e^{M \cdot t^2} \cdot dt. \quad (2)$$

where M and N are constants defined as:

$$M = \frac{2 \cdot m^*_{ev}}{\rho \cdot (\Delta\delta + \delta_0 \varepsilon_0)}; \qquad N = \sqrt{\frac{\sigma \cdot \cos\theta \cdot K}{\varepsilon_{p,0} \cdot \eta \cdot r_0}} \quad (3)$$

The parameters in equations (2) and (3) are the time t, the evaporation rate m^*_{ev}, the density ρ, the thickness δ, the porosity ε, the surface tension σ, the contact angle Θ, the permeability K, the viscosity η and the pore radius r.

Results

The actual capillary rise h_{ev} of the paper substrates samples calculated with equation (2) is plotted as a function of the time in *Figure 2*. First of all, it can be observed that the capillary rise of each sample varies depending on the fibre type used. While LFS shows a lower increase in the capillary rise, cotton

linters' increase exhibits a higher value, letting eucalyptus with the highest capillary rise of all samples. The continuous and the interrupted lines show the experimental and the theoretical (from model calculated) values, respectively. It can be seen that both values fit very good for each tested sample. Furthermore, correlation coefficients between the experimental and the theoretical h_{ev} were calculated. The results indicate values of 0.997 or above, which indicate a high accuracy of the model presented in this work.

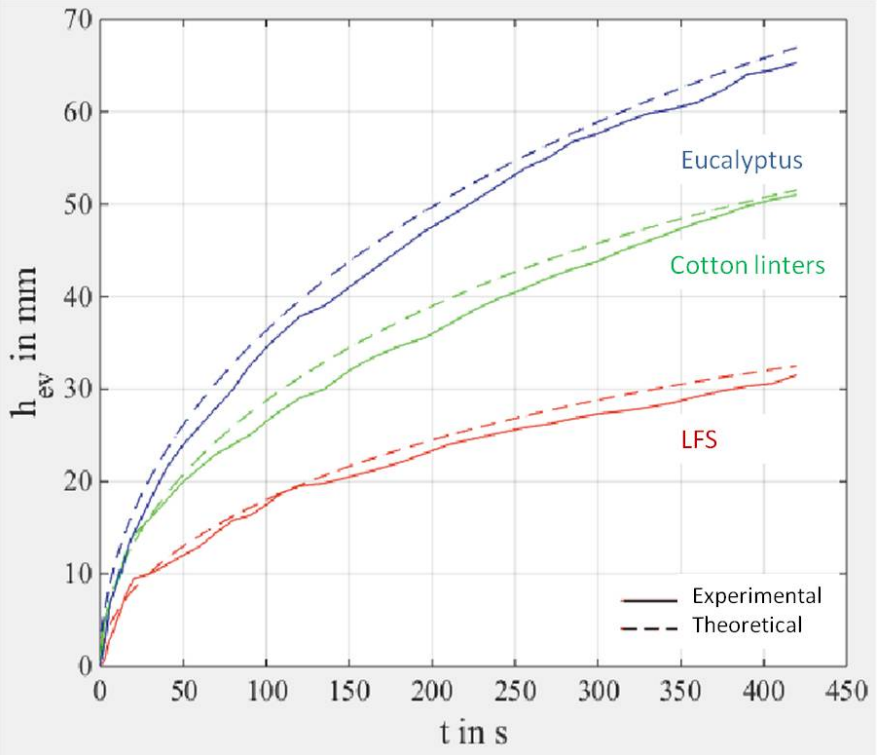

Figure 2: Mean value of the capillary rise as a function of time

Conclusions

In the present work, the capillary rise of lab-engineered paper substrates made from three different fibre types was investigated. The findings have shown that the capillary rise varies according the fibre source. In addition, a mathematical model that describes the capillary rise was introduced and compared to the experimental values. The results showed a great correlation between the theoretical and the experimental methods.

Acknowledgments

I would like to thank the "National Council of Science and Technology, CONACYT" and the "German Academic Exchange Service, DAAD" for a research scholarship.

Literature

1. Cate, D.M., et al., *Recent Developments in Paper-Based Microfluidic Devices.* Analytical Chemistry, 2015. 87(1): p. 19-41.
2. Poiseuille, J.L.M., *Recherches sur la force du coeur aortique.* Doctoral Thesis, 1828: p. 1-46.
3. Lucas, R., *Ueber das Zeitgesetz des kapillaren Aufstiegs von Flüssigkeiten.* Kolloid-Zeitschrift, 1918. 23(1): p. 15-22.
4. Washburn, E.W., *The Dynamics of Capillary Flow.* Physical Review, 1921. 17(3): p. 273-283.
5. Szekely, J., A.W. Neumann, and Y.K. Chuang, *The rate of capillary penetration and the applicability of the washburn equation.* Journal of Colloid and Interface Science, 1971. 35(2): p. 273-278.
6. Cai, J., et al., *Fractal characterization of spontaneous co-current imbibition in porous media.* Energy & Fuels, 2010. 24(3): p. 1860-1867.
7. Masoodi, R., K.M. Pillai, and P.P. Varanasi, *Darcy's law-based models for liquid absorption in polymer wicks.* AIChE Journal, 2007. 53(11): p. 2769-2782.
8. Patro, D., S. Bhattacharyya, and V. Jayaram, *Flow Kinetics in Porous Ceramics: Understanding with Non-Uniform Capillary Models.* Journal of the American Ceramic Society, 2007. 90(10): p. 3040-3046.
9. Liu, Z., et al., *Experimental and numerical studies on liquid wicking into filter papers for paper-based diagnostics.* Applied Thermal Engineering, 2015. 88: p. 280-287.

Exploring Paper/AgNW based composites for photovoltaic devices by atomic force microscopy methods

Caterina Czibula[1,3], Christian Ganser[1,3], Markus Kratzer[1], Robert Schennach[2,3], Bettina Friedel[2] and Christian Teichert[1,3]

AUTHOR INFORMATION

[1] Institute of Physics, Montanuniversitaet Leoben, Austria

[2] Institute of Solid State Physics, Graz University of Technology, Austria

[3] Christian Doppler Laboratory for Fiber Swelling and Paper Performance, Institute for Pulp, Paper and Fiber Technology, Graz University of Technology, Austria

Email: caterina-marina.czibula@stud.unileoben.ac.at

C. Czibula

To power environmentally friendly flexible electronics, a flexible organic based solar cell would also be of advantage. One possibility to realize such a solar cell is utilizing kraft pulp fiber networks as a substrate for a diode architecture, where P3HT:PCBM photovoltaic devices with conductive silver nanowire (AgNW)-coated cellulose fiber networks as a free-standing anode are used [1]. Here, atomic force microscopy (AFM) and related scanning probe microscopy techniques have been applied to study the topography and electrical properties of the paper/nanowire composite.

Due to the high porosity of the paper used, the paper sheet can be described as an arrangement of single fibers coated with AgNWs. Cellulose fibers are roughly 30 µm in diameter and have a length of about 4 mm, and the AgNWs have a diameter of about 115 nm and a length of about 20 µm – 30 µm. The composite can be seen on AFM topography images in figure 1a-c. The AgNW/cellulose anode fibers are coated with semiconductive and photoactive polymer layers, as required for a typical diode stack (see fig.3a). The devices exhibit diode behavior in the dark and a significant photoresponse under illumination [1].

In the present work, the topography of cellulose fibers/AgNW composites as well as of the different polymer layers has been studied by AFM. Furthermore,

especially the interaction between cellulose and AgNWs has been investigated to show that the AgNWs are in contact with the paper substrate. In figure 1a-c, topography images of the cellulose fibers/AgNWs composites are presented with increasing resolution. It can be seen that the AgNWs are in contact with the paper substrate which has been confirmed by analyzing line profiles of the topography images.

To further investigate the behavior of the cellulose fibers/AgNWs composite, also Kelvin Probe Force Microscopy (KPFM) [2] was applied to measure contact potential differences (CPD). In figure 1d, a clear contrast between the AgNWs and the cellulosic background is visible, which is only enhanced if a voltage is applied to the sample.

For detailed information about the interaction and contact between cellulose and AgNWs, also the behavior of spin-coated regenerated cellulose films with AgNW has been investigated. AFM topography images are presented in figure 2. It was found that the wires are underneath and also on top of the film and they are covered by dot-like agglomerates which are possibly AgCl.

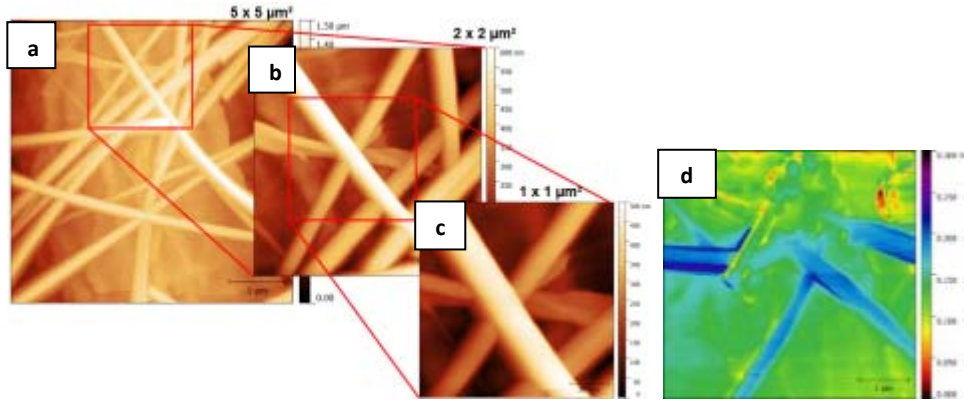

Figure 1: *(a-c) AFM topography images of cellulose fibers/AgNW composites demonstrating with increasing resolution contact between the nanowires and the cellulose fibers. A CPD image (right) of these composites reveals the contrast between AgNWs (blue) and the cellulose substrate (green).*

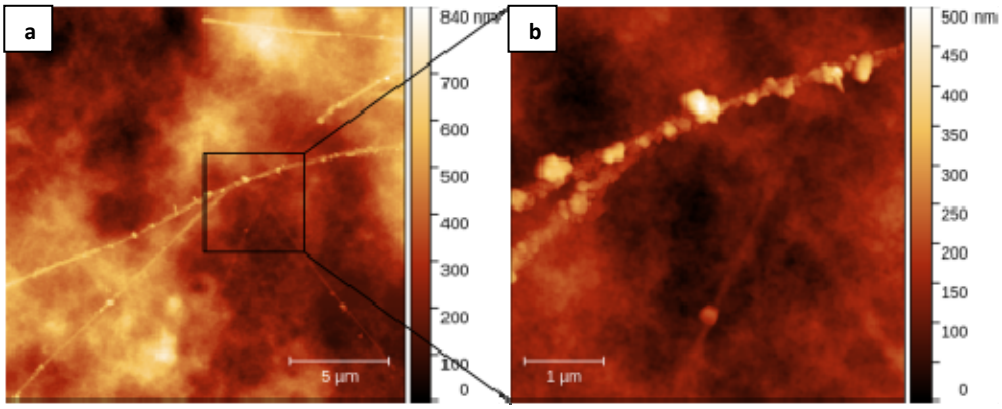

Figure 2: *(a) 20 x 20 µm² and (b) 5 x 5 µm² topography image of regenerated cellulose films with AgNWs.*

First results of a paper based photovoltaic device are presented in figure 3. In figure 3a, the architecture of the device is illustrated, whereas in figure 3b parts of the layout are shown. A 10 x 10 µm² topography image of the photovoltaic device, presented in figure 3c, proves that underneath the semiconducting P3HT:PCBM covered surface, cellulose fibers and possibly AgNWs are distinguishable.

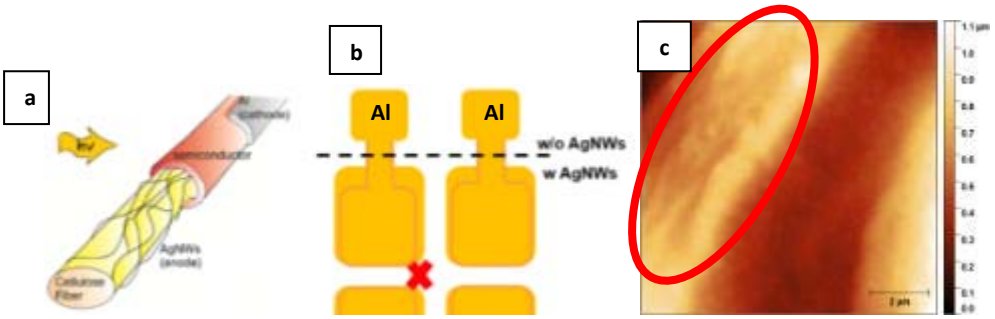

Figure 3: (a) *The scheme depicts the architecture of a paper fiber photovoltaic device based on cellulose/AgNW anodes.* ***(b)*** *The sketch shows parts of the photovoltaic device and the red cross indicates the position of the measured topography image.* ***(c)*** *A 10 x 10 µm² topography image of the cellulose fiber-based P3HT:PCBM photovoltaic device. With the red circle a cellulose fiber is marked.*

For the subsequent measurement of generated photocurrents, photoconductive AFM (PC-AFM) [3] would be the method of choice, however, this technique – operating in contact mode – cannot be applied to the fragile samples under investigation. As an alternative, photo-assisted KPFM (see e.g. [4]) operating in tapping mode will be employed under illumination with white light.

In summary, AFM and KPFM prove to be appropriate methods to investigate the surface and electrical properties of complex cellulose fiber-silver nanowire composites. Although the samples are fairly rough, we succeeded to study the interaction between cellulose fibers and films with AgNWs in detail. There is hope that photo-assisted KPFM reveals insights on the performance of novel paper fiber/AgNW/organic semiconductor based photovoltaic devices.

Literature

[1] H. Kopeinik, R. Schennach, J. Gallik, H. Plank, B. Friedel, “Photodiodes based on wood pulp fiber networks”, Cellulose **22** (2015) 3425.

[2] M. Nonnenmacher, M. P. O’Boyle, H. K. Wickramasinghe, “Kelvin Probe Force Microscopy“, Appl. Phys. Lett. **58** (1991) 2921.

[3] I. Beinik, M. Kratzer, A. Wachauer, L. Wang, C. Teichert, Y.P. Piryatinski, G. Brauer, X.Y. Chen, Y.F. Hsu, A.B. Djurišić, “Photo-response from single upright standing ZnO nanorods”, Beilstein J. Nanotechnol. **4** (2013) 208.

[4] M. Müller, M. Hývl, M. Kratzer, C. Teichert, S. Misra, M. Foldyna, L. Yu, P. Roca i Cabarrocas, T. Itoh, Z. Hájková, A. Vetushka, M. Ledinský, J. Kočka, A. Fejfar, “Investigating inhomogeneous electronic properties of radial junction solar cells using correlative microscopy”, Jap. J. Appl. Phys. **54** (2015) 08KA08.

Effect of process parameters on the dryness of molded pulp products

DIDONE MATTIA, TOSELLO GUIDO

AUTHOR INFORMATION

M. Didone

Mattia Didone, PhD Student
Technical University of Denmark,
Department of Mechanical Engineering,
Produktionstorvet
Building: 427, 314
2800 Kgs. Lyngby, Denmark
ORCID: 0000-0002-5353-7333
Homepage: http://www.mek.dtu.dk
Phone: +45 45254803

E-mail:
matdid@mek.dtu.dk

ABSTRACT

Molded pulp products are made from cellulose fibers dispersed in water then formed, drained and dried. As in the conventional papermaking process, the most energy intensive operation (including time) is drying. To gain a better understanding of the process parameters involved and to investigate their influence on the final product's dryness, two experimental plans were designed and analyzed by means of design of experiments (DOE).

A numerical simulation of the heat model was developed with the aim of finding the process time window.

MATERIALS

Test rig

The laboratory-molding machine (Figure 1) is capable of press dry a preformed paper disk of Ø100 mm. The upper half of the mold is fixed to the outer frame and is heated up to the imposed temperature. The bottom half of the mold is moved upwards by a double acting cylinder and it consists of a backing plate placed on top of a vacuum plate.

90% vacuum (i.e. 101,3 mbar in absolute pressure) is applied for a defined time in order to dry the paper disk.

Process steps:

1. Pressure is increased until the imposed limit (**p**).
2. Pressure and temperature (**T**) are kept constant for a certain time (holding time, **ht**).

3. Vacuum is applied while the mold is kept closed (vacuum time, **vt**).
4. Pressure is released by moving down the bottom half of the mold.

The variables, or factors, object of the DOE investigation are highlighted in bold.

Pulp characteristics

The pulp type used for the experiments is Kraft birch, with an average fiber length of 1 mm and width of 20 μm. Drainability is 20°SR and the water retention value is 1,078 g/g.

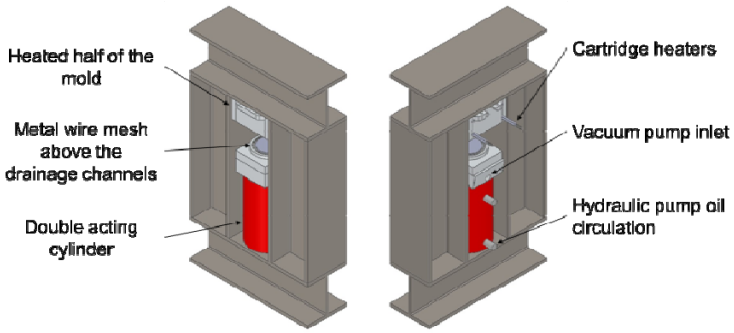

Figure 1: Scheme of the test rig used for press-dry the paper disks

NUMERICAL SIMULATION

A numerical simulation of the heat model was developed with the aim of finding the process time window. The heat is predominantly transferred from the mold to the paper disk by means of conduction along the thickness direction. The rate equation that appropriately quantifies the heat conduction is known as Fourier's law, and for the 1-D case is as follows:

$$q_x'' = -k\frac{dT}{dx} \qquad (1)$$

The equation was modelled using Crank-Nicolson method. The considered domain consists of the paper disk and the bottom half of the mold. The domain enmeshment and the boundary conditions can be seen in Figure 2.

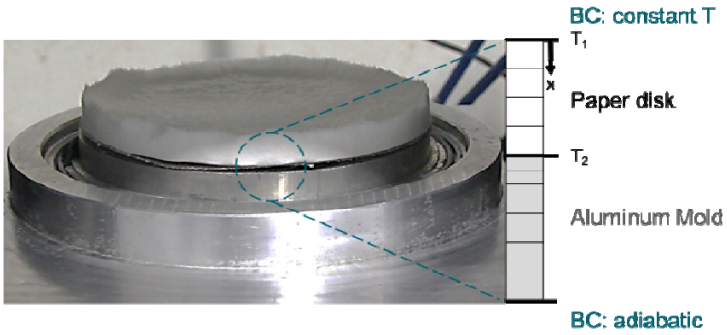

Figure 2: 1-D enmeshment of the paper disk and the aluminum mold to get the process time window via numerical simulation

The effective thermal conductivity of the paper pulp was estimated according to Maxwell's equation [1]. The results are reported in table 1

Table 1: Inputs and results of the numerical simulation

Upper mold T_1 [°C]	Initial paper T_2 [°C]	Final paper T_2 [°C]	Time [s]
110	25	55	34,5
160	25	80	41,3
210	25	105	44,8

DESIGN OF EXPERIMENTS (DOE)

Processing conditions are mainly characterized by the molding temperature, pressure and process time [2]. To investigate the influence of these variables on the final dryness of the paper disks, two experimental plans were designed and analyzed by means of design of experiments (DOE). The hypothesis of the model have been checked according to ANOVA.

The dryness is seen as an efficiency of the process, i.e. the amount of water removed by the drying process with respect to the ideal amount:

$$dryness = \frac{m_{wet} - m_{disk}}{m_{wet} - m_{dry}} \quad (2)$$

Two experimental plans were performed, in which different factors were kept fixed and the others varied. The main effects plot and the interaction plot for the two plans can be seen in Figure 3 and Figure 4 respectively.

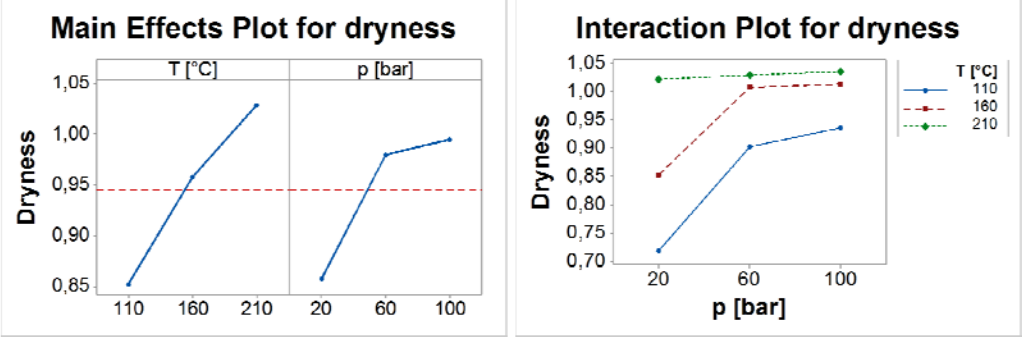

Figure 3: Main effects and interaction plot for the response dryness. First experimental plan, fixed holding time (5 s) and vacuum time (15 s).

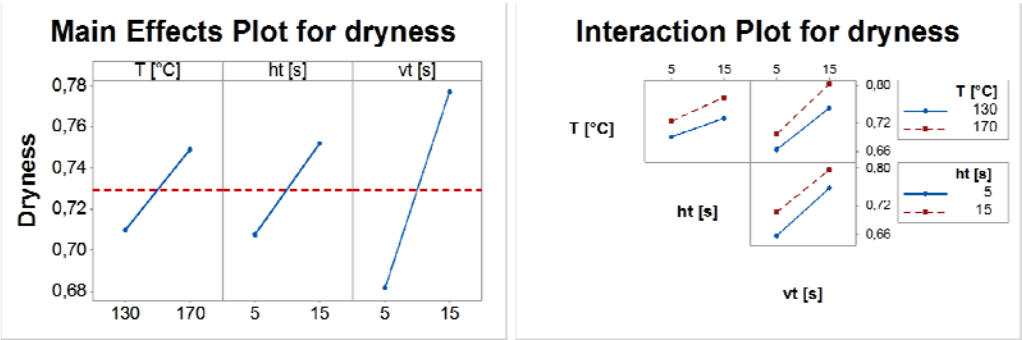

Figure 4: Main effects and interaction plot for the response dryness. First experimental plan, fixed pressure of 50 bar.

CONCLUSIONS AND OUTLOOK

- The numerical simulation showed that the process time can be shorten if both the halves of the mold are heated.
- After a certain limit, the pressure is no more beneficial for the drying process. This evidence is in accordance with the assumption given in [3], i.e. the energy transfer is independent of the pressure if the applied pressure is above 30 bar.
- The increasing of the temperature is beneficial, but a good compromise has been reached around 160°C.

ACKNOWLEDGMENT

Support from Innovation Fund Denmark, funding a consortium between DTU Mechanical Engineering, EcoXpac and Carlsberg Group, is gratefully acknowledged. Particularly, the authors express their gratitude to Christian Carlsen and all the EcoXpac team for invaluable experimental assistance.

LITERATURE

[1] M. Karlsson, *Papermaking Part 2, Drying*. TAPPI, 2000.

[2] S. T. Seana, B. Sanschagrina, B. V Koktab, and D. Maldasb, “Effects of processing variables on the mechanical properties of compression molded polystyrene-wood fiber composites,” *Die Angew. Makromol. Chemie*, vol. 184, no. 3128, pp. 157–166, 1991.

[3] J. Nilsson and S. Stenström, “Modelling of Heat Transfer in Hot Pressing and Impulse Drying of Paper,” *Dry. Technol.*, vol. 19, no. 10, pp. 2469–2485, 2001.

Modelling of stress relaxation and elastic recovery of wet paper

JARMO KOUKO[1], JOONAS SORVARI[2] AND ELIAS RETULAINEN[1]

AUTHOR INFORMATION


J. Kouko

[1] VTT Technical Research Centre of Finland Ltd,
P.O. Box 1603, FI-40101 Jyvaskyla, Finland,
[2] Lappeenranta University of Technology
P.O. Box 20, FI-53851, Lappeenranta, Finland

Email:
jarmo.kouko@vtt.fi
joonas.sorvari@lut.fi
elias.retulainen@vtt.fi

INTRODUCTION

Understanding and control of the viscoelastic behavior of paper web is important for the runnability of modern paper machines and for the success of converting processes that contain finite deformations at a high strain rate. It is well known that tension in a wet and dry paper web is non-linearly proportional to strain, and depends on the strain rate. Strain in paper is not completely recovered after the tensile load is removed, part of the recovery is time-dependent and part is non-recoverable [1]. A relaxation phase in the stress-strain cycle makes the behavior more complex and challenging.

The objective of this study was to model the rheological, time-dependent stress-strain cycle that includes a relaxation, de-loading and an elastic recovery phase. The modeling was based on experimental data that was produced for softwood and hardwood kraft pulps at different strain rates.

EXPERIMENTAL

This study is a continuation of the analysis of the tension relaxation data of wet paper that has partly been presented earlier [2-3]. Two bleached kraft pulps beaten to two levels were used: Bleached Nordic softwood (50 and 200 kWh/t) and bleached eucalyptus (100 and 200 kWh/t) kraft pulps. Additionally, the fines were removed from the 200 kWh/t refined softwood kraft pulp. 60 g/m^2 hand sheets (with white water recirculation, except for the fines-free case). Two wet pressing levels were used for varying the solids contents of the sheets: 50 kPa and 350 kPa.

The test contained a straining cycle with three (four) phases: straining, relaxation and de-straining phases (and re-straining to failure). The wet

samples were strained using three different strain rates (1, 10, and 100%/s) in the C-Impact tester [4]. The straining cycle first had a straining to 2% strain, then a 10-second relaxation phase at 2% strain followed by a de-straining to zero tension at the initial strain rate (and finally re-straining to failure).

For the linearly viscoelastic material, the relaxation modulus of the integral-based constitutive equation is commonly represented via the Prony series [5]:

$$E(t) = E_0 + \sum_{i=1}^{N} E_i e^{-t/\lambda_i} \quad (1)$$

where t is time (s), $E(t)$ is the relaxation modulus (kN/m), E_i, λ_i are non-negative constants (kN/m and s, respectively). The constants λ_i are commonly referred to as relaxation times and are often chosen equidistantly on the logarithmic time axis, one or two per decade. Due to the inertia effects, an ideal step loading relaxation test cannot be performed. It can be assumed that a large error can occur in the approximated relaxation modulus if the step strain assumption is used and the ramp time is large [5]. In this study, a simple correction method introduced by Zapas and Phillips [6] was applied for the linear model with a finite ramp time that was:

$$E(t) = \frac{\sigma(t + t_1/2)}{\varepsilon_0} \quad t \geq t_1/2 \quad (2)$$

where ε_0 is the constant strain, σ is tension (N/m) and t_1 is the ramp time. According to Sorvari [5], the Zapas-Phillips method can give accurate results in the time interval of validity, i.e., at times $t > t_1/2$. In this study, the strain rates were 1 %/s, 10 %/s and 100 %/s and the ramp times to 2% strain were 1.97 s, 0.196 s and 0.021 s, respectively. The Prony series in this study was

$$E(t) = E_0 + E_1 e^{-t/0.01} + E_2 e^{-t/0.1} + E_3 e^{-t/1} + E_4 e^{-t/10} \quad (3)$$

where E_1 and E_2 = 0, when the strain rate was 1 %/s and E_1 = 0, when the strain rate was 10 %/s. The stress-strain behavior of the wet paper was non-linear, and therefore the Prony series was applied to Schapery's nonlinear viscoelastic model [7]. The Schapery model can be utilized because it contains same structure as the linear integral model [4]. The nonlinear elasticity of the stress-strain curve of paper can be described by using hyperbolic functions. The proposed model in this study describes both time- and strain-dependent behavior and was developed from the earlier version [8]:

$$\sigma = D_0 \sinh(D_1 \varepsilon) D_T + C_0 \tanh(C_1 \varepsilon) C_T + h(\varepsilon) \int_0^t E(t - \tau) \varepsilon'(\tau) d\tau \quad (4)$$

D_T = 0 and C_T = 1, if $d\varepsilon/dt$ >= 0 or σ > 0

D_T = 1 and C_T = 0, if $d\varepsilon/dt$ < 0 or σ <= 0

At σ < 0, modeled tension is negative for a rigid material, but for paper with low bending stiffness, it can be set σ = 0

where C_0, C_1, D_0 and D_1 are constants. $h(\varepsilon)$ was constant in this study, but it will depend on the strain, in case the data has several different strain levels.

The modeling of the stress-strain curves was performed using the following procedure stages. At First the Zapas-Phillips time correction was applied to the data and then the Prony series (Eq. 3) was fitted to the time-dependent stress-relaxation phase (see Fig. 1). In the second stage the determined Prony series parameters were applied to the proposed version of the Schapery model and it was fitted to straining and de-straining phases simultaneously. In all cases, the GRG Nonlinear Solver in MS Excel was used for the nonlinear least-squares optimization to determine the material parameters.

RESULTS

The time-dependent stress relaxation phase could be modeled very well with the Prony series. Figure 1 shows a representative example of a Prony series fit on the studied relaxation data. The Prony series parameters depended on the strain rate, but in general they also showed linear relation to initial tension of the relaxation [3].

Using the Prony series together with the Schapery model, the nonlinear stress-strain cycle could be fitted with reasonable accuracy. Also the apparent master curve can be modeled very well. However, the re-straining phase (from zero tension to the apparent master curve) could not be modeled adequately with the proposed model. More investigation and development is needed for successful modeling of the subsequent re-straining phases.

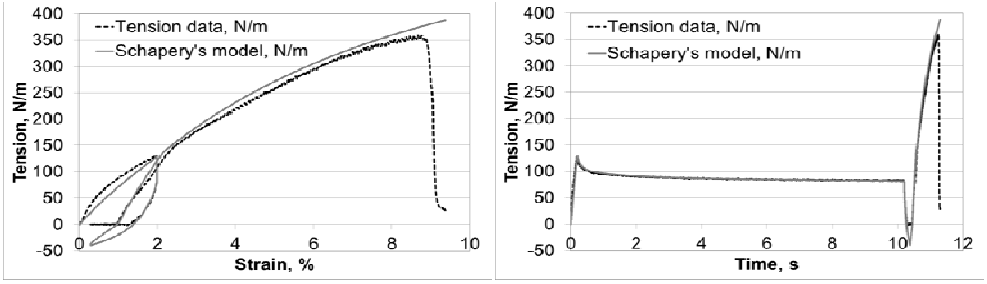

Figure 1. The straining phase is followed by the relaxation, de-straining and re-straining phases in the tensile data of wet paper. Bleached eucalyptus kraft pulp 200 kWh/t, solids content 49%, strain rate 10 %/s.

Applicability of the proposed model for tensile creep modeling was checked with simple benchmark test using ABAQUS. The proposed model presented a realistic tensile creep curve for the test case. The successful creep test encourages the continued development of the proposed model.

CONCLUSIONS

It could be concluded that the proposed nonlinear viscoelastic theory based on the Schapery model and Prony series was capable of predicting the time- and strain-dependent responses of wet paper very well at practical strain levels and time ranges.

ACKNOWLEDGEMENT
This work has been supported by the PowerBonds project belonging to the EU WoodWisdom-Net program.

REFERENCES
[1] Skowronski, J. and Robertson, A.A. The deformation properties of paper: Tensile strain and recovery. *J. Pulp Paper Sci.* 1986. Vol. 12, no. 1, pp. J20–J25.
[2] Kouko, J. and Retulainen, E. The influence of strain rate and pulp properties on the stress-strain curve and relaxation rate of wet paper. *Tappi J.* 2015. Vol. 14, no. 8, pp. 515-524.
[3] Kouko, J., Sorvari, J. and Retulainen, E. The influence of strain rate and pulp properties on the stress relaxation of wet paper – modelling of relaxation. *Submitted to Tappi J.*
[4] Kouko, J. Effects of heating, drying and straining on relaxation and tensile properties of wet paper. PhD thesis, 2014. University of Jyväskylä.
[5] Sorvari, J. Modelling methods for viscoelastic constitutive modelling for paper. PhD thesis, 2009. University of Kuopio.
[6] Zapas, L.J. and Phillips, J.C. Simple Shearing Flows in Polyisobutylene Solutions. *J. Res. Natl. Bur. Stand.* 1971. Vol. 75A, no. 1, pp. 33–40.
[7] Schapery, R.A. Nonlinear viscoelastic and viscoplastic constitutive equations based on thermodynamics. *Mech. Time-Depend. Mater.* 1997. Vol. 1, pp. 209–240.
[8] Sorvari, J., Kouko, J., Malinen, M., Kurki, M. and Hämäläinen, J. Paper as a viscoelastic material: comparison between different theories. *Int. Paper Phys. Conf.* 2007. pp. 389-396.

Characterization of the load capacity of a vulcanized fiber inner thread

Mittendorf, Roman-Marius and Künne, Bernd

AUTHOR INFORMATION


R.-M. Mittendorf


B. Künne

Technische Universität Dortmund
Institut für Konstruktion und Werkstoffprüfung
Fachgebiet Maschinenelemente
Fakultät Maschinenbau
Leonhard-Euler-Straße 5
44227 Dortmund. Germany

Email:
roman.mittendorf@tu-dortmund.de

Summary

The test results show that the load capacity and the machinability of vulcanized fiber are very good. With the established regression model the load capacity of an inner thread is calculable. At the same time this research work represents an essential step for the reactivation of an industrial interest in vulcanized fiber as a resource-saving construction material to substitute products made of plastic material.

Introduction

Vulcanized fiber is a material that is fully based on the renewable raw material cellulose and was first developed in the mid-19th century. It is made of absorbent and unsized special papers, which are joined by a merging process into one homogenous material by adding a parchmentizing solution. After bonding, the parchmentizing solution is leached out in a multistage process by using osmotic forces. As a result of the rapid development of petrochemical plastics in the period between 1930 and 1950 fundamental material science studies are missing. Consequently, there is a big lack of knowledge about processing and joining of vulcanized fiber. The aim of this research work is the characterization of the load capacity of a vulcanized fiber inner thread (M5, M6, M8, and M10) by using the method of statistical design of experiments.

Conclusions

For scientific research it has to be taken into account that vulcanized fiber is a hygroscopic material. This implies that the moisture content depends on the climatic conditions of the environment. Moisture content gains with increasing humidity as well as decreasing temperature and has a leading effect on material properties and dimensional stability. For example high material

moisture has a decreasing effect on mechanical strength properties and an increasing effect on the ductility [1], [2], [3]. Thus embedded water operates like a flexibilizer. To simulate constant testing conditions a climate chamber must be used.

At first, manufacturing methods of thread-cutting and thread-forming are preformed and analyzed. Testing conditions of T = 20 °C (temperature) and X = 40 % RH (relative humidity) are determined. Both methods are generally suitable for vulcanized fiber. In this context it has to be taken into account that the core drill hole is not standardized for the method of thread-forming. However, the size of the core drill hole has a decisive influence on the thread height and the transverse contact ratio of a bolted connection. For vulcanized fiber approximate values of steel materials are appropriate. Compared to the process of thread-cutting thread heights between 46 % and 77 % are achieved. Finally, these relatively low thread heights are typical for the process of thread-forming.

To identify the significant effects on the load capacity of an inner thread a screening-analysis with a full factorial design (scope of experiments: $n = 2^7 = 128$) has been performed. This analysis establishes that the method of thread-forming is to be preferred. The load capacity of a formed thread is about 7 % to 12 % higher caused by a continuous fiber structure and an additional material compaction. All in all, climatic conditions, coupling dimensions and testing speed have a significant effect. Furthermore the wear resistance of a vulcanized fiber inner thread has been rated as “very good”.

Subsequently, a regression analysis (CCF-design; scope of experiments: n = 130) is performed and a model for calculating thread capacity depending on the thread diameter, the length of engagement as well as the ambient temperature and the relative humidity is created. The regression model consists of 20 terms. Table 1 shows the vaild factor range.

factor	**vaild value range**
temperature T [°C]	10 … 50
relative humidity X [%]	40 … 90
thread diameter D	M5,M6,M8,M10
length of engagement m [mm]	5 …15

Table 2: Vaild factor range of the regression model [1]

To validate the model a residual analysis, an analysis of variance and a lack-of-fit test are performed and have been assessed positively. Additionally, validation tests are executed and indicate a very good prediction accuracy of the created model. Summarized, the regression model is suitable for the characterization of the load capacity of a vulcanized fiber inner thread. Figure 2 visualizes the effect of a single factor variation. To achieve high load capacity values an increase of the length of engagement m is preferable. Regarding the conditions dry climates are preferable [1]. With the results of this research work a realistic and dependable description of interactions of the system “load capacity of a vulcanized fiber inner thread” is now possible.

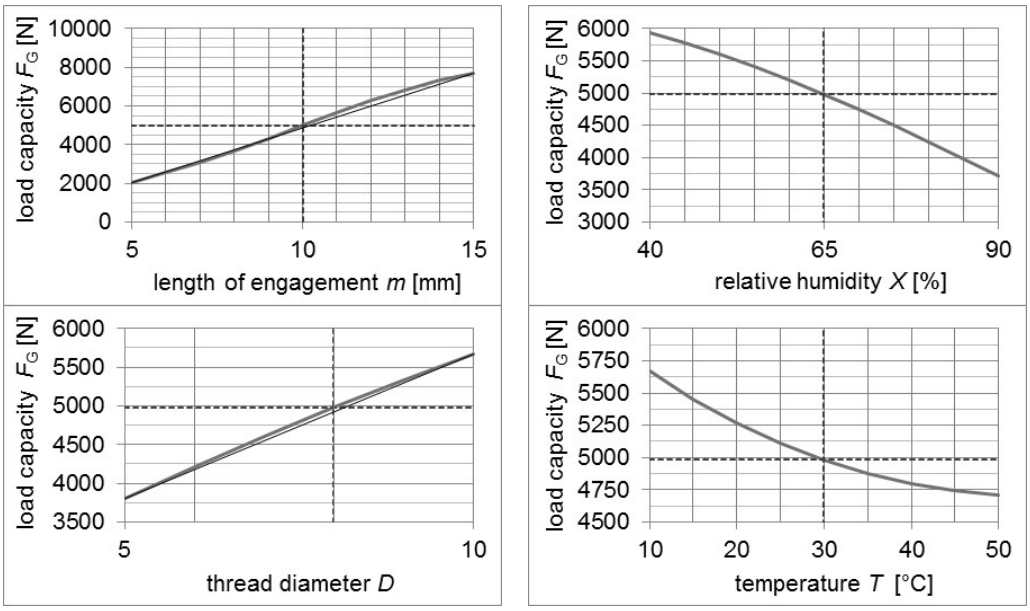

Figure 5: Effect of a single factor variation on the load capacity of a vulcanized fiber inner thread [1]

Literature

[1] Mittendorf, Roman-Marius: Entwicklung einer Richtlinie für die Auslegung von Direktschraubverbindungen in Vulkanfiber. Dissertation, Technische Universität Dortmund, Fakultät Maschinenbau, 2016.

[2] Penning, Bastian; Walther, Frank; Dumke, Dominik; Künne, Bernd: Einfluss der Verformungsgeschwindigkeit und des Feuchtegehaltes auf das quasistatische Verformungsverhalten technischer Vulkanfiber. *MP Materials Testing 55*. 2013, 4, S.276-284.

[3] Fiedler Bremer, C.; Scholz, R.; Myslicki, S.; Starke, P.; Boller, C.; Walther, F.; Krause, M.: NDT-Based Characterization of Timber and Vulcanized Fiber for Civil Infrastructure. *NDT-CE: International Symposium Non-Destructive Testing in Civil Engineering*. Berlin, 2015, S. 1-11.

Microbial Anchoring and Support System (MASS) for biocatalysts and the delivery of bioactive materials

Oscar Ivan Bernal Zuniga[1], Ph.D.; Michael Flickinger[1], Ph.D.; Joel J. Pawlak[2], Ph.D.

AUTHOR INFORMATION

J. Pawlak

[1] Department of Chemical and Biomolecular Engineering, North Carolina State University, Raleigh, North Carolina, USA

[2] Department of Forest Biomaterials, North Carolina State University, Raleigh, North Carolina. USA

Email: jjpawlak@ncsu.edu

Abstract

The delivery of bioactive living vegetative microbes and isolation of products produced catalytically by the cells using novel engineered paper-based materials has many future applications in the healthcare, agricultural, solar energy and biofuels/chemicals industries which are currently valued at >$50 billion. This proposal seeks to commercialize a novel Microbial Anchoring and Support System (MASS) to create a new cellulose fiber based biocatalysis platform that can anchor and dry-stabilize highly concentrated active microbes. This broadly applicable technology enables the *dry storage* of highly concentrated living cells in a cellulose fiber matrix for prolonged periods of time. *The MASS approach, incorporating living microbes into specialty biocatalytic papers, has a direct path for scalability and integration into existing papermaking operations.* Unique additives and materials are used during the fabrication process to protect and anchor highly concentrated microbes so that when the MASS is rehydrated we can control the activity, retention or release of the cells (engineered cell-to-fiber adhesion). Microbes may be coated on the surface of the MASS, uniformly integrated, or deposited in a distinct layer within the MASS.

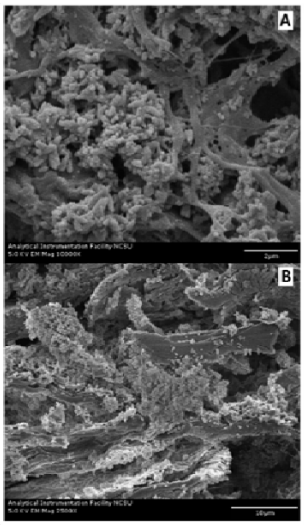

Figure 1: Proof of concept microbial paper microstructure. A. Top-view SEM micrograph of a hand-made Rps. palustris microbial paper sheet (scale bar 2µm). B. Cross-section (scale bar 10µm)

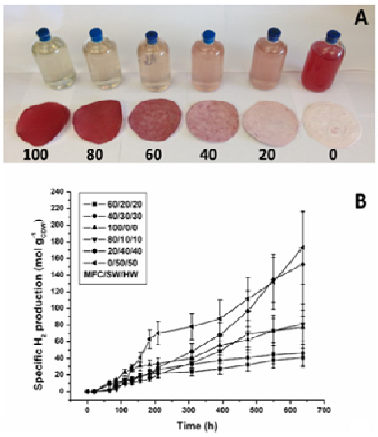

Figure 2: Vacuum-dewatered microbial paper films specific photoreactivity. A. Film/filtrate MFC series (numbers indicate MFC content (%). B. Cumulative specific H_2 production. (Error bars = 1 Std Dev, n=3)

Our research has focused on studies of model microbial systems for creating dry stabilized coated paper biocatalysts for harvesting solar energy, for recycling greenhouse gases (CO_2, CO, CH_4) or for the production of H_2 from acetate. Our results for greenhouse gas absorption and H_2 production indicate the MASS has a 10-100 fold improvement in activity of the embedded microbes (dry stabilization + intensification). This is attributed to the very high density of microbes anchored to the support and also the improved access to gases due to the porosity of the paper. The porosity and adhesion can be engineered by fiber composition and fabrication methods. This indicates that the MASS platform can be effective in intensifying and preserving microbial biological activity in a dry state before use enabling dry storage and shipping prior to re-activation. This work presents a new paradigm to use paper as an inexpensive support for large scale bio-catalytic activity for harvesting solar energy, as absorbers recycling gaseous carbon compounds or VOCs into useful products, as well as other bio-delivery mechanisms.

Evaluating the quality of recycled fibre material with a new concept

JANNE KERÄNEN AND ELIAS RETULAINEN

AUTHOR INFORMATION

J. Keränen

E. Retulainen

VTT Technical Research Centre
of Finland Ltd,
P.O. Box 1603, FI-40101
Jyväskylä, Finland

janne.keranen@vtt.fi,
elias.retulainen@vtt.fi

INTRODUCTION

Today the quality of paper for recycling is mainly estimated based on the standard grade classifications that give information on the origin and paper grade composition. However, this does not give information on the quality at the fibre level. Although recycling rates are increasing, the average age of fibres entering the mill is still low compared to what the fibres can tolerate [1-3]. Therefore, it can be argued that the characteristic phenomena in the paper recycling loop are not caused by the degradation of individual fibres, but by blending different fibre grades and non-fibre components in a non-optimal way.

THE PROPOSED NEW CONCEPT

A novel method is proposed for evaluation of the quality of fibre material used for recycling, emphasizing especially the strength related quality. The method proposes a new parameter, called Integrity value, which is an indicator of the strength potential of the pulp, and gives information on the fibre level properties. The approach is based on the fact that the strength potential of the material is of primary importance, and only sufficient strength level makes it possible to optimize other quality properties. Strength potential of material is realized when the fibres are well bonded. Integrity value is an essential component of the strength of the pulp. For lower bonding levels, the role of the integrity values is shown by this formula:

Strength = (Integrity value) * (Bonding) **(1)**

Thus the integrity value is not affected by bonding, but it is a function of several fibre level factors:

Integrity value = f (proportion of fibre material; fibre strength;

network forming potential of fibres) **(2)**

A simple equation is used for defining the integrity value:

$$\textbf{Integrity value} = (\mathbf{1} - \boldsymbol{\alpha Filler}) * (\mathbf{1} - \boldsymbol{\beta Fines}) * (\mathbf{1} - \boldsymbol{\gamma Lignin}) * \boldsymbol{L} * \frac{\boldsymbol{L}}{\boldsymbol{c}} \quad \textbf{(3)}$$

The main factors in paper for recycling that affect the strength potential are the non-fibre material (i.e. filler) [4], fines and lignin [5], fibre length (**L**) and coarseness (**c**). Although it may sound unreasonable, here fines are considered not to affect the strength potential, although it is known that fines have a definite role in contributing to inter-fibre bonding. Recycled fines have a lower bonding capability because fines with a high surface area tend to collect impurities [6]. Fines are also known to be created by the mechanical disruption of the fibre wall.

The equation (3) contains several constant parameters that need to be defined, and which can adopt different values depending on the application of the equation and how the values for different variables are determined. In the ideal case, the fibre properties can be measured in-line from pulp by using a fibre analyser.

Rough estimates for the parameters can be obtained from the literature, based on how the variables affect the tensile strength [4–6]. A first approximation is α=1.9; β=1.4 and for γ=1.2.

APPLICATION OF THE INTEGRITY VALUE

Calculation of the Integrity value for several fibre types gives results shown in Figure 1. The virgin fibre materials seem generally to have higher Integrity values than recycled pulps. Also, the deinking process in newsprint mills and screening in paperboard mill seem to increase the integrity value.

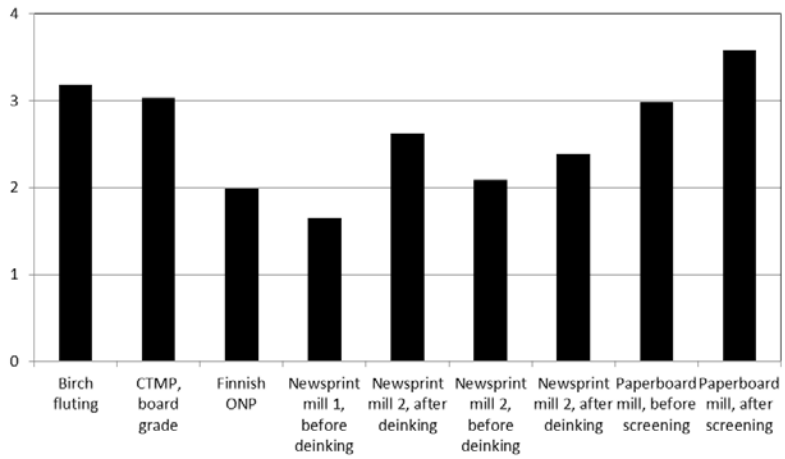

Figure 6 Calculated Integrity values for tested pulps.

Table 1 shows the reasons for changing Integrity values. Deinking reduces the filler content, reduces the fibre coarseness, and increases the curl. There is also indication of a slight increase in lignin content.

Table 3 Changes in pulp properties caused by deinking or screening

Pulp /Mill	Filler, %	Lignin, %	Fines, %	Fibre length, mm	Coarseness, mg/m	Curl, %
Newsprint mill 1, before deinking	38.6	14.8	22.8	1.17	0.24	15.5
Newsprint mill 1, after deinking	18.0	15.3	19.2	1.14	0.19	16.1
Newsprint mill 2, before deinking	26.1	13.1	19.0	1.10	0.21	14.6
Newsprint mill 2, after deinking	15.1	14.5	19.2	1.10	0.19	17.8
Paperboard mill, before screening	17.4	12.0	15.7	1.18	0.19	13.8
Paperboard mill, after screening	13.2	11.2	14.8	1.23	0.19	13.8

INTEGRITY VALUE AND STRENGHT PROPERTIES

Handsheets were made of the 9 pulps shown in Figure 1, at standard and additionally in 6 cases at elevated wet pressing levels, giving totally 16 cases. The bonding factor in equation 1 was estimated to depend mainly on the bonded area of the fibre network. The bonded area was estimated to be a linear function of density, and approach zero around at 0.3 g/cm^3 (300 kg/m^3). Figure 2 shows correlations with the tensile and SCT strengths. It is interesting that the parameter for lignin (γ=0) in this material gave the best results.

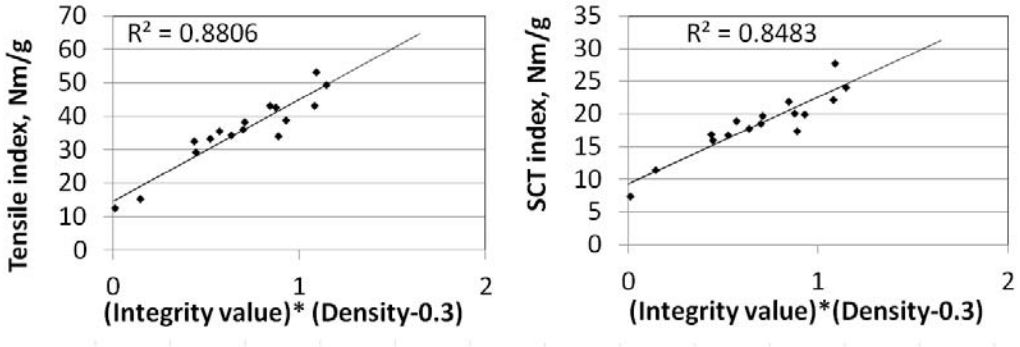

Figure 7 Correlation between measured strength values and integrity value multiplied by bonding factor. The values used for the parameters were α=0.9, β=1.59, γ=0.

CONCLUSIONS

The proposed fibre integrity value approach for recycled pulp has the potential to be used as a quality parameter for paper for recycling, although more testing is needed. The integrity value gives information on the strength potential of the fibre material. When combined with apparent fibre network density, it correlates well with several strength properties of paper. The integrity number is affected by deinking and screening. The integrity number can potentially be measured using in-line analysers.

ACKNOWLEDGEMENT

This research was part of REFFIBRE project that was in receipt of funding from the European Community's Seventh Framework Programme under grant agreement n° 604187.

REFERENCES

[1] Schabel, S., Putz H.-J. (2005), “Rohstoff Altpapier – ein Ausblick”. Wochenblatt fűr Papierfabrikation vol. 133, no 3–4, pp-103-111.

[2] Howard R.C., (1991), “The effects of recycling on paper quality”. Pap. Technol. vol. 30, no. 4, Apr. 1991, pp 20–25.
[3] Nguyen, T. L. L. (2001). “*The Impact of the Chemical Composition of Fiber Cell Walls on the Recycling Potential of Paper”*, Master’s Thesis, Asian Institute of Technology, Bangkok, Thailand.
[4] Velho, J. L. (2002). “How mineral fillers affect paper properties”, in: *Iberoamerican Congress on Pulp and Paper Research*, Campinas, Sao Paulo, Brazil.
[5] Page, D. H. et al. (1985). “Strength and Chemical Composition of Wood Pulp Fibres,” in: *Papermaking Raw Materials: Their Interactions with the Protection Process and Their Effect on Paper Properties*, Mechanical Engineering Publications Limited, London, UK. pp. 77–91.
[6] Rundlöf, M., Sjölund, A.-K., Ström, H., Asell, I., and Wågberg, L., “The effect of dissolved and colloidal substances released from TMP on the properties of TMP fines”. Nord. Pulp Pap. Res. J. vol. 15, no. 4, 2000, pp 256–265.

Edge-wrinkling in stacked sheets of paper

Louis Saes

AUTHOR INFORMATION


L. Saes

Océ Technologies B.V., Venlo, The Netherlands

Email:
louis.saes@oce.com;

A change of environmental conditions can lead to edge-wrinkling in a stack of paper sheets. We have studied this phenomenon, because in inkjet printing it is relevant to know the effects of sheet deformation on paper transport accuracy. In this contribution an introductory study is reported.

The explanation for the raise of edge-wrinkling is rather straightforward: the combination of moisture diffusion into the stack and the hygroexpansivity of paper cause the edges of the sheets to expand while the bulk does not deform. Stresses between the expanded and non-expanded parts of the sheet exceed the threshold for buckling and induce edge-wrinkling in the edges of the sheets.

Comparable phenomena, with different causes, have been studied by, for instance, Fedorchenko[1] and Liang[2]. The significance of individual contributions to the ultimate amount of edge-wrinkling differs in each of these cases.

In our study the diffusion of moisture into the stack is modeled according to the approach of Foss[3]. The parameters in this model have been determined experimentally (diffusion coefficient of moisture, exchange coefficients, moisture sorption isotherms). This provides the moisture distribution in the sheets as a function of time. For the mechanical part of the simulations, individual sheets are considered, using suitable boundary conditions. The hygroexpansivity, anisotropy of the sheet and the dependence of the elastic properties on its moisture content are taken into account. Stochastics of the phenomenon are taken into account by randomization of the initial state (flatness) of the sheet. The results are evaluated based on the wavelength and amplitude of the shape of the sheet's edge. The influences of several

parameters, the height of the stack, the penetration depth of the moisture, the thickness of the sheet, etc., on the results will be shown.

References

[1] A. I. Fedorchenko, A.-B. Wang, V. I. Mashanov, W.-P. Huang, H. H.Cheng, Strain-induced wrinkling on SiGe free standing film, Appl. Phys. Lett. **89** (2006) 043119.

[2]H. Liang, L. Mahadevan, Growth, geometry and mechanics of a blooming lily, PNAS **108** (2011) 5516.

[3]W. R. Foss, C.A. Bronkhorst, K. A. Bennet, Simultaneous heat and mass transport in paper sheets during moisture sorption from humid air, Int. J. Heat Mass Transfer **46** (2003) 2875-2886.

Paper-Based Block Copolymer and Functional Polymer membranes‡

S. Schöttner[1], C. Rüttiger[1], H.-J. Schaffrath[2], M. Biesalski[1], M.Gallei[1,*]

AUTHOR INFORMATION


S. Schöttner

[1] Macromolecular Chemistry Department, Technische Universität Darmstadt, Alarich-Weiss-Straße 4, 64287 Darmstadt, Germany

[2] Paper Technology and Mechanical Process Engineering, Technische Universität Darmstadt, Alexanderstraße 8, 64283 Darmstadt, Germany

m.gallei@mc.tu-darmstadt.de, www.makromolekulare-chemie.de

‡Results on polymer membranes were submitted for publication to the American Chemical Society

Summary

Block copolymers consist of two or more polymer segments covalently connected to each other and they have attracted enormous attention due to their unique capability of forming fascinating nanostructures in the bulk or by self-organization in solvents in the recent past. Moreover, such polymers can be addressable by external triggers representing a unique class of building blocks for the generation of novel materials.[1] Herein we focus on polymeric materials, which contain at least one functional - either chemically or physically - addressable segment. The non-solvent induced phase separation (NIPS) process is applied for nano porous structure formation on paper sheets in order to gain access to flexible integral asymmetric membranes featuring an isoporous structure on top of the paper (see Figure).[2] Additionally, we applied surface-initiated atom transfer radical polymerization protocol for the immobilization of a redox-switchable metallopolymer.[3] The obtained *smart papers* undergo efficient oxidation due to the presence of ferrocene moieties, which is accompanied with a tremendous change of polarity of the paper-metallopolymer substrate.[4] These novel functional paper materials have the potential to act as *e.g.* sensors or switchable membranes in paper-based microfluidic applications.

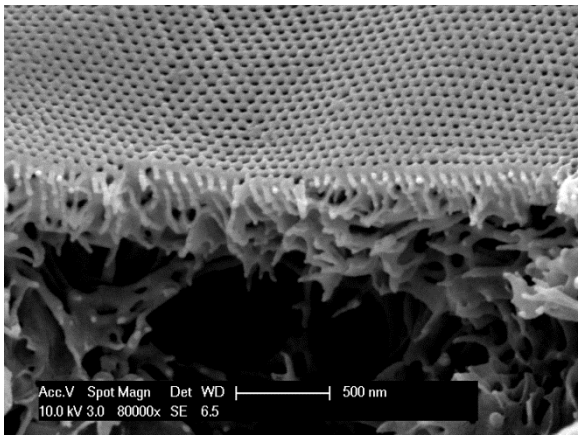

Figure 1: SEM images of functional block copolymer isoporous membranes.

Acknowledgements

M.G. thanks the Max-Buchner-Foundation and the Fonds der Chemischen Industrie for financial support of this work. This work has been partially supported in the frame of the LOEWE project iNAPO by the Hessen State Ministry of Higher Education, Research and the Arts.

Literature

[1] Stuart M. A. C., Huck W. T. S., Genzer J. *et al. Nature* 9: 101-113, 2010.

[2] Gallei M., Rangou S., Filiz V. *et al. Macromol. Chem. Phys.* 214: 1037-1046, 2013.

[3] Gallei M. *Macromol. Chem. Phys.* 215: 699-704, 2014.

[4] Rüttiger C., Biesalski, M., Gallei et al . *Polymer* 98: 429-436, 2016

Master for ming of vulcanized fibre with the pulp moulding procedure

Prof. Dr.-Ing. Bernd Künne, Dipl.-Ing. Björn Palm, Dipl.-Math. Dennis Stracke

AUTHOR INFORMATION


B. Künne

Technische Universität Dortmund
Institut für Konstruktion und Werkstoffprüfung
Fachgebiet Maschinenelemente
Fakultät Maschinenbau
Leonhard-Euler-Straße 5
44227 Dortmund

Email:
bernd.kuenne@tu-dortmund.de

Summary

The possibility to produce plates made of vulcanized fibre in the pulp moulding procedure is analysed with the help of a self-constructed apparatus. Furthermore the dependency of the samples tensile strengths on different influence factors is investigated.

Introduction / Conclusion

The assembly of three-dimensional geometries and products from conventional vulcanized fibre manufactured with the layer process is not arbitrary feasible because of the laminar structure of the paper basis. This raises the question of whether it is possible to manufacture vulcanized fibre in a master forming process, which allows the creation of diverse product geometries and an even broader spectrum of applications compared with the traditional layered product. Furthermore, with this kind of manufacturing process the raw-paper making process could be omitted, since the base material in the master forming procedure is a fibre-suspension made of fibres and a parchmentizing agent.

To evaluate the producibility, a test apparatus with a planar screen inspired by the pulp moulding procedure was built. In figure 1 the basic steps of the moulding procedure are shown. In step a) the fibres are separated, before they are mixed with the parchmentizing agent in step b). Afterwards the fibre suspension is filled into the moulding apparatus c). In step d) the

parchmentizing agent is pressed out of the apparatus through a screen at the bottom by a heated plunger. Step e) is an optional step, where the formed fibre layers are heated. The formed fibre network is washed out and dried in the last step f).

Figure 2 shows a detailed view of the used moulding apparatus including the plunger and the screen, which consists of a 3D-printed support structure (material ABS for high temperatures of up to 80 °C) and a perforated screen. The pressed out agent leaves the apparatus through an outlet on the bottom.

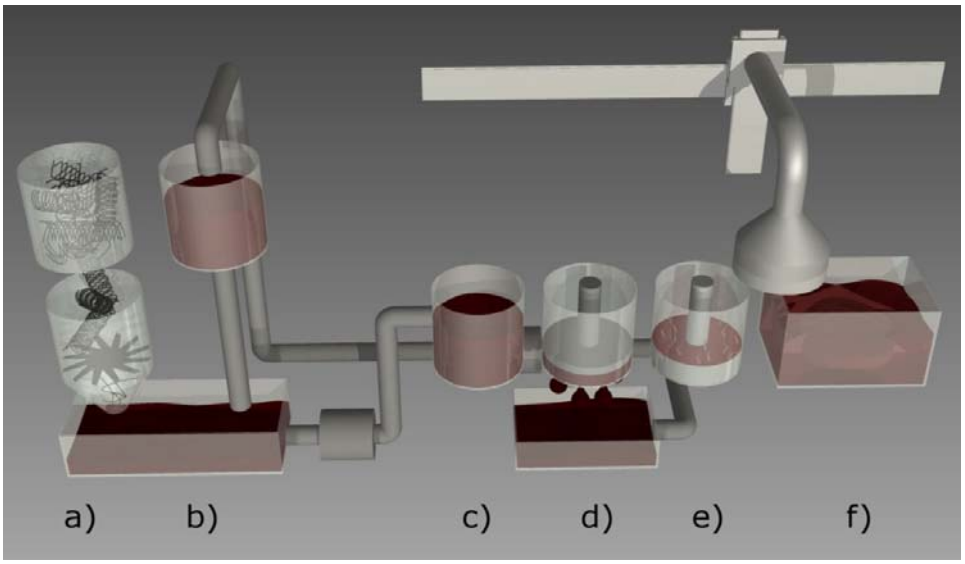

Figure 8 - Pulp moulding procedure

The fibre-suspension was made of 68-percent zinc-chloride solution mixed with cotton rags (mass-concentration of the fibre-suspension about 0.3 percent). After this the shape forming is achieved by mechanical squeezing of the suspension through the small meshed screen. In the next to last step the remaining zinc-chloride was washed out of the created vulcanized fibre fleece in a series of wash out basins with decreasing concentration, before the fleeces were dried.

The manufactured fleeces showed mechanical strengths of up to 68 MPa depending on the process parameters temperature, compression pressure and compression duration. The higher the compression pressure (with fixed temperature and fixed compression duration), the higher is the tensile

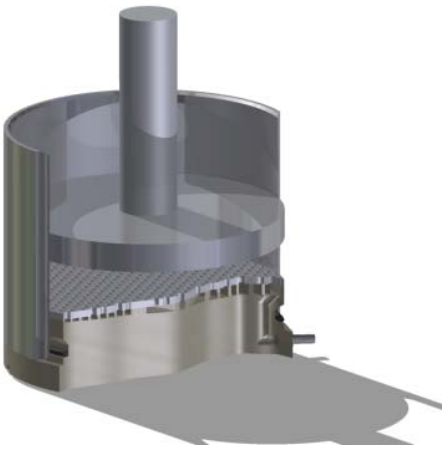

Figure 9 - moulding apparatus

strength of the samples. Same observations could be made for variation of the other two parameters (leaving the two remaining parameters constant). According to DIN 7737, traditional vulcanized fibre reaches strengths of 70 MPa in machine direction and 50 MPa in cross direction. Thus the created, in plane isotropic fleece achieves a nearly as high tensile strength as traditional vulcanized fibre products in machine direction.

One problem with the described procedure is the shrinkage which increases with increasing temperature and compression duration. An average shrinking of about 30 percent regarding the specimen area before and after the washing/drying-process could be observed. The dependency on temperature and compression duration leads to the assumption that the degree of shrinkage is highly coupled with the chemical processes during the moulding.

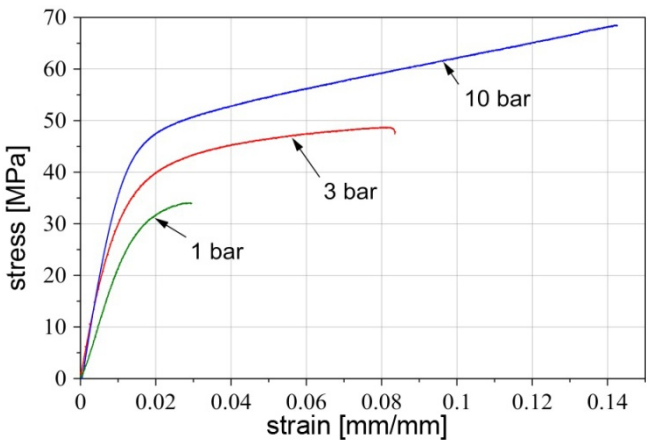

Figure 10 - stress-strain-diagrams with different compression pressures

The goal is to find an optimal balance between mechanical strength and shrinkage. Another field of interest is the substitution of used parchmentizing agents. First steps have been made to analyse the chemical sequences during the moulding process by analysing the viscosity-characteristics while fibres are dissolved in the agent. If a link could be made between the suspension viscosity and the degree of dissolution, other parchmentizing agents could be evaluated regarding their suitability for the moulding process. To summarize, the described procedure would build the basis of manufacturing entirely arbitrary geometries from a fibre-suspension without need of the paper-making process.

!

Estimating the Area in Molecular Contact using Förster Resonance Energy Transfer Microscopy (FRET)

Georg Urstöger[1, 3], Robert Schennach[2, 3], Ulrich Hirn[1, 3]

AUTHOR INFORMATION

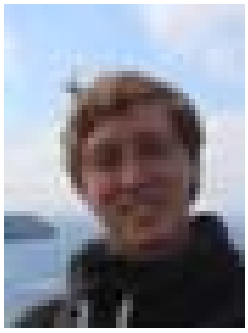
G. Urstöger

[1] Institute for Paper, Pulp and Fiber Technology, Graz University of Technology

[2] Institute for Solid State Physics, Graz University of Technology

[3] CD-Laboratory for fiber swelling and paper performance

Inffeldgasse 23, 8010 Graz, Austria

Email:
georg.urstoeger@tugraz.at

Summary

Tensile strength and binding properties of paper have been thoroughly investigated for the past 50 years. However, recent studies have shown that the binding mechanisms of fibers are more complex than previously thought. The area in molecular contact, necessary for all molecular interactions but especially for interdiffusion, is the key factor quantifying hydrogen, van der Waals and Coulomb bonds between the fibers. Therefore, determining the area in molecular contact is essential to quantify the binding energy. For this purpose, fiber-fiber joints were investigated by Förster resonance energy transfer microscopy (FRET). This method is based on the dipole interaction of two dyes which are being covalently bound to the individual fiber surfaces. The dyes on the fibers (donor dye on fiber 1 and acceptor dye on fiber 2) are being excited by incident light of a certain wavelength. If the two fibers are close together (~1-10 nm) during this process, a part of the energy transfer between the chromophores happens non-radiative through a so called Förster transfer. In this work the area of molecular contact has been measured by FRET and polarized light microscopy.

Introduction

Starting with the rigoros investigations of paper strength properties by Page et al. in the 60s, a vast progress in understanding paper was made. This strong

theoretical groundwork forms the basis of today's scientific investigation in the paper industry. However due to the improvement of technical methods, we believe it is worth taking a second look at some of the basics with the aim of improving our knowledge of paper. This work therefor continues to investigate the area in molecular contact of bound cellulose fibers as it was done previously by E. Gilli and Kappel et al. to get a better understanding of the bonding mechanisms between cellulose structures. [1–3]

The method we concentrate on is called Förster Resonance Energy Transfer (FRET). This method makes use of two chromophores, a donor and an acceptor, which can interact when they come into proximity (1 – 10 nm) by Förster energy transfer. Förster transfer is a form of dipole-dipole interaction which occurs when a photon (type 1) excites the donor molecule to a state where it forms an oscillating dipole. When the acceptor is close enough and the energy levels of the donor and the acceptor overlap to a certain extent, the donor can transfer its energy to the acceptor. Subsequently the acceptor can relax into its ground state under the emission of another photon (type 2) with a wavelength higher than the initial one. The increased occurrence of type 2 photons can be detected and statements about the proximity of the two chromophores can be made. We therefore have a method to determine if two bonded cellulose fibers exhibit contact on a molecular level.

The fibers used were from industrial softwood kraft pulp. The fibers were fractionated with a Bauer McNett unit and only the longest remaining fraction of fibers was used. The two chromophores used were 7-(diethylamino)coumarin-3-carbohydrazide as a donor and Fluorescein-5-thiosemicarbazide as an acceptor. The chromophores were bought from Santa Cruz Biotechnology. The dying process was adapted from Thomson et al..[4] Fiber crossings were prepared manually by overlaying individual fibers in a drop of water on a Teflon sheet. A second Teflon sheet was carefully put on top of the first sheet and subsequently put into a Rapid Köthen sheet dryer. As the chromophores are light sensitive the exposure to light was kept at a minimum throughout the preparation process. The fiber crossings were then investigated by a microscope with three different filter sets corresponding to the excitation and emission maxima of the chromophores. The data was analyzed by an in house written Matlab script based on a FRET analysis algorithm from Gordon et al., and Acceptor-photobleach method.[5] For imaging an Optimos model from QI Imaging was used. The camera has a

monochrome sensor with high resolution and sensitivity. As a light source the KL-2500 from Leica was used.

Conclusion

Fiber crossings of fibers dyed at different concentrations were investigated. An exemplary bond is displayed in figure 1. Since the algorithms employed to achieve the FRET images are only valid for the bonded area and break down beyond the borders of the bond only the bonded area is displayed.

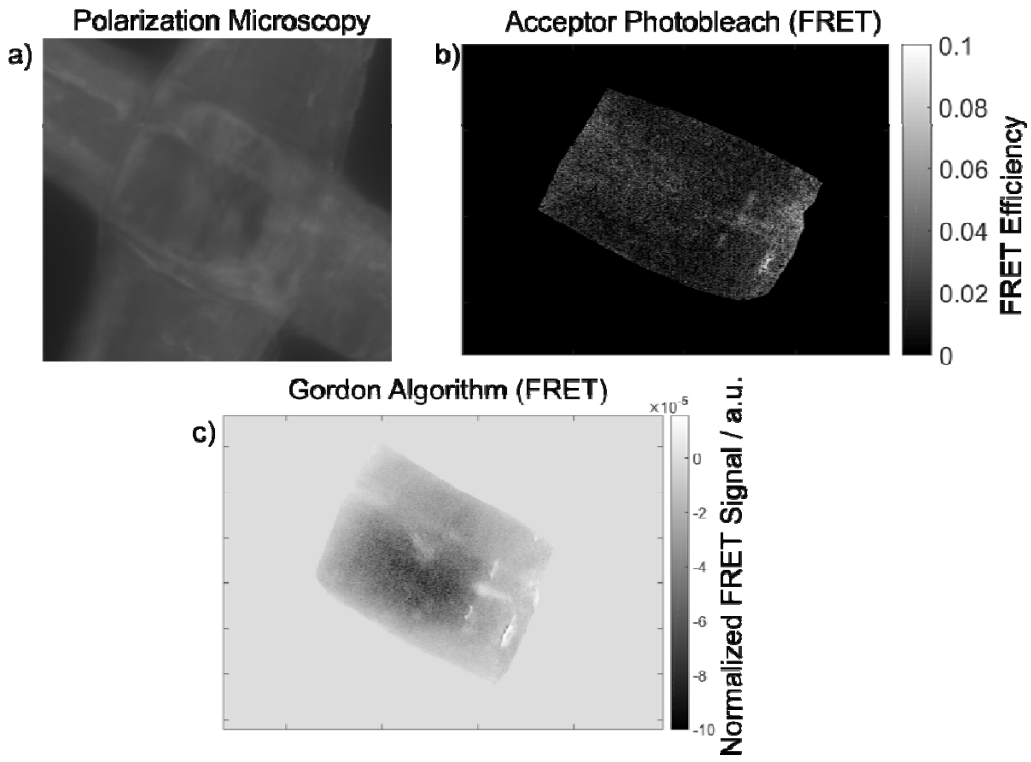

Figure 1: *Fiber crossing analyzed with polarization microscopy and acceptor photobleach method. The fibers were dyed at a concentration of 1.6 and 0.8 mmol/L of acceptor and donor dye, respectively. Although the bonded area is not evident in the polarization microscopy it becomes clearer in the acceptor photobleach image (b). Acceptor Photobleach and Gordon Algorithm should be in agreement show however quite different results.*

When looking at the polarization microscopy image it is far from evident to what degree the two fibers are bonded. Employing the Acceptor Photobleach method to analyze the bond results in an image like in figure 1b) can improve our knowledge of this joint. The FRET efficiency in the image is low and seems to be quite homogeneously distributed over the bond.

The picture c) in figure 1 shows the evaluation of the same bond with the Gordon algorithm. The result of this algorithm should be in agreement with the

acceptor photobleach method in figure 1b) however it does not agree at all. As can be seen in the figure the signal from the bonded area is mostly below zero which is physically impossible. Since the acceptor photobleach method is less prone to experimental errors we believe that either the setup for the Gordon algorithm includes an inadequate part or that more rigorous corrections to the raw data need to be made.

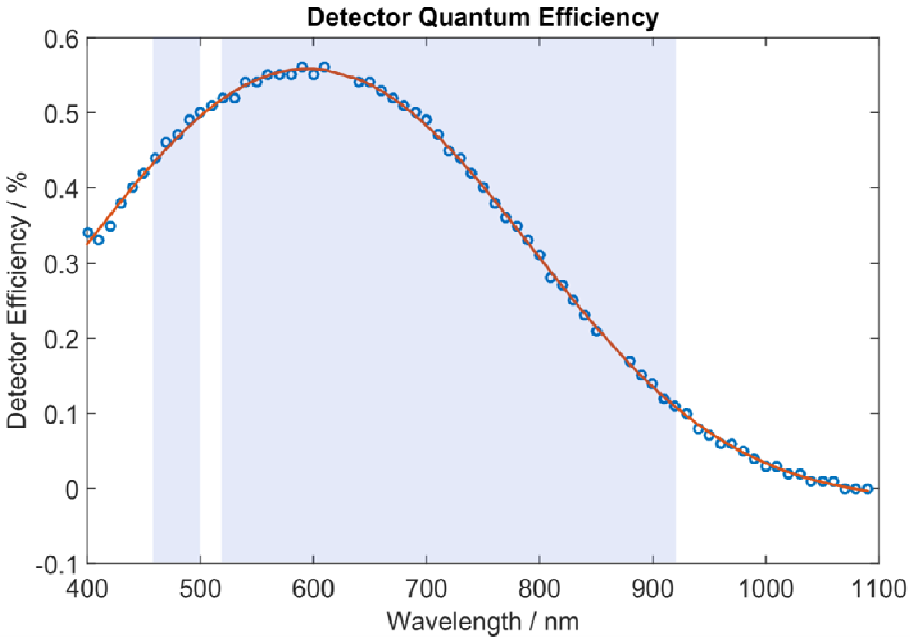

Figure 2: *Detector quantum efficiency. Example of one of the corrections that need to be made in order to account for eventuality in the experiment. When light at different positions (blue regions) of the visible spectrum is detected the data needs to be corrected according to the quantum efficiency.*

An example of such a correction can be seen in figure 2. When images are being recorded at different positions in the visible spectrum, as portrayed by the blue areas, it needs to be accounted for when the data is analyzed. Also a rigorous error analysis needs to be developed, adequate for this problem to confirm the significance of the results.

Literature

[1] E. Gilli, L. Kappel, U. Hirn, and R. Schennach, Compos. Interfaces **16**, 901 (2009).

[2] U. Hirn and R. Schennach, Sci. Rep. **5**, 10503 (2015).

[3] Kappel, Nord. Pulp Pap. Res. J. **24**, 199 (2009).

[4] C.I. Thomson, R.M. Lowe, and A.J. Ragauskas, Carbohydr. Polym. **69**, 799 (2007).

[5] G.W. Gordon, G. Berry, X.H. Liang, B. Levine, and B. Herman, Biophys. J. **74**, 2702 (1998).

Continuous production of plasticized cellulosic composites with a paper machine

Tervahartiala, Tero and Valkama, Jukka

AUTHOR INFORMATION

Papiertechnik
Duale Hochschule Baden-Württemberg Karlsruhe
Baden-Wuerttemberg
Cooperative State University Erzbergerstraße 121
- 76133 Karlsruhe - Germany

Email:
tervahartiala@dhbw-karlsruhe.de

Summary
Project COMPAC (Plasticised Cellulosic Composites for Packaging Materials) aims to integrate a production process of an ACC to a conventional paper and board making process. By developing a strong bio-based material for the packaging industry COMPAC project will create value for our project partners by reducing transport costs, increasing the value of the products and replacing non-recyclable materials. During two pilot trials on a pilot scale paper machine (PM) with machine width of 550 mm and speeds up to 30 m/s a proof of concept has been achieved.

COMPAC is a 3 year EU funded Woodwisdom Eranet+ project running until 14.07.2017 and includes universities and industry partners from Germany, Finland and Sweden.

Introduction
Within project COMPAC alternative methods for plasticizing paper materials into ACC (all cellulosic composites) or CCC (cellulose containing composites), in order to use conventional paper machines for the production of a strong, fully biodegradable and bio-based material. Furthermore, the focus was in acceleration of the plasticization in order to produce the composite material in a continuous process and replacement of environmentally very problematic chemicals needed for the vulcanization that makes the processing costly.

Traditionally the plasticization of cellulosic material is done by partially dissolving and re-crystallizing a cellulosic fibre web by using vulcanization technique and chemicals i.e. sulphuric acid or zinc chloride. In its simplest form vulcanisation of a cellulosic fibre web is a 3 step process: impregnation, washing and drying. In this process the vulcanisation chemical works as a catalyst and ideally in the end product no traces of chemicals can be found and the product is 100% cellulosic. This makes the washing step crucial and the limiting factor regarding process speeds and material thickness. Strong vulcanized fibre materials have been used for a long time in several

applications ranging from housing for electronics and products like, sealing rings or panels.

Rapid plasticization of natural cellulosic fibres by using different fibre sources (conventional paper pulps) were first studied in the laboratory in order to understand the material behaviour. Extensive cellulosic fibre material screening studies using anisotropic laboratory paper sheets showed improvement of mechanical strength properties cross the board and increase in density from 500 kg/m³ up to 1100 kg/m³. Tensile strength of the sheet material increased by more than 300% as well as elongation at break by more than 100%. Interestingly different fibre sources react very differently to plasticisation, this enables a broad field of specialised applications where with various treatment times and fibre mixes product properties can be widened.

Alternative chemical systems were researched in pre-studies. For the continuous processing of CCC a caustic/urea based plasticization system was used and successfully tested with a paper machine production. The paper web was produced by using a Fourdrinier-type paper machine and plasticized at the size press unit. The base paper had a basis weight of 100 g/m^2. During the pilot trials on a pilot scale paper machine (PM) with machine width of 550 mm and speeds up to 30 m/s was used. The plasticized paper produced in pilot trials showed equal properties to the laboratory tests. Both off-line (roll-to-roll) and on-line production was tested. Patents for the production methods have been applied.

By developing a strong bio-based material for example for the packaging industry the transport costs can be reduced, but also value increasing barrier properties are generated.

Conclusions

Plasticised fibre material, including vulcanised fibre, has potential in packaging and consumer applications. All-cellulose or all-cellulosic composites (when not using 100% cellulose pulps) can be produced on a paper machine. This proof of concept very well may be the answer to cost-effective production of a sheet-like natural fibre composite.

Advanced Structure Research of Functional Cellulose and Paper Materials by Solid-State Dynamic Nuclear Polarization (DNP)

Li Zhao,[a] Gerd Buntkowsky,[a] Kai Zhang,[b] Markus Gallei,[c] Torsten Gutmann[a]

AUTHOR INFORMATION


Li Zhao

[a] Eduard-Zintl-Institute
for Inorganic Chemistry and Physical Chemistry
Technical University Darmstadt, Alarich-Weiss-Str. 4
D-64287 Darmstadt, Germany

[b] Wood Technology and Wood Chemistry
Georg-August University Göttingen
Büsgenweg 4
37077 Göttingen, Germany

[c] Ernst-Berl-Institute
for Chemical Engineering and Macromolecular Science
Technical University Darmstadt
Alarich-Weiss-Str. 4
D-64287 Darmstadt, Germany

Email:
zhao@chemie.tu-darmstadt.de

A full paper-version is intended to be published. Please contact the author for further information.

KRÜSS

Advancing your Surface Science

Dr. Martin Kirchner
Technical Consultant at KRÜSS

WHO CAN HELP TO WRITE NEW CHAPTERS IN THE HISTORY OF PAPER SURFACE TREATMENT?

WE CAN. AT KRÜSS.

Mobile Surface Analyzer – MSA

www.kruss.de

Engagierte Mitarbeiter, innovative Produkte und modernste Technologien sind auch weiterhin die Garanten für den weltweiten Erfolg der Koehler Paper Group.

UNTERNEHMEN MIT ZUKUNFT – PAPER FOR THE FUTURE

Papierfabrik August Koehler SE
Hauptstraße 2 · D-77704 Oberkirch
Telefon +49 7802 81-0 · Fax +49 7802 81-4330

www.koehlerpaper.com

Koehler
PAPER GROUP


MITSUBISHI
PAPER MILLS
LIMITED
HiTec Paper.
Innovativ
und flexibel.
Mitsubishi HiTec Paper steht für innovative Produktentwicklungen und Spezialpapiere höchster Qualität. Natürlich stehen wir in engem Kontakt zu Kunden, Endanwendern, OEMs und Hochschulen und orientieren unsere Innovationen an aktuellen und zukünftigen Marktanforderungen.
Sechs unterschiedliche Streichtechnologien stehen für die Realisierung unserer Produkt-innovationen zur Verfügung. Für spezielle Funktionsstriche auf eigenen Basispapieren. State-of-the-art und sehr flexibel.
Digitaldruck
Fälschungs- und Produktsicherheit
Funktions- und Barriere-Striche
Speziallösungen für die Verpackungsindustrie
Mitsubishi HiTec Paper Europe GmbH
www.mitsubishi-paper.com
innovations.mpe@mitsubishi-paper.com

Schabel, Samuel; Schaffrath, Heinz-Joachim (eds.)
„Progress in Paper Physics Seminar 2016 Conference Proceedings“
Darmstadt, 2016

Print ISBN 978-3-00-054001-1